



HAL
open science

Metal nanoparticles embedded in ligand-functionalized water-soluble core-shell polymers for application in aqueous biphasic hydrogenation

Chantal Joseph Abou-Fayssal

► **To cite this version:**

Chantal Joseph Abou-Fayssal. Metal nanoparticles embedded in ligand-functionalized water-soluble core-shell polymers for application in aqueous biphasic hydrogenation. Coordination chemistry. Université Paul Sabatier - Toulouse III; Polytekniske laereanstalt, Danmarks tekniske universitet, 2023. English. NNT : 2023TOU30237 . tel-04643484

HAL Id: tel-04643484

<https://theses.hal.science/tel-04643484>

Submitted on 10 Jul 2024

HAL is a multi-disciplinary open access archive for the deposit and dissemination of scientific research documents, whether they are published or not. The documents may come from teaching and research institutions in France or abroad, or from public or private research centers.

L'archive ouverte pluridisciplinaire **HAL**, est destinée au dépôt et à la diffusion de documents scientifiques de niveau recherche, publiés ou non, émanant des établissements d'enseignement et de recherche français ou étrangers, des laboratoires publics ou privés.



THÈSE



**En vue de l'obtention du
DOCTORAT DE L'UNIVERSITÉ DE TOULOUSE**

Délivré par l'Université Toulouse 3 - Paul Sabatier

Cotutelle internationale: Université technique du Danemark

**Présentée et soutenue par
Chantal JOSEPH ABOU-FAYSSAL**

Le 30 novembre 2023

**Synthèse et confinement de nanoparticules métalliques dans des
polymères amphiphiles à coeur-coquille pour application en
catalyse biphasique**

Ecole doctorale : **SDM - SCIENCES DE LA MATIERE - Toulouse**

Spécialité : **Chimie Organométallique et de Coordination**

Unité de recherche :
LCC - Laboratoire de Chimie de Coordination

Thèse dirigée par
Eric MANOURY et Anders RIISAGER

Jury

Mme Audrey DENICOURT-NOWICKI, Rapporteure

M. Cyril GODARD, Rapporteur

M. Esben THORMANN, Examineur

Mme Martine URRUTIGOÏTY, Examinatrice

M. Eric MANOURY, Directeur de thèse

M. Anders RIISAGER, Co-directeur de thèse

PhD Dissertation

Metal nanoparticles embedded in ligand-functionalized water-soluble core-shell polymers for application in aqueous biphasic hydrogenation

Chantal JOSEPH ABOU-FAYSSAL

September 2023



Supervisors


Prof. Anders RIISAGER, Professor, DTU Chemistry

Dr. Eric MANOURY, Research Director, LCC - CNRS

Dr. Karine PHILIPPOT, Research Director, LCC - CNRS

Co-Supervisor

Dr. Martin NIELSEN, Associate Professor, DTU Chemistry

À tous les cèdres de ma vie 

Acknowledgments

First and foremost, I would like to extend my sincere appreciation to my esteemed jury members Dr. Audrey DENICOURT-NOWICKI, Prof. Cyril GODARD, and Prof. Esben THORMANN. I wish to express my gratitude to them for agreeing to be the referees for this thesis project. Your willingness to be a part of my thesis committee is a source of great honor for me.

The Danish Technical University and Université de Toulouse III Paul Sabatier are acknowledged for their support. The European Union's Horizon 2020 research and innovation program the Marie Skłodowska-Curie grant agreement No. 860322 (CCIMC project) is acknowledged for the scholarship.

To my esteemed supervisors and mentors, I wish to express my heartfelt appreciation for your profound impact on my academic journey. Your words and our discussions have transformed this experience into a cherished memory, and you will forever stand as the steadfast pillar in the splendid garden of my life. Dr. Karine PHILIPPOT, Dr. Eric MANOURY, Dr. Martin NIELSEN and Prof. Anders RIISAGER your wisdom, guidance, and patience have been invaluable to me. I have learned a lot from you, and I am deeply grateful for the opportunities you have provided. Dr. PHILIPPOT, I will forever hold close to the simple yet profoundly heartwarming phrase you shared with me, "Profite bien et garde les couleurs en tête." It exemplifies an exceptionally gracious heart! Dr. MANOURY, your words, during my moments of vulnerability, served as the spark that reignited my strength and determination. 'Tu es une femme forte, mais tu ne le sais pas encore. Tu le verras.' Prof. RIISAGER, I will forever remember your specific words following our three-hour meeting, 'I guess in life, you're an initiator,' and your unwavering support, which transformed this encounter into a unique human experience, guided by an exceptional leader.

Prof. Rinaldo POLI, expressing the sheer delight of having met you and the profound gratitude for working with you and your unwavering presence, help, advice, support,

and motivation, during those pivotal moments of my Ph.D. journey, is a challenge I wholeheartedly embrace. I can aptly describe you by saying you're a testament to the wisdom of life, akin to the finest wine. Thank you, for the passion you've instilled in me.

I couldn't have envisioned having more exceptional advisors and mentors throughout my Ph.D. studies.

My secondment experience at *Institut Français du Pétrole, Énergies Nouvelles* has been amazing, and it's all thanks to the guidance, mentorship, and hospitality of Dr. Lionel MAGNA. Your willingness to share your knowledge, provide valuable insights, and offer support significantly impacted my professional growth.

I also want to acknowledge the incredible teams I have had the privilege of working with. Both groups at *Laboratoire de Chimie de Coordination: Group of 'Ligands, Complex Architectures, and Catalysis', 'Engineering of Metal Nanoparticles'*, and at the Centre for Catalysis and Sustainable Chemistry '*RIISAGER group*'. I also want to acknowledge the unforgettable memories with exceptional people: Eng. Sandrine VINCENDEAU, Dr. Agnès LABANDE, Dr. Christophe FLIEDEL, Dr. Hui WANG, Dr. Leonhard SCHILL, and Dr. Rosa AXET. Your dedication and collaborative spirit have made every challenge surmountable, and every success a shared victory.

I would like to express my gratitude to the incredible two colleagues of office C226, Dr. Maxime MICHELAS and Dr. Illia RUZHYLO.

A very sincere and deep acknowledgment to Dr. Mahmoud IBRAHIM.

To my co-workers and colleagues, your presence has made the workplace a second home, and I am thankful for the friendships that have blossomed from our professional interactions.

To my soulmate **Eleonora** AR. N., to my friends, **Ramy** N., **Laureine** BK. AF., **Lina** F., **Layal** F., **Si-belle** F., **Barbara** AT., **Georges** A., **Roger** K., **Amedeo** C., **Nina** H., **Elie** M.,

Josette R., Taline S., Rita T., Maxime M., Illia R. and Julian S. . Last, but never least, to my mother, **Samira**, who taught me to spread my wings and fly 'روحي اسبقي نجوم السما'. To my father, **Joseph**, who taught me that my world may shake but will never fall apart 'الأرض بتهتز وما بتوقع'. To my uncle **Samir**, who taught me to love unconditionally and to give without limit, to you **Chady**, to you **Elham**, to my angel in heaven **Sami**, I still feel your presence by the love you created in my heart. My family and friends, your support, understanding, and love have been my anchor during both the highs and lows of my journey. Your belief in me has been a constant source of motivation. Cheers to more memories with very good wine!

This letter serves as a small token of my appreciation for every one of you. Without your support, I would not be here today or have grown as a person and a professional. Your contributions have made an indelible mark on my life. I look forward to continuing this journey, knowing that I am fortunate to have such an incredible network of individuals by my side.

I am excited to see what the future holds, and I hope to continue making you all proud. Once again, thank you from the bottom of my heart for everything you have done.

Mes Cèdres, your support means the world to me.

To Beirut, Lebanon.

For you are with me [Psalm 23:4].

Chantal JOSEPH ABOU-FAYSSAL

Chantal J. Abou Fayssal

Preface

This PhD work has received funding from the European Union Horizon 2020 research and innovation program under the Marie Skłodowska-Curie grant agreement No. 860322 (CCIMC project). It was carried out in the framework of a joint agreement between the Technical University of Denmark (DTU) and Université Paul Sabatier Toulouse III (UPS-Toulouse III) for three years, from October 2020 to September 2023. The work was carried out at the *Centre of Catalysis and Sustainable Chemistry (CSC)* under the supervision of Prof. Anders RIISAGER, in Lyngby, Denmark, and the *Laboratoire de Chimie de Coordination*, in the team “*Ligands, Complex Architectures and Catalysis (LAC₂)*” under the supervision of Dr. Eric MANOURY and the team “*Engineering of Metal Nanoparticles*” under the supervision of Dr. Karine PHILIPPOT, in Toulouse, France. A secondment of two months was performed at *Institut Français du Pétrole, Energies Nouvelles (IFPEN)* under the supervision of Dr. Lionel MAGNA, in Solaize, France.

This thesis focuses on the generation of metal nanoparticles embedded in ligand-functionalized water-soluble core-shell polymers for application in aqueous biphasic hydrogenation catalysis. Chapter I is a bibliographic survey on polymeric nanoreactors and metal nanoparticles. Special attention is given to core-crosslinked micelles and Rh nanoparticles, respectively. Chapter II consists of the materials and methods used during the research work. Chapters III-VI are dedicated to the results and discussions of the different studies with detailed descriptions. Finally, Chapter VIII summarizes the main conclusions and perspectives achieved in the completed projects and propose directions for future research.

Abstract

Metallic nanoparticles (MNPs) garner substantial attention in the field of catalysis due to their remarkable high surface-to-volume ratio that includes a high number of potential active sites. The confinement of MNPs significantly impacts their stability and catalytic performance. Biphasic applications are particularly attractive as they facilitate catalyst recovery and recycling by simple phase separation. Micellar catalysis, where the catalyst is tethered to the hydrophobic core of a surfactant, that self-assembles into micellar nanoreactors is of particular interest. Inspired by previous research work, this project focuses on the synthesis of unimolecular nanosized polymeric reactors and the confinement of rhodium nanoparticles (RhNPs) within their cores, for their application in aqueous biphasic hydrogenation. To circumvent extraction of the NPs upon recycling, as previously encountered with triphenylphosphine-functionalized polymer cores in the presence of O-based solvent, the use of triphenylphosphine oxide (TPPO) as core-anchor was developed. The aim was to have core-ligands which interact more strongly with the RhNPs surface, and thus provide a more efficient confinement and resultant higher performance for hydrogenation catalysis. Experiments were performed using core-crosslinked micelles with a polycationic (CCM-C) or polyanionic (CCM-A) shell, where TPPO functions were grafted by copolymerization with styrene of 4-styryldiphenylphosphine oxide (SDPPO), both synthesized by reversible addition-fragmentation chain transfer (RAFT) polymerization. The in-situ generation of the RhNPs using $[\text{Rh}(\text{COD})(\mu\text{-Cl})_2]$ as precursor proved unsuccessful, suggesting that Rh^I binding by TPPO to yield $[\text{RhCl}(\text{COD})(\text{TPPO}@CCMs)]$ was insufficiently strong to cleave the di- $\mu\text{-Cl}$ -bridge in the precursor complex. However, two alternative approaches were successfully developed for the generation of RhNP-TPPO@CCMs, consisting of either an ex-situ synthesis of RhNPs in the presence of stabilizers followed by their transfer to the CCM cores, and a one-pot synthesis approach. The resulting RhNP-TPPO@CCMs latexes showed a very high catalytic activity for the aqueous biphasic hydrogenation of styrene, and they proved reusable in multiple catalytic runs without any perceptible RhNPs loss during the intermediate product extractions with diethyl ether. The RhNP-TPPO@CCMs latexes were also proven efficient for the hydrogenation of other alkenes, alkynes, and carbonyl substrates.

Resumé

Metal nanopartikler (MNPs) har betydelig opmærksomhed inden for katalyse på grund af deres bemærkelsesværdige høje overflade-til-volumen-forhold, som giver potentielt mange katalytiske aktive sites. MNPs's stabilitet og katalytiske ydeevne øges markant når de indesluttet, og det er attraktivt at anvende sådanne katalysatorer i bifasiske systemer, hvor katalysatorseparation og -genbrug kan foregå ved simpel faseadskillelse. Specielt katalyse med micellære nanoreaktorer hvor katalysatoren er bundet til den hydrofobe kerne af et overfladeaktivt stof er interessant. Inspireret af tidligere forskning fokuserer dette projekt på syntese af unimolekylære nano-polymer reaktorer med rhodium NPs indesluttet i kernerne, samt anvendelse af de resulterende katalystorer til vandig bifasisk hydrogenering. For at undgå ekstraktion af RhNPs fra katalysatorerne med opløsningsmidler indeholdende oxygenatomer under deres genbrug, som ellers tidligere er fundet for polymerkerner funktionaliseret med triphenylphosphin, blev triphenylphosphinoxid (TPPO) udviklet som kerneanker. Formålet var, at have ligander bundet i kernen som effektivt forankrer RhNP via stærk interaktion med deres overflade, og dermed opnå bedre katalysatorer til hydrogenering. Forsøg blev udført ved kernekrydsbundne miceller syntetiseret med både polykationisk (CCM-C) og polyanionisk (CCM-A), hvor TPPO er bundet gennem co-polymerisering med styren fra 4-styryldiphenylphosphinoxid (SDPPO) via reversibel addition-fragmentations kædeoverførsel (RAFT). In-situ generering af RhNP med kompleksforbindelsen $[Rh(COD)(\mu-Cl)]_2$ lykkedes dog ikke, hvilket antydede at bindingen mellem Rh^I og TPPO ikke var tilstrækkelig stærk til at danne $[RhCl(COD)(TPPO@CCM)]$ ud fra dimeren ved at bryde $di-\mu-Cl$ -brobindingen. Imidlertid blev der udviklet to alternative syntesemetoder til at fremstille RhNP-TPPO@CCM'er, som bestod af hhv. ex-situ syntese af RhNP'er med stabilisatorer efterfulgt af overførsel til CCM-kernerne, samt en et-trins syntese der kombinerer RhNP syntese og overførsel. De fremstillede RhNP-TPPO@CCM-latexer udviste meget høj katalytisk aktivitet i vandig bifasisk hydrogenering af styren, og kunne genanvendes i flere på hinanden følgende reaktioner uden tab af RhNP ved ekstraktion af de dannede produkter med diethylether. RhNP-TPPO@CCM-latexerne var også effektive til hydrogenering af andre alkaner, alkener og carbonylforbindelser.

Résumé

Les nanoparticules métalliques (MNPs) suscitent une attention considérable dans le domaine de la nanocatalyse en raison de leur rapport surface/volume remarquablement élevé qui leur confère un grand nombre de sites actifs potentiels. Le confinement des MNPs a un impact significatif sur leur stabilité et leur performance catalytique. Leurs utilisations en conditions biphasiques sont particulièrement intéressantes car elles facilitent la récupération et le recyclage du catalyseur par une simple séparation de phase. La catalyse micellaire, où le catalyseur est lié au noyau hydrophobe d'un surfactant, qui s'auto-assemble en nanoréacteurs micellaires, est d'un intérêt particulier. Inspiré par de travaux antérieurs, ce projet se concentre sur la synthèse de réacteurs polymériques nanométriques unimoléculaires et sur le confinement de nanoparticules métalliques à l'intérieur de leurs noyaux, en vue de leur application dans l'hydrogénation biphasique aqueuse. Pour résoudre le problème d'extraction des MNPs rencontré précédemment avec des polymères fonctionnalisés dans leur cœurs par la triphénylphosphine en présence d'un solvant à base d'O, l'utilisation de l'oxyde de triphénylphosphine (TPPO) a été développée. L'objectif était d'avoir des ligands de coeur interagissant plus fortement avec la surface des nanoparticules de rhodium (RhNPs), pour obtenir un confinement plus efficace des MNPs et, au-delà, une performance plus élevée en catalyse d'hydrogénation. Des synthèses ont été réalisées avec des micelles réticulées à enveloppe polycationique (CCM-C) ou polyanionique (CCM-A) où les fonctions TPPO ont été greffées par copolymérisation avec le styrène de l'oxyde de 4-styryldiphénylphosphine (SDPPO), tous deux obtenues par polymérisation par transfert de chaîne par addition-fragmentation réversible (RAFT). Si la génération *in situ* de RhNPs à partir de $[\text{Rh}(\text{COD})(\mu\text{-Cl})_2]$ a échoué, sans doute parce que la liaison du Rh^I par le TPPO pour obtenir $[\text{RhCl}(\text{COD})(\text{TPPO}@CCMs)]$ n'était pas assez forte pour rompre le pont di- $\mu\text{-Cl}$ dans le dimère $[\text{Rh}(\text{COD})(\mu\text{-Cl})_2]$, deux approches différentes aboutissant à la génération de RhNP-TPPO@CCMs ont été développées avec succès. L'une en deux étapes, en une synthèse *ex-situ* des RhNPs en présence de ligands stabilisants, suivie de leur transfert au coeur des CCMs. L'autre par une protocole en une seule étape. Les latex RhNP-TPPO@CCMs résultants ont montré une activité catalytique très élevée pour l'hydrogénation biphasique aqueuse du styrène, se révélant réutilisables dans de multiples cycles catalytiques sans aucune perte visible de RhNPs pendant les étapes intermédiaires d'extractions des produits avec le diéthylether. Les latex RhNP-TPPO@CCMs se sont également révélés efficaces pour l'hydrogénation d'autres alcènes, alcynes et substrats carbonylés.

List of Publications

- [1] H. Wang, C. J. Abou-Fayssal, C. Fliedel, E. Manoury, R.Poli. Phosphine-Functionalized Core-Crosslinked Micelles and Nanogels with an Anionic Poly(styrenesulfonate) Shell: Synthesis, Rhodium(I) Coordination and Aqueous Biphasic Hydrogenation Catalysis, *Polymers* 14 (2022) 4937 <https://doi.org/10.3390/polym14224937>. **Published.**
- [2] C.J. Abou-Fayssal, C. Fliedel, R. Poli, A. Riisager, K. Philippot, E. Manoury, Confinement of Rh nanoparticles in triphenylphosphine oxide-2 functionalized core-crosslinked micelles for aqueous biphasic hydrogenation catalysis, *Materials Today Chemistry* (2023). **Manuscript Accepted.**
- [3] C.J. Abou-Fayssal, R. Poli, K. Philippot, A. Riisager, E. Manoury, Polymeric nanoreactors for catalytic applications. **Manuscript Submitted.**
- [4] C. J. Abou-Fayssal, L. Schill, R. Poli, E. Manoury, K. Philippot, A. Riisager. Aqueous biphasic hydrogenation with one-pot-synthesized Rh nanoparticles in polycationic-shell, triphenylphosphine oxide-functionalized core-cross-linked micelles. **Manuscript Submitted.**
- [5] C. J. Abou-Fayssal, R. Poli, E. Manoury, A. Riisager, K. Philippot. Rh nanoparticles confined in novel polyanionic core-crosslinked micelles with triphenylphosphine oxide-functionalization: Synthesis, characterization, and application in aqueous biphasic hydrogenation. **Manuscript in Preparation.**
- [6] C. J. Abou-Fayssal, R. Poli, E. Manoury, Anders Riisager, K. Philippot. Ni nanoparticles confined in cross-linked micelles and application in aqueous biphasic hydrogenation: Influence of the support on catalytic performance. **Manuscript in Preparation.**

List of Conferences and Workshops

- 1- **3rd Trans Pyrenean Meeting in Catalysis (TrapCat³) – Toulouse, France**
(November 2023)

Contribution: Oral Communication - One-pot synthesized Rh nanoparticles in polycationic-shell core-cross-linked micelles as efficient catalyst for aqueous biphasic hydrogenation

- 2- **International School on Innovations in Homogeneous and Supported Homogeneous Catalysis – Bucharest, Romania** (April 2023)

Contribution: My thesis in 180 min and Poster - Confinement of Rh nanoparticles in novel core-crosslinked micelles with a polycationic shell and a triphenylphosphine oxide-functionalized core for aqueous biphasic catalytic hydrogenation

- 3- **DTU Chemistry's annual PhD Symposium 2022 - Snekkersten, Denmark**
(November 2022)

Contribution: Oral Communication - Metal nanoparticles embedded in ligand-functionalized core-shell polymers for biphasic hydrogenation catalysis.

- 4- **Cutting-Edge Homogeneous Catalysis workshop – CEHC-2 - Leipzig, Germany** (March 2022)

Contribution: Poster and Flash Presentation - Metal nanoparticles embedded in ligand-functionalized core-shell polymers for biphasic hydrogenation catalysis.

2nd Prize award of the New Journal of Chemistry for poster presentation

- 5- **Hetero-elements and Coordination Chemistry: from Concepts to Application - 4th HC3A Meeting - Barcelona, Spain** (January 2022)

Contribution: Oral communication - Biphasic catalysis with Rh nanoparticles confined in cationic polymeric nanoreactors with functionalized triphenylphosphine oxide ligands.

- 6- **DTU Chemistry's annual PhD Symposium 2021 - Snekkersten, Denmark**
(November 2021)

Contribution: Poster - Biphasic catalysis with Rh nanoparticles confined in cationic polymeric nanoreactors with functionalized triphenylphosphine oxide ligands.

- 7- **Cutting-Edge Homogeneous Catalysis workshop – CEHC-1 - Toulouse, France** (May 2021)

Contribution: Poster - Biphasic Catalysis with metal nanoparticles inside polymeric nanoreactors.

List of abbreviations and symbols

I. Symbols

D_z	Z-average size, intensity-weighted harmonic mean particle diameter
PDI	Polydispersity Index
M_w	Weight-Average Molecular Weight
M_n	Number-Average Molecular Weight
DP_n	Degree of Polymerization
s	singlet NMR resonance
d	doublet NMR resonance
t	t triplet NMR resonance
q	quadruplet NMR resonance
m	multiplet NMR resonance
b	broad NMR resonance
Đ	Dispersity

II. Abbreviations

4VP	4-Vinylpyridine
ACPA	4,4'-Azobis(4-Cyanopentanoic Acid)
acac	Acetylacetonato
CCM	Core-Crosslinked Micelle
CCM-A	CCM With a Polyanionic Outer Shell
CCM-C	CCM With a Polycationic Outer Shell
CCM-N	CCM With a Neutral Outer Shell
CMC	Critical Micelle Concentration
CTPPA	4-Cyano-4-Thiothiopropyl-Sulfanyl Pentanoic Acid
d_m	Mean diameter
DLS	Dynamic Light Scattering

EDX	Energy Dispersive X-ray
E_a	Activation Energy
GC	Gas Chromatography
ICP-MS	Inductively Coupled Plasma Mass Spectrometry
macroRAFT	Macromolecular RAFT Agent
NMR	Nuclear Magnetic Resonance
NPs	Nanoparticles
P(4VPMe⁺I)	Poly(1-Methyl-4-Vinylpyridinium Iodide)
P4VP	Poly(4-Vinylpyridine)
PAA	Polyacrylic Acid
PEG	Poly(Ethylene Glycol)
PEGMA	Poly(Ethylene Glycol) Methacrylate
PEOMA	Poly(Ethylene Oxide) Methyl Ether Methacrylate
PISA	Polymerization Induced Self-Assembly
PMAA	Polymethacrylic Acid
ppm	part per million
PSt	Polystyrene
RAFT	Reversible Addition-Fragmentation Chain-Transfer
rpm	revolutions per minute
SDPP	(4-Styryl)diphenylphosphine
SDPPO	(4-Styryl)diphenylphosphine oxide
SDPPS	(4-Styryl)diphenylphosphine sulfide
SS-Na⁺	Sodium 4-Vinylbenzenesulfonate
St	Styrene
TEM	Transmission Electron Microscopy
TOF	TurnOver Frequency
TON	TurnOver Number
TOP	Tri-n-octylphosphine

TPP	Triphenylphosphine
TPPO	Triphenylphosphine Oxide
TPPS	Triphenylphosphine Sulfide
XPS	X-ray Photoelectron Spectroscopy

Table of Contents

Chapter I: Bibliographic Survey	1
I.1. Introduction	1
I.2. Catalysis within confined spaces	5
I.3. Macromolecular nanoreactors	6
<i>I.3.1. Polymer micelles</i>	<i>7</i>
<i>I.3.2. Polymersomes</i>	<i>12</i>
<i>I.3.3. Unimolecular nanoreactors</i>	<i>15</i>
<i>I.3.3.1. Shell cross-linked micelles</i>	<i>15</i>
<i>I.3.3.2. Core cross-linked micelles</i>	<i>19</i>
<i>I.3.3.2.1 Core cross-linked micelles with RhNP-TPP@CCM-C</i>	<i>29</i>
I.4. Metal Nanoparticles	29
I.5. Synthesis of Metal Nanoparticles	33
I.6. Chemical synthesis of MNPs	34
<i>I.6.1. Chemical reduction</i>	<i>36</i>
<i>I.6.2. Organometallic approach</i>	<i>39</i>
I.7. Rhodium Nanoparticles in Catalysis	41
I.8. MNPs confined inside CCM-C for application in aqueous biphasic hydrogenation catalysis	55
I.9. Summary	56
I.10. Scope of the PhD thesis work	57
I.10. References	58
Chapter II : Experimental section	78
II.1. Material and Method	78
<i>II.1.1. General Method</i>	<i>78</i>
<i>II.1.2. Autoclave used at the Technical University of Denmark</i>	<i>79</i>
<i>II.1.3. Autoclave used at Laboratoire de Chimie de Coordination</i>	<i>79</i>
<i>II.1.4. Autoclave used at Institut Français du Pétrole, Energies Nouvelles</i>	<i>80</i>
<i>II.1.5. Set-up used in LCC vs DTU</i>	<i>81</i>
II.2. Characterization techniques	81
<i>II.2.1. Nuclear magnetic resonance (NMR) spectroscopy</i>	<i>79</i>
<i>II.2.2. Dynamic light scattering (DLS)</i>	<i>82</i>
<i>II.2.3. Transmission electron microscopy (TEM)</i>	<i>83</i>
<i>II.2.4. Gas chromatography (GC)</i>	<i>84</i>
<i>II.2.5. Inductive coupled plasma mass spectrometry (ICP-MS)</i>	<i>84</i>
<i>II.2.6. X-ray photoelectron spectroscopy (XPS)</i>	<i>85</i>
<i>II.2.7. Thermal gravimetric analysis (TGA)</i>	<i>85</i>
<i>II.2.8. Fourier-transform infrared spectroscopy (FTIR)</i>	<i>86</i>
II.3. Synthesis of novel core-crosslinked micelles functionalized with triphenylphosphine oxide.	86
<i>II.3.1. Synthesis of monomers</i>	<i>86</i>

II.3.1.1. (4-styryl)diphenylphosphine oxide (SDPPO).	86
II.3.1.2. (4-styryl)diphenylphosphine oxide (SDPPS).	87
II.3.2. Preparation of $R_0-(4VPMe^+I)_{140}-b-St_{50}-b-(St_{0.9-co}-SDPPO_{0.1})_{300}-SC(S)SnPr$ (chain extension with styrene and SDPPO, step 4).	87
II.3.3. Preparation of $R_0-(4VPMe^+I)_{140}-b-St_{50}-b-(St_{0.9-co}-SDPPO_{0.1})_{300}-b-(St_{0.9-co}-DEGDMA_{0.1})_{150}-SC(S)SnPr$ core-crosslinked micelles (CCM-C latex).	88
II.3.4. Preparation of $R_0-(4VPMe^+I)_{140}-b-St_{50}-b-(St_{0.9-co}-SDPPS_{0.1})_{300}-SC(S)SnPr$ (chain extension with styrene and SDPPO, step 4).	88
II.3.5. Preparation of $R_0-(4VPMe^+I)_{140}-b-St_{50}-b-(St_{0.9-co}-SDPPS_{0.1})_{300}-b-(St_{0.9-co}-DEGDMA_{0.1})_{150}-SC(S)SnPr$ core-crosslinked micelles (CCM-C latex).	88
II.4. Synthesis of RhNPs and the RhNP-TPPO@CCM-C latex	89
II.4.1. Synthesis of RhNPs stabilized by pyridine and TPP	89
II.4.2. Synthesis of RhNP-TPPO@CCM-C latex	89
II.5. One-pot synthesis of RhNP-TPPO@CCM-C	90
II.5.1. Synthesis without added base	90
II.5.2. Synthesis with added base	90
II.5.3. Catalyst poisoning experiment	90
II.6. Synthesis of cross-linked micelles with a polycationic shell and a pyridine/triphenylphosphine-functionalized core	91
II.6.1. Preparation of $R_0-(4VPMe^+I)_{140}-b-St_{50}-b-(St_{0.9-co}-SDPP_{0.05}-VP_{0.05})_{300}-SC(S)SnPr$ (chain extension with styrene and SDPP and 4VP, step 4).	91
II.6.2. Preparation of $R_0-(4VPMe^+I)_{140}-b-St_{50}-b-(St_{0.9-co}-SDPP_{0.05}-VP_{0.05})_{300}-b-(St_{0.9-co}-DEGDMA_{0.1})_{150}-SC(S)SnPr$ core-crosslinked micelles (CCM-C latex).	91
II.7. Synthesis of cross-linked micelles with a polyanionic shell and a triphenylphosphine oxide functionalized core.	92
II.7.1. Synthesis of phosphine oxide-functionalized copolymer nanoreactors with an anionic $P(SS^-Na^+)$ shell.	92
II.7.2. Preparation of $R_0-(SS^-Na^+)_{140}-b-St_{50}-b-(St_{0.9-co}-SDPPO_{0.1})_{300}-SC(S)SnPr$ amphiphilic block copolymers.	92
II.7.3. Preparation of CCM with a 90:10 St/DEGDMA core: crosslinking of the $R_0-(SS^-Na^+)_{140}-b-St_{50}-b-(St_{0.9-co}-SDPPO_{0.1})_{300}-SC(S)SnPr$ amphiphilic block copolymers.	92
II.8. Synthesis of RhNPs-TPPO@CCM-A	93
II.8.1. In Ex-situ procedure	93
II.8.2. One-pot synthesis of RhNP-TPPO@CCM-A	93
II.9. General procedure for metal NPs-catalyzed biphasic hydrogenation	94
II.9.1. Aqueous biphasic hydrogenation	95
II.9.2. Catalyst recycling experiments	95
II.9.3. Corrected TOF calculations for RhNPs	95
II.10. Nickel nanoparticle synthesis	96
II.10.1. Synthesis of NiNPs conducted without H_2	96
II.10.2. Synthesis of NiNPs conducted under H_2	96
II.10.3. Synthesis of NiNPs conducted with H_2 using IFPEN reactors (30 mL)	96

II.10.4. Hydrogenation of 3-hexyne using IFPEN reactors (30 mL)	97
II.10.5. Corrected TOF calculations for NiNPs	98
II.11. References	98
Chapter III: Confinement of Rh nanoparticles in core-crosslinked micelles functionalized with triphenylphosphine oxide for aqueous biphasic hydrogenation catalysis	100
III.1. Introduction	100
III.2. Polymer synthesis and characterization	101
III.2.1. Attempts to oxidize TPP in the core of the CCM-C	101
III.2.1.1. Oxidation by S_8	103
III.2.1.2. Oxidation by air	103
III.2.2. Synthesis of TPPE@CCM-C (E = S, O) by copolymerization using oxidized monomers	103
III.2.2.1. Characterization of TPPS@CCM-C	105
III.2.2.2. Characterization of TPPO@CCM-C	107
III.2.2.3. Choice of CCM-C for Rh nanoparticle confinement for catalytic hydrogenation	108
III.3. Generation of Rhodium Nanoparticles	109
III.3.1. Kinetic study on the decomposition of $[Rh(COD)(\mu-Cl)]_2$	110
III.3.2. Generation of RhNPs in optimized conditions	111
III.4. Transfer of the RhNPs to the CCM-C core	113
III.5. Catalytic hydrogenation with RhNP-TPPO@CCM-C done at LCC	114
III.6. Catalytic studies of the hydrogenation of styrene (at DTU)	118
III.6.1. Hydrogenation of styrene using the colloidal RhNP suspension in toluene	119
III.6.2. Hydrogenation of styrene with RhNP-TPPO@CCM-C	120
III.7. Summary and Outlook	129
III.8. References	129
Chapter IV: Aqueous biphasic hydrogenation with one-pot-synthesized Rh nanoparticles in polycationic-shell and triphenylphosphine oxide-functionalized core-cross-linked micelles	135
IV.1. Introduction	135
IV.2. One-pot synthesis and characterization of RhNP-TPPO@CCM-C	136
IV.3. Aqueous biphasic hydrogenation with RhNP-TPPO@CCM-C	141
IV.3.1. Hydrogenation of styrene without base additive	141
IV.3.2. Hydrogenation of styrene with base additive	146
IV.3.3. Hydrogenation of styrene in the presence of Hg	148
IV.3.4. Hydrogenation of other substrates	149
IV.4. Summary and Outlook	151
IV.5. References	152
Chapter V : Synthesis and characterization of novel cross-linked micelles with polycationic shell and pyridine/triphenylphosphine-functionalized core.	156
V.1. Introduction	156
V.2. Polymer synthesis and characterization	156

V.3. [Rh(COD)(μ-Cl)₂ precatalyst coordination	160
V.4. Aqueous biphasic catalysis with Rh-VP-TPP@CCM-C	162
<i>V.4.1. Aqueous biphasic hydrogenation with Rh^I</i>	162
<i>V.4.1. Attempts to generate RhNP-VP-TPP@CCM-C</i>	162
V.5. Summary and Outlook	163
V.6. References	163
Chapter VI: Rh nanoparticles confined in novel polyanionic core-crosslinked micelles with triphenylphosphine oxide-functionalization: Synthesis, characterization, and application in aqueous biphasic hydrogenation	165
VI.1. Introduction	165
VI.2. Polymer synthesis and characterization	166
VI.3. Synthesis and characterization of RhNPs-TPPO@CCM-A	168
<i>VI.3.1. Ex-situ synthesis of RhNPs and transfer to TPPO@CCM-A</i>	168
<i>VI.3.2. One-pot synthesis of RhNPs-TPPO@CCM-A</i>	169
<i>VI.3.2.1. Characterization of RhNPs-TPPO@CCM-A</i>	170
VI.4. Hydrogenation catalysis with one-pot synthesized RhNPs-TPPO@CCM-A	173
<i>VI.4.1. Styrene hydrogenation</i>	173
<i>VI.4.2. Acetophenone hydrogenation</i>	178
VI.5. Summary and Outlook	180
VI.6. References	181
Chapter VII: Synthesis and characterization of nickel nanoparticles and their application in catalysis	183
VII.1. Introduction	183
VII.2. NiNPs synthesis and characterization	185
VII.3. Semi-hydrogenation of 3-hexyne with NiNPs	191
VI.4. One-pot synthesis of NiNP-TPPO@CCM-A latex	193
VII.5. Summary and Outlook	194
VII.6. References	195
Chapter VIII: Conclusion and Perspective	200
Appendix A	204
Appendix B	208
Appendix C	210
Appendix D	215
Appendix E	217

Chapter I: Bibliographic Survey

This chapter focuses on catalytic applications within confined spaces of polymeric nanoreactors. It delves into the fundamental concepts of nanotechnologies and the interests of metal nanoparticles (MNPs) in catalysis. The chapter begins by introducing polymeric nanoreactors and highlighting their primary roles in catalysis. The subsequent section is dedicated to core-crosslinked micelles (CCM), providing insights into the latest developments in this field, including the first use of MNP@CCM by our group. Then the significance of MNPs and the methods for their chemical synthesis are described before commenting recent works on the utilization of rhodium nanoparticles (RhNPs) in hydrogenation catalysis. The introductory section of this chapter (Section I-III), is related to article No. 3 in the list of publications mentioned earlier in this manuscript.

I.1. Introduction

Catalysis is a key technology for our society with extensive contributions in diverse areas such as energy, chemicals and food production, cosmetics, health, *etc.* [1,2]. Heterogeneous catalysis, where the catalyst and the substrate are in two different phases, provides easy catalyst separation and reuse, which often results in extended catalyst lifetime and use of less solvents. These features have made heterogeneous catalysts predominant in industry (about 80% of processes). However, heterogeneous catalytic systems typically require harsher reaction conditions than homogeneous analogs and this may lead to lower selectivities. Heterogeneous systems may also suffer from mass transport limitations, which may decrease the catalytic activity. In addition, the exploration of reaction kinetics and mechanistic understanding are often more problematic for heterogeneous catalysts. Conversely, homogeneous catalytic systems usually provide high activities and selectivities under milder reaction conditions. They also allow easier mechanistic investigations. However, since the

catalyst and the substrate coexist in the same physical phase (typically a liquid phase), these systems inherently suffer from difficult catalyst separation and reuse. Hence, down-stream separation procedures such as precipitation, extraction, or ultrafiltration are typically required to recover the catalyst, which are operations requiring additional equipment, undesirable large amounts of solvent, and extra costs (Table I.1).

Table I.1. Comparison between heterogeneous and homogeneous catalysis [1,2].

	Heterogeneous	Homogeneous
Catalyst form	Solid, often metal or metal oxide	Metal complex
Mode of use	Fixed bed or slurry	Dissolved in the reaction medium
Solvent	Usually not required	Usually required
Selectivity	Difficult to control	High and easily tailored
Stability	Stable to high temperature	Decomposes at >100 °C
Recyclability	Easy	Can be very difficult
Cost	Low	High
Catalyst life	Long, regeneration feasible	Short, difficult regeneration
Diffusion limitations	Susceptible, to be eliminated with proper reaction conditions	Can be overcome by optimization of stirring
Reaction kinetics and mechanisms	Complex, difficult to establish	Relatively easy to establish
Special reaction	Haber process	Methanol carbonylation

To circumvent these issues, several strategies have been implemented for the recycling of homogeneous catalysts in large-scale processes. These strategies include: (1) employing specially designed membranes capable of selectively percolating catalyst-supporting molecules (such as dendrimers or colloids) through micro-/ultra-/nanofiltration or reverse osmosis processes [3,4], tailored to the size and geometry of the catalyst; (2) utilizing biphasic catalysis, where the catalyst is immobilized in a separate, immiscible liquid phase from that of the reaction products [3] (for instance, the Rhône-Poulenc/Ruhrchemie hydroformylation of propene and butene involving water as the immiscible phase [5]); and (3) employing catalyst confinement techniques, where the catalyst support can be a solid phase with the molecular catalyst

either grafted onto the surface or enclosed within the pores of insoluble polymers (such as resins), inorganic oxides (like silica and alumina), or carbon materials (including carbon black, carbon nanotubes, and graphene), known as heterogenized homogeneous catalysis, or a separate liquid phase, referred to as liquid/liquid biphasic catalysis. The latter strategy is an effective and low-cost solution to preserve the catalytic performance and facilitate catalyst recovery. Whatever the catalyst support, solid or liquid, catalyst confinement approaches combine the benefits of homogeneous and heterogeneous catalysis. This is also possible *via* micro-heterogenization using colloidal assemblies [3], also referred to as nanoreactors.

As defined by the National Nanotechnology Initiative (NNI), *nanotechnology is the scientific field dedicated to the synthesis, engineering, and creation of materials and functional systems at the nanometer scale, ranging from 1 to 100 nm* [6]. The lower limit is constrained by the size of individual atoms, as fundamental building blocks of materials [6]. On the other hand, the upper limit (approximately 100 nm), represents a level at which the specific phenomena exhibited by nanomaterials start to diminish. The prefix "nano" finds its origin in the Greek word "*νᾶνος*" or the Latin word "*nannus*", both meaning "dwarf." It was officially adopted as an SI prefix, indicating 10^{-9} of an SI base unit, during the 11th "Conférence Générale des Poids et Mesures (CGPM)" in 1960 [7]. Polymeric nanoreactors that contain covalently linked ligands in their core architecture offer an interesting approach for anchoring and protecting the catalyst from the surrounding environment, while facilitating its recovery and recycling [4]. One of the prominent techniques for catalyst recovery and recycling is liquid/liquid biphasic catalysis using two immiscible liquid phases, one containing the catalyst and the other one containing the reaction products and any unreacted substrate [5,8,9]. In this approach, the two phases can be separated by a simple decantation, thus facilitating the reuse of the catalyst phase without the introduction of any thermal or chemical stress. Four distinct operational modes for the catalyzed transformation may be associated to the liquid/liquid biphasic approach (Figure I.1), as exemplified in the

case of the biphasic aqueous catalysis [5]: (i) homogeneous in the aqueous catalyst phase, if the substrate is sufficiently water-soluble; (ii) homogeneous in the substrate/product phase, if the catalyst is sufficiently soluble in the substrate phase or can be transported there by a temperature stimulus (thermomorphic approach) [10–12] or by a phase-transfer agent; (iii) interfacial when neither component is sufficiently soluble in the other component phase and the transformation occurs exclusively at the interface; (iv) homogeneous within nanoreactors, which are held as a stable dispersion in a phase different from that of the substrates/products [13,14].

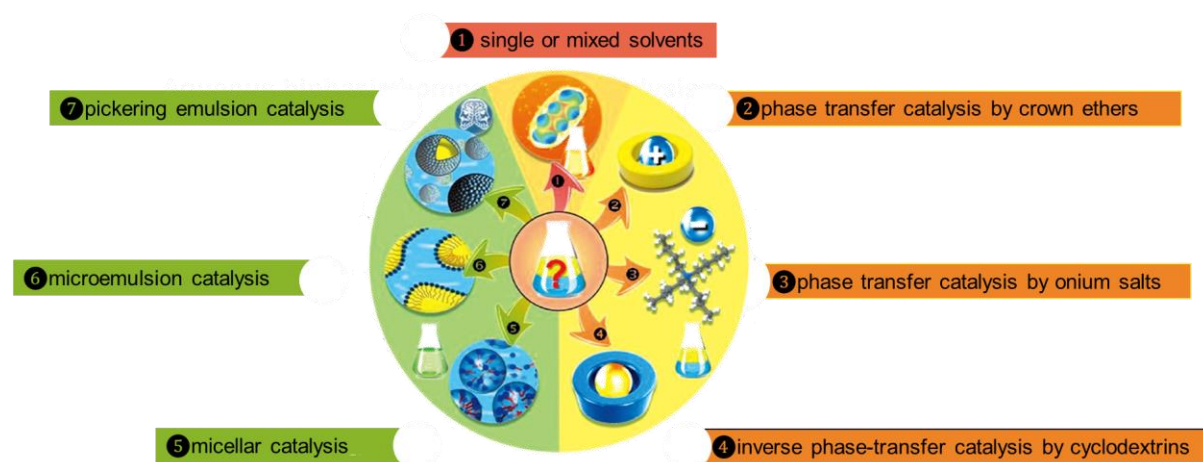


Figure I.1. Different implementations of liquid/liquid biphasic catalysis. (Adapted from [9] and used with permission from John Wiley and Sons ©).

The latter approach, with the catalyst confinement within a small container, can allow precise control over its interaction with the substrate. This can lead to different reaction pathways compared to the free catalyst, resulting in significantly improved selectivities compared to the non-confined analogs [15,16]. The catalyst host can either be molecular or macromolecular, and the latter type of nanoreactors are described herein.

A powerful toolbox is available to access a wide array of polymeric nanoreactors [9,10] through controlled and living polymerization techniques [17] such as reversible addition-fragmentation chain transfer (RAFT) polymerization (*vide infra*, section I.3.3.2), ring-opening anionic, -cationic and -metathesis polymerization (AROP, CROP

and ROMP), and atom transfer radical polymerization (ATRP). These polymerization methods have successfully been used to synthesize various nanoreactor architectures for application in catalysis, including self-assembled micelles, multifunctional micelles [18], polymersomes [19–24], and star polymers [25]. In all cases, a common aim is to embed and protect the catalyst while allowing the substrate to easily reach the reactive site and the products to migrate back toward the bulk phase.

The following section provides an overview of the currently known polymer-based nanoreactor systems used in biphasic catalysis, designed from macromolecular building blocks. Special attention is given to CCMs obtained by RAFT polymerization. The progress made on the synthesis of this particular type of unimolecular nanoreactors and on their use in micellar-type aqueous biphasic catalysis will be highlighted.

I.2. Catalysis within confined spaces

One of the captivating approaches in homogeneous biphasic catalysis is micellar catalysis. Each micelle is an independent reaction locus and can thus be described as a catalytic “nanoreactor” [4,15,16,18,20,26–31]. It is necessary to distinguish between two fundamentally different implementations of micelles in catalysis [32]. In the initially developed one, the catalyst is dissolved in the aqueous phase, or held close to the micellar surface by Coulombic forces (if the catalyst has an opposite charge to that of the micelle surface) or by covalent grafting. In this case, the catalytic reaction occurs at the interface between the bulk aqueous phase and the nanoreactor core where the hydrophobic substrate is located. The beneficial effect of the micelles is thus merely the increase of the water/organic interface, thus improving mass transport kinetics in an interfacial catalysis approach. This is what the “micellar catalysis” terminology has typically been referring to, but a more appropriate description should be “micelle-aided catalysis”. This topic has been extensively reviewed and will not be considered here [1,33–38]. The second type of micellar catalysis, developed more recently, deals

with systems where the catalyst is embedded, by interaction with core-anchored ligands, in the hydrophobic core of the micelles. In this case, the catalytic reaction occurs in the homogeneous environment of the hydrophobic micellar core, benefitting from a high local concentration of both substrate and catalyst [15,32]. The kinetics of the overall transformation can thus favorably compare with that of the analogous homogeneous process.

The first report on micellar catalysis dates back to 1970 [39], when many developments were conducted focusing on both preparation, characteristics as well as catalytical applications [33,34,39–47]. O'Reilly *et al.* [48], Handa *et al.* [49], and Lee *et al.* [50] focused for example on Suzuki-Miyaura cross couplings, whereas Lipshutz and Ghorai [51] developed a polyethylene-hydroquinone-sebacic acid (PQS) micellar catalyst system for aldol reactions in water.

I.3. Macromolecular nanoreactors

For micelles generated by amphiphilic macromolecules, different morphologies can be formed depending on the packing parameter p that was first defined by Israelachvili [52] through Equation (1), where v is the volume, a_0 is the optimal area of the head group and l_c is the length of the hydrophobic tail.

$$p = v/a_0 \cdot l_c \quad (1)$$

Spherical micelles are obtained when $p \leq 1/3$ whereas worm-like micelles are formed when $1/3 \leq p \leq 1/2$. If $p \geq 1/2$, vesicles are formed. Within each morphology group, a smaller size leads to a higher interface area and thus improves the kinetics of mass transport between the hydrophobic bulk phase and the nanoobject core. Another factor that also plays a major role is the hydrophobicity of the local pocket [53]. Self-assembled nanoreactors are non-covalent macromolecular entities assembled from their initial building blocks [20,22–24,54]. This type of nanoreactors form good compartmentalization of catalytic systems, providing advantages on the kinetics

(faster reaction rate) and on thermodynamics (lowering the energy of the transitional state). In an aqueous medium, the formation of amphiphilic micelles that tend to assemble above the so-called “critical aggregation concentration” leads to complex supramolecular architectures depending on the structure of the molecular amphiphiles [55]. As a function of the parameter “ p ” defined above, three different morphologies can be observed, combining the following terms of Gibbs free energy [26]:

- (i) a favorable entropic contribution resulting from the assembly of the hydrophobic parts of the molecule,
- (ii) a tendency of amphiphiles to minimize unfavorable lipophilic-water interaction by closely packing and to spread apart as the result of electrostatic repulsion between the hydrophilic head groups, defined as surface term,
- (iii) a limitation to the possible geometry of aggregation, requiring that the hydrophobic cores only assemble in water or polar solvent, defined as the packing parameter explained previously.

It is important to note that the described aggregates have dimensions in the nanometer regime. Furthermore, the inclusion of catalytic sites in these molecular aggregates, whether by polymerization or by the coordination of the pre-catalyst, results in the formation of nanoreactors. In such nanoreactors, the reaction selectivity can be modified by tuning the nature of the monomers in the core block.

1.3.1. Polymer micelles

Polymer micelles [56–59] (PMs) are normally described as aggregates formed by the self-association of amphiphilic polymers owing to hydrophobic interactions between polymer molecules, but interactions may also be electrostatic or *via* hydrogen bonds or coordination bonds. The morphology of these block copolymer micelles resembles that of molecular surfactant micelles and can be divided into various nanostructures,

such as spherical or cylindrical micelles and vesicles, where the hydrophobic polymer chains form the core and the hydrophilic polymer chains form the shell when dispersed in aqueous media. The morphology of the PMs depends on the ratio between the hydrophobic and hydrophilic chains, capable of accommodating the catalyst [56]. PMs are efficient systems for the encapsulation of hydrophobic compounds due to the hydrophobic nature of their core and the hydrophilic corona, and these nanoreactors have many applications besides catalysis, especially in the medical field for, *e.g.* drug delivery [60,61] and magnetic resonance imaging (MRI) [62].

Chen and coworkers [63] have described the synthesis and application of thermo-responsive polymer micelle-based nanoreactors containing polyoxometalates (POMs) and poly(*N*-isopropylacrylamide)-*b*-poly(L-lysine) (PNIPAM-*b*-PLys-POM) electrostatically linked *via* the POM and amino groups of poly(L-lysine) for catalytic wet hydrogen peroxide oxidation (CWPO) of phenol. Similarly, Suzuki *et al.* [64] performed Pd-catalyzed Mizoroki-Heck coupling of iodobenzene and *n*-butyl acrylate in aqueous solution using thermo-responsive PMs based on poly(*N*-isopropylacrylamide) (PNIPAAm), which is known as an efficient thermo-responsive polymer due to its lower critical solution temperature (LCST) of 32 °C in water [65] (Figure I.2).

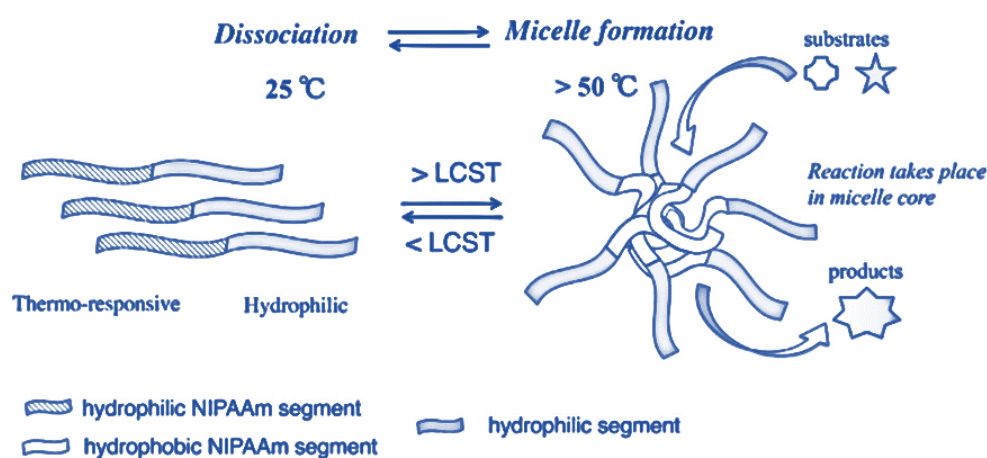
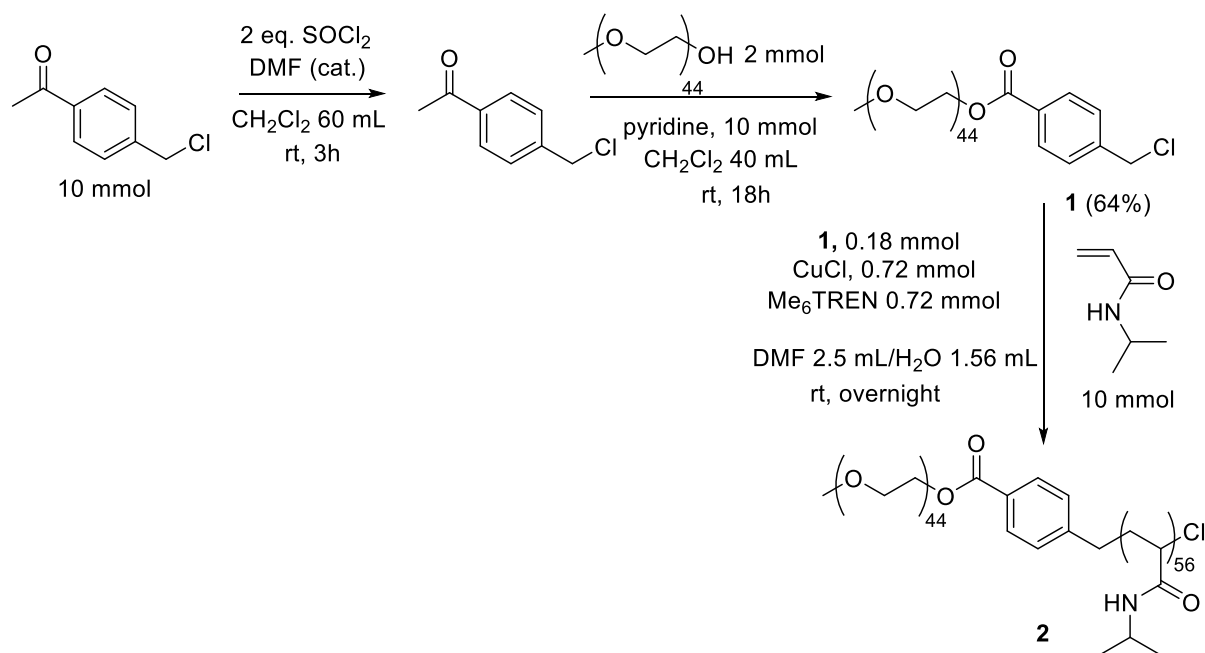


Figure I.2. Thermo-responsive micelles switched on/off by temperature. (Adapted from [65] and used with permission from Elsevier ©).

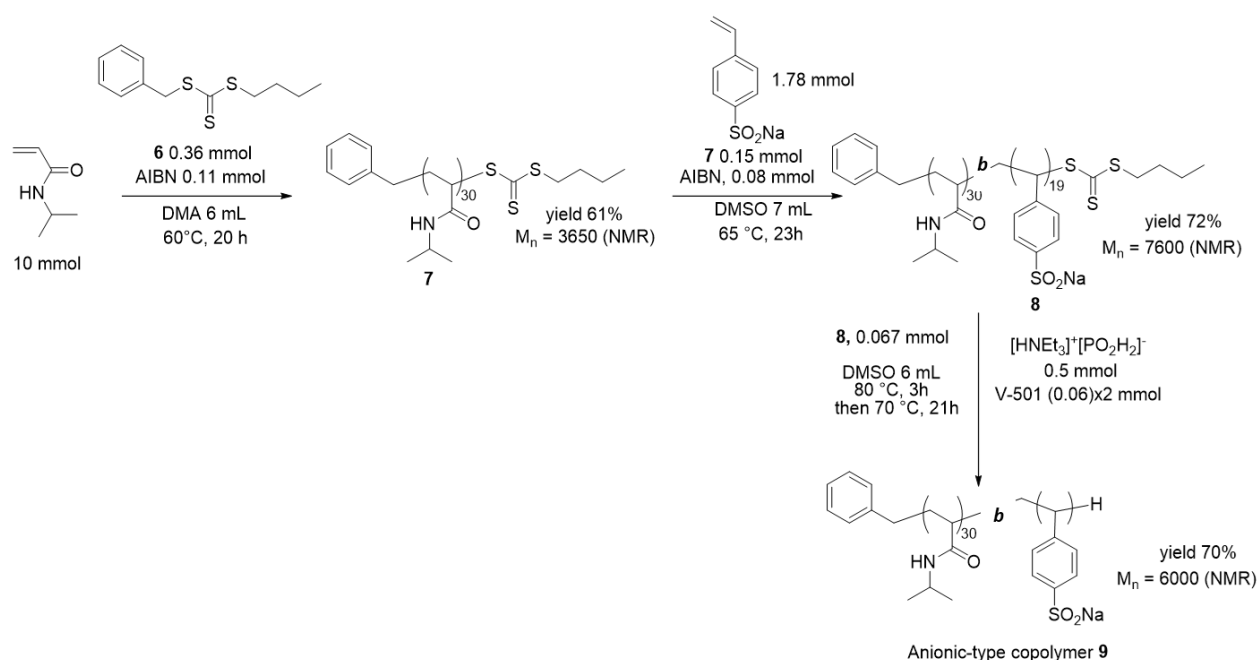
The thermo-responsive amphiphilic block copolymer NIPAAm **2** with a neutral poly(ethylene glycol) (PEG) chain was prepared from **1** *via* ATRP (Scheme I.1). The resulting block copolymer had a narrow size distribution (15-20 nm at 25 °C) and was water-soluble at room temperature but when heated up to 60 °C the polymer was insoluble, and the solution became opaque. Characterization by dynamic light scattering (DLS) demonstrated that the formation of the PMs by **2** was thermo-induced and the switchable nature improved product extraction. The PMs also limited the use of organic solvent for product separation from the aqueous reaction mixture, but 2 mol% of Pd was required to obtain good product yield in the palladium-catalyzed Mizoroki-Heck cross-coupling [65].



Scheme I.1. Preparation of NIPAAm-*b*-PEG **2** with PEGylated ATRP agent. (Adapted from [65]).

In a follow-up work [65], NaCl was introduced to the block polymer containing proline to lower the solubility of the organic solute in the aqueous phase and help directing it to the core of the PMs. This “salting-out” protocol led to the design of a new thermo-responsive block copolymer with an anionic sodium sulfate segment, PNIPAAm-*b*-PSSNa **9**, also prepared using RAFT polymerization. In the synthesis protocol, *N*-isopropylacrylamide and sodium *p*-styrenesulfonate were polymerized in

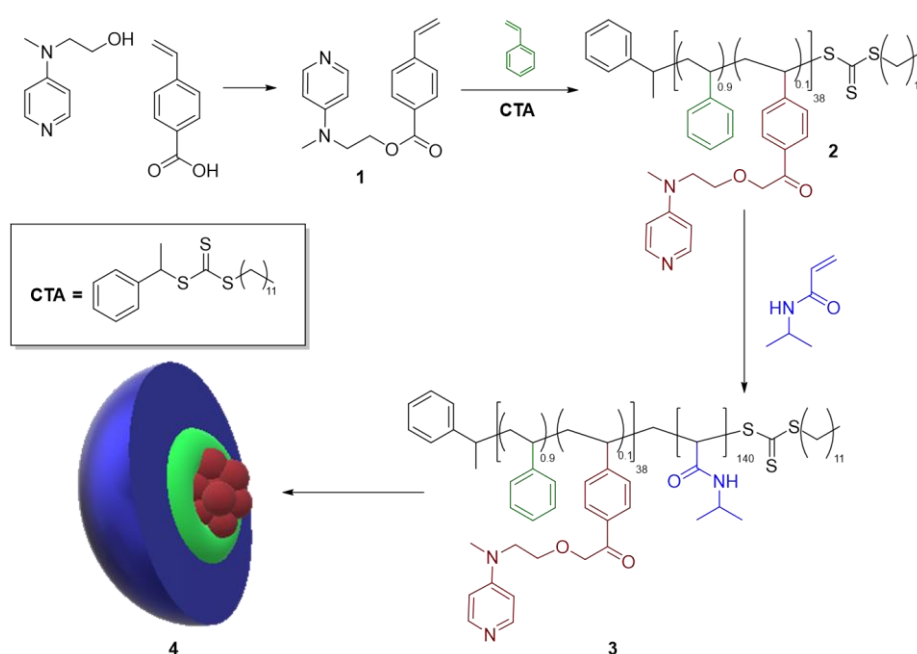
the presence of the RAFT agent **6** forming **7**, followed by depolymerization of *p*-styrenesulfonate by a radical desulfurization process that led to the removal of trithiocarbonate moiety at the end of the polymer-chain to yield the anionic-type copolymer (Scheme I.2). A larger particle size was obtained with the anionic PMs compared to the neutral one, likely due to electrostatic repulsion among the anionic polymer chains. Further analysis also showed that the anionic copolymer exhibited its LCST behavior at 40-55 °C. When the aqueous Pd-catalyzed Mizoroki-Heck coupling of iodobenzene and *n*-butyl acrylate was performed with **9** using 0.5 mol% Pd, a better yield (though moderate) was obtained compared to the previous reaction with the neutral copolymer and 2 mol% Pd (Scheme I.2), thus demonstrating how rational PM design can improve catalytic performance.



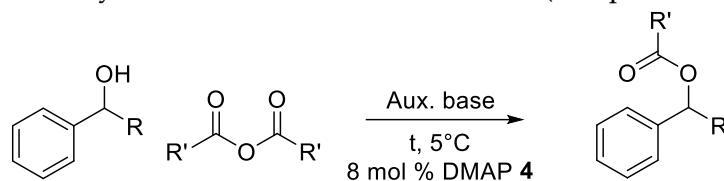
Scheme I.2. Preparation of PNIPAAm-b-PSSNa **9** by RAFT polymerization. (Adapted from [65]).

The introduction of the catalyst in the core of the micellar nanoreactors can be realized in different ways, either by polymerizing a pre-catalyst-functionalized monomer into the hydrophobic compartment, followed by self-assembly, or by ligand exchange between a molecular pre-catalyst, introduced by mass transport inside the already assembled micelles, to a core-anchored ligand. An example of the former method [66]

is the copolymerization of styrene and a functionalized styrene containing a 4-(dimethylamino)pyridine (DMAP) organocatalyst, using the RAFT technique, to yield a hydrophobic macroRAFT agent **2**, which was then chain-extended with a hydrophilic poly(N-isopropylacrylamide) (PNIPAM) block (Scheme I.3). The catalytic activity of the compartmentalized organocatalyst in the core was found to be high, improving in some reactions the DMAP-catalyzed acylation reaction of alcohols with anhydrides, with rates up to 100 times compared to those for unsupported DMAP in organic solvents (Table I.2). Additionally, these catalytic nanoreactors were recycled up to six times without losing catalytic activity.



Scheme I.3. Four-step synthesis of micelles (**4**) containing the DMAP functionality covalently attached to the hydrophobic core. (Adapted from [66]).

Table I.2. Acylation reactions in the micelles **4**. (Adapted from [66]).

Entry	R	R'	Conversion (%) (15 min)	Conversion (%) (24 h)
1	CH ₃	CH ₃	26	32
2	CH ₂ CH ₃	CH ₃	28	29
3	CH ₃	CH ₂ CH ₂ CH ₃	47	53
4 ^b	CH ₃	CH ₂ CH ₂ CH ₃	65	66
5 ^b	CH ₂ CH ₃	CH ₂ CH ₂ CH ₃	94	98

^aAll reactions contained 8 mol % DMAP, [OH] = 0.02 M, 1.5 equiv of auxiliary base (TEA), 1 equiv of alcohol, and 3 equiv of anhydride. Conversions determined by HPLC measurements with mesitylene as the internal standard. ^bN,N-Diisopropylethylamine (DIPEA) was used as auxiliary base instead of TEA.

Despite their successful applications, these and other micellar catalysts have one major drawback: the equilibrium between micelles and free surfactant macromolecules. The presence of the equilibrium can lead to undesired formation of stable emulsions, slow micelle/product separation caused by excessive swelling, and catalyst loss through the formation of Langmuir-Blodgett films at the liquid/liquid interface and/or inverse micelles in the bulk organic phase [67]. Another major drawback related to thermo-responsive PMs is their dynamic nature that renders them sensitive to their environment. To circumvent these issues, the micelles can be turned into unimolecular persistent objects by cross-linking, which can be accomplished by various strategies as described below. These cross-linked PMs constitute an attractive alternative with improved characteristics and catalytical behavior.

1.3.2. Polymersomes

The stability of micelle- and vesicle-based systems depends on the environment, such as the temperature of the solution and the concentration of the surfactant. To obtain better-defined and more stable systems, macromolecular polymers have been

considered as alternative nanoreactors, with a higher kinetic stability compared to the self-assembled molecular surfactant (*vide supra*). When vesicles are self-assembled from macromolecular amphiphiles (or block copolymers), they usually are referred to as polymersomes. Polymersomes [68–72] have increased rigidity and stability compared to micelles and vesicles, and their structure can vary from simple coil-like diblock copolymers to rod-like, rod-coil diblock or multiblock polymers with or without additional cross-linker groups [73]. The variation in composition can be tuned by varying the relative block lengths, which results in modified size, structure, polarity, and permeability of the polymersomes.

Eisenberg and coworkers [74] were the first to generate a block copolymer system with six different morphologies of "crew-cut" aggregates of polystyrene-*b*-poly(acrylic acid) block copolymers. Shortly after, Meijer and coworkers [75] reported the synthesis of polystyrene-poly(propylene)imine, thus starting a new research line based on the relation between amphiphilic properties and molecular structure towards the preparation of many other polymersomes by various approaches [76–78] and with different application scope. For enzymatic ring-opening polymerization, Nolte and coworkers [79] developed polystyrene-polyisocyanopeptide (PS-PIAT) based polymersomes, while van Hest and coworkers [80] reported a polymersome-stabilized Pickering emulsion at the water/oil interface that was later applied in biphasic enzymatic catalysis. In addition, Lecommandoux, van Hest, and coworkers [81] reported a cascade reaction in which small polymersomes were loaded into larger ones, resulting in a multi-compartmentalized polymersome-in-polymerosome system (Figure I.3).

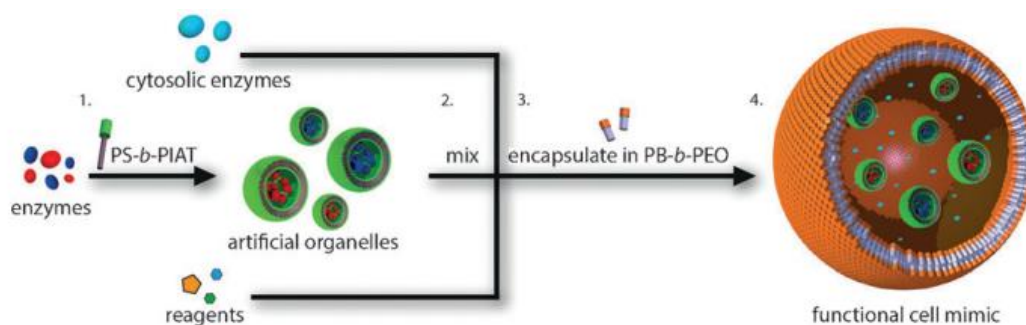
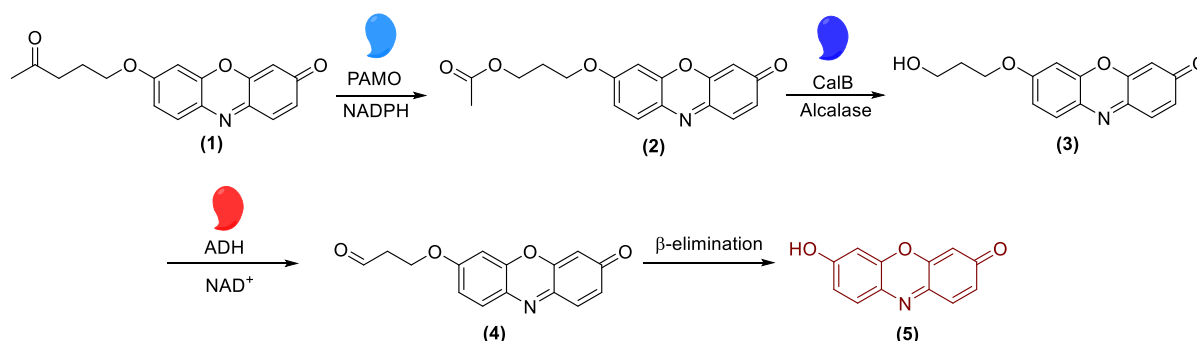


Figure I.3. Multi-compartmentalized polymersome-in-polymerosome system. (Adapted from [81] and used with permission from John Wiley and Sons ©).

To demonstrate the functional and structural control of the system, they investigated a model reaction with isolated enzymes in the different compartments. The first step of the reaction was a Baeyer-Villiger oxidation of a substituted hydroxyphenoxazinone ketone **1**. The resulting ester **2** was then hydrolyzed with a lipase (enzyme) to form the corresponding primary alcohol **3**, which was subsequently oxidized by alcohol dehydrogenase and a cofactor nicotinamide adenine dinucleotide (NAD) to yield the corresponding aldehyde product **4**. The final step of the catalytic transformation was a spontaneous β -elimination leading to 7-hydroxy-3H-phenoxazin-3-one-10-oxide **5** (Scheme I.4). The concept of enzyme compartmentalization in the cascade reaction spatially separated incompatible enzymes to retain their functionality, thus resembling the intracellular organization of eukaryotic cells. This concept allows to separate and conduct incompatible reactions simultaneously in a confined environment with increased efficiency and is a very powerful tool in materials chemistry.



Scheme I.4. Enzymatic cascade reactions in multi-compartmentalized polymersomes. (Adapted from [81]).

Using the micellar or vesicular approaches, may lead to the formation of stable emulsions due to the excessive swelling of the micellar core [82]. In addition, parameters such as temperature, dilution, and others (*e.g.*, the composition of the mixed solvent) [83–86] determine the equilibrium between micelles/vesicles and free amphiphilic arms. An alternative and promising method to overcome these disadvantages is to cross-link all surfactant molecules to form unimolecular nanoobjects [32,54,87].

I.3.3. Unimolecular nanoreactors

I.3.3.1. Shell cross-linked micelles

Wooley and coworkers [88] introduced a method to prepare functionalized micelles from low polydispersity macromolecules with a defined structure and an immobilized permeable cross-linked shell and labile core. Unlike dendrimers [89] the resulting shell-cross-linked knedel-like (SCK) particles have greater peripheral functions and nanometer-size diameters, and are therefore more considered a hybrid between dendrimers, hollow spheres, latex particles, and block copolymer micelles (Figure I.4). The SCKs were prepared by a two-step synthesis procedure using a block copolymer of polystyrene and poly(4-vinyl pyridine), PSt-*b*-PVP, prepared by anionic polymerization. The PSt served as the hydrophobic block and the quaternized PVP generated the hydrophilic block and introduced the cross-linkable group. Besides micellar catalysis [88], the SCKs find many applications in other fields such as, *e.g.* recording materials, hydraulic fluids, delivery processes, phase transfer reactions, solvation, coatings, and fillers.

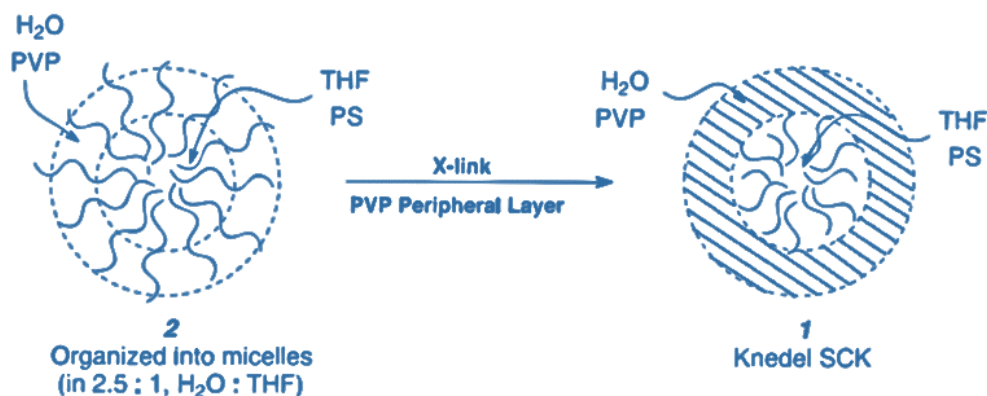
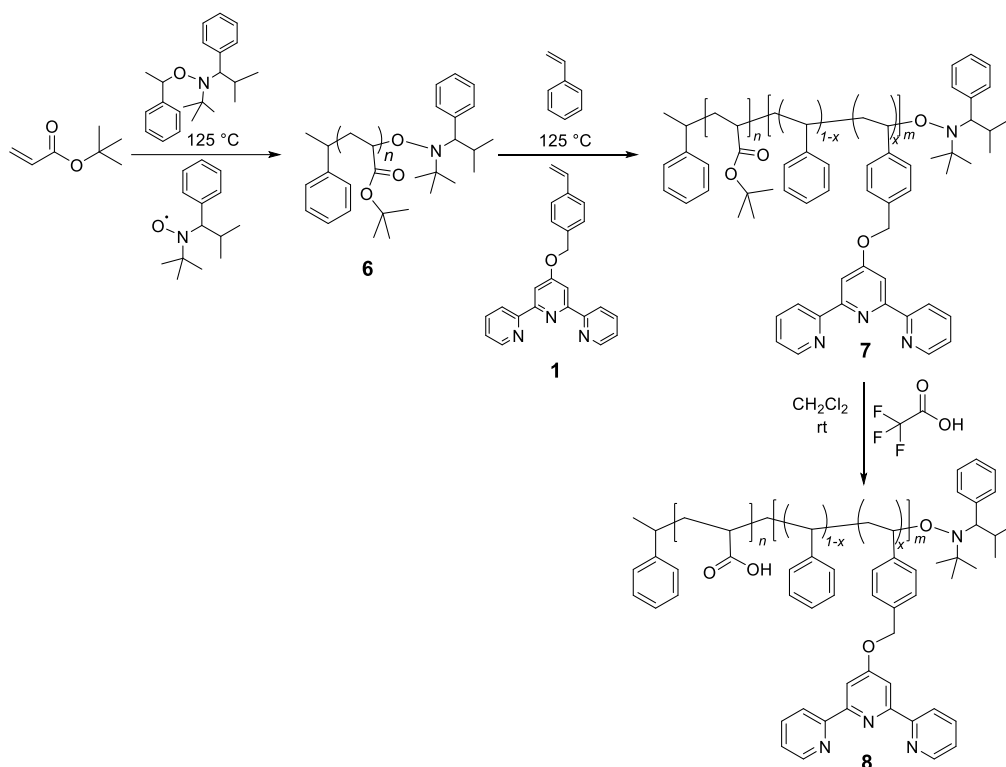


Figure I.4. Schematic representation of the basic approach for the formation of SCK's. Micellization of amphiphilic **2** is followed by cross-linking through the styrene side chains located in the peripheral water to yield **1**. (Adapted from [88] and used with permission from American Chemical Society ©).

O'Reilly and coworkers [90] reported the co-polymerization of an amphiphilic copolymer in which the hydrophobic domain was selectively functionalized with terpyridine groups using nitroxide-mediated polymerization (NMP) techniques, that has been extensively studied and optimized by Schubert and coworkers [91,92] (Scheme I.5). The resulting shell cross-linked micelles (SCMs) (Figure I.5) were then modified by metal ion complexation, notably Cu^+ , and used as catalysts for 1,3-dipolar cycloaddition reactions ("click reactions") of azido- and alkynyl-functionalized small molecules [90].



Scheme I.5. Synthesis of a tert-butyl acrylate block **6** using NMP, followed by chain extension to block copolymer **7** that incorporates terpyridine functionality, and then formation of an amphiphilic diblock copolymer **8** with terpyridine functionality embedded within the hydrophobic segment. (Adapted from [90]).

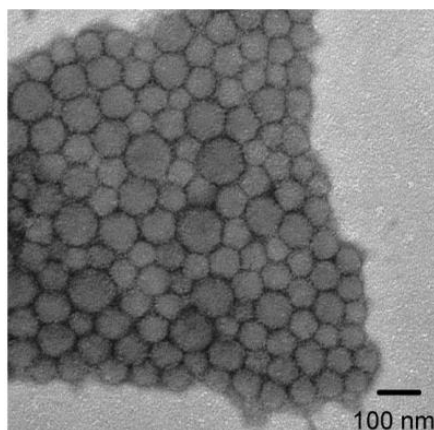
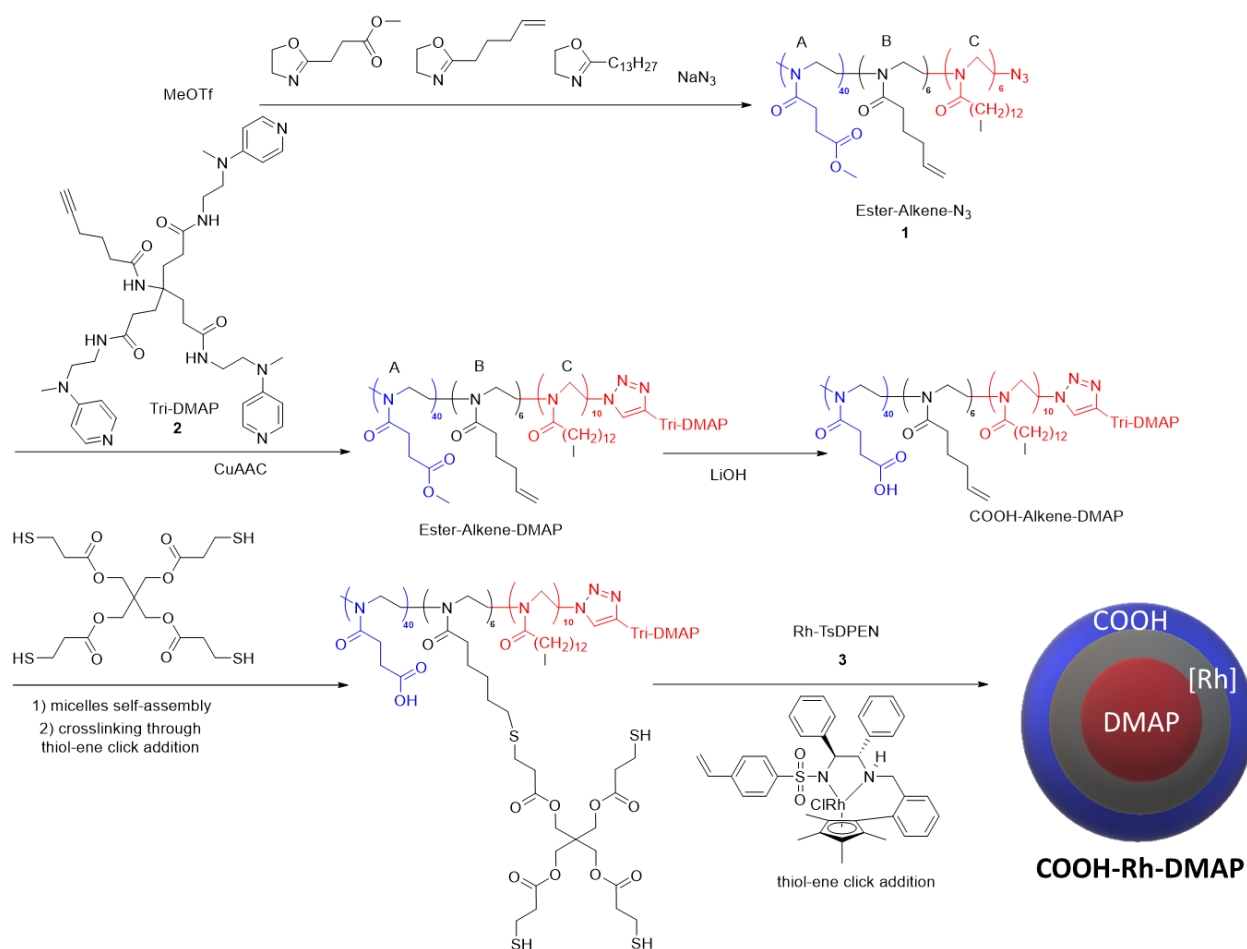


Figure I.5. Representative transmission electron microscopy (TEM) images of SCM. (Adapted from [90] and used with permission from American Chemical Society ©).

Weck and coworkers [93] have also reported the synthesis of various SCMs and their catalytic applications [94]. Initially, they reported the synthesis of poly(norbornene) block copolymer-based amphiphilic ABC triblock copolymers *via* ring-opening metathesis polymerization (ROMP) [93]. The middle block (B block) was functionalized with a photochemically active cinnamate group for crosslinking, and

the terminal hydrophobic block (C block) contained a Co-salen ligand. The Co-salen functionalized SCMs catalysts were then used for hydrolytic kinetic resolution (HKR) of epichlorohydrin. They showed that the structure of the SCM catalysts was stabilized by the cross-linked shell, which assisted recyclability of the catalysts. Then they also prepared SCMs containing Co^{III}-salen cores from amphiphilic poly(2-oxazoline) triblock copolymers [94] and studied substrate selectivity in HKR with various terminal epoxides. More recently, they also developed trifunctional SCMs for enantioselective three-step domino catalysis [95], which were based on poly(2-oxazoline) synthesized through living cationic ring-opening polymerization [96,97] that permitted compartmentalization of three incompatible catalysts. The SCM consisted of carboxylic acids in the hydrophilic outer shell, Rh-based *N*-tosylated 1,2-diphenyl-1,2-ethylenediamine (Rh-TsDPEN) in the intermediate cross-linked shell, and 4-dimethylaminopyridine (DMAP) in the hydrophobic core. The spatial architecture of each catalyst was designed to selectively exploit the path of the substrate during each step of the reaction; the first step involved ketal hydrolysis to the corresponding prochiral ketone, the second step asymmetric transfer hydrogenation (ATH) to yield an enantio-enriched secondary alcohol, and the final step selective acylation to the desired ester product (Scheme I.6). Higher conversions were observed with more hydrophobic ketals and anhydrides, and the role of the intermediate shell cross-linked layer in preventing deactivation of the DMAP catalyst supported inside the micellar core was also shown.



Scheme I.6. Synthesis of the trifunctional SCM nanoreactor COOH-Rh-DMAP. (Adapted from [95]).

Optimally, SCMs act as nano-incubators for loaded catalysts and protect the catalyst from passivation or deactivation. However, the cross-linked shell also introduces a physical barrier between the hydrophobic core and the hydrophilic shell, which can lower the mass transport of certain chemicals and limit SCMs applicability for certain catalytical transformations.

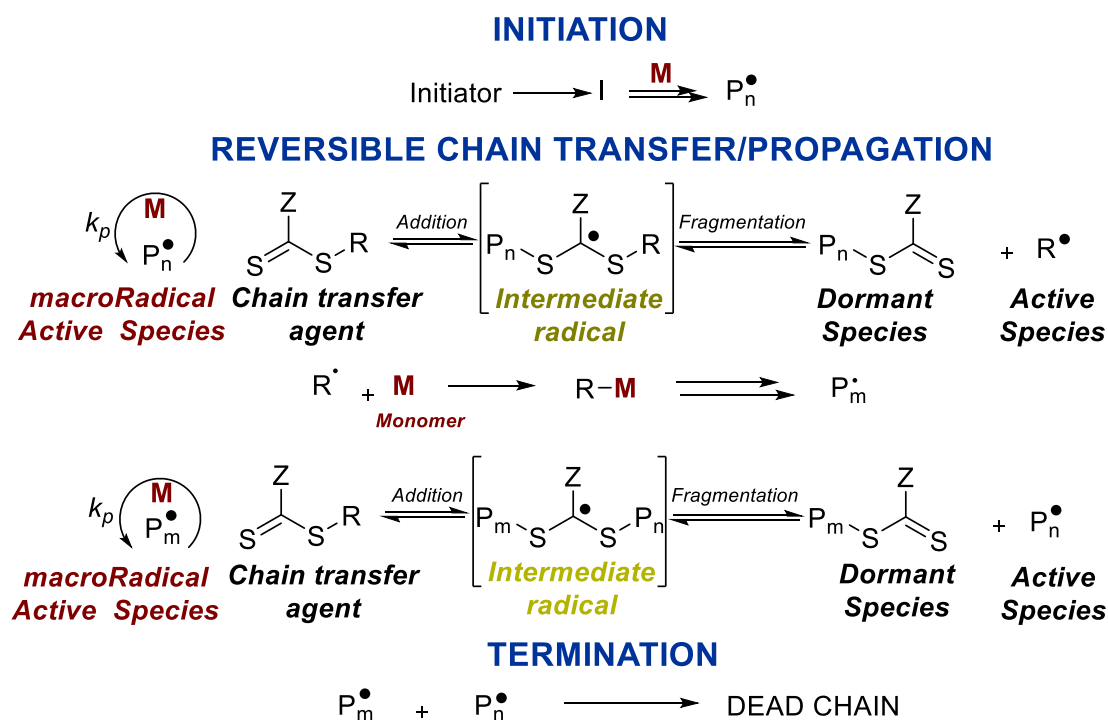
I.3.3.2. Core cross-linked micelles

To circumvent the mass transport restrictions of SCMs, other polymeric structures have been developed. The first structure, called Core-Crosslinked Micelle (CCM), consists of ligand-functionalized amphiphilic diblock copolymers that are cross-linked at the end of the hydrophobic chain. This provides star-block unimolecular nano-objects where the ligands are located on flexible arms outside of the cross-linked

area. The second structure, known as NanoGel (NG), features a fully cross-linked core, with the catalyst binding sites being situated within the cross-linked core [82]. Various strategies have been reported in the literature for the synthesis of CCMs, including ATRP, as used by Sawamoto and Terashima [98]. They were the first to use NG-type nanoreactors in catalysis, loaded with molecular Ru-based catalysts [32,99–102], and RAFT-mediated polymerization-induced self-assembly (PISA) [103]. The latter strategy is a particularly attractive approach as it allows to produce block copolymer nano-objects with a full synthesis protocol under one-pot conditions. An extensive examination of various synthetic approaches for CCMs falls outside the purview of this PhD work, where the primary focus lies on the application of the RAFT polymerization approach for the synthesis of CCMs. For a more comprehensive understanding of alternative methods, readers are encouraged to explore the literature references [104–109].

In RAFT-PISA, a water-soluble homopolymer (A) is prepared by homogeneous polymerization of a water-soluble monomer and then chain-extended using a hydrophobic monomer in water [103]. The polymerization starts slowly as a suspension polymerization, with the monomer droplets providing the monomer molecules to the growing water-soluble chains. Beyond a certain length of the second block (B), self-assembly of the AB diblock copolymer occurs to yield micelles. Then, the residual monomer is incorporated into the micellar cores and the process continues rapidly as a dispersion polymerization. The morphology of the resulting block copolymers varies in correspondence to the degree of polymerization (as described previously) [53]. RAFT polymerization proceeds in the same way as classical free-radical polymerization (*i.e.*, initiation, propagation, and termination), but with additional reversible addition-fragmentation steps, uses a large amount of thiocarbonylthio compounds as controlling agents (CTAs), and a comparatively low concentration of radical initiator. The CTAs react through a RAFT reaction with the (macro)radicals formed in the presence of monomer by an exchange mechanism

between the active species and the dormant chains by the formation of an intermediate radical (Scheme I.7).



Scheme I.7. Schematic overview of RAFT polymerization. (Adapted from [53]).

Stenzel and coworkers [110] used RAFT polymerization technique to synthesize poly(2-hydroxyethyl acrylate)-poly(*n*-butyl acrylate) block copolymers using either poly(2-hydroxyethylacrylate) or poly(*n*-butyl acrylate) macromolecular RAFT (macroRAFT) agents with narrow molecular weight distributions. These macroRAFT agents were further extended by polymerization of a diacrylate monomer, yielding core-crosslinked micelles. No catalytic applications were described for these CCMs. Furthermore, three generations of CCMs with amphiphilic unimolecular polymer-based nanoreactors [82] having neutral (CCM-N), cationic (CCM-C), and anionic (CCM-A) shells, respectively, have been prepared by RAFT. Loaded with molecular complexes, in particular with rhodium containing ones, they have been used for aqueous biphasic hydrogenation and hydroformylation catalysis (Figure I.6) [111].

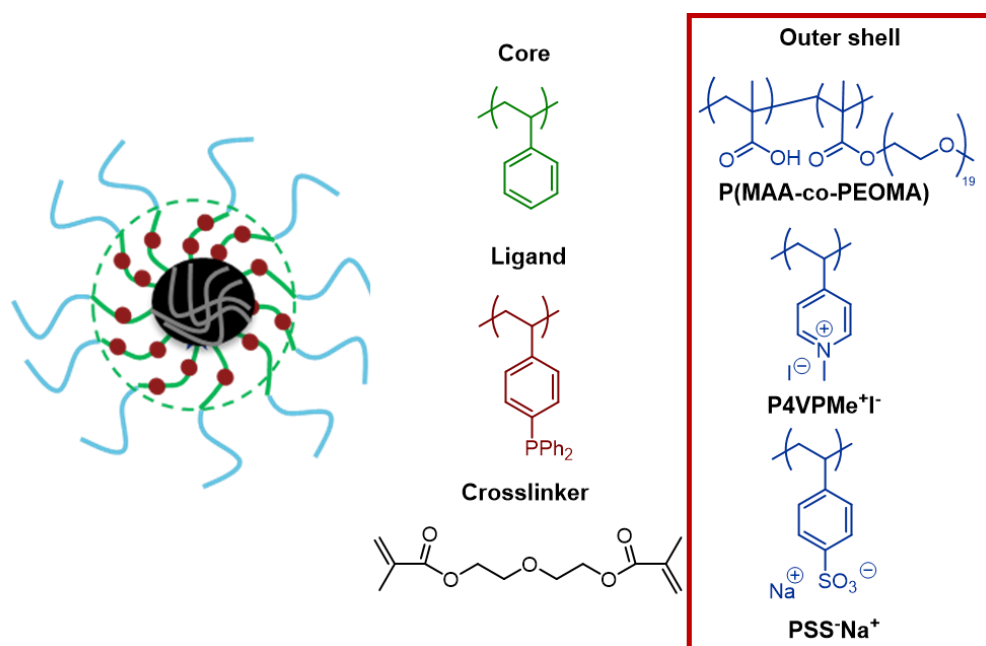
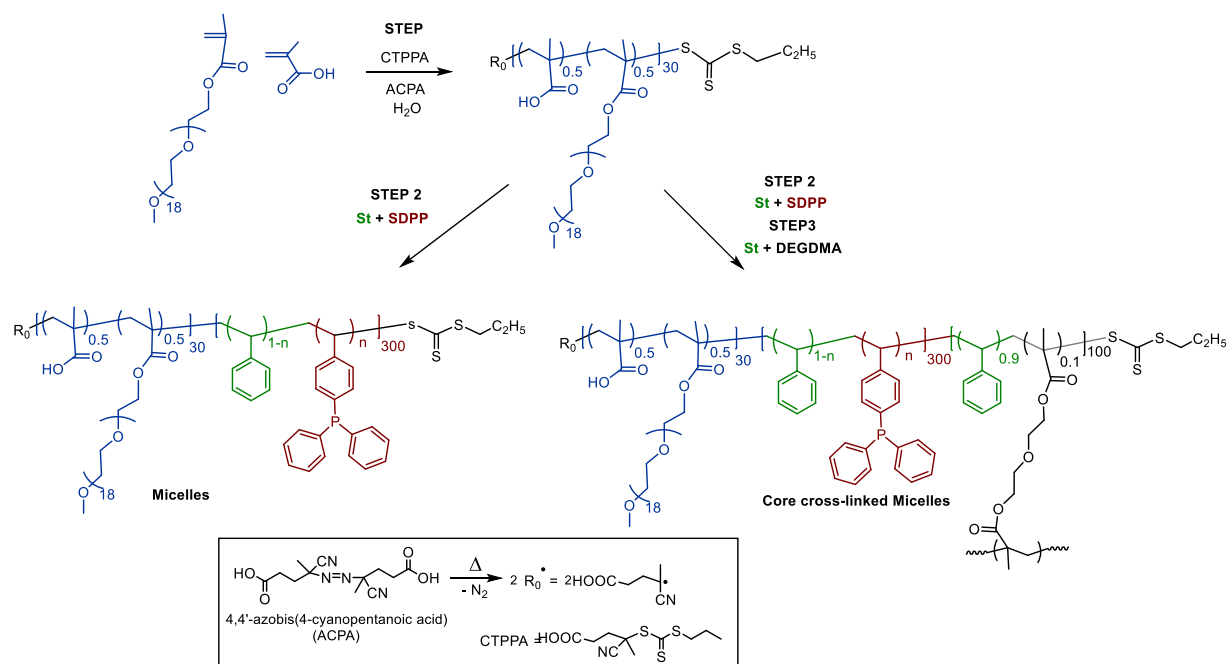


Figure I.6. Three generations of CCMs with triphenylphosphine (TPP) core and different outer shells.

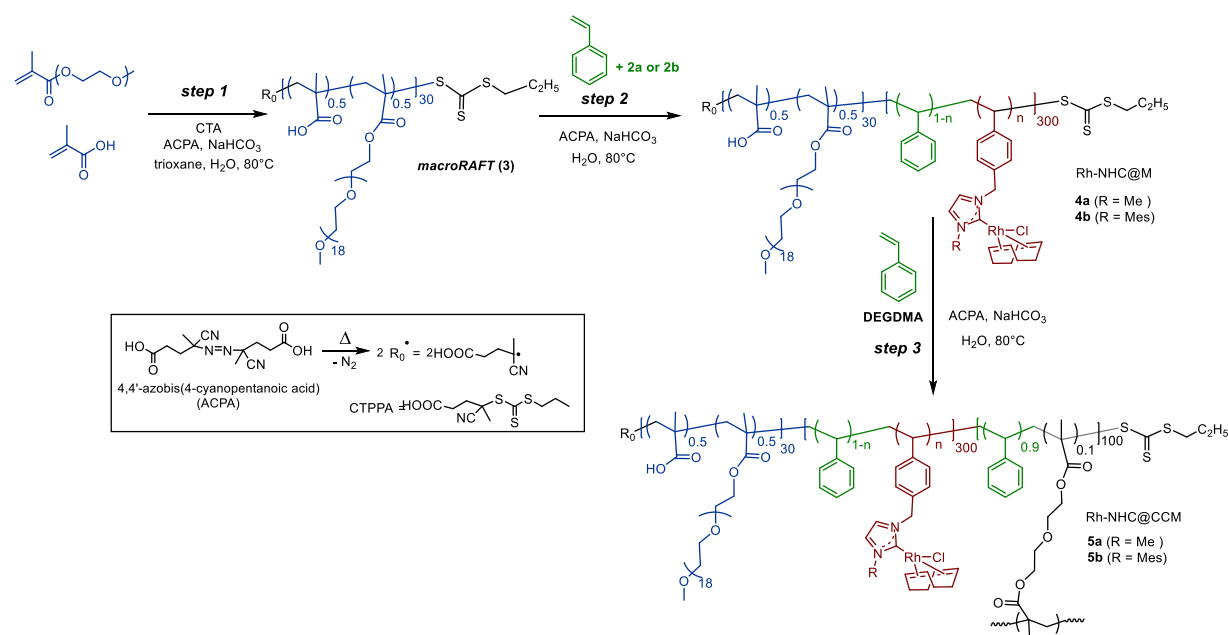
The first generation CCM-N [112] was designed with an uncharged water-soluble shell by copolymerization of methacrylic acid (MAA) and poly(ethylene oxide) methyl ether methacrylate (PEOMA) to generate a P(MAA-*co*-PEOMA) macroRAFT agent (Scheme I.8). Addition of styrene (St) and DPPS (diphenylphosphinostyrene) as core ligands generated P(MAA-*co*-PEOMA)-*b*-P(St-*co*-DPPS) amphiphilic block copolymers that self-assembled into well-defined micellar particles ($d = 72$ nm), which were crosslinked using diethylene glycol dimethacrylate (DEGDMA) forming CCM-N ($d = 79$ nm). The average formula of the single polymer chains is $R_0-(MAA_{0.5-co}PEOMA_{0.5})_{30b}-(St_{1-n-co}DPPS_n)_{300b}-(St_{0.9-co}DEGDMA_{0.1})_{100}SC(S)SPr$, with the chain ends ($R_0 = C(CH_3)(CN)CH_2CH_2COOH$ and $SC(S)SPr$) provided by the CTA. The uniformity of the CCM-Ns was demonstrated by size exclusion chromatography (SEC), TEM, and DLS analyses, which also evidenced the latex stability. Moreover, nuclear magnetic resonance (NMR) spectroscopy and DLS confirmed the transport of hydrophobic molecules across the hydrophilic shell into the polymer core to be fast leading to increased particle size owing to the particle swelling ($d = 117$ nm).



Scheme I.8. General strategy of RAFT-mediated emulsion polymerization for the synthesis of various types of core-shell nanoreactors. (Adapted from [112]).

As a proof-of-principle application, the CCM-Ns were loaded with $[\text{Rh}(\text{acac})(\text{CO})_2]$ (acac = acetylacetonate) and evaluated for aqueous biphasic hydroformylation of 1-octene [113]. High activity, low isomerization, as well as good stability and recyclability (Rh leaching of a few ppm), were found, but the system was moderately mass-transfer limited at high rhodium concentrations and non-negligible leaching appeared to result from particle aggregation. Subsequent follow-up studies addressed the metal leaching mechanism [114], the metal migration and cross-exchange in amphiphilic core-shell polymer latexes [115], and mass-transport limitations [116]. Later, Poli, Manoury, and coworkers [117] extended the family of ligand-functionalized CCMs using the same synthesis protocol to include the bidentate Nixantphos ligand in the CCM-N. After loading with $[\text{Rh}(\text{acac})(\text{CO})_2]$ the system was also applied to the aqueous biphasic hydroformylation of 1-octene, where only moderate activity (mass-transfer limitation) but excellent regioselectivity was found for the formation of *n*-nonanal.

A convergent synthesis of polymeric nanoreactors containing polymerizable Rh^I-NHC^R complexes [43] was then developed (Scheme I.9). TEM images of the resulting Rh-NHC^R@CCM nanoreactors with R = Me (**5a**) and R = Mes (**5b**) (Figure I.7) revealed formation of particles with a broad size distribution and non-spherical shape together with spherical shape (diameter of 123 ± 19 nm), respectively. Under optimized reaction conditions, the **5b** nanoreactors yielded good activity and excellent recyclability for styrene hydrogenation with Rh-leaching < 0.6 ppm per reaction cycle (measured by inductively coupled plasma mass spectrometry, ICP-MS) after some initial decomposition of the Rh-complex by cleavage of the Rh-NHC bond in the initial two runs (Table I.3, entries 1 and 2). Despite the encouraging recyclability results, mass-transfer limitations and impractical slow separation of the catalyst and reaction mixture remained for this catalyst, like for the other CCM-N catalysts.



Scheme I.9. Synthesis of Rh-NHC^R@CCMs **5a** (R = *N*-mesitylimidazole (Me)) and **5b** (R = *N*-mesitylimidazole (Mes)) by RAFT-PISA polymerization. (Adapted from [43]).

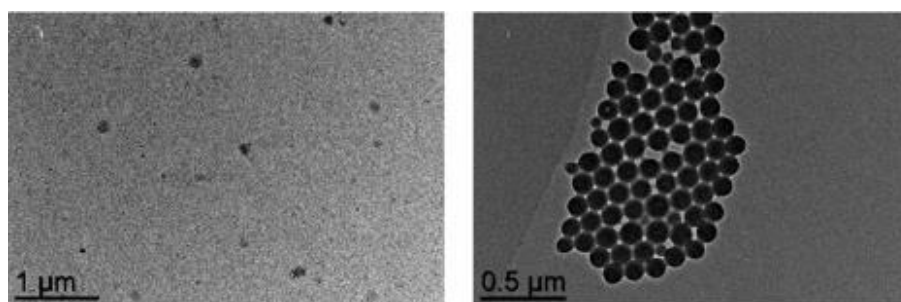
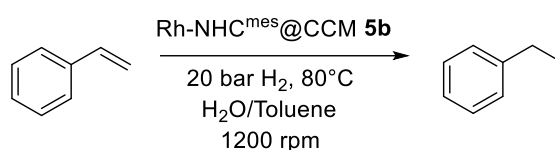


Figure I.7. TEM images of Rh-NHC^R@CCMs **5a** (left) and **5b** (right) (numbers as in Scheme I.9). (Adapted from [43] and used with permission from Royal Society of Chemistry ©).

Table I.3. Recycling study of Rh-NHC^{Mes}@CCM **5b** (number as in Figure I.7) catalyst in styrene hydrogenation. (Adapted from [43]).

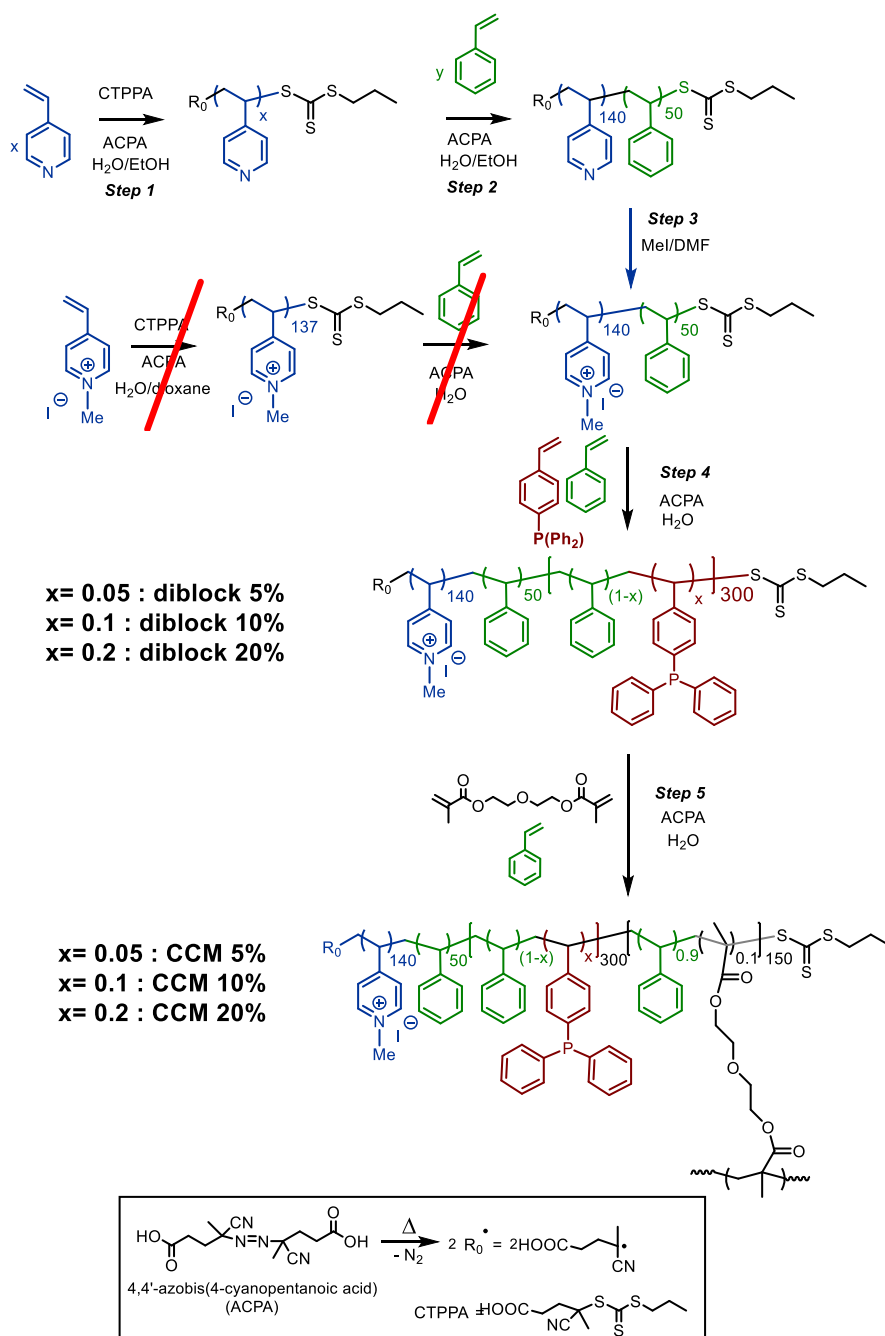


Entry	Run	Molar St/Rh ratio	St Conversion ^a (%)	EB Selectivity ^a (%)	Rh leaching ^b (ppm)
1	1st		>99.5	>99.5	0.87
2	2nd		>99.5	>99.5	1.47
3	3rd	1000/1	>99.5	>99.5	0.24
4	4th		>99.5	>99.5	0.34
5	5th		>99.5	>99.5	0.21
6	1st		73	>99.5	0.39
7	2nd		77	>99.5	0.61
8	3rd	10 000/1	>99.5	>99.5	0.54
9	4th		>99.5	>99.5	0.31
10	5th		98	>99.5	0.13

Conditions: styrene (79.3 mg, 0.75 mmol), CCM **5b** (85 mg, 7.9×10^{-7} mol of Rh for St/Rh: 1000/1 or 8.5 mg, 7.9×10^{-8} mol of Rh for St/Rh:10 000/1), decane (31.5 mg, 0.225 mmol), toluene (1 mL)/water (0.5 mL). ^a Measured by GC. ^b Measured by ICP-MS. St: Styrene, EB: ethylbenzene.

To circumvent the mass-transfer and separation issues with CCM-N, a second generation of CCM nanoreactors with an outer polycationic shell (CCM-C) based on poly(1-methyl-4-vinylpyridinium) (CCM-Cs) was subsequently developed *via* RAFT polymerization [118]. The macroRAFT agent was synthesized by RAFT polymerization of 4-vinylpyridine (4VP) in aqueous ethanol, followed by a chain extension with a PSt block and quaternization of the P4VP block. A core-anchored

triphenylphosphine (TPP) ligand functionality, diluted in styrene was introduced by chain extension in a fourth synthetic step and the CCM-C was finally formed in a fifth step by core cross-linking by a DEGDMA)/St (10:90) mixture [119] (Scheme I.10). All obtained polymers ($x = 5, 10$ or 20%) were shown by DLS and TEM analyses to have spherical morphology, a narrow size distribution ($d = 130-150$ nm) and a positive zeta potential.



Scheme I.10. Synthesis of CCM-C. (Adapted from [119]).

After loading with $[\text{Rh}(\text{COD})(\mu\text{-Cl})_2]$, the aqueous biphasic hydrogenation of 1-octene and styrene revealed improved mass transport properties and superior performance of the CCM-Cs, in terms of both catalytic activity, stability, and recovery, relative to the neutral-shell analogs [119]. Importantly, also less catalyst leaching occurred due to an enhanced ability of the polycationic shell to confine the nanoreactors in the aqueous phase. Moreover, in substrate scope investigations where the catalytic hydrogenation of acetophenone was attempted, the $[\text{RhCl}(\text{COD})(\text{TPP}@ \text{CCM-C})]$ latex turned black, suggesting the reduction of the molecular Rh^{I} complex to Rh^0 metal. In retrospect, this method has proven highly effective in generating RhNPs within the core of CCMs (Figure I.8), sparking further investigations into biphasic hydrogenation involving RhNPs [120]. This objective was the focus of the current PhD project. Specifically, addressing significant challenges encountered during the previous work, which will be discussed in the concluding section of this chapter.

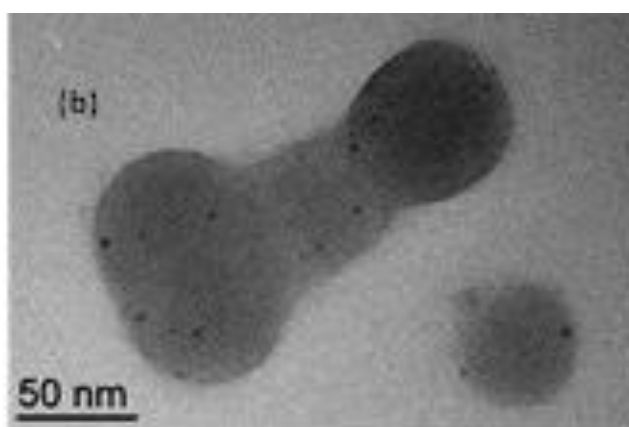


Figure I.8. TEM image of RhNPs generated in the core of CCM-C. (Adapted from [120] and used with permission from Royal Society of Chemistry ©).

To address the substrate scope limitation of the CCM-C nanoreactors (*vide infra* section I.8), a third generation of phosphine-functionalized CCM nanoreactors was developed with a polyanionic poly(styrene sulfonate)-based shell [13]. The synthesis route was identical to those used for the syntheses of CCM-N and CCM-C described above, except for using the water-soluble sodium styrene sulfonate monomer in the first step (Scheme I.11, Figure I.9) [13].

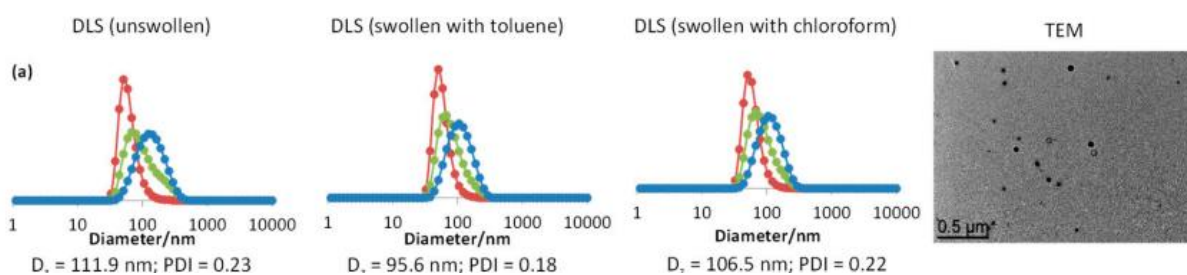
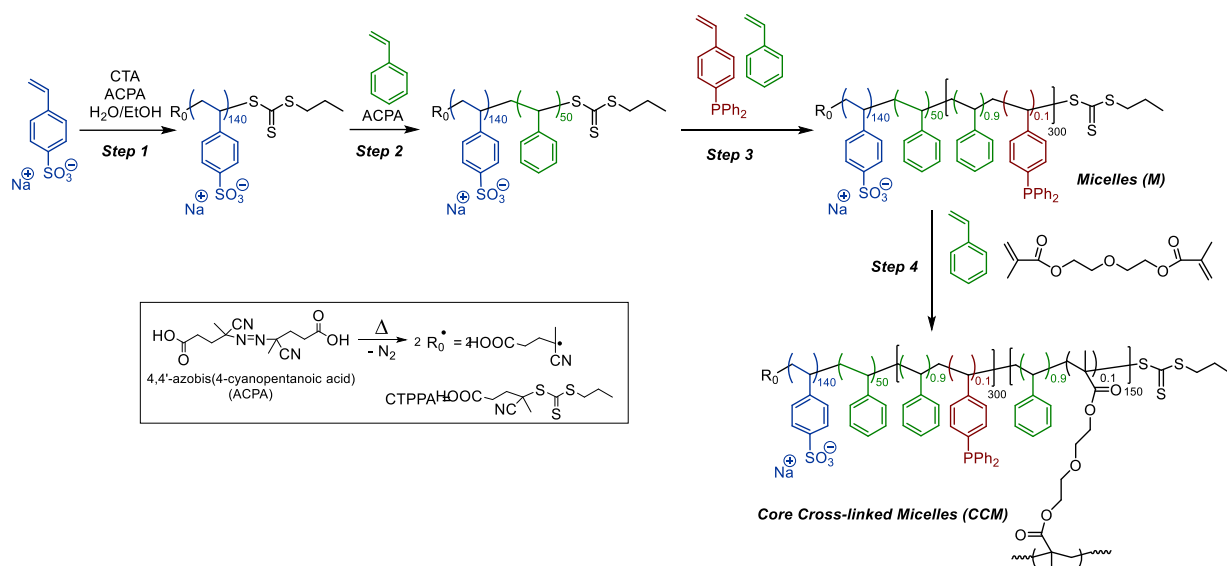


Figure I.9. DLS (before and after swelling with toluene or chloroform) and TEM image of the CCM-A. Color coding for the DLS size distributions: number (red), volume (green), and intensity (blue). (Adapted from [13] and used with permission from Elsevier ©).

For application in aqueous biphasic styrene hydrogenation, the CCM-A nanoreactors were loaded with $[\text{Rh}(\text{COD})(\mu\text{-Cl})_2]$, as previously done for the CCM-N and CCM-C counterparts (*vide supra*). However, the interaction between the Rh dimer complex and the outer shell of the CCM-A limited the transfer of the metal complex to the core, presumably *via* chelating Rh^{I} -sulfonate complex formation. However, this bottleneck could be circumvented by “dilution” of the shell with a neutral monomer (PEOMA), forming a mixed polyanionic CCM with lower surface charge density, which allowed Rh^{I} complexation in the core. Nevertheless, these CCM nanoreactors had inferior performance compared to equivalent nanoreactors with neutral and polycationic shells, which seemed to stem from catalyst alterations induced by migration of the Rh centers towards the shell sulfonate groups [13,111]. Thus, despite significant progress

in the development of CCMs, further improvements are still needed to obtain efficient and durable nanoreactor systems for aqueous biphasic hydrogenation catalysis.

I.3.3.2.1. Core cross-linked micelles with RhNP-TPP@CCM-C

In contrast to what was observed during styrene hydrogenation, an unexpected change occurred in the catalytic mixture of Rh-TPP@CCM-C, when acetophenone was used as substrate, namely a dark coloration (*vide supra*, section I.3.3.2). This change indicated that the molecular Rh precatalyst underwent reduction to its metallic form, potentially leading to the formation of RhNPs. This suggested that in the presence of a low concentration of phosphine ligands (initially using P/Rh ratios of 1/1 or 2/1), styrene might hinder the reduction of the Rh^I center. This protective effect can be attributed to styrene π -acidity, unlike acetophenone. This finding triggered further research aiming at expanding the scope of the CCMs to synthesize RhNPs embedded within ligand-functionalized water-soluble core-shell polymers for applications in aqueous biphasic hydrogenation.

I.4. Metal Nanoparticles

While metal nanoparticles (MNPs) and derived nanomaterials have been extensively utilized due to their unique properties, various methods for their preparation have been developed throughout history, notably during the 15th and 16th centuries [121]. However, the first scientifically documented synthesis of nanoparticles dates back to 1857 when M. Faraday [122] published his findings on the formation of a deep red colloidal gold solution through the reduction of chloroaurate ($[\text{AuCl}_4^-]$) using white phosphorus in CS_2 . Faraday's interest extended to the optical properties of the resulting isolated colloids, noting color changes from deep red bluish to green under pressure. In 1861, T. Graham [123] introduced the term "colloid" for the first time in his discussions on liquid diffusion, derived from the French word "colle" meaning "glue". The field of nanotechnology continued to evolve, drawing the attention of

more researchers, and achieving significant milestones. For instance, in 1902 R.W. Wood discovered Surface Plasmon Resonance (SPR) [124,125], and G. Mie's work in 1908 on the scattering and absorption of electromagnetic fields by nanospheres explained how particle size affects color changes (notably observed in gold particles) [126]. A breakthrough in the study of MNPs occurred in 1931 with the invention of TEM by M. Knoll and E. Ruska, for which Ruska was awarded the Nobel Prize in 1986 [127]. A few years later in 1937, M. von Ardenne developed the scanning electron microscope [128]. All these advancements set the stage for R. Feynman's 1959 address, "*There's Plenty of Room at the Bottom*," delivered at the American Physical Society meeting at California Institute of Technology (CalTech) [129]. In this influential talk, Feynman invited the research community to explore the manipulation of matter at the atomic scale, a field later termed "nanotechnology" by N. Taniguchi in 1974 [6].

During the past 30 years, the scientific and engineering communities have witnessed a surge in interest and investments in the realms of nanoscience and nanotechnology [130]. One of the primary driving factors behind the advancement of this field is the immense potential offered by MNPs, across various scientific domains, including chemistry [131], physics, biology, medicine, electronics [132], and materials science. The fascination with MNPs, also referred to as "nanoclusters" [133], largely stems from their unique state of matter, which positions them at the interface between individual atoms and bulk materials. These entities are larger than metal-based molecules yet remain small enough to avoid classification as bulk metals. Consequently, they do not conform to the strict rules of either absolute quantum chemistry or classical physics as metal-complexes and metal bulks but exhibit unique properties that deviate significantly from conventional expectations.

In chemistry, bulk materials are defined as the compounds that exist in their macroscopic form, meaning they are present in quantities substantial enough to be visible and manageable without the need for specialized equipment. These bulk materials typically consist of a multitude of atoms, molecules, or ions arranged in a

three-dimensional structure. On the other hand, as previously defined, MNPs and nanomaterials fall within the size range of 1-100 nm. They are composed of a relatively small number of metal atoms in comparison to bulk materials. Due to their nanoscale dimensions and high surface area-to-volume ratio, the MNPs exhibit properties that can significantly diverge from those of their bulk counterparts. It is worth noting that MNPs and bulk metals represent two distinct forms of a metal, each manifesting distinct properties, and behaviors because of differences in size and structure. As an illustration, in 1987, Haruta demonstrated that gold, long regarded as chemically inert, undergoes a significant transformation when reduced to the nanoscale (<5 nm) [134]. At this size range, gold can serve as a highly efficient catalyst in the oxidation of carbon monoxide. In particular, MNPs often display enhanced mechanical, optical, electrical, and catalytic properties when contrasted with their bulk counterparts. These enhancements primarily stem from quantum confinement effects, which can be explained by the behavior of matter and energy at small scale. Conversely, bulk materials have properties that align with classical physics and are not substantially influenced by quantum effects at the nanoscale. As described by Schmid [135], the quantum size effect can be illustrated in the following manner: when transitioning from a three-dimensional electronic system (bulk materials) to a zero-dimensional system (quantum dots), there is a gradual reduction in the density of available electronic states. In practical terms, a NP typically encompasses hundreds or even thousands of atoms. What is crucial to note is that electrons confined within such a NP possess discrete energy levels, replacing the previously continuous density of states existing in the bulk materials (Figure I.10) [136–138].

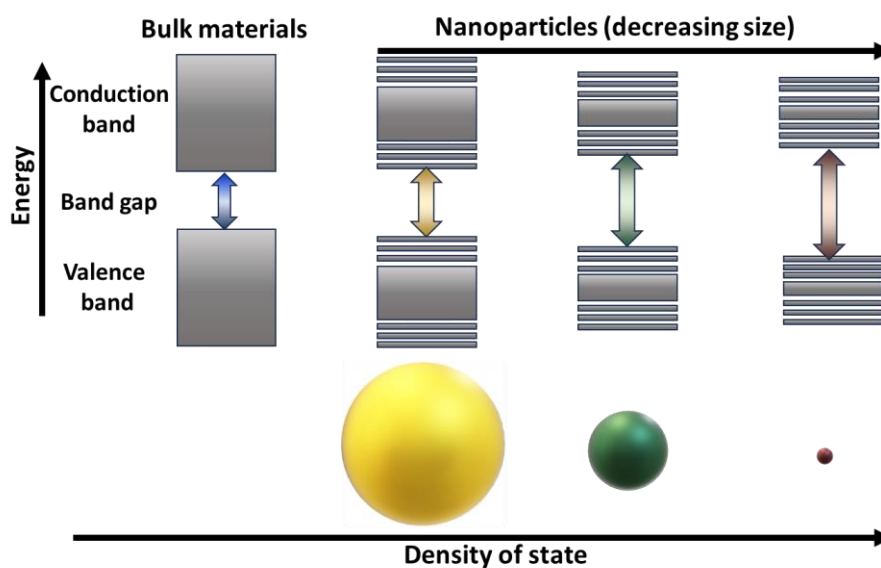


Figure I.10. Comparative representation of the electronic states in bulk metals and MNPs.

Regarding their electrical and optical characteristics, colloidal solutions of MNPs, particularly gold and silver, exhibit highly appealing properties. These properties stem from their distinct interactions with light within the visible to near-infrared (NIR) spectra, coupled with unexpected changes in conductivity behavior. Notably, these properties prove to be significantly dependent on the shape and size of the NPs, unlike their behavior in the bulk state. For example, gold spheres with diameters of 1 μm , 1 cm, or 1 mm all appear shiny and exhibit the typical gold color associated with metallic properties like malleability and conductivity when viewed at the macroscopic level [139–141]. However, as these gold spheres reduce in size to the nanoscale, their properties undergo remarkable transformations. At the nanoscale, the color of gold particles becomes highly sensitive to their size. For instance, gold spheres with a diameter of 13 nm, when suspended in a solution (forming a colloidal solution), exhibit a distinct red color. As the size decreases to less than 10 nm, gold loses its metallic properties and can no longer conduct electricity (Figure I.11) [141].

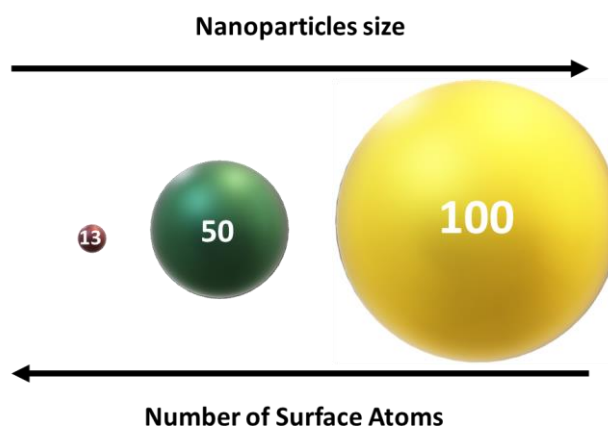


Figure I.11. Different colors for colloidal solutions of AuNPs depending on their size in nanometers (nm). (Adapted from [139–141]).

At the fundamental scientific level, the appeal of MNPs primarily arises from their distinctive electronic characteristics, which are brought about by their nanoscale dimensions [142]. Consequently, the investigation of size-dependent phenomena, where finite size effects become prominent, is a matter of great significance. The interest of MNPs with precisely controlled characteristics lies in their ability to unlock a wide range of applications, enabling tailored solutions in areas ranging from medicine and electronics to energy and the environment. This level of control inspired researchers and engineers to develop synthesis methods to have well-defined MNPs.

1.5. Synthesis of Metal Nanoparticles

In the literature, various techniques for producing MNPs have been documented over time, from historical methods to contemporary ones. To be deemed effective, a synthesis method must meet several criteria, including the precise control of size, shape, and crystal structure, as well as maintaining stable chemical and physical properties [133]. It should also manage the rate of aggregation, minimize impurities, and allow for scalability and reproducibility at minimal costs. According to Horikoshi and Serpone [143], the MNP synthesis techniques can be categorized into two main groups (Figure I.12) [138,144].

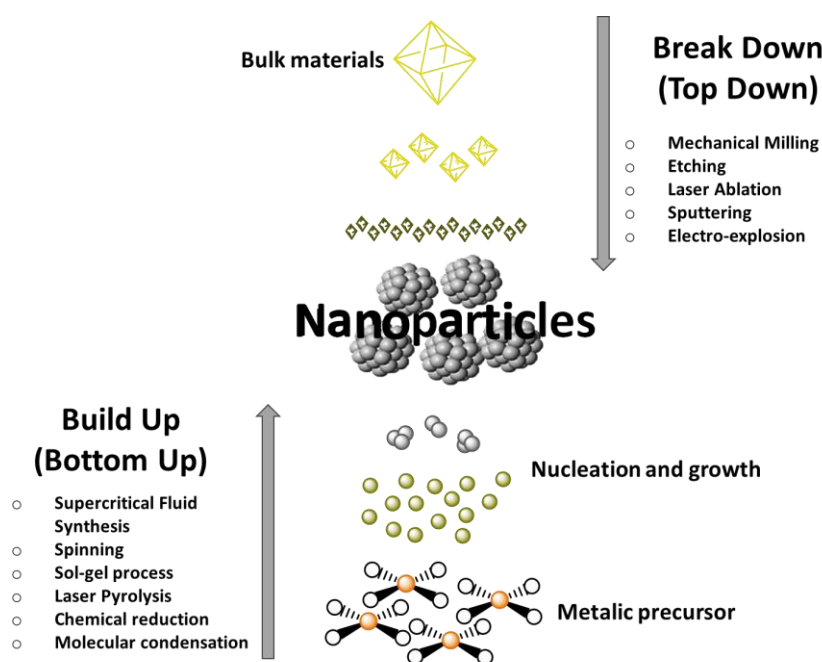


Figure I.12. Synthesis of MNPs *via* top-down and bottom-up approaches. Top Down = physical, Bottom Up = chemical.

The first group corresponds to the "breakdown" or "top-down" methods, wherein external forces are applied to solid materials, causing them to fragment into smaller particles. These methods typically involve dry or wet physical grinding techniques, subjecting bulk matter to shocks, compression, or friction. However, a drawback is the difficulty in achieving highly dispersed particles due to simultaneous condensation during the pulverization (grinding) step. Wet grinding can partially mitigate this issue by reducing condensation [145]. The second group assembles the "build-up" or "bottom-up" methods, which generate MNPs starting from gas or liquid atoms through atomic transformation or molecular condensation. The bottom-up approach is broadly categorized into gaseous- and liquid-phase methods. Gaseous-phase methods, while minimizing the presence of organic impurities compared to liquid-phase ones, require complex vacuum equipment, which comes with disadvantages including high costs and low productivity. Liquid-phase methods are the primary routes for NP synthesis, offering a wide range of options. For instance, the chemical reduction method is a commonly used solution synthesis method. Its principal advantage lies in the ability to produce particles of varying sizes and shapes, such as nanorods, nanowires, nanoprisms, nanoplates, and hollow NPs[136]. This method

allows for the fine-tuning of NP morphology and size by adjusting different variables, including the metal source, reducing agent [146,147], stabilizer [142], solvent [148], reaction time, and temperature [149].

1.6. Chemical synthesis of MNPs

Nucleation, namely the formation of the initial nuclei, stands as the pivotal phase in the synthesis of MNPs. In homogeneous nucleation, metal atoms or ions in the solution collide and aggregate to form small clusters of atoms referred to as nuclei. This typically occurs in a supersaturated solution where the concentration of metal ions exceeds their solubility limit. Nucleation is followed by the growth of NPs, which can be attributed to the attachment of monomers, metal ions, or atoms, to the nuclei present in solution. This attachment can be controlled through various chemical and physical parameters, or by Ostwald Ripening where larger NPs grow at the expense of smaller ones [150–155]. Ostwald Ripening happens because smaller NPs have a higher surface energy, and atoms from these smaller particles dissolve and redeposit onto larger ones, causing them to grow (Figure I.13). Factors influencing nucleation and growth steps in the synthesis of MNPs are the following:

1. **Precursor Concentration** [156]: The concentration of metal ions or atoms in the solution plays a crucial role. Higher concentrations can lead to more nucleation events, while lower concentrations may result in slower or no nucleation.
2. **Temperature** [151]: Temperature affects both nucleation and growth. Higher temperatures often accelerate these processes by providing more kinetic energy for atoms to collide and attach to nuclei.
3. **Reducing Agents** [157]: In some synthesis methods, reducing agents are used to convert metal ions into atoms, facilitating nucleation and growth. The choice of reducing agent can impact the rate of both steps and consequently the size of the NPs.

4. **Stabilizing Agents** [154]: Stabilizing agents (polymers, ligands, ionic liquids, *etc.*) are generally required to control particle size and prevent agglomeration by creating a protective layer around the NPs.
5. **pH** [150]: The pH of the solution can influence the surface charge of NPs and affect their stability and growth.
6. **Reaction Time** [155]: The duration of the reaction determines the extent of nucleation and growth. Longer reaction times may lead to larger NPs, due to Ostwald ripening phenomenon.

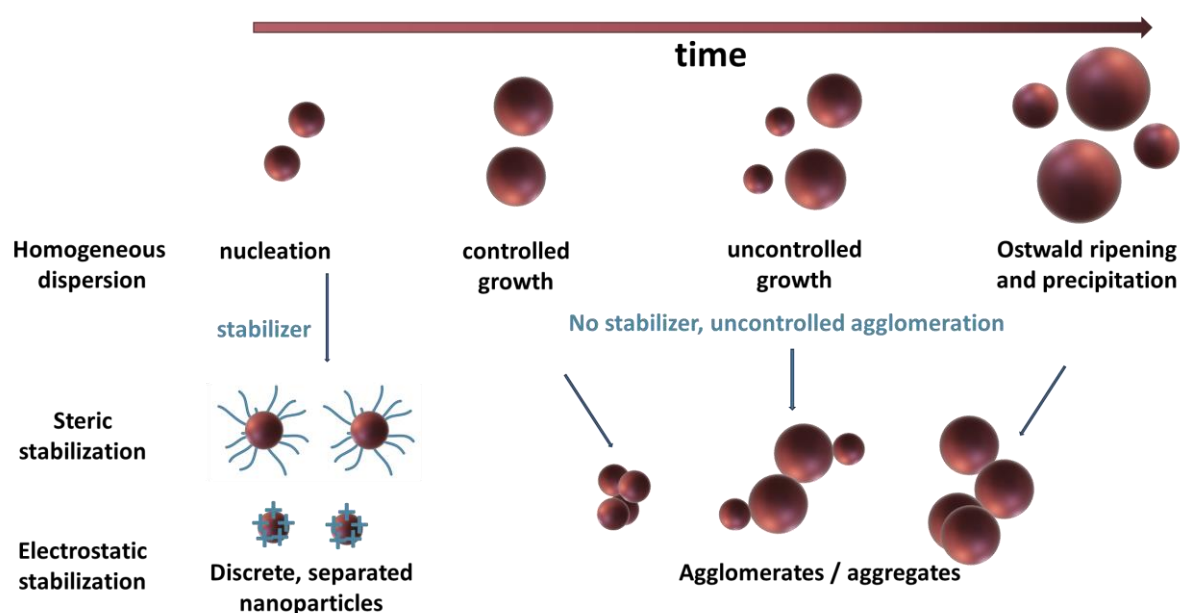


Figure I.13. Schematic presentation of (metal) NPs growth and stabilization. (Adapted from [153]).

1.6.1. Chemical Reduction

The chemical reduction of transition metal salts in the presence of stabilizing agents to produce zero-valent metal colloids in either aqueous or organic environments was initially documented in 1857 by Faraday [122]. This approach has since evolved into one of the most commonly used and potent synthetic methods in this field. The first reliable and standardized procedures for generating metal colloids, such as 20 nm gold colloids through the reduction of $[\text{AuCl}_4]^-$ using sodium citrate, were established

by Turkevich [158]. Additionally, he proposed a mechanism outlining the gradual formation of nanoclusters involving nucleation, growth, and agglomeration, a concept that remains fundamentally valid. Over time, this model has been further refined using data from modern analytical techniques and the latest findings in thermodynamics and kinetics, as described in Figure I.14 [157].

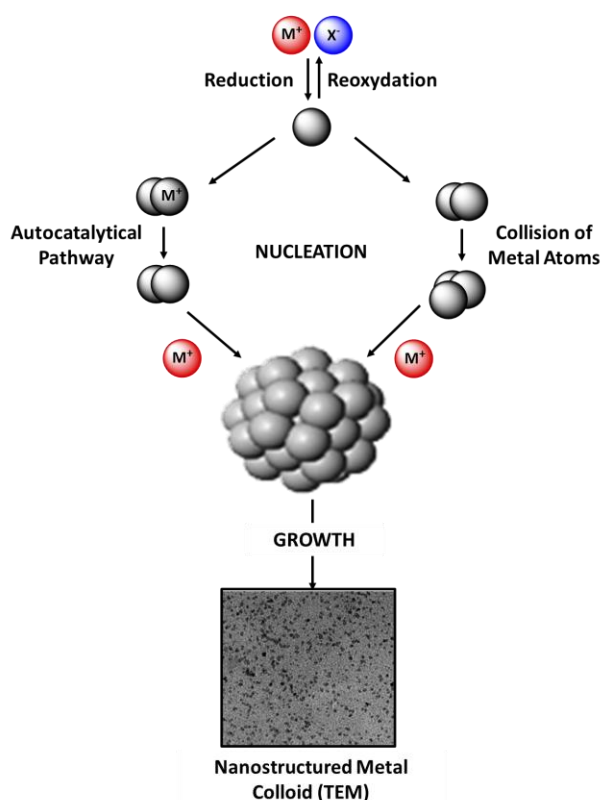


Figure I.14. Synthesis of MNPs by chemical reduction. (Adapted from [157]).

In the early stages of nucleation, the metal salt undergoes reduction, producing zero-valent metal atoms. These atoms can interact within the solution, colliding with additional metal ions, metal atoms, or clusters to form irreversible "seeds" that serve as the foundation for stable metal nuclei. The size of initial "seeds" and nuclei can be considerably less than 1 nm, contingent upon factors such as the strength of metal-metal bonds and the disparity between the redox potentials of the metal salt and the applied reducing agent. To maintain stability and prevent agglomeration of growing NPs, the addition of protective agents is essential. Indeed, in solution the MNPs are close enough to each other to be affected by van der Waals forces. If there isn't anything to oppose these forces, then the NPs will aggregate which will lead to a

change of size and properties, for example, in activity by lowering the active surface area. There are two primary modes of stabilization:

1. **Electrostatic Stabilization** [157]: relying on Coulombic repulsion forces between particles, resulting from the electrical double layer formed by ions adsorbed at the particle surface. For instance, sodium citrate can create electrostatic stabilization. An example is the preparation of gold sols through the reduction of $[\text{AuCl}_4]^-$ in the presence of sodium citrate.
2. **Steric Stabilization**[157]: achieved by employing sterically bulky organic molecules that act as protective shields on the metal surface. This prevents nanometallic cores from aggregating by keeping them separated. Various protective agents are reported in the literature, including polymers, block copolymers, P-, N- and S-donor molecules (*e.g.*, phosphines, amines, thioethers), solvents like THF, THF/MeOH, and propylene carbonate, long-chain alcohols, surfactants, and organometallic compounds. Typically, lipophilic protective agents yield metal colloids able to afford stable dispersions in organic media, referred to as "organosols", while hydrophilic agents result in colloidal dispersions stable in water, known as "hydrosols."

The chemical reduction of transition metal salts stands as one of the most widely used techniques for producing MNPs in solution, primarily for applications in catalysis, but not only. This reduction process can be controlled by using diverse reducing agents, including alcohols [157], polyol [159], dihydrogen [157], sodium borohydrate [160,161], and more. Furthermore, zero-valent MNPs can also be produced by treating metal-organic complexes, typically in a hydrogen (H_2) atmosphere or by employing sodium borohydride (NaBH_4).

The aqueous reduction of metal salts is a well-known technique due to several advantages: (i) the commercial availability of the required chemicals, (ii) ease of handling as the process is relatively straightforward, (iii) cost-effectiveness, since it is

an affordable method for obtaining MNPs, (iv) versatile stabilizing agents such as polymers, ammonium salts, long-chain alkanethiols, amines, fatty acids, *etc.*, can be employed to tailor the properties of the resulting NPs and lastly, (v) diverse reduction paths including the use of hydrides, hydrogen, as well as physical methods such as UV-Vis or gamma radiation [160,162].

1.6.2. Organometallic approach

The physical and chemical characteristics of MNPs are influenced by various factors, including particle size and size distribution, crystalline structure, particle shape, surface properties, their organization into nanomaterials, and their dispersibility [142]. These factors, in turn, rely on effective control and reproducibility in the synthesis process and particle stability. Traditionally, polymers have been the most commonly used tools to stabilize NPs. However, they may not be suitable for specific chemical or physical applications. Consequently, there has been significant works in the use of ligands able to coordinate to the particle surface. Thus, development of efficient methods that allow controlling the characteristics of MNPs in a reproducible manner is a fundamental objective. The use of organometallic chemistry techniques was found to be an efficient means for the formation of well-controlled nanostructures [142,153]. The synthesis of MNPs by the organometallic approach is based on using an organometallic or metal-organic complex as the source of metal in combination with a suitable stabilizing agent among various functional organic molecules [163], surfactants [164], polymers, dendrimers [40], ionic liquids [165], *etc.*

The choice of organometallic precursors is governed by their ability to be decomposed under mild reaction conditions. Their decomposition is generally performed using a gas that can be either H₂ or CO to give the naked zero-valent metal atoms (Figure I.15). The choice of the stabilizer is fundamental as it will influence the growth, stability, and surface chemistry of the nanostructures, in addition to its potential role for any target application.

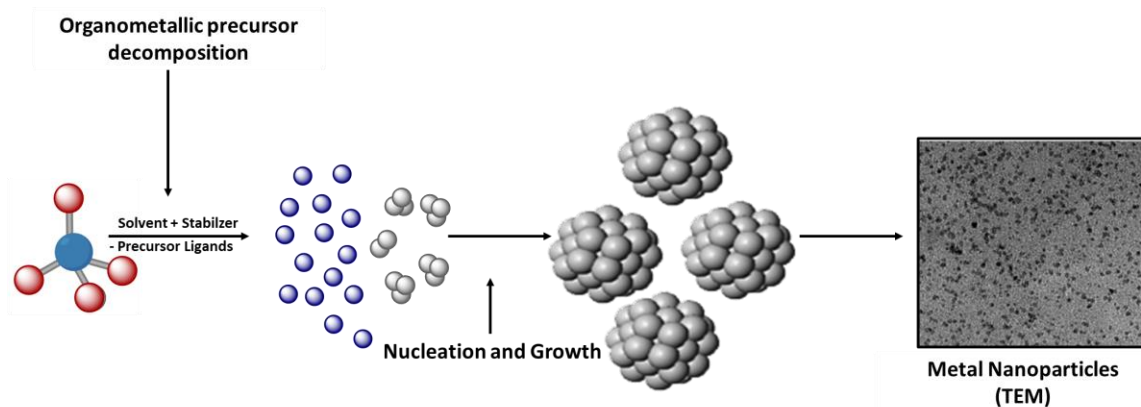


Figure I.15. Schematic representation of the organometallic approach for the synthesis of MNPs.

H_2 can decompose complexes by reduction of their ligands or reducing the metal precursors when they are not in the zero-valent oxidation state. CO can displace ligands present in the coordination sphere of the metal center by simple substitution (leading to an unstable intermediate). Whatever the gas used for the decomposition, it leads to the release of naked and free metal atoms in solution. These atoms will tend to associate together to form the seeds, that are the center of growth of the particles. The stabilizers will interact chemically with the surface of the growing particles or make a steric barrier around them, thus controlling their size by preventing them from excessive agglomeration.

Olefinic and allylic complexes stand out as the most appealing category of metal precursors. This is because the unsaturated ligands undergo a transformation into alkanes that do not interfere with the surface of the NPs when subjected to mild reaction conditions under H_2 pressure. For instance, compounds like $[Rh(\eta^3-C_3H_5)_3]$ [163,166] ($\eta^3-C_3H_5$ = allyl ligand), $[Ni(COD)_2]$ [167] (COD = 1,5-cyclooctadiene), $[Ru(COD)(COT)]$ (COT = 1,3,5,7-cyclooctatetraene) [168,169], $[Re_2(C_3H_5)_4]$ [170], and others, readily decompose when exposed to a low H_2 pressure (1-3 bar), making them excellent sources for MNPs. Additionally, metal complexes that contain ligands that can lead to potential stabilizing molecules for the particles are also of interest. Examples of such complexes include $[Rh(acac)(C_8H_{12})]$ or $[Ni(acac)_2]$ [171] (acac = acetylacetonato) which release acacH. While carbonyl complexes have been successful

used for synthesizing MNPs, notable examples being $\text{Co}_2(\text{CO})_8$, $\text{Rh}_6(\text{CO})_{16}$, and $\text{Ir}_4(\text{CO})_{12}$ [172,173], there is a significant drawback. These complexes require high temperatures for decomposition, and the release of CO molecules known to coordinate to the surface of MNPs can obstruct active sites, which can be particularly negative for catalytic applications.

The advantages of the organometallic approach can be succinctly outlined by (i) the variety of usable complexes, including carbonyl or olefinic complexes of transition metals and amido complexes featuring zero-valent metals or metals in a low oxidation state [174,175], (ii) the use of diverse reactions pathways, since organometallic reactions cover a spectrum of chemical processes, such as the cleavage of carbon-metal or nitrogen-metal bonds, ligand hydrogenation, ligand displacement, and nitrogen-metal hydrogenolysis, (iii) operations under mild conditions of temperature (often at or around room temperature), and pressure (1-3 bar) thus reducing energy requirements and facilitating implementation, and (iv) precise control over both the composition of the metal cores and of the stabilizing layer, most often consisting of organic molecules surrounding the MNPs.

I.7. Rhodium Nanoparticles in Catalysis

Nanocatalysis [176,177] has emerged as an attractive field between homogeneous and heterogeneous catalysis as it offers unique solutions to meet the requirements for catalyst enhancement. The aim is to develop well-defined catalysts that consist of MNPs combining the advantageous characteristics of both homogeneous and heterogeneous catalysts, such as high efficiency, selectivity, stability, and ease of recovery/recycling [149,178–180]. Despite being one of the rarest and most expensive metals, Rh stands out among other noble metals for its exceptional and frequently unparalleled catalytic properties, particularly in hydrogenation and hydroformylation reactions, also at the nanoscale regime [181]. Various methods have been developed to synthesize small-sized RhNPs [181,182]. The most widely known

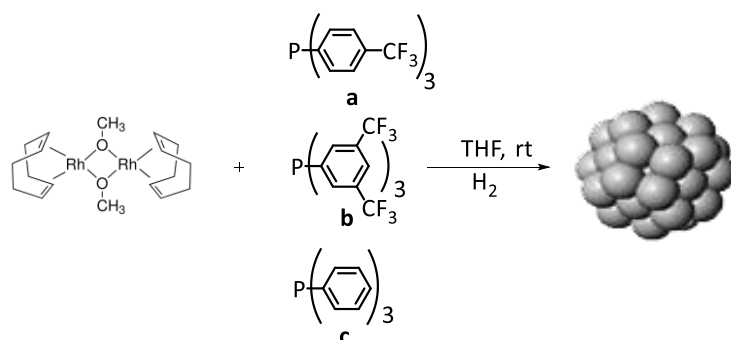
method involves reducing the metal salt $\text{RhCl}_3 \cdot 3\text{H}_2\text{O}$ [161,164] but the organometallic approach based on the use of Rh complexes such as $[\text{Rh}(\eta^3\text{-C}_3\text{H}_5)_3]$ [166,183] has also proved useful to generate well-controlled RhNPs. As mentioned above, RhNPs are widely recognized for their exceptional catalytic activity in hydrogenation reactions, on a broad range of reactants and functional groups. RhNPs systems are often stabilized by surfactants, polymers, and macromolecules, but also by ligands, predominantly P- and N-based ligands. Selected studies relevant to this PhD work will be hereafter described.

Delmas and coworkers [156] investigated the impact of various factors on the stability of polymer stabilized RhNPs. The RhNPs synthesis was achieved by the chemical reduction of $\text{RhCl}_3 \cdot 3\text{H}_2\text{O}$ in the presence of polyvinylpyrrolidone (PVP), resulting in 2 nm-sized particles. The obtained colloids exhibited impressive catalytic performance in the hydrogenation of 1-octene (50 °C, 3 bar H_2 , 2750 rpm), and could be reused multiple times without any loss in activity, surpassing the performance of conventional Rh complexes in biphasic liquid-liquid conditions. TEM analyses of the spent PVP-RhNPs revealed no change in the NP size and indicated the presence of both rhodium oxide and metallic Rh. The kinetics of 1-octene hydrogenation have been investigated considering its parallel isomerization reaction [156]. Various parameters have been studied, including 1-octene concentration, catalyst concentration, hydrogen pressure, and temperatures (29.8 °C – 49.8 °C). The reaction rate was found to be first-order with respect to the rhodium concentration, to the hydrogen pressure, and to the 1-octene concentration. The activation energies were found remarkably low, especially for the primary 1-octene hydrogenation reaction (14.1 kJ/mol). This suggests the presence of significant diffusional limitations within the polymer layer surrounding the colloidal particles. Indeed, the apparent activation energy is determined by turnover frequency (TOF) which is a measure of the rate at which a reaction proceeds, typically expressed as the amount of substrate transformed per active catalyst surface per unit of time (*e.g.*, per hour) [184,185]. In chemical

reactions, the rate can be influenced by both the intrinsic kinetics of the reaction and the mass transport of reactants and products to and from the catalytic sites [186,187]. When diffusional limitations are present, even if the reactant molecules possess the required energy to overcome the activation energy barrier, the rate of reaction may be determined by the number of reactants accessing the catalytic sites. Mass transfer coefficients play a vital role in this context. A low mass transfer coefficient signifies a slow transfer rate of reactants between the bulk fluid and the catalyst surface, which can lead to diffusion limitations. The combination of low mass transfer and diffusional limitations can result in very slow reaction rates, which in turn lead to low TOFs and are indicative of a low apparent activation energy and *vice-versa* [187].

Choukroun, Chaudret, Philippot, and coworkers [188] reported the synthesis of PVP-RhNPs using the organometallic dimer complex $[\text{RhCl}(\text{C}_2\text{H}_4)]_2$ as precursor in THF. They explored the hydrogenation of various substrates, including benzene, phenylacetylene, norbornene, quinoline, and adiponitrile. The PVP-RhNPs catalyst was used in both heterogeneous and dispersed forms under biphasic conditions (liquid/liquid), where the catalyst was dispersed in water. In both cases, the catalytic reaction exhibited kinetics characterized by zero-order with respect to the substrate and first-order with respect to H_2 and the Rh concentration. Interestingly, the highest hydrogenation rate was observed when benzene was employed under biphasic conditions. The Rh-PVP catalyst demonstrated also remarkable efficiency in the hydrogenation of norbornene, quinoline, and adiponitrile, leading to the formation of norbornane, tetrahydroquinoline, and 6-aminocapronitrile, respectively.

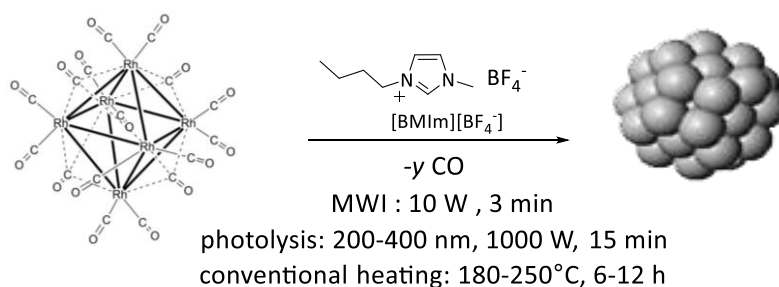
Gómez, Masdeu-Bulto, and coworkers [189] reported the synthesis of RhNPs using $[\text{Rh}(\mu\text{-OMe})(\text{COD})]_2$ as precursor and fluorinated phosphine ligands in THF (Scheme I.12), and the use of the resulting nanocatalysts in the hydrogenation of arene derivatives in both organic solvent (THF) and supercritical carbon dioxide (sCO_2).



Scheme I.12. Synthesis of RhNPs stabilized by phosphine **c** and fluorinated phosphine ligands **a–b**. (Adapted from [188]).

Both TPP (**c**) as well as the fluorinated ligand (**a**) were effective in stabilizing the RhNPs. The less-hindered fluorinated ligand (**a**) yielded the smallest NPs with an average mean diameter of 1.7 ± 0.4 nm (2.5 ± 0.9 nm for Rh-**c**), when (**b**) yielded large NPs. When the RhNPs systems were used for hydrogenation reactions of substrates, such as styrene, *p*-methylanisole, and (2-methylallyloxy)benzene, the reaction rates were slower in *s*CO₂ compared to THF, possibly due to different solubilities of the RhNPs in *s*CO₂ vs THF. Also, the predominant product formed in the hydrogenation of styrene in THF with Rh-**a** or Rh-**c** catalysts was ethylcyclohexane (selectivity >99%), whereas the selectivity shifted towards the olefinic group with ethylbenzene (EB) as the primary product using *s*CO₂. This observation suggested a robust interaction between the phenyl groups of the substrates and the NPs surface, however, the RhNPs were also agglomerated after the hydrogenation in *s*CO₂.

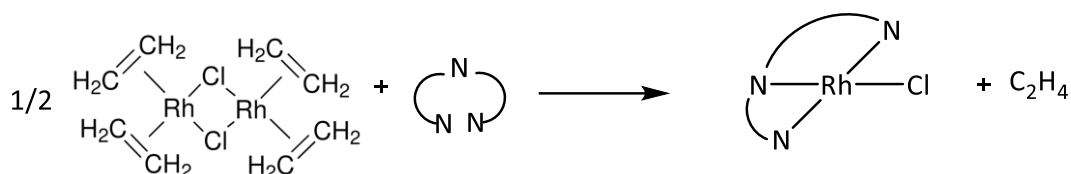
Janiak and coworkers [190] reported the synthesis of RhNPs in the ionic liquid (IL) 1-butyl-3-methylimidazolium tetrafluoroborate ([BMIm][BF₄]) using [Rh₆(CO)₁₆] as precursor applying various preparation methods (microwave (MWI), photolytic, or thermal decomposition). They obtained RhNPs of different sizes depending on the synthesis pathway. For instance, RhNPs of 1.7 ± 0.3 nm were formed under MWI conditions, compared to 1.9 ± 0.3 nm with photocatalytic decomposition and 3.5 ± 0.8 nm for thermal decomposition (Scheme I.13).



Scheme I.13. Microwave, photocatalytic and thermal decomposition of $[\text{Rh}_6(\text{CO})_{16}]$ in the IL $[\text{BMIm}][\text{BF}_4]$ to RhNPs. (Adapted from [190]).

The dispersions of the RhNPs in $[\text{BMIm}][\text{BF}_4]$ resulting from the syntheses were used directly in the liquid-liquid biphasic hydrogenation of cyclohexene to cyclohexane (10 bar H_2 , 90 °C), where the systems proved highly active (TOFs of 695-810 h^{-1}) and easily recyclable. Notably, an activity increase was observed from the second catalytic run which was attributed to an induction period, and a gradual rise in the activity after each catalyst recycle was explained by a surface restructuring.

Vallribera and coworkers [191] reported the hydrogenation of aromatic compounds catalyzed by RhNPs generated from rhodium bis(imino)pyridine complexes prepared from $[\text{Rh}(\mu\text{-Cl})(\eta^2\text{-C}_2\text{H}_4)_2]_2$ dimer (Scheme I.14). The synthesis of the RhNPs (1 bar H_2 , 2-propanol solvent, 60 °C, with K^tBuO) led to 1.5 ± 0.2 nm sized NPs which were found active in the hydrogenation of benzene, toluene, *p*-xylene, styrene, *R*-methylstyrene, biphenyl, aniline, phenol, and pyridine, under mild conditions (1 bar H_2 , 60 °C). Remarkably, when deposited onto alumina these RhNPs maintained their catalytic activity without substantial alteration with Hg^0 poisoning indicating a heterogeneous-type catalysis. The ability of Hg^0 to poison metal-particle heterogeneous catalysts, by forming an amalgam with the metal or adhering to its surface, has been widely used to distinguish homogeneous versus heterogeneous catalysis. This experimental procedure consists of adding Hg^0 to the reaction solution. The inhibition of the catalytic activity by Hg^0 is evidence of a heterogeneous catalyst; if Hg^0 does not suppress catalysis (negative result) the presence of a homogeneous catalyst is suggested [192].



Scheme I.14. Preparation of the bis(imino)pyridine complexes from $[\text{Rh}(\mu\text{-Cl})(\eta^2\text{-C}_2\text{H}_4)_2]_2$ in the presence of 2,6-bis{1-(phenyl)iminoethyl}pyridine pincer type ligands. (Adapted from [191]).

Moore and coworkers [165] described the synthesis of RhNPs stabilized by phosphine-functionalized imidazolium ionic liquids (FILs), $[\text{BDMI}][\text{NTf}_2]$ ($[\text{BDMI}] = 1\text{-alkyl-2,3-dimethylimidazolium}$, $\text{NTf}_2 = \text{bis(trifluoromethanesulfonyl)imide}$) using $[\text{Rh}(\eta^3\text{-C}_3\text{H}_5)_3]$ complex as precursor [164]. The precursor decomposed under 4 bar H_2 into Rh^0 and volatile propane, thus leaving no impurity at the NP surface (Figure I.16).

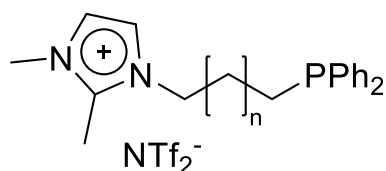


Figure I.16. Phosphine-functionalized $[\text{BDMI}][\text{NTf}_2]$ ILs ($n = 1$ and 9) used as stabilizers for the generation of RhNPs. (Adapted from [165]).

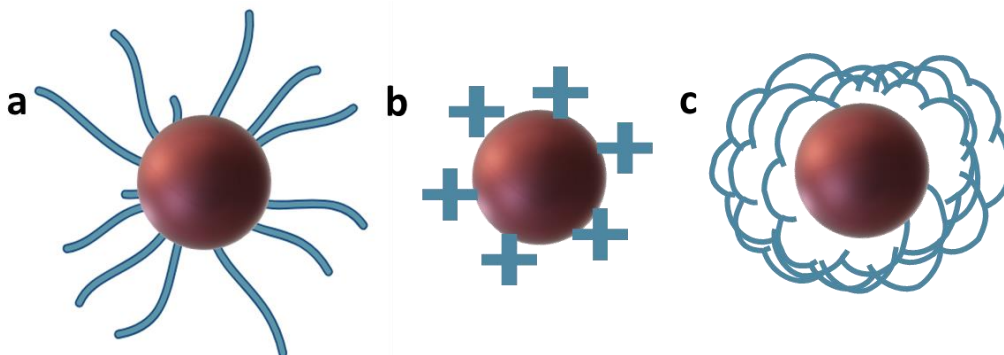
The IL-stabilized RhNPs were applied in the hydrogenation of toluene, styrene, and xylenes under mild conditions (40 bar H_2 , 75 °C, 3 h). The results for toluene hydrogenation to methylcyclohexane indicated that the FILs enhanced the catalytic activity, allowed recycling of the RhNPs, and prolonged the lifetime of the RhNPs catalysts compared to those stabilized by an unfunctionalized IL or a TPP ligand. A comparative analysis of the size and dispersion of the RhNPs before and after catalysis (Table I.4) provided an explanation of the observed differences, as TEM analysis of the RhNPs synthesized without IL stabilizers tended to aggregate. An induction time was also observed in the hydrogenation of styrene and *p*-xylene, which may be explained by a restructuring of the NP surface under catalytic conditions that led to higher TOFs in the consecutive runs. Despite this, the IL-RhNPs systems proved recyclable up to six runs with these substrates.

Table I.4. TEM characterization of RhNPs before catalysis and after catalyst recycling in toluene hydrogenation^a. (Adapted from [165]).

Entry	Stabilizer	RhNP size (nm)		
		Before catalysis	After Run 1	After Run 10
1	None	Clusters	2.3 ± 0.8	Aggregates
2	IL (n = 1) ^b	2.4 ± 0.6	2.3 ± 0.5	1.5 ± 0.4
3	IL (n = 9) ^b	2.0 ± 0.5	1.7 ± 0.3	1.9 ± 0.5
4	TPP	1.5 ± 0.4	Clusters	Aggregates

^a Catalysis conditions: Rh precursor (0.05 mmol), ligand (0.05 mmol), IL (1 mL), toluene (5.0 mmol, 100 equiv.), 40 bar H₂, 75 °C, 3 h. ^b Phosphine-functionalized 1-alkyl-2,3-dimethylimidazolium bis(trifluoromethanesulfonyl)imide) ILs with n = 1 and 9, see Figure I.16.

Rossi and coworkers [193] described the synthesis of RhNPs using RhCl₃·3H₂O as Rh source and 1-octadecanethiol (ODT; covalently coordinated ligand; **a**), tetraoctylammonium bromide (TOAB; electrostatic stabilization; **b**) or polyvinyl alcohol (PVA; steric stabilization; **c**) as stabilizers (Figure I.17). Their study focused on evaluating the influence of the three RhNPs systems, each characterized by distinct mechanisms for NP stabilization, in hydrogenation catalysis.

**Figure I.17.** Stabilization of RhNPs using **a** covalent linkage (ODT ligand), **b** electrostatic interaction (TOAB surfactant), and **c** steric stabilization (PVA polymer). (Adapted from [193]).

First, they observed a significant impact of the stabilizer on the RhNPs size (Figure I.18), obtaining an average diameter of 4.0 ± 1.0 nm when using ODT as stabilizer *vs* 2.3 ± 0.4 nm in the case of TAOB and 4.2 ± 1.2 nm with PVA. The RhNPs were then tested in the hydrogenation of cyclohexene either as soluble systems or after deposition onto a functionalized silica-coated magnetite NP support (FFSi).

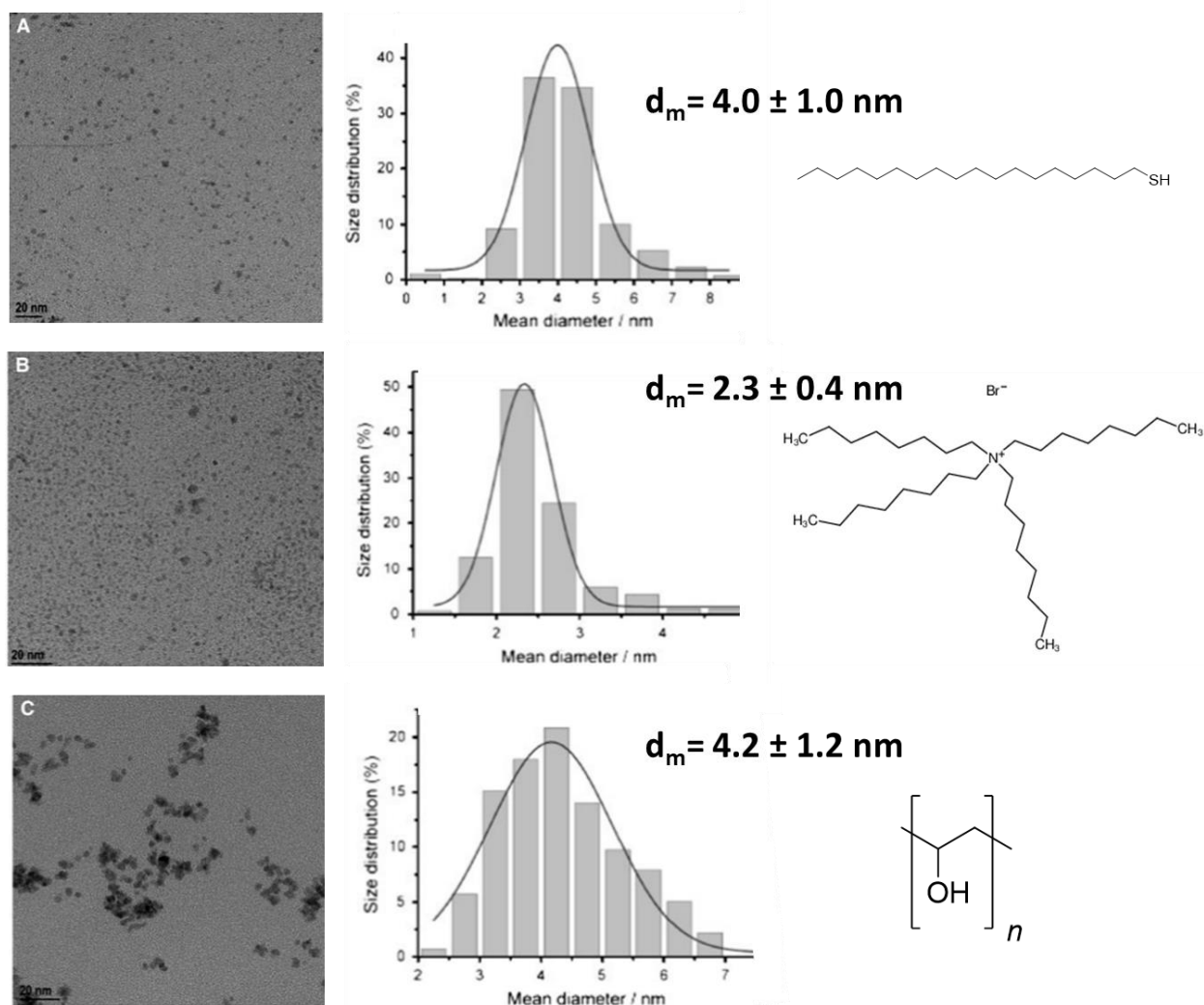


Figure I.18. TEM images of A) Rh-ODT **a**, B) Rh-TOAB **b**, and C) Rh-PVA **c** NPs and their corresponding size distribution histograms. ODT: covalently coordinated ligand, TOAB: tetraoctylammonium bromide, PVA: polyvinyl alcohol. (Adapted from [193] and used with permission from Springer Nature ©).

Table I.5. Hydrogenation of cyclohexene using soluble RhNPs. (Adapted from [193]).

Entry	Catalyst	TON ^a	Activation Time (h) ^b	Time (h) ^c	TOF (cTOF) (h ⁻¹) ^d
1	Rh-ODT	35600	4.8	>24	248 (795)
2	Rh-TOAB	35600	0.14	0.65	127300 (242940)
3	Rh-TOAB	71200	0.16	0.78	384170 (733150)
4	Rh-TOAB	142400	0.21	1.26	431970 (824370)
5	Rh-TOAB	284800	0.1	1.22	684240 (1305800)
6	Rh-TOAB	569600	0.30	1.00	185900 (354770)
7	Rh-PVA	35600	0.11	1.67	30960 (99230)
8	Rh-PVA	71200	0.12	1.8	55670 (178430)
9	Rh-PVA	142400	0.18	2	103990 (333300)
10	Rh-PVA	284800	0.36	3.6	120650 (386700)
11	Rh-PVA	569600	0.46	7.4	162680 (521410)

Reaction conditions (solventless): Cyclohexene (14.6 mmol), catalyst (0.052–0.4 μmol of Rh), 75 $^{\circ}\text{C}$, 6 atm of H_2 . ^a Turnover number expressed as moles of the substrate transformed per moles of catalyst. ^b Time interval without consumption of hydrogen. ^c Time interval required for each cycle reaction completion estimated by H_2 consumption curves (99 % conversion as determined by GC). ^d Initial turnover frequency expressed as moles of the substrate transformed per moles of catalyst per h and in parentheses TOF is corrected per moles of surface Rh atoms.

The Rh–ODT NPs gave almost no catalytic activity, while the Rh–PVA NPs as well as the Rh–TOAB NPs exhibited distinct and similar activities both in solution (as part of aqueous biphasic catalysis), and when immobilized onto functionalized silica with amine groups (FFSiNH₂) that were prepared by adding the pre-formed colloidal NPs to the FFSiNH₂ support. Furthermore, the RhNPs stability was found dependent on the stabilizer used for the synthesis as well as the functionalization of the support before RhNPs immobilization. Through optimization of the catalyst synthesis and reaction conditions, they achieved remarkable TOFs, reaching as high as $\sim 700000 \text{ h}^{-1}$ while maintaining the stability and recyclability of the RhNPs catalyst (Table I.5).

Quaternary ammonium salts have also proven effective capping agents to efficiently stabilize transition metal nanospecies in various biphasic catalytic reactions. Roucoux and Denicourt-Nowicki [194] studied the catalytic performance of colloidal suspensions of RhNPs stabilized by hydroxycetylammmonium surfactants and their chiral counterparts, generated by chemical reduction of RhCl_3 with sodium borohydride (Figure I.19). The nature of the surfactant (length of the alkyl chain) was

shown to influence the NP size and morphology. These RhNPs, acted as micellar nanoreactors, demonstrating their significance as catalysts in the pure biphasic hydrogenation of diverse lipophilic aromatic derivatives.

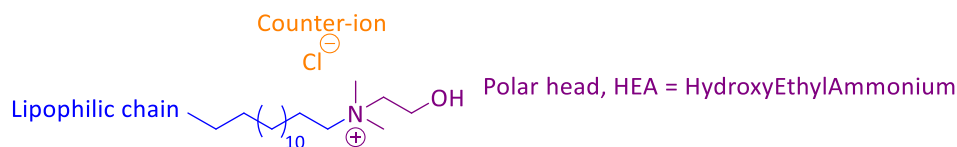


Figure I.19. Quaternary ammonium surfactants used to stabilize RhNPs for application in biphasic hydrogenation of arene derivatives. HEA16Cl (16 designating the number of carbons in the lipophilic chain). (Adapted from [194]).

Catalytic studies performed under mild conditions (1 bar H₂, room temperature) achieving notably high TOF values. Moreover, the ability to easily adjust the associated counter-ion or the polar head of the surfactant allowed for fine-tuning of particle size, morphology, aqueous suspension stability, and catalytic properties. As a result, these nanoreactors, formed by confining metallic nanospecies within surfactant micelles, exhibited remarkable catalytic activity in the reduction of aromatic compounds (Table I.6). They also offered the advantage of easy recyclability in biphasic setups.

Table I.6. Biphasic hydrogenation of arene derivatives with HEA16Cl-capped Rh⁰ colloids.^a (Adapted from [194]).

Entry	Substrate	Product Yield ^b (%)	Time (h)	TOF ^c (h ⁻¹)
1	Toluene	Methylcyclohexane (100)	3.6	83
2	Anisole	Methoxycyclohexane (70)/cyclohexanone (30)	4	75
3	Ethylbenzoate	Ethylcyclohexanoate (100)	4.7	64
4	Aniline	Cyclohexylamine (100)	10	30
5	o-Xylene	1,2-Dimethylcyclohexane (cis/trans: 91/9)	5.3	57
6	m-Xylene	1,3-Dimethylcyclohexane (cis/trans: 80/20)	6.8	44
7	p-Xylene	1,4-Dimethylcyclohexane (cis/trans: 65/35)	4.1	73
8	Chlorobenzene	Cyclohexane (100)	1.7	-
9	2-Chloroanisole	Methoxycyclohexane (53)/cyclohexanone (47)	11	34

^a Reaction conditions: Rh (3.8×10^{-5} mol), [Substrate]/[Metal]/[Surfactant] = 100/1/2, H₂O, 1 bar H₂, 20 °C.

^b Determined by gas chromatography. ^c Turnover frequency determined by number of moles of consumed H₂ per mole of introduced Rh per hour.

Godard and coworkers [195], studied the catalytic performance of phosphine- and phosphite-stabilized RhNPs in hydrogenation reaction. The RhNPs were synthesized by the organometallic approach starting from $[\text{Rh}(\eta^3\text{-C}_3\text{H}_5)_3]$ precursor and using TPP **1** and triphenylphosphite **2** as model ligands, in various P/Rh ratios (Figure I.20).

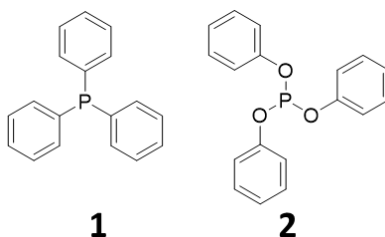


Figure I.20. The TPP **1** and triphenylphosphite **2** ligands used for the synthesis of RhNPs. (Adapted from [195]).

Regardless of the P/Rh ratio, crystalline NPs were formed that consistently displayed a size of *ca.* 2 nm, a spherical shape, and a face-centered cubic (fcc) structure. In the hydrogenation of styrene (40 bar H_2 , 80 °C), complete conversion of styrene was observed in all cases (Table I.7). However, the selectivity towards either EB or the fully hydrogenated product, ethylcyclohexane, was found to be significantly affected by the ligand coverage. TPP-stabilized RhNPs (Rh1 systems), quantitatively led to the fully hydrogenated product (methylcyclohexane), whatever the P/Rh ratio used for the synthesis (Entries 1-3).

Table I.7. Catalytic hydrogenation of styrene using phosphine- and phosphite-stabilized RhNPs^a. (Adapted from [195]).

Entry	NPs	d_m (nm)	Conversion (%) ^b	Selectivity (%)	
				Ethylbenzene ^b	Ethylcyclohexane ^b
1	Rh1-0.2	1.47 ± 0.28	100	-	100
2	Rh1-0.4	1.52 ± 0.21	100	-	100
3	Rh1-0.6	1.46 ± 0.25	100	-	100
4	Rh2-0.1	1.57 ± 0.23	100	26	73
5	Rh2-0.2	1.55 ± 0.31	100	87	13
6	Rh2-0.4	1.52 ± 0.23	100	97	3
7	Rh2-0.6	1.65 ± 0.30	100	100	0

^a General conditions: 1.24 mmol of substrate, 2 mol% of RhNPs, 10 ml of heptane, 80 °C, 40 bar H_2 , 16 h. ^b Determined by GC.

Conversely, triphenylphosphine-stabilized RhNPs (Rh₂ systems) showed a steadily increase of selectivity from 26 to 100% for EB as the ligand coverage on the catalyst increased between P/Rh = 0.2 and P/Rh = 0.6 (Entries 4-7).

A study involving CO adsorption on the surface of the NPs and IR spectroscopy evidenced that less Rh sites were available to form Rh(CO)₂ species at high phosphite coverage due to the coordination of ligands. In contrast, a low ligand coverage led to more Rh(CO)₂ species as the result of more accessible Rh sites for CO coordination. These results allowed to correlate between the quantity of active sites for the hydrogenation catalysis with the ligand coverage. The authors concluded that at high ligand coverage, the sites responsible for the hydrogenation of arenes were blocked by the stabilizer, allowing only hydrogenation of the vinyl unit of the substrate, and providing a high selectivity for EB.

Philippot, Rossi, and coworkers [196] reported a comparative analysis of the surface reactivity of RhNPs stabilized by a polymer *vs* phosphine/diphosphine ligands as components of supported catalysts in the hydrogenation of cyclohexene under solventless conditions (the substrate acted as dispersion medium for the RhNPs). Well-defined and very small RhNPs were synthesized through the organometallic synthesis, using [Rh(η^3 -C₃H₅)₃] as the metal source, PVP as stabilizer and TPP as a monophosphine and 1,4-bis(diphenyl)phosphinobutane (dppb) as diphosphine. These NPs had mean sizes of 2.2, 1.3, and 1.7 nm, respectively (Figure I.21).

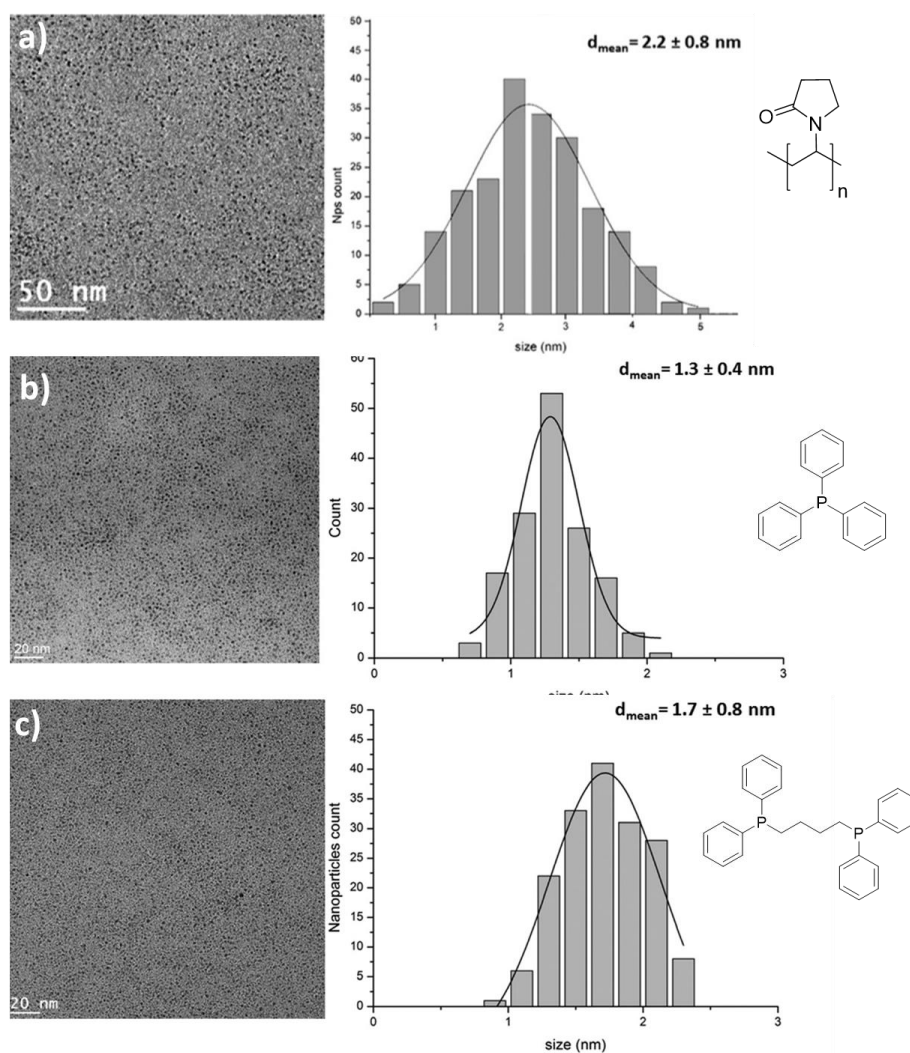


Figure I.21. TEM images and size distribution histograms of a) PVP- b) TPP- and c) dpbb-stabilized RhNPs. (Adapted from [196] and used with permission from Royal Society of Chemistry ©).

Among the stabilizers tested, the PVP-stabilized RhNPs exhibited the highest catalytic activity (Table I.8). This can be attributed to the more accessible metallic surface, as PVP interaction with Rh surface atoms is weaker compared to that in phosphine-stabilized NPs, where phosphines strongly coordinate with NPs surfaces. Interestingly, no significant difference was observed between the two phosphines, indicating that they both interacted or blocked the surface Rh atoms to a similar extent. However, electronic, or facet-directed effects induced by the phosphine ligands could not be ruled out. To further explore the catalytic potential of these RhNPs, they were deposited onto an amino-functionalized silica-coated magnetite (FFSiNH₂) support (also used previously, see above) by impregnation leading to supported Rh

nanocatalysts with uniform particle dispersion throughout the support. These nanocatalysts demonstrated improved catalytic performance in cyclohexene hydrogenation under similar reaction conditions as colloidal particles. Once again, the RhPVP-stabilized NPs proved to be the most active catalyst, and no discernible difference was observed between TPP and dppb ligands after immobilization. This suggested that the phosphine ligands continued to strongly coordinate with the metal surface after particle immobilization, affecting catalysis.

Table I.8. Hydrogenation of cyclohexene^a. (Adapted from [196]).

Catalyst	Induction time ^b (h)	Time ^c (h)	TOF ^d (cTOF) (h ⁻¹)
RhPVP	0.25	2.50	3500 (6730)
RhPVP@FFSiNH ₂ †	0.05	0.58	105700 (203270)
RhTPP	0.07	1.67	3800(5000)
RhTPP@FFSiNH ₂	0.15	1.50	23650 (31120)
Rhdppb	0.05	2.14	2800(4516)
Rhdppb@FFSiNH ₂	0.23	1.80	24850 (40080)

^a Reaction conditions (solventless): cyclohexene (29.2 mmol, 2.4 g), Rh catalyst (7.3 μmol), mol substrate per mol catalyst = 4000, †cyclohexene (14.6 mmol, 1.2 g), Rh catalyst (0.4 μmol), mol substrate per mol catalyst = 36500, 75 °C, 6 bar H₂. ^b Time interval without consumption of dihydrogen. ^c Time interval required for each cycle reaction completion estimated by H₂ consumption curves (>99% conversion as determined by GC). ^d Turnover frequency (TOF) expressed as moles of the substrate transformed per mole of catalyst per h at < 20% conversion. In parenthesis, TOF corrected per mol of surface Rh atoms.

Additionally, the authors took advantage of the magnetic properties of the support to facilitate the catalyst reuse in successive hydrogenation cycles. In the case of RhPVP@FFSiNH₂, a more active surface was obtained after successive reactions, likely due to progressive elimination of PVP from the RhNPs as the result of washing treatment. The immobilization of PVP-stabilized RhNPs thus appeared as an excellent strategy to retain and even enhance the catalytic performance of the NPs, as the polymer could be removed without compromising stability. The results obtained with Rh-dppb@FFSiNH₂ and RhPPh₃@FFSiNH₂ nanocatalysts confirmed the catalytic performance observed with colloidal RhNPs, suggesting that phosphine ligands remained strongly coordinated to the metal surface and were not displaced during immobilization or recycling experiments, thus leading to lower performance than PVP-systems. This study highlighted the interest in the organometallic approach for

preparing very small and stable RhNPs with different surface properties that can be deposited onto a support to improve stability and facilitate recycling. If the use of phosphines as stabilizing ligands resulted in the formation of smaller NPs, it also led to less active nanocatalysts. This relies on the strong coordination of the ligand at the Rh surface blocking some surface atoms, thus limiting the surface reactivity even after several catalytic recycles for supported nanocatalysts.

All the preceding research studies emphasize the need to design nanocatalysts with a right balance between a small NP size (to have a high number of potential active sites) and an accessible surface (to allow the reactivity), while being sufficiently stable to allow good recyclability. In the next section, previous results in the use of polymeric micelles as nanoreactors to confine RhNPs for hydrogenation catalysis will be described.

I.8. MNPs confined inside CCM-C for application in aqueous biphasic hydrogenation catalysis

As discussed earlier in this chapter (section I.3.3.2.1), an unexpected darkening of the color occurred in the reaction mixture when acetophenone was hydrogenated using a [RhCl(COD)(TPP@CCM-C)] latex catalyst. Such color change typically designates the formation of MNPs, and a further study was performed involving the generation of RhNPs in TPP@CCM-C for application in hydrogenation catalysis [120].

The RhNP-TPP@CCM-C system was initially tested in aqueous biphasic hydrogenation of acetophenone, but only low conversions were obtained unless high temperature (90 °C) was used. The slow reaction rate was attributed to a poor mass transport of the acetophenone into the CCM-C core, owing to a possible electrostatic interaction between its carbonyl group and the cationic pyridinium functions present in the polymer shell [120]. Conversely, RhNP-TPP@CCM-C showed excellent performance in the hydrogenation of 1-octene and styrene, with full conversion and full selectivity towards the hydrogenation of the olefinic group. Notably, the catalytic

activity was superior to that of Rh^I molecular system. RhNP-TPP@CCM-C proved also recyclable for styrene hydrogenation in four runs without loss of activity and with the RhNPs remaining well-dispersed, when toluene was used for product recovery/catalyst recycling. However, when using diethyl ether as extraction solvent a dramatic loss of activity was observed. This phenomenon was attributed to an extraction of the RhNPs from the CCM-C core driven by diethyl ether, an oxygen-based solvent (Figure I.22).

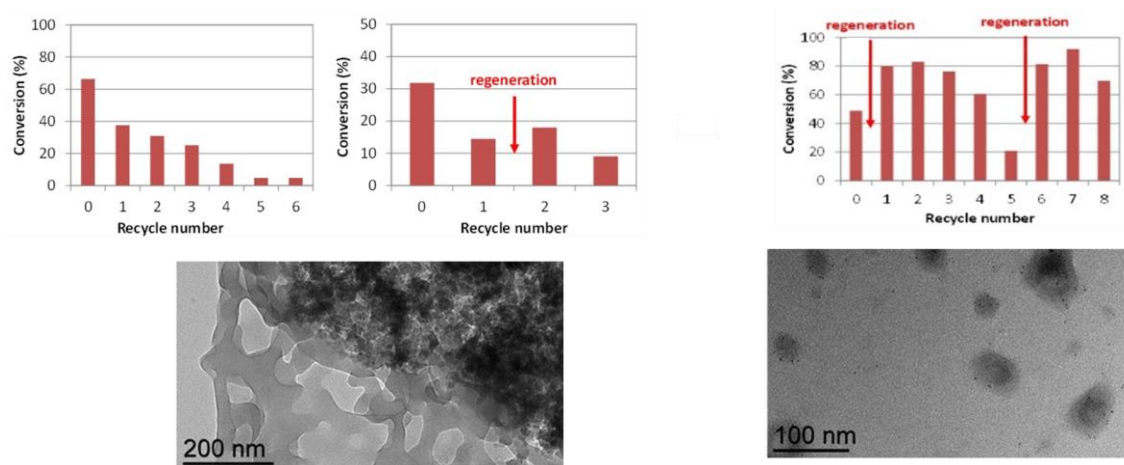


Figure I.22. Recycling tests in the hydrogenation of styrene with RhNP-TPP@cCCM using diethyl ether (left) and toluene (right) as extraction solvent (25 °C, 0.5 h, styrene/Rh = 2000/1) (top). TEM images of the recovered catalyst latexes after the final run (bottom). (Adapted from [120] and used with permission from Royal Society of Chemistry ©).

I.9. Summary

Nanostructured materials with high specific surface area offer many advantages in catalysis. In this chapter, major developments in the synthesis and catalytic applications of self-assembled nanoreactors made from amphiphilic macromolecules such as polymer micelles, polymersomes and unimolecular nanoreactors were first highlighted. The approaches using macromolecular nanoreactors as potential catalyst supports, hold many advantages owing to the diverse synthesis strategies for the generation and tuning of the nanoreactors, which could be of interest for industrial

applications. In particular, unimolecular nanoreactors have been the topic of extensive recent research. The perspectives of these systems are numerous, owing to their modularity and simple syntheses, notably by the RAFT-PISA protocol, which provides access to ligand-functionalized CCM nanoreactors. In such nanoreactors, the chemical nature and the degree of polymerization of the core and the shell, the type and density of the core-anchored ligands, as well as the nature of the coordinated metal pre-catalyst can all be readily varied. This makes the unimolecular nanoreactors highly adaptable and applicable to aqueous biphasic catalysis, thus providing new avenues of research with several potential applications.

In the second part of this chapter, the interests of nanosized catalysts, and in particular of RhNPs in hydrogenation catalysis have been presented. This section finished by describing work, where the formation of RhNPs was observed when working with a molecular Rh-complex@CCM-C system, that were active in the hydrogenation of acetophenone and styrene.

I.10. Scope of the PhD thesis work

The above-described discovery of the formation of catalytically active RhNPs in the TPP@CCM-C system forms the foundation of the research work conducted in this PhD thesis work. The overarching research aim of the work was to develop novel solutions to improve the confinement of MNPs, mainly RhNPs, in the CCM-C, to have performant, stable, and recyclable catalytic systems for aqueous biphasic liquid-liquid hydrogenation catalysis as application focus.

To achieve this goal, synthesis tools from CCM polymer chemistry and organometallic nanochemistry were combined and multiple approaches to achieve the sub-objectives outlined below were explored. The primary research outcomes are presented in the following chapters. Novel polymer syntheses incorporating TPPO ligands and polycationic or polyanionic shells were developed to enhance the confinement of

RhNPs and to address substrate limitations, respectively, with the aim of refining their activity, selectivity, and scope. Additionally, CCMs functionalized with different ligands, namely 4-vinylpyridine (VP) and (4-Styryl)diphenylphosphine (SDPP), were developed to further investigate their potential applications in aqueous biphasic hydrogenation and to assess the influence of the support material on catalytic performance. Figure I.23 provides a comprehensive overview of this PhD study's scope.

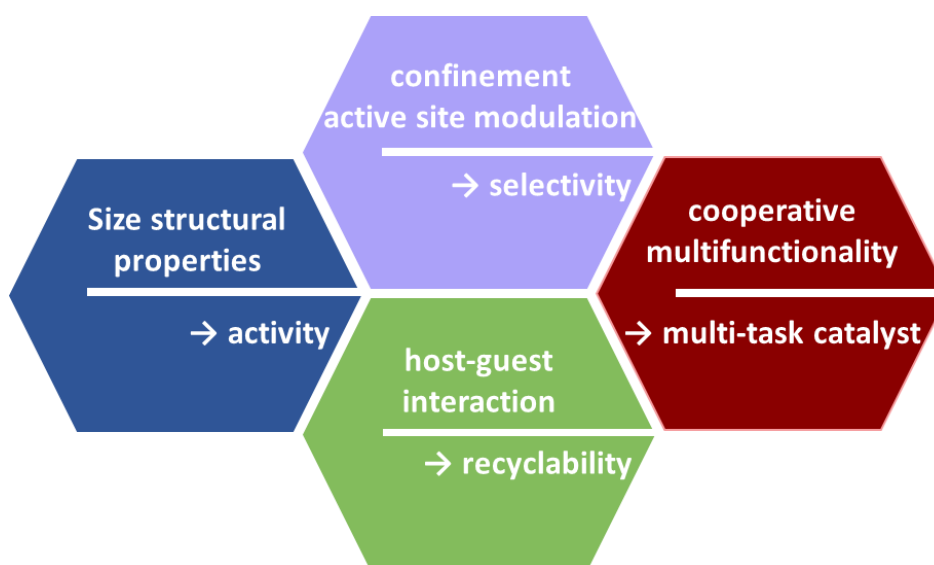


Figure I.23. Scope of the PhD study.

I.11. References

- [1] M. Niyaz Khan, *Micellar Catalysis*; CRC Press (2006) ISBN 9780429133749, <https://doi.org/10.1201/9781420015843>
- [2] Sheldon RA, Arends I, Hanefeld U. *Green Chemistry and Catalysis*. New York: John Wiley & Sons 295 (2007) <https://doi.org/10.1002/9783527611003.ch7>
- [3] O. Nuyken, P. Persigehl, R. Weberskirch *Amphiphilic Poly(Oxazoline)s - Synthesis and Application for Micellar Catalysis*. *Macromol. Symp.* (2002) 163–173, [https://doi.org/10.1002/1521-3900\(200201\)177:1<163::AID-MASY163>3.0.CO;2-W](https://doi.org/10.1002/1521-3900(200201)177:1<163::AID-MASY163>3.0.CO;2-W)

- [4] M. T. De Martino, L. K. E. A. Abdelmohsen, F. P. J. T. Rutjes, J. C. M. van Hest. Nanoreactors for green catalysis. *Beilstein J. Org. Chem.* 14 (2018) 716–33. <https://doi.org/10.3762/bjoc.14.61>
- [5] E. Wiebus, B. Cornils, *Biphasic Systems: Water – Organic, Catalyst Separation, Recovery and Recycling, Catalysis by Metal Complexes* Springer, Dordrecht 30 (2006). https://doi.org/10.1007/1-4020-4087-3_5
- [6] F. Allhoff, P. Lin, D. Moore, *What is nanotechnology and why does it matter? : from science to ethics*, Wiley-Blackwell, (2010) Online ISBN:9781444317992 <https://doi.org/10.1002/9781444317992>
- [7] E.G. Barillon, Onzième Conférence Générale Des Poids Et Mesures, *Comptes Rendus* (1960) 87 <https://doi.org/10.59161/CGPM1960RES12E>
- [8] R. V. Chaudhari, B.M. Bhanage, R. M. Deshpande, H. Delmas, Enhancement of interfacial catalysis in a biphasic system using catalyst-binding ligands, *Nature* 373 (1995) 501-503. <https://doi.org/10.1038/373501a0>
- [9] M. Pera-Titus, L. Leclercq, J.M. Clacens, F. De Campo, V. Nardello-Rataj, Pickering interfacial catalysis for biphasic systems: From emulsion design to green reactions, *Angew. Chem. Int. Ed.* 54 (2015) 2006-2021. <https://doi.org/10.1002/anie.201402069>
- [10] Y. Zhou, Z. Guo, W. Hou, Q. Wang, J. Wang, Polyoxometalate-based phase transfer catalysis for liquid-solid organic reactions: A review. *Catal. Sci. Technol.* 5 (2015) 4324–4335. <https://doi.org/10.1039/c5cy00674k>
- [11] M. Mkosza, M. Fedoryski, Phase Transfer Catalysis-Basic Principles, Mechanism and Specific Features, *Russ. Chem. Bull.* 60 (2011) 2141-2146. <https://doi.org/10.1007/s11172-011-0332-3>
- [12] T. Ooi, K. Maruoka, Recent advances in asymmetric phase-transfer catalysis, *Angew. Chem. Int. Ed.* 46 (2007) 4222–4266. <https://doi.org/10.1002/anie.200601737>
- [13] H. Wang, C. Fliedel, E. Manoury, R. Poli, Core-crosslinked micelles with a poly-anionic poly(styrene sulfonate)-based outer shell made by RAFT polymerization, *Polymer (Guildf)* 243 (2002) 124640. <https://doi.org/10.1016/j.polymer.2022.124640>
- [14] H. Wang, L. Vendrame, C. Fliedel, S. Chen, F. Gayet, F. D’Agosto, M. Lansalot, E. Manoury, R. Poli, Triphenylphosphine-Functionalized Core-Cross-Linked Micelles and Nanogels with a Polycationic Outer Shell: Synthesis and Application in Rhodium-Catalyzed Biphasic Hydrogenations, *Chem. Eur. J.* 27 (2021) 5205–5214, <https://doi.org/10.1002/chem.202004689>

- [15] S.H.A.M. Leenders, R. Gramage-Doria, B. De Bruin, J.N.H. Reek, Transition metal catalysis in confined spaces, *Chem. Soc. Rev.* 44 (2015) 433–448. <https://doi.org/10.1039/c4cs00192c>
- [16] C. Gaeta, P. La Manna, M. De Rosa, A. Soriente, C. Talotta, P. Neri, Supramolecular Catalysis with Self-Assembled Capsules and Cages: What Happens in Confined Spaces, *ChemCatChem* 13 (2021) 1638–1658. <https://doi.org/10.1002/cctc.202001570>
- [17] A. Kilbinger, Controlled and Living Polymerizations. From Mechanisms to Applications. Edited by A. H. E. Müller and K. Matyjaszewski, *Angew. Chem. Int. Ed.* 49 (2010) 1191–1192. <https://doi.org/10.1002/anie.200907064>
- [18] A.H. Gröschel, A.H.E. Müller, Self-assembly concepts for multicompartment nanostructures, *Nanoscale*. 7 (2015) 11841–11876. <https://doi.org/10.1039/c5nr02448j>
- [19] C. Bouilhac, E. Cloutet, D. Taton, A. Deffieux, R. Borsali, H. Cramail, Block copolymer micelles as nanoreactors for single-site polymerization catalysts, *J. Polym. Sci. A Polym. Chem.* 47 (2009) 197–209. <https://doi.org/10.1002/pola.23142>
- [20] J.I. van der Vlugt, T.S. Koblenz, J. Wassenaar, J.N.H. Reek, Chemistry in Self-Assembled Nanoreactors, *Molecular Encapsulation: Organic Reactions in Constrained Systems*, (eds U.H. Brinker and J.-L. Mieusset) (2010) 145–174. <https://doi.org/10.1002/9780470664872.ch6>
- [21] M. Wang, Y. Min, J. Huang, Y. Shi, X. Dong, X. Zhou, X. Yu, D. Qi, Z. Hua, T. Chen, Self-Assembled Catalytic Nanoreactors from Molecular Brushes by Utilizing Postpolymerization Modification for Catalyst Attachment, *ACS Appl. Polym. Mater.* 4 (2022) 1411–1421. <https://doi.org/10.1021/acsapm.1c01484>
- [22] W. Demos, C.R. Bittencourt, L. Nardino, F. Nome, A.P. Gerola, Self-Assembled Multifunctional Nanoreactors for Dephosphorylation Reactions, *ACS Appl. Nano Mater.* 4 (2021) 644–651. <https://doi.org/10.1021/acsanm.0c02943>
- [23] M. Kuepfert, E. Ahmed, M. Weck, Self-Assembled Thermoresponsive Molecular Brushes as Nanoreactors for Asymmetric Aldol Addition in Water, *Macromolecules* 54 (2021) 3845–3853. <https://doi.org/10.1021/acs.macromol.0c02708>
- [24] B.M. Rossbach, K. Leopold, R. Weberskirch, Self-assembled nanoreactors as highly active catalysts in the hydrolytic kinetic resolution (HKR) of epoxides in water, *Angew. Chem. Int. Ed.* 45 (2006) 1309–1312. <https://doi.org/10.1002/anie.200503291>
- [25] J.M. Ren, T.G. McKenzie, Q. Fu, E.H.H. Wong, J. Xu, Z. An, S. Shanmugam, T.P. Davis, C. Boyer, G.G. Qiao, Star Polymers, *Chem. Rev.* 116 (2016) 6743–6836 <https://doi.org/10.1021/acs.chemrev.6b00008>

- [26] D.M. Vriezema, M.C. Aragonès, J.A.A.W. Elemans, J.J.L.M. Cornelissen, A.E. Rowan, R.J.M. Nolte, Self-assembled nanoreactors, *Chem. Rev.* 105 (2005) 1445–1489. <https://doi.org/10.1021/cr0300688>
- [27] R. Syah, M. Zahar, E. Kianfar, Nanoreactors: Properties, applications and characterization, *Int J Chem React Eng.* 19 (2021) 981–1007. <https://doi.org/10.1515/ijcre-2021-0069>
- [28] P. Cotanda, N. Petzetakis, R.K. O'reilly, Catalytic polymeric nanoreactors: More than a solid supported catalyst, *MRS Commun.* 2 (2012) 119–126. <https://doi.org/10.1557/mrc.2012.26>
- [29] C. Deraedt, D. Astruc, Supramolecular nanoreactors for catalysis, *Coord. Chem. Rev.* 324 (2016) 106–122. <https://doi.org/10.1016/j.ccr.2016.07.007>
- [30] V. Mouarrawis, R. Plessius, J.I. van der Vlugt, J.N.H. Reek, Confinement effects in catalysis using well-defined materials and cages, *Front Chem.* 6 (2018). <https://doi.org/10.3389/fchem.2018.00623>
- [31] M.R. Buchmeiser, Catalysis in Confined Spaces, *ChemCatChem* 13 (2021) 785–786. <https://doi.org/10.1002/cctc.202001941>
- [32] R. Poli (Editor), *Effects of Nanoconfinement on Catalysis*, Springer International Publishing (2017), ISBN: 978-3-319-50205-2, <http://www.springer.com/series/5964>
- [33] G. La Sorella, G. Strukul, A. Scarso, Recent advances in catalysis in micellar media, *Green Chem.* 17 (2015) 644–683. <https://doi.org/10.1039/c4gc01368a>
- [34] T. Dwars, E. Paetzold, G. Oehme, Reactions in micellar systems, *Angew. Chem. Int. Ed.* 44 (2005) 7174–7199. <https://doi.org/10.1002/anie.200501365>
- [35] B. Cornils, W. A Herrmann, M. Beller, R. Paciello, Editors, *Applied Homogeneous Catalysis with Organometallic Compounds: A Comprehensive Handbook in Four Volumes*, Wiley-VCH (2017), ISBN: 9783527651733 <https://doi.org/10.1002/9783527651733>
- [36] A. G. Volkov (Editor), *Interfacial Catalysis*, Marcel Dekker, Inc.: New York, Basel. 2003, ISBN 0-8247-0839-3 <https://doi.org/10.1201/9780203910429>
- [37] O. Nuyken, R. Weberskirch, T. Kotre, D. Schönfelder, A. Wörndle, *Polymers for Micellar Catalysis, Polymeric Materials in Organic Synthesis and Catalysis*, Wiley-VCH (2005) 277–304. <https://doi.org/10.1002/3527601856.ch6>

- [38] D. J. Cole-Hamilton, Homogeneous Catalysis--New Approaches to Catalyst Separation, Recovery, and Recycling, *Science* 299 (2003) 1702-1706. <https://doi.org/10.1126/science.1081881>
- [39] E. J. Fendler, J. H. Fendler, Micellar Catalysis in Organic Reactions: Kinetic and Mechanistic Implications, V. Gold (Editor), *Adv. Phys. Org. Chem.* 8 (1970) 271-406. ISBN: 9780120335084. [https://doi.org/10.1016/S0065-3160\(08\)60323-8](https://doi.org/10.1016/S0065-3160(08)60323-8)
- [40] D. Christophe, S. Lionel, E. Laetitia, R. Jaime, A. Didier, "Click" dendrimers as efficient nanoreactors in aqueous solvent: Pd nanoparticle stabilization for sub-ppm Pd catalysis of Suzuki–Miyaura reactions of aryl bromides, *Chem. Commun.* 49 (2013) 8169–8171. <https://doi.org/10.1039/c3cc45132a>
- [41] J. Lu, J. Dimroth, M. Weck, Compartmentalization of Incompatible Catalytic Transformations for Tandem Catalysis, *J. Am. Chem. Soc.* 137 (2015) 12984–12989. <https://doi.org/10.1021/jacs.5b07257>
- [42] L. Onel, N.J. Buurma, Reactivity in organized assemblies, *Annu. Rep. Prog. Chem. Section B* 106 (2010) 344–375. <https://doi.org/10.1039/b927079p>
- [43] S.S. Sambou, R. Hromov, I. Ruzhylo, H. Wang, A. Allandrieu, C. Sabatier, Y. Coppel, J.C. Daran, F. Gayet, A. Labande, E. Manoury, R. Poli, Amphiphilic polymeric nanoreactors containing Rh(I)-NHC complexes for the aqueous biphasic hydrogenation of alkenes, *Catal Sci Technol.* 11 (2021) 6811–6824. <https://doi.org/10.1039/d1cy00554e>
- [44] G. Delaittre, C. Dire, J. Rieger, J.L. Putaux, B. Charleux, Formation of polymer vesicles by simultaneous chain growth and self-assembly of amphiphilic block copolymers, *Chem. Commun.* (2009) 2887–2889. <https://doi.org/10.1039/b903040a>
- [45] M. Steinbeck, G.D. Frey, W.W. Schoeller, W.A. Herrmann, Synthesis and characterization of chiral mono N-heterocyclic carbene-substituted rhodium complexes and their catalytic properties in hydrosilylation reactions, *J. Organomet. Chem.* 696 (2011) 3945–3954. <https://doi.org/10.1016/j.jorganchem.2011.04.001>
- [46] M.R. Nabid, Y. Bide, H40-PCL-PEG unimolecular micelles both as anchoring sites for palladium nanoparticles and micellar catalyst for Heck reaction in water, *Appl. Catal. A Gen.* 469 (2014) 183–190. <https://doi.org/10.1016/j.apcata.2013.09.016>
- [47] M. Galetti, S. Rossi, C. Caffarra, A. G.Gerboles, M. Miragoli, Chapter 9 - Innovation in nanomedicine and engineered nanomaterials for therapeutic purposes, Nelson Marmioli, Jason C. White, Jing Song (Editors), *Micro and Nano Technologies, Exposure to Engineered Nanomaterials in the Environment*, Elsevier (2019) 235-262, ISBN: 9780128148358. <https://doi.org/10.1016/B978-0-12-814835-8.00009-1> .

- [48] R.K. O'Reilly, C.J. Hawker, K.L. Wooley, Cross-linked block copolymer micelles: Functional nanostructures of great potential and versatility, *Chem Soc Rev.* 35 (2006) 1068–1083. <https://doi.org/10.1039/b514858h>
- [49] S. Handa, J.D. Smith, M.S. Hageman, M. Gonzalez, B.H. Lipshutz, Synergistic, and selective copper/ppm Pd-Catalyzed Suzuki–Miyaura couplings: In water, mild conditions, with recycling, *ACS Catal.* 6 (2016) 8179–8183. <https://doi.org/10.1021/acscatal.6b02809>
- [50] M. Lee, C.J. Jang, J.H. Ryu, Supramolecular reactor from self-assembly of rod-coil molecule in an aqueous environment, *J. Am. Chem. Soc.* 126 (2004) 8082–8083. <https://doi.org/10.1021/ja048264z>
- [51] B.H. Lipshutz, S. Ghorai, PQS: A new platform for micellar catalysis. RCM reactions in water, with catalyst recycling, *Org. Lett.* 11 (2009) 705–708. <https://doi.org/10.1021/ol8027829>
- [52] J.N. Israelachvili, D.J. Mitchell, B.W. Ninham, Theory of self-assembly of lipid bilayers and vesicles, *Biochim. Biophys. Acta* 470 (1977) 185–201. [https://doi.org/10.1016/0005-2736\(77\)90099-2](https://doi.org/10.1016/0005-2736(77)90099-2)
- [53] F. D'Agosto, J. Rieger, M. Lansalot, RAFT-Mediated Polymerization-Induced Self-Assembly, *Angew. Chem. Int. Ed.* 59 (2020) 8368–8392. <https://doi.org/10.1002/anie.201911758>
- [54] Y. Wang, X. Zhu, Nanofabrication within unimolecular nanoreactors, *Nanoscale* 12 (2020) 12698–12711 <https://doi.org/10.1039/d0nr02674c>
- [55] W. Blokzijl, J.B.F.N. Engberts, Hydrophobic Effects. Opinions and Facts, *Angew. Chem. Int. Ed.* 32 (1993) 1545–1579. <https://doi.org/10.1002/anie.199315451>
- [56] S.Yusa, P. Bahadur, H. Matsuoka, T. Sato, Editors, *Polymer Micelles*, *Polymers* (2018) ISBN 978-3-03842-808-4. <https://doi.org/10.3390/books978-3-03842-808-4>
- [57] A.O. Moughton, M.A. Hillmyer, T.P. Lodge, Multicompartment block polymer micelles, *Macromolecules* 45 (2012) 2–19. <https://doi.org/10.1021/ma201865s>
- [58] R.K. O'Reilly, Spherical polymer micelles: Nanosized reaction vessels, *Philos. Trans. Royal Soc. A* 365 (2007) 2863–2878. <https://doi.org/10.1098/rsta.2007.0019>
- [59] S.E. Webber, *Polymer Micelles: An Example of Self-Assembling Polymers*, *J. Phys. Chem. B* 102(15) (1998) 2618–2626. <https://doi.org/10.1021/jp980386o>
- [60] P. Zhang, X. Zhang, C. Li, S. Zhou, W. Wu, X. Jiang, Target-Amplified Drug Delivery of Polymer Micelles Bearing Staudinger Ligation, *ACS Appl. Mater. Interfaces.* 11 (2019) 32697–32705. <https://doi.org/10.1021/acsami.9b10295>

- [61] G. Yang, L. Xiao, L. Lamboni, *Bioinspired materials science and engineering*, John Wiley & Sons, Inc (2018). Online ISBN:9781119390350. <https://doi.org/10.1002/9781119390350>
- [62] C.M. Ellis, D. Yuan, F.E. Mózes, J.J. Miller, J.J. Davis, Reversible pH-responsive MRI contrast with paramagnetic polymer micelles, *Chem. Commun.* 59 (2023) 1605–1608. <https://doi.org/10.1039/d2cc06255k>
- [63] X. Wu, Y. Hu, X. Wang, L. Chen, Thermo-responsive polymer micelle-based nanoreactors for intelligent polyoxometalate catalysis, *Catal. Commun.* 58 (2015) 164–168. <https://doi.org/10.1016/j.catcom.2014.09.016>
- [64] N. Suzuki, T. Takabe, Y. Yamauchi, S. Koyama, R. Koike, M. Rikukawa, W.T. Liao, W.S. Peng, F.Y. Tsai, Palladium-catalyzed Mizoroki-Heck reactions in water using thermoresponsive polymer micelles, *Tetrahedron* 75 (2019) 1351–1358. <https://doi.org/10.1016/j.tet.2019.01.047>
- [65] N. Suzuki, R. Akebi, T. Inoue, M. Rikukawa, Y. Masuyama, Asymmetric Aldol Reaction On Water Using An Organocatalyst Tethered On A Thermoresponsive Block Copolymer, *Curr. Organocatal.* 3 (2016) 306-314. <https://doi.org/10.1246/cl.130711>
- [66] P. Cotanda, A. Lu, J.P. Patterson, N. Petzetakis, R.K. O'Reilly, Functionalized organocatalytic nanoreactors: Hydrophobic pockets for acylation reactions in water, *Macromolecules* 45 (2012) 2377–2384. <https://doi.org/10.1021/ma2027462>
- [67] J. C. Ravey and M. Buzier, *Macro- and microemulsions: theory and applications: based on a symposium sponsored by the Division of Industrial and Engineering Chemistry at the 186th Meeting of the American Chemical Society, Washington, D.C., ACS Symposium Series 272 (1985) 253-263* <http://books.google.com/books?id=E8hQAAAAAYAAJ>
- [68] R. Bleul, R. Thiermann, M. Maskos, Techniques to Control Polymersome Size, *Macromolecules* 48 (2015) 7396–7409. <https://doi.org/10.1021/acs.macromol.5b01500>
- [69] L.K.E.A. Abdelmohsen, R.S.M. Rikken, P.C.M. Christianen, J.C.M. van Hest, D.A. Wilson, Shape characterization of polymersome morphologies via light scattering techniques, *Polymer (Guildf)* 107 (2016) 445–449. <https://doi.org/10.1016/j.polymer.2016.06.067>
- [70] E. Lorenceau, A.S. Utada, D.R. Link, G. Cristobal, M. Joanicot, D.A. Weitz, Generation of polymerosomes from double-emulsions, *Langmuir* 21 (2005) 9183–9186. <https://doi.org/10.1021/la050797d>

- [71] H.K. Cho, I.W. Cheong, J.M. Lee, J.H. Kim, Polymeric nanoparticles, micelles and polymersomes from amphiphilic block copolymer, *Korean J. Chem. Eng.* 27 (2010) 731–740. <https://doi.org/10.1007/s11814-010-0216-5>
- [72] J. Lefley, C. Waldron, C.R. Becer, Macromolecular design and preparation of polymersomes, *Polym. Chem.* 11 (2020) 7124–7136. <https://doi.org/10.1039/d0py01247e>
- [73] D.E. Discher, A. Eisenberg, Polymer vesicles, *Science* 297 (2002) 967–973. <https://doi.org/10.1126/science.1074972>
- [74] L. Zang, A. Eisenberg, Multiple Morphologies of "Crew-Cut" Aggregates of Polystyrene-*b*-poly(acrylic acid) Block Copolymers, *Science* 268 (1995) 1728–1731. <https://doi.org/10.1126/science.268.5218.1728>
- [75] J.C.M. Hest, van, D.A.P. Delnoye, M.W.P.L. Baars, M.H.P. Genderen, van, E.W. Meijer Polystyrene-dendrimer amphiphilic block copolymers with a generation-dependent aggregation, *Science* 268 (1995) 1592–1595. <https://doi.org/10.1126/science.268.5217.1592>
- [76] H.C. Shum, D.A. Weitz, Multicompartment polymersome gel for encapsulation, *Soft Matter*. 7 (2011) 8762–8765. <https://doi.org/10.1039/c1sm06026k>
- [77] N.P. Kamat, J.S. Katz, D.A. Hammer, Engineering polymersome protocells, *J Phys Chem. Lett.* 2 (2011) 1612–1623. <https://doi.org/10.1021/jz200640x>
- [78] H. Che, J.C.M. van Hest, Adaptive Polymersome Nanoreactors, *ChemNanoMat*. 5 (2019) 1092–1109. <https://doi.org/10.1002/cnma.201900245>
- [79] M. Nallani, H.P.M. de Hoog, J.J.L.M. Cornelissen, A.R.A. Palmans, J.C.M. van Hest, R.J.M. Nolte, Polymersome nanoreactors for enzymatic ring-opening polymerization, *Biomacromolecules* 8 (2007) 3723–3728. <https://doi.org/10.1021/bm7005938>
- [80] Z. Wang, M.C.M. van Oers, F.P.J.T. Rutjes, J.C.M. van Hest, Polymersome Colloidosomes for Enzyme Catalysis in a Biphasic System, *Angew. Chem.* 124 (2012) 10904–10908. <https://doi.org/10.1002/ange.201206555>
- [81] R.J.R.W. Peters, M. Marguet, S. Marais, M.W. Fraaije, J.C.M. van Hest, S. Lecommandoux, Cascade Reactions in Multicompartmentalized Polymersomes, *Angew. Chem.* 126 (2014) 150–154. <https://doi.org/10.1002/ange.201308141>
- [82] E. Manoury, F. Gayet, F. D'Agosto, M. Lansalot, H. Delmas, C. Julcour, J.-F. Blanco, L. Barthe, R. Poli, Core-Cross-Linked Micelles and Amphiphilic Nanogels as Unimolecular Nanoreactors for Micellar-Type, Metal-Based Aqueous Biphasic

Catalysis, In: Poli, R. (eds) Effects of Nanoconfinement on Catalysis. Fundamental and Applied Catalysis. Springer, (2017) 147–172. https://doi.org/10.1007/978-3-319-50207-6_7

[83] Y. Chevalier, T. Zemb, The structure of micelles and microemulsions, Rep. Prog. Phys. 53 (1990) 279 <https://doi.org/10.1088/0034-4885/53/3/002>

[84] D. J. Mitchell, B. W. Ninham, Micelles, Vesicles and Microemulsions, J. Chem. Soc. Faraday Trans. 2 (1981) 601-629. <https://doi.org/10.1039/F29817700601>

[85] J.F. Gohy, Block copolymer micelles, Adv. Polym. Sci. 190 (2005) 65–136. https://doi.org/10.1007/12_048

[86] M.J. Blandamer, P.M. Cullis, L.G. Soldi, J.B.F.N. Engberts, A. Kacperska, N.M. Van Os, M.C.S. Subha, Thermodynamics of micellar systems: comparison of mass action and phase equilibrium models for the calculation of standard Gibbs energies of micelle formation. Adv. Colloid Interface Sci. 58 (1995) 171–209. [https://doi.org/10.1016/0001-8686\(95\)00252-1](https://doi.org/10.1016/0001-8686(95)00252-1)

[87] P. Qu, M. Kuepfert, E. Ahmed, F. Liu, M. Weck, Cross-Linked Polymeric Micelles as Catalytic Nanoreactors, Eur. J. Inorg. Chem. 2021 (2021) 1420–1427. <https://doi.org/10.1002/ejic.202100013>

[88] K.I. Bruce Thurmond, T. Kowalewski, K.L. Wooley, Water-Soluble Knedel-like Structures: The Preparation of Shell-Cross-Linked Small Particles, J. Am. Chem. Soc. 118 (1996) 7239–7240. <https://doi.org/10.1021/JA961299H>

[89] M. Petriccone, R. Laurent, C.-O. Turrin, R.M. Sebastián, A.-M. Caminade, Specific Bifunctionalization on the Surface of Phosphorus Dendrimers Syntheses and Properties, Organics 3 (2022) 240–261. <https://doi.org/10.3390/org3030018>

[90] A.D. Levins, X. Wang, A.O. Moughton, J. Skey, R.K. O'Reilly, Synthesis of core functionalized polymer micelles and shell cross-linked nanoparticles, Macromolecules 41 (2008) 2998–3006. <https://doi.org/10.1021/ma702702j>

[91] H. Hofmeier, U.S. Schubert, Recent developments in the supramolecular chemistry of terpyridine-metal complexes, Chem. Soc. Rev. 33 (2004) 373–399. <https://doi.org/10.1039/b400653b>

[92] U. S Schubert, C. Eschbaumer, O. Hien, P. R Andres, 4'-Functionalized 2,2':6',2''-terpyridines as building blocks for supramolecular chemistry and nanoscience, Tetrahedron Lett. 42 (2001) 4705-4707. [https://doi.org/10.1016/S0040-4039\(01\)00796-1](https://doi.org/10.1016/S0040-4039(01)00796-1)

- [93] Y. Liu, V. Piñón, M. Weck, Poly(norbornene) block copolymer-based shell cross-linked micelles with Co(III)-salen cores, *Polym. Chem.* 2 (2011) 1964–1975. <https://doi.org/10.1039/c1py00151e>
- [94] Y. Liu, Y. Wang, Y. Wang, J. Lu, V. Piñón, M. Weck, Shell cross-linked micelle-based nanoreactors for the substrate-selective hydrolytic kinetic resolution of epoxides, *J. Am. Chem. Soc.* 133 (2011) 14260–14263. <https://doi.org/10.1021/ja206644d>
- [95] M. Kuepfert, A.E. Cohen, O. Cullen, M. Weck, Shell Cross-Linked Micelles as Nanoreactors for Enantioselective Three-Step Tandem Catalysis, *Chem. Eur. J.* 24 (2018) 18648–18652. <https://doi.org/10.1002/chem.201804956>
- [96] M. Glassner, M. Vergaelen, R. Hoogenboom, Poly(2-oxazoline)s: A comprehensive overview of polymer structures and their physical properties, *Polym. Int.* 67 (2018) 32–45. <https://doi.org/10.1002/pi.5457>
- [97] B. Verbraeken, B.D. Monnery, K. Lava, R. Hoogenboom, The chemistry of poly(2-oxazoline)s, *Eur. Polym. J.* 88 (2017) 451–469. <https://doi.org/10.1016/j.eurpolymj.2016.11.016>
- [98] A.F. Cardozo, E. Manoury, C. Julcour, J.F. Blanco, H. Delmas, F. Gayet, R. Poli, Preparation of Polymer Supported Phosphine Ligands by Metal-Catalyzed Living Radical Copolymerization and Their Application to Hydroformylation Catalysis, *ChemCatChem* 5 (2013) 1161–1169. <https://doi.org/10.1002/cctc.201200446>
- [99] T. Terashima, M. Ouchi, T. Ando, M. Sawamoto, Oxidation of sec-alcohols with Ru(II)-bearing microgel star polymer catalysts via hydrogen transfer reaction: Unique microgel-core catalysis, *J. Polym. Sci. A Polym. Chem.* 49 (2011) 1061–1069. <https://doi.org/10.1002/pola.24501>
- [100] T. Terashima, M. Ouchi, T. Ando, M. Sawamoto, Thermoregulated phase-transfer catalysis via PEG-armed Ru(II)-bearing microgel core star polymers: Efficient and reusable Ru(II) catalysts for aqueous transfer hydrogenation of ketones, *J. Polym. Sci. A Polym. Chem.* 48 (2010) 373–379. <https://doi.org/10.1002/pola.23794>
- [101] M. Ouchi, T. Terashima, M. Sawamoto, Transition metal-catalyzed living radical polymerization: Toward perfection in catalysis and precision polymer synthesis, *Chem. Rev.* 109 (2009) 4963–5050. <https://doi.org/10.1021/cr900234b>
- [102] T. Terashima, M. Kamigaito, K.Y. Baek, T. Ando, M. Sawamoto, Polymer catalysts from polymerization catalysts: Direct encapsulation of metal catalyst into star polymer core during metal-catalyzed living radical polymerization, *J. Am. Chem. Soc.* 125 (2003) 5288–5289. <https://doi.org/10.1021/ja034973l>

- [103] S.L. Canning, G.N. Smith, S.P. Armes, A Critical Appraisal of RAFT-Mediated Polymerization-Induced Self-Assembly, *Macromolecules* 49 (2016) 1985–2001. <https://doi.org/10.1021/acs.macromol.5b02602>
- [104] Y. Niu, Y. Lu, Construction of pH-responsive core crosslinked micelles via thiol-yne click reaction, *J. Appl. Polym. Sci.* 139 (2022) e52753 <https://doi.org/10.1002/app.52753>
- [105] K. Shiraishi, S.I. Yusa, M. Ito, K. Nakai, M. Yokoyama, Photo irradiation-induced core crosslinked poly(ethylene glycol)-block-poly(aspartic acid) micelles: Optimization of block copolymer synthesis and characterization of core crosslinked micelles, *Polymers (Basel)* 9 (2017) 710 <https://doi.org/10.3390/polym9120710>
- [106] S. Kramer, K.O. Kim, R. Zentel, Size Tunable Core Crosslinked Micelles from HPMA-Based Amphiphilic Block Copolymers, *Macromol. Chem. Phys.* 218 (2017) 1700113. <https://doi.org/10.1002/macp.201700113>
- [107] X. Zhang, H. Dong, S. Fu, Z. Zhong, R. Zhuo, Redox-Responsive Micelles with Cores Crosslinked via Click Chemistry, *Macromol. Rapid Commun.* 37 (2016) 993–997. <https://doi.org/10.1002/marc.201600049>
- [108] J. He, Y. Xia, Y. Niu, D. Hu, X. Xia, Y. Lu, W. Xu, pH-responsive core crosslinked polycarbonate micelles via thiol-acrylate Michael addition reaction, *J. Appl. Polym. Sci.* 134 (2017) 44421 <https://doi.org/10.1002/app.44421>
- [109] L. Tian, L. Yam, J. Wang, H. Tat, K.E. Uhrich, Core crosslinkable polymeric micelles from PEG-lipid amphiphiles as drug carriers, *J. Mater. Chem.* 14 (2004) 2317–2324. <https://doi.org/10.1039/b401398k>
- [110] L. Zhang, K. Katapodi, T.P. Davis, C. Barner-Kowollik, M.H. Stenzel, Using the reversible addition-fragmentation chain transfer process to synthesize core-crosslinked micelles, *J. Polym. Sci. A Polym. Chem.* 44 (2006) 2177–2194. <https://doi.org/10.1002/pola.21328>
- [111] H. Wang, C.J. Abou-Fayssal, C. Fliedel, E. Manoury, R. Poli, Phosphine-Functionalized Core-Crosslinked Micelles and Nanogels with an Anionic Poly(styrenesulfonate) Shell: Synthesis, Rhodium(I) Coordination and Aqueous Biphasic Hydrogenation Catalysis, *Polymers (Basel)* 14 (2022) 4937. <https://doi.org/10.3390/polym14224937>
- [112] X. Zhang, A.F. Cardozo, S. Chen, W. Zhang, C. Julcour, M. Lansalot, J.F. Blanco, F. Gayet, H. Delmas, B. Charleux, E. Manoury, F. D'Agosto, R. Poli, Core-Shell Nanoreactors for Efficient Aqueous Biphasic Catalysis, *Chem. Eur. J.* 20 (2014) 15505–15517. <https://doi.org/10.1002/chem.201403819>

- [113] A.F. Cardozo, C. Julcour, L. Barthe, J.F. Blanco, S. Chen, F. Gayet, E. Manoury, X. Zhang, M. Lansalot, B. Charleux, F. D'Agosto, R. Poli, H. Delmas, Aqueous phase homogeneous catalysis using core-shell nanoreactors: Application to rhodium-catalyzed hydroformylation of 1-octene, *J. Catal.* 324 (2015) 1–8. <https://doi.org/10.1016/j.jcat.2015.01.009>
- [114] S. Chen, F. Gayet, E. Manoury, A. Joumaa, M. Lansalot, F. D'Agosto, R. Poli, Coordination Chemistry Inside Polymeric Nanoreactors: Interparticle Metal Exchange and Ionic Compound Vectorization in Phosphine-Functionalized Amphiphilic Polymer Latexes, *Chem. Eur. J.* 22 (2016) 6302–6313. <https://doi.org/10.1002/chem.201504923>
- [115] S. Chen, E. Manoury, F. Gayet, R. Poli, Coordination chemistry inside polymeric nanoreactors: Metal migration and cross-exchange in amphiphilic core-shell polymer latexes, *Polymers (Basel)* 8 (2016) 26. <https://doi.org/10.3390/polym8020026>
- [116] A. Joumaa, S. Chen, S. Vincendeau, F. Gayet, R. Poli, E. Manoury, Rhodium-catalyzed aqueous biphasic hydrogenation of alkenes with amphiphilic phosphine-containing core-shell polymers, *Mol. Catal.* 438 (2017) 267–271. <https://doi.org/10.1016/j.mcat.2017.06.005>
- [117] A. Joumaa, F. Gayet, E.J. Garcia-Suarez, J. Himmelstrup, A. Riisager, R. Poli, E. Manoury, Synthesis of nixantphos core-functionalized amphiphilic nanoreactors and application to rhodium-catalyzed aqueous biphasic 1-octene hydroformylation, *Polymers (Basel)* 12 (2020), 1107. <https://doi.org/10.3390/POLYM12051107>
- [118] H. Wang, L. Vendrame, C. Fliedel, S. Chen, F. Gayet, E. Manoury, X. Zhang, F. D'agosto, M. Lansalot, R. Poli, Core-Cross-Linked Micelles Made by RAFT Polymerization with a Polycationic Outer Shell Based on Poly(1-methyl-4-vinylpyridinium), *Macromolecules.* 53 (2020) 2198–2208. <https://doi.org/10.1021/acs.macromol.9b02582>
- [119] H. Wang, L. Vendrame, C. Fliedel, S. Chen, F. Gayet, F. D'Agosto, M. Lansalot, E. Manoury, R. Poli, Triphenylphosphine-Functionalized Core-Cross-Linked Micelles and Nanogels with a Polycationic Outer Shell: Synthesis and Application in Rhodium-Catalyzed Biphasic Hydrogenations, *Chem. Eur. J.* 27 (2021) 5205–5214. <https://doi.org/10.1002/chem.202004689>
- [120] H. Wang, A.M. Fiore, C. Fliedel, E. Manoury, K. Philippot, M.M. Dell'Anna, P. Mastrorilli, R. Poli, Rhodium nanoparticles inside well-defined unimolecular amphiphilic polymeric nanoreactors: Synthesis and biphasic hydrogenation catalysis, *Nanoscale Adv.* 3 (2021) 2554–2566. <https://doi.org/10.1039/d1na00028d>

- [121] L.B. Hunt, The True Story of Purple of Cassius. *Gold Bull* 9, (1976) 134–139. <https://doi.org/10.1007/BF03215423>
- [122] Crellius, D. Laurentius. “Nova Experimenta Chemica Quae Ad Penitiorem Acidi e Pinguedine Eruti Cognitionem Valere Videntur. Scriebat D. Laurentius Crellius, Gulielmo Huntero, M. D. S. R. S.” *Philos. trans. R. Soc. Lond., A* (1782): 8–34. <http://www.jstor.org/stable/106445> .
- [123] T. Graham, Liquid Diffusion Applied to Analysis, *Philos. trans. R. Soc. Lond., A*, 151 (1861) 183-224 <https://about.jstor.org/terms>.
- [124] P. Adogu, I. Udigwe, G. Udigwe, C. Ubajaka, Wood, R. W. *Philosophical Magazine Series 6* 1902, 4, 396, *Int J Clin Med.* 05 (2014) 940–948. <https://doi.org/10.4236/ijcm.2014.515126>
- [125] C.G. Abbot, Wood, R. W. *Philosophical Magazine Series 6* 1912, 24, 316, *The London, Edinburgh, and Dublin Philosophical Magazine and Journal of Science.* 18 (1909) 32–35. <https://doi.org/10.1080/14786440708636670>
- [126] B. Stout, N. Bonod, Gustav Mie: the man, the theory. *Photoniques.* (2020) 22–26. <https://doi.org/10.1051/photon/202010122>
- [127] D. G. Rickerby, G. Valdrè, U. Valdrè, *Impact of Electron and Scanning Probe Microscopy on Materials Research*, Springer Dordrecht, (1999) ISBN : 978-0-7923-5940-1 <https://doi.org/10.1007/978-94-011-4451-3>
- [128] M. Von Ardenne, P. Hawkes, T. Mulvey, On the history of scanning electron microscopy, of the electron microprobe, and of early contributions to transmission electron microscopy, *Adv in Imaging and Elect Physics.* 220 (2021) 25–50. <https://doi.org/10.1016/bs.aiep.2021.08.002>
- [129] P. Mulvaney, Nanoscience vs nanotechnology-defining the field, *ACS Nano.* 9 (2015) 2215–2217. <https://doi.org/10.1021/acsnano.5b01418>
- [130] C.A. Mirkin, The beginning of a small revolution, *Small.* 1 (2005) 14–16. <https://doi.org/10.1002/sml.200400092>
- [131] G. Prieto, J. Zečević, H. Friedrich, K.P. De Jong, P.E. De Jongh, Towards stable catalysts by controlling collective properties of supported metal nanoparticles, *Nat Mater.* 12 (2013) 34–39. <https://doi.org/10.1038/nmat3471>
- [132] N. Nitta, F. Wu, J.T. Lee, G. Yushin, Li-ion battery materials: Present and future, *Mat Today.* 18 (2015) 252–264. <https://doi.org/10.1016/j.mattod.2014.10.040>

- [133] John D. Aiken, Richard G. Finke, A review of modern transition-metal nanoclusters: their synthesis, characterization, and applications in catalysis, *J Mol Cat : Chem* 145(1-2) (1999) 1-44, [https://doi.org/10.1016/S1381-1169\(99\)00098-9](https://doi.org/10.1016/S1381-1169(99)00098-9)
- [134] M. Okumura, T. Fujitani, J. Huang, T. Ishida, A Career in Catalysis: Masatake Haruta, *ACS Catal.* 5 (2015) 4699–4707. <https://doi.org/10.1021/acscatal.5b01122>
- [135] G. Schmid, Large metal clusters and colloids — Metals in the embryonic state. In: Rehage, H., Peschel, G. (eds) *Structure, Dynamics and Properties of Disperse Colloidal Systems*. Prog. Colloid Polym. Sci, Steinkopff. 111. (1998). <https://doi.org/10.1007/BFb0118109>
- [136] E. Roduner, Size matters: Why nanomaterials are different, *Chem Soc Rev.* 35 (2006) 583–592. <https://doi.org/10.1039/b502142c>
- [137] A.P. Alivisatos, Semiconductor Clusters, Nanocrystals, and Quantum Dots, *Science*, 271(5251) (1996) 933–937 <https://doi.org/10.1126/science.271.5251.933>
- [138] P. Khanna, A. Kaur, D. Goyal, Algae-based metallic nanoparticles: Synthesis, characterization and applications, *J Microbiol Methods*. 163 (2019). <https://doi.org/10.1016/j.mimet.2019.105656>
- [139] C. Contini, J.W. Hindley, T.J. Macdonald, J.D. Barritt, O. Ces, N. Quirke, Size dependency of gold nanoparticles interacting with model membranes, *Commun Chem.* 3 (2020). <https://doi.org/10.1038/s42004-020-00377-y>
- [140] P. Suchomel, L. Kvitek, R. Prucek, A. Panacek, A. Halder, S. Vajda, R. Zboril, Simple size-controlled synthesis of Au nanoparticles and their size-dependent catalytic activity, *Sci Rep.* 8 (2018). <https://doi.org/10.1038/s41598-018-22976-5>
- [141] R. Jin, Y. Cao, C.A. Mirkin, K.L. Kelly, G.C. Schatz, J.G. Zheng, Photoinduced conversion of silver nanospheres to nanoprisms, *Science* (1979). 294 (2001) 1901–1903. <https://doi.org/10.1126/science.1066541>
- [142] C. Amiens, D. Ciuculescu-Pradines, K. Philippot, Controlled metal nanostructures: Fertile ground for coordination chemists, *Coord Chem Rev.* 308 (2016) 409–432. <https://doi.org/10.1016/j.ccr.2015.07.013>
- [143] A. de la Hoz, A. Loupy, *Microwaves in organic synthesis*, Wiley-VCH Verlag GmbH & Co (2012) Online ISBN:9783527651313 <https://doi.org/10.1002/9783527651313>
- [144] N. Baig, I. Kammakakam, W. Falath, I. Kammakakam, Nanomaterials: A review of synthesis methods, properties, recent progress, and challenges, *Mater Adv.* 2 (2021) 1821–1871. <https://doi.org/10.1039/d0ma00807a>

- [145] S. Sakthivel, V. V. Krishnan, B. Pitchumani, Influence of suspension stability on wet grinding for production of mineral nanoparticles, *Particuology*. 6 (2008) 120–124. <https://doi.org/10.1016/j.partic.2007.12.001>
- [146] Y. Guari, C. Thieuleux, A. Mehdi, C. Reyé, R.J.P. Corriu, S. Gomez-Gallardo, K. Philippot, B. Chaudret, R. Dutartre, In situ formation of gold nanoparticles within functionalized ordered mesoporous silica via an organometallic “chimie douce” approach, *Chem Comm.* (2001) 1374–1375. <https://doi.org/10.1039/b102575a>
- [147] M. Brust, M. Walker, D. Bethell, D.J. Schiffrin, R. Whyman, Synthesis of Thiol-derivatised Gold Nanoparticles in a Two-phase Liquid-Liquid System, *J. Chem. Soc. Chem. Commun.* (1994) 801-802. <https://doi.org/10.1039/C39940000801>
- [148] H. Bönemann, G. A. Braun, W. Brijoux, R. Brinkmann, A. Schulze Tilling, K. Seevogel, K. Siepen. Nanoscale colloidal metals and alloys stabilized by solvents and surfactants Preparation and use as catalyst precursors. *J Organomet. Chem* 520 (1996) 143-162. [https://doi.org/10.1016/0022-328X\(96\)06273-0](https://doi.org/10.1016/0022-328X(96)06273-0)
- [149] C. Burda, X. Chen, R. Narayanan, M.A. El-Sayed, Chemistry and properties of nanocrystals of different shapes, *Chem Rev.* 105 (2005) 1025–1102. <https://doi.org/10.1021/cr030063a>
- [150] K.J. Klabunde, Ryan. Richards, *Nanoscale materials in chemistry.*, Wiley, 2009. online ISBN:9780470523674 <https://doi.org/10.1002/9780470523674>
- [151] A. Pitto-Barry, N.P.E. Barry, Effect of Temperature on the Nucleation and Growth of Precious Metal Nanocrystals, *Angew Chem* 131 (2019) 18653–18657. <https://doi.org/10.1002/ange.201912219>
- [152] H. Goesmann, C. Feldmann, Nanoparticulate functional materials, *Angew Chem Int Ed* 49 (2010) 1362–1395. <https://doi.org/10.1002/anie.200903053>
- [153] S. Wegner, C. Janiak, Metal Nanoparticles in Ionic Liquids, *Top Curr Chem.* 375 (2017). <https://doi.org/10.1007/s41061-017-0148-1>
- [154] T.P. Doan-Nguyen, S. Jiang, K. Koynov, K. Landfester, D. Crespy, Ultrasmall Nanocapsules Obtained by Controlling Ostwald Ripening, *Angew Chem Int Ed.* 60 (2021) 18094–18102. <https://doi.org/10.1002/anie.202103444>
- [155] E.Y. Bol’Shagin, V.I. Roldughin, Kinetics of nucleation and growth of metal nanoparticles in the presence of surfactants, *Colloid Journal.* 74 (2012) 649–654. <https://doi.org/10.1134/S1061933X12060038>

- [156] A Borsla, A.M Wilhelm, H Delmas, Hydrogenation of olefins in aqueous phase, catalyzed by polymer-protected rhodium colloids: kinetic study, *Cat Today*, 66(2–4) (2001) 389–395 [https://doi.org/10.1016/S0920-5861\(00\)00635-0](https://doi.org/10.1016/S0920-5861(00)00635-0)
- [157] H. Bönemann, R.M. Richards, Nanoscopic metal particles - Synthetic methods and potential applications, *Eur J Inorg Chem.* (2001) 2455–2480. [https://doi.org/10.1002/1099-0682\(200109\)2001:10<2455::aid-ejic2455>3.0.co;2-z](https://doi.org/10.1002/1099-0682(200109)2001:10<2455::aid-ejic2455>3.0.co;2-z)
- [158] Turkevich, J., & Kim, G. Palladium: preparation and catalytic properties of particles of uniform size. *Science (New York, N.Y.)*, 169(3948) (1970) 873–879. <https://doi.org/10.1126/science.169.3948.873>.
- [159] F. Fievet, S. Ammar-Merah, R. Brayner, F. Chau, M. Giraud, F. Mammeri, J. Peron, J.Y. Piquemal, L. Sicard, G. Viau, The polyol process: a unique method for easy access to metal nanoparticles with tailored sizes, shapes and compositions, *Chem Soc Rev.* 47 (2018) 5187–5233. <https://doi.org/10.1039/c7cs00777a>
- [160] A. Denicourt-Nowicki, A. Roucoux, Odyssey in Polyphasic Catalysis by Metal Nanoparticles, *Chemical Record.* (2016) 2127–2141. <https://doi.org/10.1002/tcr.201600050>
- [161] N.T.T. Chau, S. Handjani, J.P. Guegan, M. Guerrero, E. Monflier, K. Philippot, A. Denicourt-Nowicki, A. Roucoux, Methylated β -Cyclodextrin-Capped Ruthenium Nanoparticles: Synthesis Strategies, Characterization, and Application in Hydrogenation Reactions, *ChemCatChem.* 5 (2013) 1497–1503. <https://doi.org/10.1002/cctc.201200718>
- [162] F. Martinez-Espinar, P. Blondeau, P. Nolis, B. Chaudret, C. Claver, S. Castellón, C. Godard, NHC-stabilised Rh nanoparticles: Surface study and application in the catalytic hydrogenation of aromatic substrates, *J Catal.* 354 (2017) 113–127. <https://doi.org/10.1016/j.jcat.2017.08.010>
- [163] E. Guyonnet Bilé, R. Sassine, A. Denicourt-Nowicki, F. Launay, A. Roucoux, New ammonium surfactant-stabilized rhodium(0) colloidal suspensions: Influence of novel counter-anions on physico-chemical and catalytic properties, *Dalton Trans* 40 (2011) 6524–6531. <https://doi.org/10.1039/c0dt01763a>
- [164] S.A. Stratton, K.L. Luska, A. Moores, Rhodium nanoparticles stabilized with phosphine functionalized imidazolium ionic liquids as recyclable arene hydrogenation catalysts, *Catal Today.* 183 (2012) 96–100. <https://doi.org/10.1016/j.cattod.2011.09.016>
- [165] M.R. Axet, S. Castellón, C. Claver, K. Philippot, P. Lecante, B. Chaudret, Chiral diphosphite-modified rhodium(0) nanoparticles: Catalyst reservoir for styrene

hydroformylation, *Eur J Inorg Chem.* (2008) 3460–3466. <https://doi.org/10.1002/ejic.200800421>

[166] L. Zaramello, B.L. Albuquerque, J.B. Domingos, K. Philippot, Kinetic investigation into the chemoselective hydrogenation of α,β -unsaturated carbonyl compounds catalyzed by Ni(0) nanoparticles, *Dalton Trans.* 46 (2017) 5082–5090. <https://doi.org/10.1039/c7dt00649g>

[167] J. Creus, L. Mallón, N. Romero, R. Bofill, A. Moya, J.L.G. Fierro, R. Mas-Ballesté, X. Sala, K. Philippot, J. García-Antón, Ruthenium Nanoparticles Supported on Carbon Microfibers for Hydrogen Evolution Electrocatalysis, *Eur J Inorg Chem.* 2019 (2019) 2071–2077. <https://doi.org/10.1002/ejic.201801438>

[168] P. Lara, K. Philippot, B. Chaudret, Organometallic Ruthenium Nanoparticles: A Comparative Study of the Influence of the Stabilizer on their Characteristics and Reactivity, *ChemCatChem.* 5 (2013) 28–45. <https://doi.org/10.1002/cctc.201200666>

[169] T. Ayvalı, P. Lecante, P.F. Fazzini, A. Gillet, K. Philippot, B. Chaudret, Facile synthesis of ultra-small rhenium nanoparticles, *Chem Comm.* 50 (2014) 10809–10811. <https://doi.org/10.1039/c4cc04816d>

[170] S. Carencó, C. Boissière, L. Nicole, C. Sanchez, P. Le Floch, N. Mézailles, Controlled design of Size-tunable monodisperse nickel nanoparticles, *Chem Mat.* 22 (2010) 1340–1349. <https://doi.org/10.1021/cm902007g>

[171] E. Redel, R. Thomann, C. Janiak, Use of ionic liquids (ILs) for the IL-anion size-dependent formation of Cr, Mo and W nanoparticles from metal carbonyl $M(\text{CO})_6$ precursors, *Chem Comm.* (2008) 1789–1791. <https://doi.org/10.1039/b718055a>

[172] C. Amiens, B. Chaudret, D. Ciuculescu-Pradines, V. Collière, K. Fajerweg, P. Fau, M. Kahn, A. Maisonnat, K. Soulantica, K. Philippot, Organometallic approach for the synthesis of nanostructures, *New J Chem.* 37 (2013) 3374–3401. <https://doi.org/10.1039/c3nj00650f>

[173] L.M. Martínez-Prieto, B. Chaudret, Organometallic Ruthenium Nanoparticles: Synthesis, Surface Chemistry, and Insights into Ligand Coordination, *Acc Chem Res.* 51 (2018) 376–384. <https://doi.org/10.1021/acs.accounts.7b00378>

[174] C. Pan, K. Pelzer, K. Philippot, B. Chaudret, F. Dassenoy, P. Lecante, M.J. Casanove, Ligand-stabilized ruthenium nanoparticles: Synthesis, organization, and dynamics, *J Am Chem Soc.* 123 (2001) 7584–7593. <https://doi.org/10.1021/ja003961m>

[175] P. Serp, K. Philippot Editors, *Nanomaterials in Catalysis* Wiley-VCH (2012). Online ISBN:9783527656875. <https://doi.org/10.1002/9783527656875>

- [176] D. Astruc Editor, *Nanoparticles and Catalysis*, Wiley-VCH, (2007). Online ISBN:978352762132.3 <https://doi.org/10.1002/9783527621323>
- [177] B. Chaudret, K. Philippot, *Organometallic nanoparticles of metals or metal oxides*, *Oil and Gas Science and Technology*. 62 (2007) 799–817. <https://doi.org/10.2516/ogst:2007062>
- [178] A. Roucoux, J. Schulz, H. Patin, *Reduced transition metal colloids: A novel family of reusable catalysts?*, *Chem Rev.* 102 (2002) 3757–3778. <https://doi.org/10.1021/cr010350j>
- [179] D. Astruc, F. Lu, J.R. Aranzaes, *Nanoparticles as recyclable catalysts: The frontier between homogeneous and heterogeneous catalysis*, *Angew Chem Int Ed.* 44 (2005) 7852–7872. <https://doi.org/10.1002/anie.200500766>
- [180] M. Guerrero, N.T.T. Chau, S. Noël, A. Denicourt-Nowicki, F. Hapiot, A. Roucoux, E. Monflier, K. Philippot, *About the Use of Rhodium Nanoparticles in Hydrogenation and Hydroformylation Reactions*, *Curr Org Chem* 17 (2013) 364-399 <https://doi.org/10.2174/1385272811317040006>
- [181] J.L. Castelbou, E. Bresó-Femenia, P. Blondeau, B. Chaudret, S. Castellón, C. Claver, C. Godard, *Tuning the selectivity in the hydrogenation of aromatic ketones catalyzed by similar ruthenium and rhodium nanoparticles*, *ChemCatChem.* 6 (2014) 3160–3168. <https://doi.org/10.1002/cctc.201402524>
- [182] M. Ibrahim, R. Poreddy, K. Philippot, A. Riisager, E.J. Garcia-Suarez, *Chemoselective hydrogenation of arenes by PVP supported Rh nanoparticles*, *Dalton Trans.* 45 (2016) 19368–19373. <https://doi.org/10.1039/C6DT03668F>
- [183] S. Kozuch, J.M.L. Martin, *“Turning over” definitions in catalytic cycles*, *ACS Catal.* 2 (2012) 2787–2794. <https://doi.org/10.1021/cs3005264>
- [184] M. Boudart, "A Aldag, J.E. Benson, N.A. Dougharty, G. Girvin Harkins, *On the Specific Activity of Platinum Catalysts*, n.d.
- [185] H. Rafatijo, D.L. Thompson, *General application of Tolman’s concept of activation energy*, *J Chem Phys.* 147 (2017). <https://doi.org/10.1063/1.5009751>
- [186] Z.A. Piskulich, O.O. Mesele, W.H. Thompson, *Removing the barrier to the calculation of activation energies: Diffusion coefficients and reorientation times in liquid water*, *J Chem Phys.* 147 (2017). <https://doi.org/10.1063/1.4997723>
- [187] J.L. Pellegatta, C. Blandy, V. Collière, R. Choukroun, B. Chaudret, P. Cheng K. Philippot. *Catalytic investigation of rhodium nanoparticles in the hydrogenation of*

benzene and phenylacetylene. *J Mol Catal A-chem* 178 (2002) 55-61
[https://doi.org/10.1016/s1381-1169\(01\)00298-9](https://doi.org/10.1016/s1381-1169(01)00298-9)

[188] M. V. Escárcega-Bobadilla, C. Tortosa, E. Teuma, C. Pradel, A. Orejón, M. Gómez, A.M. Masdeu-Bultó, Ruthenium, and rhodium nanoparticles as catalytic precursors in supercritical carbon dioxide, *Catal Today*. 148 (2009) 398–404.
<https://doi.org/10.1016/j.cattod.2009.07.112>

[189] C. Vollmer, E. Redel, K. Abu-Shandi, R. Thomann, H. Manyar, C. Hardacre, C. Janiak, Microwave irradiation for the facile synthesis of transition-metal nanoparticles (NPs) in ionic liquids (ILs) from metal-carbonyl precursors and Ru-, Rh-, and Ir-NP/IL dispersions as biphasic liquid-liquid hydrogenation nanocatalysts for cyclohexene, *Chem Eur J*. 16 (2010) 3849–3858. <https://doi.org/10.1002/chem.200903214>

[190] M.L. Buil, M.A. Esteruelas, S. Niembro, M. Oliván, L. Orzechowski, C. Pelayo, A. Vallribera, Dehalogenation and hydrogenation of aromatic compounds catalyzed by nanoparticles generated from rhodium bis(imino)pyridine complexes, *Organomet*. 29 (2010) 4375–4383. <https://doi.org/10.1021/om1003072>

[191] J.A. Widegren, R.G. Finke, A review of the problem of distinguishing true homogeneous catalysis from soluble or other metal-particle heterogeneous catalysis under reducing conditions, *J Mol Catal A Chem*. 198 (2003) 317–341.
[https://doi.org/10.1016/S1381-1169\(02\)00728-8](https://doi.org/10.1016/S1381-1169(02)00728-8)

[192] S.A. Stratton, K.L. Luska, A. Moores, Rhodium nanoparticles stabilized with phosphine functionalized imidazolium ionic liquids as recyclable arene hydrogenation catalysts, *Catal Today*. 183 (2012) 96–100.
<https://doi.org/10.1016/j.cattod.2011.09.016>

[193] L.M. Rossi, L.L.R. Vono, M.A.S. Garcia, T.L.T. Faria, J.A. Lopez-Sanchez, Screening of soluble rhodium nanoparticles as a precursor for highly active hydrogenation catalysts: The effect of the stabilizing agents, *Top Catal*. 56 (2013) 1228–1238. <https://doi.org/10.1007/s11244-013-0089-z>

[194] A. Denicourt-Nowicki, A. Roucoux, From hydroxycetylammmonium salts to their chiral counterparts. A library of efficient stabilizers of Rh(0) nanoparticles for catalytic hydrogenation in water, *Catal Today*. 247 (2015) 90–95.
<https://doi.org/10.1016/j.cattod.2014.05.031>

[195] J.L. Castelbou, P. Blondeau, C. Claver, C. Godard, Surface characterization of phosphine and phosphite stabilized Rh nanoparticles: a model study, *RSC Adv*. 5 (2015) 97036–97043. <https://doi.org/10.1039/c5ra21835g>

[196] M. Ibrahim, M.A.S. Garcia, L.L.R. Vono, M. Guerrero, P. Lecante, L.M. Rossi, K. Philippot, Polymer: Versus phosphine stabilized Rh nanoparticles as components of

supported catalysts: Implication in the hydrogenation of cyclohexene model molecule, Dalton Trans. 45 (2016) 17782–17791. <https://doi.org/10.1039/c6dt03104h>

Chapter II: Experimental section

II.1. Material and Method

II.1.1. General Method

All manipulations were carried out using Schlenk-line techniques under an inert atmosphere of dry argon. Toluene (99%, Sigma-Aldrich; dried on SPS), diethyl ether (>99%, Sigma Aldrich), mercury (Hg, 99.9999 Suprapur©, Sigma-Aldrich; Note: Hg should be handled with utmost care using proper safety precautions), phenylacetylene (98%, Sigma-Aldrich), *cis*-stilbene (96%, Sigma-Aldrich), 5-nonanone (98%, Sigma-Aldrich), 3-hexyne (>99%, Sigma Aldrich), *trans*-2-hexen-1-al (98%, Sigma-Aldrich), 2-cyclohexan-1-one (≥95%, Sigma-Aldrich), (4-Styryl)diphenylphosphine (SDPP, 97%, Aldrich), 4,4'-azobis(4-cyanopentanoic acid) (ACPA, >98%, Fluka), diethylene glycol dimethacrylate (DEGDMA, 95%, Sigma-Aldrich) and hydrogen (99.999%, Air Liquid), sodium 4-vinylbenzenesulfonate (SS-Na⁺, >90%, Aldrich), tri-n-octylphosphine (TOP, >97%, Sigma Aldrich), deuterated chloroform (CDCl₃, 99.8 atom %D, Sgima-Aldrich), deuterated dimethyl sulfoxide (DMSO-d₆, 99.9 atom %D, Sigma-Aldrich), deuterated water (D₂O, 99.8 atom %D, Sigma-Aldrich), N,N-dimethylformamide (DMF anhydrous, 99.8%, Sigma-Aldrich), hydrogen peroxide (H₂O₂, 34.5-36.5% Sigma-Aldrich), sodium bicarbonate (NaHCO₃, ≥99.7% Sigma-Aldrich), sodium chloride (NaCl, ≥99.0% Sigma-Aldrich), triethylamine (NEt₃, ≥99.5%, Sigma-Aldrich), iodomethane (MeI, ≥99.0%, Sigma-Aldrich), pyridine (≥99.0%, Sigma-Aldrich), triphenylphosphine (TPP, 99%, Sigma-Aldrich), triphenylphosphine oxide (TPPO 99%, Sigma-Aldrich), Chloro(1,5-cyclooctadiene)rhodium(I) dimer ([Rh(COD)(μ-Cl)]₂, >98%, Sigma-Aldrich), Bis(1,5-cyclooctadiene)nickel(0) ([Ni(COD)₂], >98%, Sigma-Aldrich), Nickel(II) acetylacetonate ([Ni(acac)₂], >98%, Sigma-Aldrich), were used as received. 4-Vinyl pyridine (4VP, 95%, Sigma), styrene (St, 99%, Acros), and oleylamine (>97%, Sigma

Aldrich) were distilled under reduced pressure prior to use. The RAFT agent 4-cyano-4-thiothiopropylsulfanyl pentanoic acid (CTPPA) or R_0 -SC(S)*SnPr* ($R_0 = C(CH_3)(CN)CH_2CH_2COOH$) [1] and 1-methyl-4-vinylpyridinium iodide (4VPM e^+I^-) were prepared according to previously described methods [2]. The R_0 -(4VPM e^+I^-) $_{140}$ -SC(S)*SnPr* and R_0 -(SS $^-Na^+$) $_{140}$ -*b-St* $_{50}$ -SC(S)*SnPr* macroRAFT agent were synthesized as described in a recent contribution [3]. The deionized water used for the syntheses and for the dynamic light scattering (DLS) analyses was obtained from a Purelab Classic UV system (Elga Lab-Water).

II.1.2. Autoclaves used at the Technical University of Denmark

The autoclaves used for the syntheses of RhNPs and for the catalytic hydrogenations have a volume of 15 mL and were homebuilt. A typical reaction procedure was performed in a 40 x 20 mm vial, and a magnetic crossbar (Figure II.1)

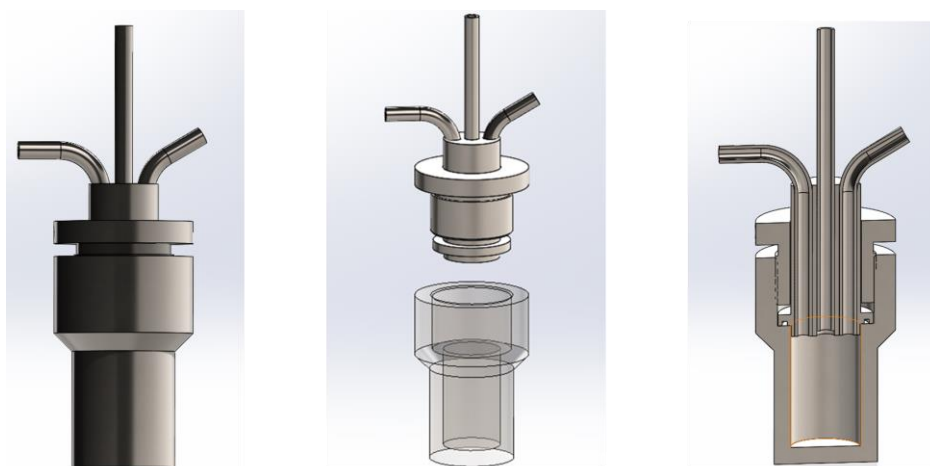


Figure II.1. Autoclaves used in the syntheses of RhNPs and the catalytical studies at DTU.

II.1.3. Autoclaves used at Laboratoire de Chimie de Coordination

The 4650 Series Reactors have a capacity of 100 ml (Figure II.2). Typical reaction procedure was performed in a 45 x 15mm vial and the stirring was ensured by a standard cylindrical magnetic stir bar.

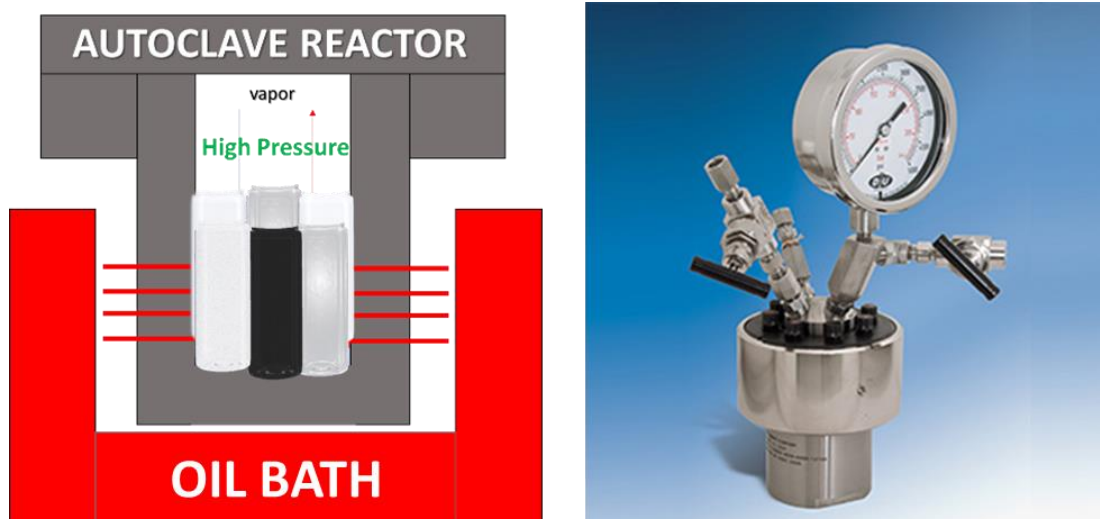


Figure II.2. Autoclaves used in the syntheses of RhNPs and the catalytic studies at LCC.

II.1.4. Autoclaves used at Institut Français du Pétrole, Energies Nouvelles

The autoclaves used for the syntheses of NiNPs and for the catalytic hydrogenations have a volume of 30 mL provided by IFPEN. A typical reaction procedure was performed directly in the reactors with mechanical stirring (Figure II.3).

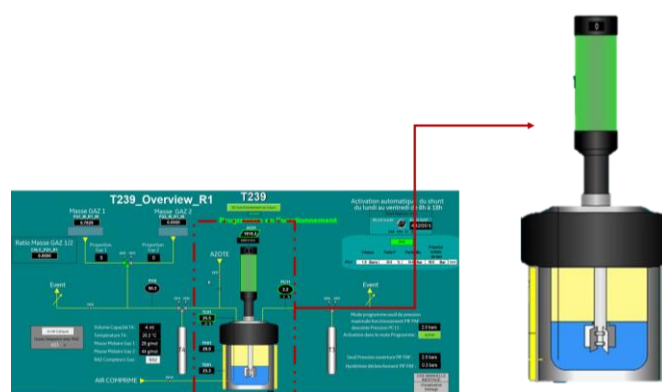


Figure II.3. Autoclaves used in the syntheses of NiNPs and the catalytic studies at IFPEN.

II.1.5. Set-up used in LCC vs DTU

The first catalytic studies, conducted at LCC, made use of a 100 mL autoclave, the reaction vessel was a 45 x 15mm vial and the stirring was ensured by a standard cylindrical magnetic stir bar. At DTU, on the other hand, the equipment consisted of

a 15 mL autoclave, a 40 x 20 mm vial, and a magnetic cross bar. These differences alerted us to the possible existence of different diffusion conditions (Figure II.4).

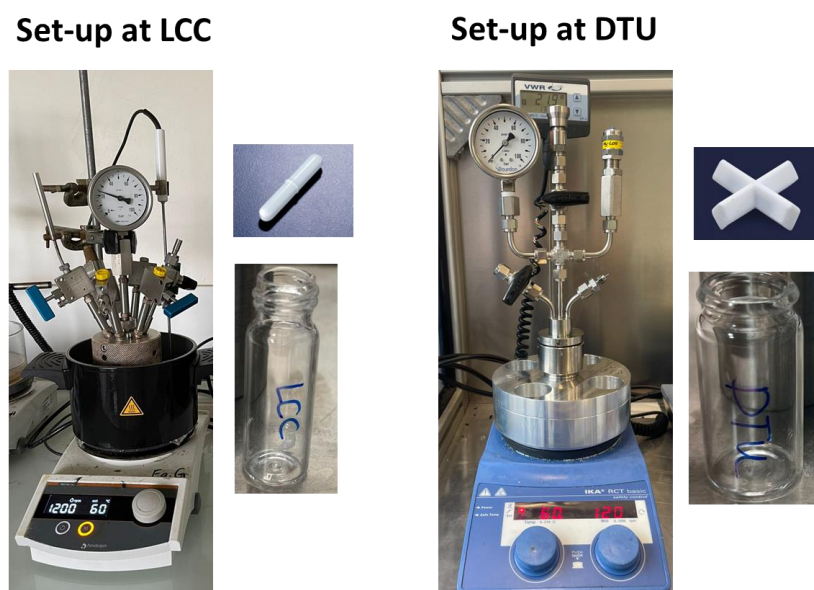


Figure II.4. Set-up used for MNPs synthesis and catalysis, in LCC (left) vs DTU (right)

II.2. Characterization techniques

II.2.1. Nuclear magnetic resonance (NMR) spectroscopy

Liquid NMR spectra were recorded in 5 mm diameter tubes at 300 K on Bruker Avance III 300 or 400 MHz spectrometers. The ^1H and ^{13}C chemical shifts were determined using the residual peak of the deuterated solvent as internal standard and are reported in ppm (δ) relative to tetramethylsilane. Peaks are labeled as singlet (s), doublet (d), triplet (t), quadruplet (q), multiplet (m) and broad (br). For the synthesis of the macroRAFT agent, the monomer conversion was monitored by ^1H NMR in $\text{DMSO-}d_6$ at room temperature by the relative integration of the protons of the internal reference (1,3,5-trioxane, δ 5.20) and the vinylic protons. All the polymerization steps were followed to completion (full consumption of monomers) by ^1H NMR.

II.2.2. Dynamic light scattering (DLS)

The z-average diameters of the polymer particles (D_z) and the polydispersity index (PDI) were obtained with a Malvern Zetasizer NanoZS equipped with a He-Ne laser ($\lambda = 633 \text{ nm}$), operating at 300 K. Samples were analyzed after dilution (with deionized water), either unfiltered or after filtration through a $0.45 \mu\text{m}$ pore-size membrane. The procedure without filtration allowed verification of the presence of agglomerates. Each value was the average of five measurements. In each figure, the curves labeled N, V and I represent the instrumental responses in number, volume, and intensity, respectively.

Dynamic light scattering (DLS) (Figure II.5) technique relies on the interaction of light with particles in motion. At any given moment, the suspended particles occupy specific positions within the area where the scattering occurs. These particles scatter light towards a detector, but the phases of the scattered light waves differ due to variations in the phases of incident light they encounter at their respective positions, as well as differences in the distances between particles and the detector [4,5].

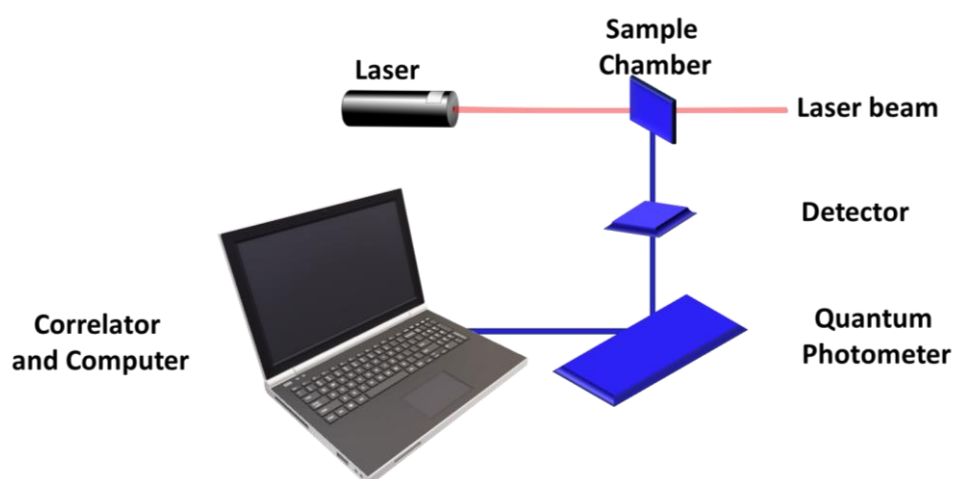


Figure II.5. Schematic diagram of a DLS spectrometer.

II.2.3. *Transmission electron microscopy (TEM)*

Morphological analyses of copolymer nanoobjects and RhNPs were carried out with a JEOL JEM 1400 transmission electron microscope working at 120 kV (Centre de Microcaractérisation Raimond Castaing, UAR 3623, Toulouse, France). Diluted aqueous samples were dropped on a formvar/carbon-coated copper grid and dried under vacuum for 24 h before measurements.

Transmission Electron Microscopy (TEM) is an extremely useful method for studying nanomaterials. It allows us to directly see these materials and obtain accurate measurements of particle or grain size, size distribution, and the overall shape.. This microscopic technique functions by directing a stream of electrons through a thin specimen, engaging with the specimen as it traverses through it. The interaction of these electrons with the specimen generates an image, which is subsequently magnified and directed onto an imaging apparatus, a layer of photographic film, or captured by a sensor like a camera. Notably, TEM surpasses traditional light-based imaging methods by delivering significantly greater resolution, exceeding them by a factor of approximately 1000. However, it's worth noting that TEM does possess some limitations, including the production of monochromatic (black and white) images, the requirement for substantial financial investment, sensitivity to magnetic particles, and potential issues related to structural rearrangement and particle agglomeration. Despite these constraints, TEM remains the primary choice for determining the size and size distribution of nanoparticle samples in most cases [6].

Energy-dispersive X-ray spectroscopy (EDS, also known as EDX or XEDS) systems are commonly incorporated within electron microscopy apparatus. This analytical method is employed to perform elemental analysis or chemical profiling of a specimen. EDS effectively segregates the distinct X-rays associated with various elements found in the specimen, which are emitted when the electron beam interacts with the sample and subsequently transforms them into an energy spectrum. Through

this process, it becomes feasible to ascertain the presence and quantity of specific elements within a given sample, both qualitatively and quantitatively.

II.2.4. Gas chromatography (GC)

Quantitative determination of products and residual substrates in organic phases after catalysis was conducted with an Agilent 6890N gas chromatograph equipped with an HP-5MS capillary column (30 m × 250 μm × 0.25 μm) and a flame ionization detector (FID), using helium as carrier gas. The peak assignment was assisted by separate GC mass spectrometry (GC-MS) analyses (Agilent 6850-5975C). Conversion and selectivity were assessed by constructing calibration curves using commercially available expected reaction products. The mass balance was calculated using the substrate consumption and product yield using mainly decane as an internal standard.

II.2.5. Inductively coupled plasma mass spectrometry (ICP-MS)

Rh metal leaching into the organic phase after catalysis was quantified by high-resolution ICP-MS using an XR Thermo Scientific Element. For the sample preparation, the recovered organic phase was diluted in water using a 104 volumetric dilution factor, high enough to ensure complete dissolution. In practice, a 100 mL volumetric flask was filled 2/3 with Milli-Q water, then 10 μl of the organic product phase was introduced using a precision pipette. The borders were rinsed and the flask was introduced into an ultrasound bath for 15 min. The dilution was then completed with Milli-Q water to the 100 mL mark, followed by further sonication for 45 min. Standards were prepared using $[\text{Rh}(\text{COD})(\mu\text{-Cl})_2]$ dissolved in toluene, attaining Rh concentrations in aqueous solution in the 1-100 ppt range. The relative standard deviation on the measurements used for the calibration was 3% [7].

II.2.6. X-ray photoelectron spectroscopy (XPS)

XPS analyses were performed using a Thermo Scientific system at room temperature using AlK α radiation (1484.6 eV) and a spot size of 400 μm . A flood gun was used to reduce sample charging effects and the obtained spectra were further corrected by setting the C 1s binding energy at 284.8 eV. Data processing was done using the Avantage 4.87 software.

XPS is an analytical technique used to study the surface properties of materials (Figure II.6). It provides information about the elemental composition, chemical state, and electronic state of the outermost atomic layers of a material [8].

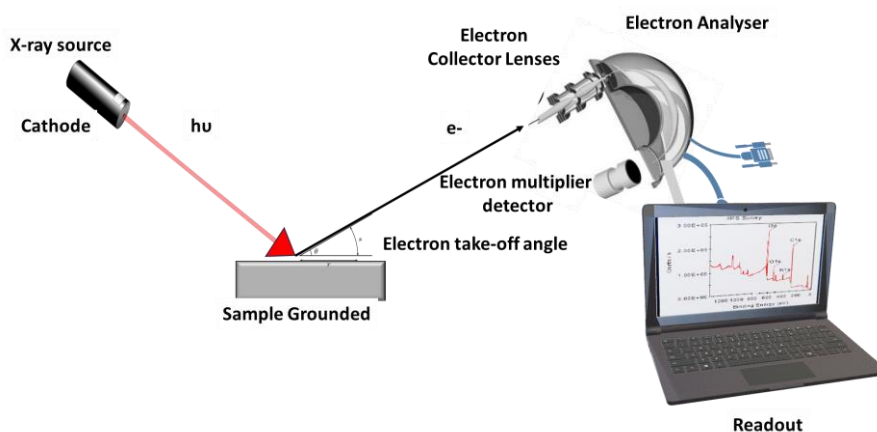


Figure II.6. Schematic diagram of an XPS spectrometer.

II.2.7. Thermal gravimetric analysis (TGA)

Thermal gravimetric analyses were carried out on a Mettler Toledo TGA/DSC 3+ instrument under a N_2 flow. Samples were placed into an alumina crucible and then heated from 27 $^\circ\text{C}$ to 800 $^\circ\text{C}$ at a heating rate of 10 $^\circ\text{C}/\text{min}$. They were used to investigate the polymer and the catalyst stability, by studying the decomposition temperature of both.

II.2.8. Fourier-transform infrared spectroscopy (FTIR)

The FTIR spectra of freeze-dried samples were measured using a PerkinElmer Spectrum 100 FT-IR spectrometer equipped with diamond attenuated total reflectance (ATR) mode. Each measurement consisted of an average of two scans (600–4000 cm^{-1}) with background correction.

II.3. Synthesis of novel core-crosslinked micelles functionalized with triphenylphosphine oxide.

II.3.1. Synthesis of monomers

II.3.1.1. (4-styryl)diphenylphosphine oxide (SDPPO).

To a round bottom flask containing SDPP (2.65 g, 0.07 mmol) and H_2O_2 (2.4 mL, 0.07 mol, 1 equivalent) was added 20 mL of CH_2Cl_2 . The reaction was kept stirring overnight at room temperature. The resulting product was recrystallized from dichloromethane/pentane yielding a dispersed white solid ($y = 86\%$) [9]. The ^1H , ^{13}C , and ^{31}P NMR spectra (CDCl_3) perfectly match with those already reported for this compound [9] (See Appendix A1-4).

^1H NMR: (δ , ppm, CDCl_3): 7.73-7.62 (m, 6H, Ph); 7.60-7.52 (m, 2H, Ph); 7.52-7.45 (m, 6H, Ph); 4.49 (m, 1H, subst. Cp); 6.76 (dd, $J_{\text{HH}} = 17.6$ Hz, $J_{\text{HH}} = 10.9$ Hz, 1H, $\underline{\text{CH}}$ vinyl); 5.87 (d, $J_{\text{HH}} = 17.6$ Hz, 1H, $\underline{\text{CH}}$ vinyl); 5.40 (d, $J_{\text{HH}} = 10.9$ Hz, 1H, $\underline{\text{CH}}$ vinyl);

$^{31}\text{P}\{^1\text{H}\}$ NMR: (δ , ppm, CDCl_3): 28.91;

$^{13}\text{C}\{^1\text{H}\}$ NMR: (δ , ppm, CDCl_3): 141.01 (d, $J_{\text{CP}} = 2.9$ Hz, quat Ph $\underline{\text{C}}$ -vinyl); 135.93 (d, $J_{\text{CP}} = 1.7$ Hz, CH vinyl); 132.58 (d, $J_{\text{CP}} = 104$ Hz, quat Ph); 132.41 (d, $J_{\text{CP}} = 10.2$ Hz, CH Ph); 132.08 (d, $J_{\text{CP}} = 9.9$ Hz, CH Ph); 131.95 (d, $J_{\text{CP}} = 2.8$ Hz, CH Ph); 131.57 (d, $J_{\text{CP}} = 101$ Hz, quat Ph); 128.52 (d, $J_{\text{CP}} = 12.1$ Hz, CH Ph); 128.22 (d, $J_{\text{CP}} = 12.4$ Hz, CH Ph); 116.57 (s, CH_2 vinyl).

II.3.1.2. (4-styryl)diphenylphosphine sulfide (SDPPS).

To a round bottom flask containing SDPP (2.65 g, 0.07 mmol) and S₈ (89.6 g, 0.35 mmol, 5 equivalents) was added 20 mL of CH₃Cl. The reaction was kept stirring overnight at 40 °C. The resulting product was recrystallized from dichloromethane/pentane yielding a dispersed white solid (y = 73%). The ¹H, ¹³C, and ³¹P NMR spectra (CDCl₃) perfectly match with those already reported for this compound[9] (See Appendix A5-7).

¹H NMR: (δ, ppm, CDCl₃): 7.73-7.62 (m, 6H, Ph); 7.60-7.52 (m, 2H, Ph); 7.52-7.45 (m, 6H, Ph); 4.49 (m, 1H, subst. Cp); 6.76 (dd, J_{HH} = 17.6 Hz, J_{HH} = 10.9 Hz, 1H, CH vinyl); 5.85 (d, J_{HH} = 17.6 Hz, 1H, CH vinyl); 5.40 (d, J_{HH} = 10.9 Hz, 1H, CH vinyl);

³¹P{¹H} NMR: (δ, ppm, CDCl₃): 42.9;

¹³C{¹H} NMR: (δ, ppm, CDCl₃): 141.01 (d, J_{CP}=2.9 Hz, quat Ph C-vinyl); 135.93 (d, J_{CP} = 1.7Hz, CH vinyl); 132.58 (d, J_{CP}=104 Hz, quat Ph); 132.41 (d, J_{CP} = 10.2 Hz, CH Ph); 132.08 (d, J_{CP} = 9.9 Hz, CH Ph); 131.95 (d, J_{CP} = 2.8 Hz, CH Ph); 131.57 (d, J_{CP}=101 Hz, quat Ph); 128.52 (d, J_{CP}=12.1 Hz, CH Ph); 128.22 (d, J_{CP}=12.4 Hz, CH Ph); 116.57 (s, CH₂ vinyl).

II.3.2. Preparation of R₀-(4VPMe⁺I)₁₄₀-b-St₅₀-b-(St_{0.9}-co-SDPPO_{0.1})₃₀₀-SC(S)SnPr (chain extension with styrene and SDPPO, step 4).

The first three steps of the polymer synthesis were carried out as described in the previous work done in our group by Dr. Hui Wang [1].

A portion of the [R₀-(4VPMe⁺I)₁₄₀-b-St₅₀-SC(S)SnPr]·14DMF polymer resulting from the three-step synthesis above (1 g, 24.3 μmol) was dissolved in 19 mL of degassed water to afford a pale yellow opalescent dispersion. To this mixture was added 1,3,5-trioxane (26.3 mg, 0.29 mmol), degassed styrene (0.75 mL, 0.68 g, 6.55 mmol, 270 equiv. per chain) and SDPPO (0.22 g, 0.73 mmol, 30 equiv. per chain). Then a degassed

ACPA/NaHCO₃ (14 mg/14 mg) stock solution (0.7 mL, 14.01 mg ACPA, 5 μmol) was added and the resulting reaction mixture was stirred at 80 °C for 8.5 h, yielding a white opalescent stable dispersion. The resulting polymer, R₀-(4VPMe⁺I)₁₄₀-b-St₅₀-b-(St_{0.9}-co-SDPPO_{0.1})₃₀₀-SC(S)SnPr, has a theoretical molar mass of 78337 g mol⁻¹.

II.3.3. Preparation of R₀-(4VPMe⁺I)₁₄₀-b-St₅₀-b-(St_{0.9}-co-SDPPO_{0.1})₃₀₀-b-(St_{0.9}-co-DEGDMA_{0.1})₁₅₀-SC(S)SnPr core-crosslinked micelles (CCM-C latex).

To a Schlenk tube containing the entire aqueous suspension of the R₀-(4VPMe⁺I)₁₄₀-b-St₅₀-b-(St_{0.9}-co-SDPPO_{0.1})₃₀₀-SC(S)SnPr polymer prepared in step 4 were successively added degassed styrene (0.35 g, 3.36 mmol, 138 equiv. per chain), DEGDMA (0.09 g, 0.36 mmol, 15 equiv. per chain), and a degassed ACPA/NaHCO₃ stock solution (0.7 mL, 14.01 mg ACPA, 5 μmol). The resulting reaction mixture was stirred at 80 °C for 8.5 h, resulting in the complete conversion of both monomers (followed by ¹H NMR in DMSO-*d*₆ on periodically withdrawn aliquots of the reaction mixture). The final polymer latex has a theoretical molar mass (per RAFT CTA) of 96835 g mol⁻¹ with a polymer content of 12.3 wt.%.

II.3.4. Preparation of R₀-(4VPMe⁺I)₁₄₀-b-St₅₀-b-(St_{0.9}-co-SDPPS_{0.1})₃₀₀-SC(S)SnPr (chain extension with styrene and SDPPS, step 4).

(The polymerization procedure of SDPPS is the same as the one described below, however by using SDPPS monomer instead of SDPPO).

[R₀-(4VPMe⁺I)₁₄₀-b-St₅₀-SC(S)SnPr]·14DMF (1 g, 24.3 μmol), degassed water 19 mL, 1,3,5-trioxane (27 mg, 0.29 mmol), degassed styrene (0.75 mL, 0.68 g, 6.55 mmol, 270 equiv. per chain) and SDPPS (0.24 g, 0.75 mmol, 30 equiv. per chain). Degassed ACPA/NaHCO₃ (14 mg/14 mg) stock solution (0.7 mL, 14.01 mg ACPA, 5 μmol). T= 80 °C for 8.5 h.

II.3.5. Preparation of $R_0-(4VPMe^+I^-)_{140}-b-St_{50}-b-(St_{0.9-co}-SDPPS_{0.1})_{300}-b-(St_{0.9-co}-DEGDMA_{0.1})_{150}-SC(S)SnPr$ core-crosslinked micelles (CCM-C latex).

$R_0-(4VPMe^+I^-)_{140}-b-St_{50}-b-(St_{0.9-co}-SDPPS_{0.1})_{300}-SC(S)SnPr$ polymer as prepared in step 4, degassed styrene (0.39 g, 3.37 mmol, 138 equiv. per chain), DEGDMA (0.09 g, 0.36 mmol, 15 equiv. per chain), and a degassed ACPA/ $NaHCO_3$ stock solution (0.7 mL, 14.01 mg ACPA, 5 μ mol). T = 80 °C for 8.5 h.

II.4. Synthesis of RhNPs and the RhNP-TPPO@CCM-C latex

II.4.1. Synthesis of RhNPs stabilized by pyridine and TPP

$[Rh(COD)(\mu-Cl)]_2$ (5.45 mg, 11.6 μ mol), TPP (5.8 mg, 22.1 μ mol, 1 equiv. per Rh), pyridine (2 μ L, 1.75 mg, 22.1 μ mol, 1 equiv. per Rh), and 0.5 mL of toluene were mixed by magnetic stirring for 5 min in a Schlenk tube and then transferred to a glass vial (40 x 20 mm), which was placed into an autoclave. The autoclave was then charged with 20 bar of H_2 and placed in an aluminum heating block at 60 °C. After stirring (1200 rpm) for 20 h, the autoclave was carefully depressurized and the vial containing a black colloidal suspension of RhNPs in toluene was removed under argon.

II.4.2. Synthesis of RhNP-TPPO@CCM-C latex

The prepared CCM-C latex (1 mL, 51.14 μ mol of P=O ligands) was mixed with water (3 mL) and toluene (4 mL) in a Schlenk tube, and magnetically stirred for 5 min to induce the CCM core swelling. Then, 0.5 mL of the separately prepared colloidal suspension of RhNPs (11.6 μ mol, P=O: Rh ratio of 4:1) in toluene was added and the mixture was vigorously stirred (1200 rpm) at room temperature for 5 min, whereafter the aqueous phase became greyish and the toluene phase completely colorless (stirring was stopped at regular intervals to assess the reaction progress with phase-separation occurring within < 1 min). The resulting RhNP-TPPO@CCM-C latex had a volume of 5.5 mL.

II.5. One-pot synthesis of RhNP-TPPO@CCM-C

II.5.1. Synthesis without added base

The TPPO@CCM-C latex [10] (1 mL, 51.1 μmol of TPPO ligands) was dispersed in water (4 mL). Then toluene was added (4 mL) and the suspension was vigorously stirred for 15 min to swell the CCM-C cores. Afterward, a toluene solution (3.2 mL) of $[\text{Rh}(\text{COD})(\mu\text{-Cl})_2]$ (3.6 mg, 7.43 μmol) was added, and the mixture was magnetically stirred (1200 rpm) for 5 min before transferring to a glass vial (40 x 20 mm), which was placed into an autoclave. The autoclave was then charged with 20 bar of H_2 and positioned in an aluminum heating block at 60 °C. After stirring for another 20 h, the autoclave was carefully depressurized and the colorless transparent toluene (top phase) was removed from the vial by decantation. The remaining aqueous black latex was used for catalysis.

II.5.2. Synthesis with added base

An identical procedure to that of the previous section was carried out with the addition, after the CCM-C core swelling, of $[\text{Rh}(\text{COD})(\mu\text{-Cl})_2]$ (3.6 mg, 7.43 μmol) and either pyridine (2.9 mg, 37 μmol) or triethylamine (3.71 mg, 37 μmol). The resulting latexes were washed with diethyl ether (3×1 mL) before catalysis.

II.5.3. Catalyst poisoning experiment

Mercury (Hg) was added to a reaction vial containing the RhNP-TPPO@CCM-C latex (1 mL, 10.1 μmol of TPPO ligands, 1.8 μmol of Rh) in large excess ($\text{Hg/Rh} = 500/1$) and stirred (1200 rpm) at 25 °C for 5 h. Afterward, the vial was charged with styrene ($\text{St/Rh} = 5000/1$) under argon and placed in the autoclave. Then, the autoclave was charged

with 20 bar of H₂ positioned in an aluminum heating block at 25 °C, regulated with a digital thermostat, and stirred (1200 rpm, crossbar) for 0.25 h. After the set time, the product recovery and analysis were carried out according to the same protocol described above for the hydrogenation experiments.

II.6. Synthesis of cross-linked micelles with a polycationic shell and a pyridine/triphenylphosphine-functionalized core

II.6.1. Preparation of $R_0-(4VPMe^+I)_{140}-b-St_{50}-b-(St_{0.9}-CO-SDPP_{0.05}-VP_{0.05})_{300}-SC(S)SnPr$ (chain extension with styrene and SDPP and 4VP, step 4).

A portion of the $[R_0-(4VPMe^+I)_{140}-b-St_{50}-SC(S)SnPr] \cdot 14DMF$ polymer resulting from the three-step syntheses described above (Section II.3.2) (1 g, 24.3 μ mol) was dissolved in 10 mL of degassed water to afford a pale yellow opalescent dispersion. To this mixture was added 1,3,5-trioxane (46.3 mg, 0.61 mmol), degassed styrene (0.7 mL, 0.63 g, 6.09 mmol, 270 equiv. per chain), SDPP (0.11 g, 0.39 mmol, 15 equiv. per chain) and 4VP (0.05 mL, 0.05 mg, 0.4 mmol, 15 equivalents). Then a degassed ACPA/NaHCO₃ (14 mg/14 mg) stock solution (0.7 mL, 14.01 mg ACPA, 5 μ mol) was added and the resulting reaction mixture was stirred at 80 °C for 8.5 h, yielding a white opalescent stable dispersion. The resulting polymer, $R_0-(4VPMe^+I)_{140}-b-St_{50}-b-(St_{0.9}-CO-SDPP_{0.05}-VP_{0.05})_{300}-SC(S)SnPr$, has a theoretical molar mass of 73783 g.mol⁻¹.

II.6.2. Preparation of $R_0-(4VPMe^+I)_{140}-b-St_{50}-b-(St_{0.9}-CO-SDPP_{0.05}-VP_{0.05})_{300}-b-(St_{0.9}-CO-DEGDMA_{0.1})_{150}-SC(S)SnPr$ core-crosslinked micelles (CCM-C latex).

To a Schlenk tube containing the entire aqueous suspension of the, $R_0-(4VPMe^+I)_{140}-b-St_{50}-b-(St_{0.9}-CO-SDPP_{0.05}-VP_{0.05})_{300}-SC(S)SnPr$ polymer prepared in step 4 were successively added degassed styrene (0.37 g, 3.43 mmol, 138 equiv. per chain), DEGDMA (0.08 g, 0.36 mmol, 15 equiv. per chain), and a degassed ACPA/NaHCO₃ stock solution (0.7 mL, 14.01 mg ACPA, 5 μ mol). The resulting reaction mixture was

stirred at 80 °C for 8.5 h, resulting in the complete conversion of both monomers (followed by ^1H NMR in $\text{DMSO-}d_6$ on periodically withdrawn aliquots of the reaction mixture). The final polymer latex has a theoretical molar mass (per RAFT CTA) of 91477 g mol^{-1} with a polymer content of 16.63 wt.%.

II.7. Synthesis of cross-linked micelles with a polyanionic shell and a triphenylphosphine oxide functionalized core.

II.7.1. Synthesis of phosphine oxide-functionalized copolymer nanoreactors with an anionic $P(\text{SS}^-\text{Na}^+)$ shell.

The synthesis of the latexes followed the same procedure, as their phosphine-functionalized nanoreactors analogs also optimized by Dr. Hui Wang and reported in the literature [3,11].

II.7.2. Preparation of $R_0-(\text{SS}^-\text{Na}^+)_{140}\text{-}b\text{-St}_{50}\text{-}b\text{-}(\text{St}_{0.9}\text{-}co\text{-SDPPO}_{0.1})_{300}\text{-SC(S)SnPr}$ amphiphilic block copolymers.

To the pale-yellow latex of the $R_0-(\text{SS}^-\text{Na}^+)_{140}\text{-}b\text{-St}_{50}\text{-SC(S)SnPr}$ macroRAFT agent (0.04 mmol of polymer, corresponding to 0.56 mmol of SS^-Na^+ units, 3 mL of water) in a Schlenk tube under Argon were added degassed styrene (1.24 mL, 1.12 g, 10.75 mmol; 270 equiv. per chain) and SDPPO (0.344 g, 1.20 mmol; 30 equiv. per chain) and trioxane (*ca.* 90 mg) as an internal standard. A portion of a degassed ACPA/ NaHCO_3 stock solution (0.11 mL, 2.2 mg ACPA, $7.96 \mu\text{mol}$) was then added and the resulting reaction mixture was stirred at 80 °C for 4.5 h, yielding a white opalescent stable dispersion. The resulting polymer has a theoretical molar mass of 66869 g mol^{-1} . The weight percent polymer in the latex is 19.4%.

II.7.3. Preparation of CCM with a 90:10 St/DEGDMA core: crosslinking of the $R_0-(SSNa^+)_{140}-b-St_{50}-b-(St_{0.9}-co-SDPPO_{0.1})_{300}-SC(S)SnPr$ amphiphilic block copolymers.

To the total volume of the $R_0-(SSNa^+)_{140}-b-St_{50}-b-(St_{0.9}-co-SDPPO_{0.1})_{300}-SC(S)SnPr$ latex obtained as described above (0.04 mmol of polymer) were successively added DEGDMA (0.133 mL, 144.3 mg, 0.6 mmol; 15 equiv. per chain), styrene (0.62 mL, 561.6 mg, 5.4 mmol; 135 equiv. per chain) and the degassed ACPA/NaHCO₃ stock solution (0.11 mL, 2.2 mg ACPA, 7.96 μmol). The resulting reaction mixtures were stirred at 80 °C for 4 h resulting in complete comonomer consumption (¹H NMR monitoring in DMSO-d₆) to yield the CCM $R_0-(SSNa^+)_{140}-b-(St_{0.9}-co-SDPPO_{0.1})_{300}-b-(DEGDMA_{0.1}-co-St_{0.9})_{150}-SC(S)SnPr$. The resulting polymer has a theoretical molar mass of 86254 g mol⁻¹. Polymer content: 14.4%, [TPPO] = 65.3 μmol mL⁻¹.

II.8. Synthesis of RhNPs-TPPO@CCM-A

II.8.1. In Ex-situ procedure

1 mL of the prepared CCM latex (containing 9.3 μmol of P=O ligands) was mixed with 3 mL of H₂O and 4 mL of toluene in a Schlenk tube, and magnetically stirred for 5 min to induce the CCM core swelling. Then, 0.5 mL of a separately prepared colloidal suspension of RhNPs (2.3 μmol, P=O: Rh ratio of 4:1) in toluene (see section II.3.4.1) was added and the mixture vigorously stirred (1200 rpm) at room temperature for 5 min, whereafter the aqueous phase became greyish and the toluene phase completely colorless (stirring was stopped at regular intervals to assess the reaction progress with phase-separation occurring < 1 min). The resulting latex had a volume of 5.5 mL.

II.8.2. One-pot synthesis of RhNP-TPPO@CCM-A

The TPPO@CCM-A latex dispersed in water (6 mL, 71.3 μmol of P=O ligands) was core swollen by toluene (8 mL) for 15 min. Afterward, a toluene solution (3.2 mL) of

[Rh(COD)(μ -Cl)]₂ (6.2 mg, 12.2 μ mol) was added and the mixture was magnetically stirred (1200 rpm) for 5 min and transferred to a glass vial (40 x 20 mm), which was placed into an autoclave. The autoclave was then charged with 20 bars of H₂ and positioned in an aluminum heating block at 60 °C. After stirring (1200 rpm) for 20 h, the autoclave was carefully depressurized and the vial containing the catalyst as a black latex (bottom phase) and a colorless transparent toluene (top phase) was used for catalysis after separation.

II.9. General procedure for metal NPs-catalyzed biphasic hydrogenation

II.9.1. Aqueous biphasic hydrogenation

To a glass vial containing the RhNP@CCM-C latex (0.5 mL, 4.9 μ mol of P=O ligands, 1.05 μ mol of Rh) were added the desired amounts of styrene (see Results and Discussion) and decane (internal standard; substrate/internal standard molar ratio *ca.* 4). The vial was then placed inside a custom-made autoclave, charged with 20 bar of H₂ and placed in an aluminum heating block (Figure II.7) at the desired temperature with magnetic stirring (1200 rpm) for a chosen reaction time. After the set time the stirring was stopped, the autoclave was slowly vented, the vial was removed (under argon) and the reaction mixture was allowed to phase separate. After completing phase separation, the latex was extracted with diethyl ether or toluene (3 x 0.3 mL), applying 5 min of stirring (1200 rpm) followed by 5 min for phase separation without stirring for each extraction (these operations were carried out in air). Lastly, the combined organic phase was analyzed by GC and the catalyst activity was calculated as turnover frequency (TOF) and corrected TOF (*c*TOF, see section II.7.3 below).

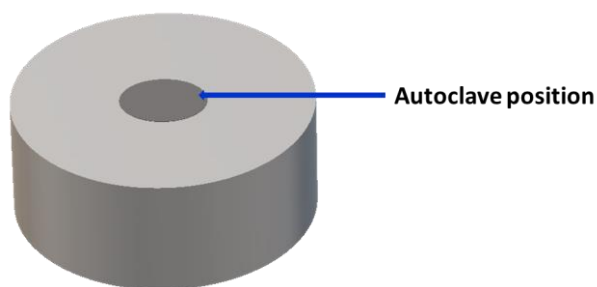


Figure II.7. Aluminium heating block used at DTU

II.9.2. Catalyst recycling experiments

After the product separation and extraction, the vial containing the RhNP@CMM latex from the hydrogenation experiment was charged directly with fresh substrate (same amount as in the initial run), followed by a new catalytic run and then by the product separation procedure according to the above-described protocol. All catalytic results were generally reproduced within $\pm 5\%$.

II.9.3. Corrected TOF calculations for RhNPs

“Indeed, the catalytic activity, for a valid comparison, must be referred to the number of exposed surface atoms of a specified kind. Thus a convenient way to express catalytic activity is by means of a turnover number equal to the number of reactant molecules converted per minute per catalytic site for given reaction conditions.”[12]

The catalyst activity is expressed as turnover frequency (TOF) and calculated as moles of substrate converted per moles of Rh in the catalyst per hour (assuming all Rh atoms are active). The corrected TOF (*c*TOF) is based on the surface Rh atoms, as calculated from Eq. 1-5.

The moles of surface Rh atoms ($n_{Rh,surface}$) were obtained considering spherical NPs having a closed packed structure (fcc), the radius of the sphere being the average measured from the TEM images, and a Rh atom diameter (D_{Rh}) of 0.27 nm.

$$N_{Rh,surface} = \frac{N_{Rh,shell}}{N_{Rh,total}} = \frac{(N_{calc} \times V_{Rh,shell})/V_{Rh,cell}}{(N_{calc} \times V_{Rh,total})/V_{Rh,cell}} = \frac{V_{Rh,shell}}{V_{Rh,total}} = \frac{V_{Rh,total} - V_{Rh,cc}}{V_{Rh,total}} \quad (1)$$

$$V_{Rh,total} = \frac{4}{3}\pi R_{RhNP}^3 \quad (2)$$

$$V_{Rh,core} = \frac{4}{3}\pi(R_{RhNP} - D_{Rh})^3 \quad (3)$$

$$n_{Rh,surface} = 0.74 \times n_{Rh,total} \quad (4)$$

$$cTOF = \frac{n_{substrate\ converted}}{n_{Rh,surface} \times time} \quad (5)$$

II.10. Nickel nanoparticle synthesis

II.10.1. Synthesis of NiNPs conducted without H₂

0.48 mmol of oleylamine (0.13 mg, 0.15 mL, 22 equiv.) was introduced into a round-bottom Schlenk flask, followed by a degassing process under vacuum conditions for 15 minutes. Ni(acac)₂ (6 mg, 21.8 μmol, 1 equiv.) or Ni(COD)₂ (6 mg, 23.4 μmol, 1 g, 1 equiv.) and tri-*n*-octylphosphine (TOP, 8.08 mg, 23.4 μmol, 1 equiv.) were subsequently added, under a nitrogen atmosphere, to the flask containing the oleylamine. The resulting mixture was degassed again and placed under a nitrogen atmosphere. Following this, the mixture was heated to 215 °C using a heating mantle.

II.10.2. Synthesis of NiNPs conducted under H₂

[Ni(COD)₂] (6 mg, 2.18 mmol, 1 equiv.) or [Ni(acac)₂] (6 mg, 2.34 mmol, 1 equiv.), TPP (5.72 mg, 2.18 mmol, 1 equiv.) and pyridine (4 μL, 3.92 mg, 4.96 mmol, 22 equiv.), were mixed by magnetic stirring for 5 min in a Schlenk tube and then transferred to a glass vial (40 x 20 mm), which was placed into an autoclave. The autoclave was then charged with 20 bar of H₂ and placed in an aluminum heating block at 110 °C. After stirring (1200 rpm) for 20 h, the autoclave was carefully depressurized and the vial

containing a black colloidal suspension of NiNPs in pyridine was removed under argon.

II.10.3. Synthesis of NiNPs conducted with H₂ using IFPEN reactors (30 mL)

[Ni(COD)₂] (3 mg, 1.09 mmol, 1 equiv.) or [Ni(acac)₂] (3 mg, 1.17 mmol, 1 equiv.), TPP (2.86 mg, 1.09 mmol, 1 equiv.) and pyridine (10.6 mL, 10.4 g, 0.13 mol, 121 equiv.) were mixed by magnetic stirring for 5 min in a Schlenk tube and then transferred to the reactor of 30 mL. The mixture was heated up to 110 °C under mechanical stirring at 1200 rpm, then charged with 20 bar of H₂, for 20 h. After the set reaction time, the reactor was automatically cooled down, then depressurized, then filled with N₂, and the suspension was withdrawn from the reactor with a sterilized needle. The syringe containing the black colloidal suspension of NiNPs in pyridine was then added to a Schlenk flask under Ar, and placed in a glovebox.

II.10.4. Hydrogenation of 3-hexyne using IFPEN reactors (30 mL)

The desired volume (See Chapter VII, Results and Discussion) of the suspension was withdrawn and added to a Schlenk flask. The desired amount of 3-hexyne in cyclohexane was added, an aliquot was withdrawn from the reaction mixture, dioxane was added as an external standard and the mixture was analyzed by ¹H NMR in CDCl₃ (t₀). The mixture was then transferred to the reactor under Ar. The mixture was heated up to 60 °C under mechanical stirring (1200 rpm), then charged with 20 bar of H₂. After the set reaction time (See Chapter VII – Results and Discussion), the reactor was cooled down, depressurized, and then filled with N₂, and the suspension was withdrawn from the reactor with a sterilized needle. An aliquot was withdrawn from the reaction mixture, dioxane was added as an external standard and the mixture was analyzed by ¹H NMR in CDCl₃ (t_f).

II.10.5. Corrected TOF calculations for NiNPs

The catalyst activity is expressed as turnover frequency (TOF) and calculated as moles of substrate converted per moles of Ni in the catalyst per hour (assuming all Ni atoms are active). The corrected TOF (*c*TOF) is based on the surface Ni atoms, as calculated from Eq. 1-5 (Section II.9.3.).

The moles of surface Ni atoms ($n_{Ni,surface}$) were obtained considering spherical NPs having a closed packed structure (fcc), the radius of the sphere being the average measured from the TEM images, and a Ni atom diameter (D_{Ni}) of 0.248 nm

II.11. References

- [1] H. Wang, L. Vendrame, C. Fliedel, S. Chen, F. Gayet, E. Manoury, X. Zhang, F. D'agosto, M. Lansalot, R. Poli, Core-Cross-Linked Micelles Made by RAFT Polymerization with a Polycationic Outer Shell Based on Poly(1-methyl-4-vinylpyridinium), *Macromolecules*. 53 (2020) 2198–2208. <https://doi.org/10.1021/acs.macromol.9b02582>
- [2] S. Alunni, V. Laureti, L. Ottavi, R. Ruzziconi, Catalysis of the β -elimination of HF from isomeric 2-fluoroethylpyridines and 1-methyl-2-fluoroethylpyridinium salts. Proton-activating factors and methyl-activating factors as a mechanistic test to distinguish between concerted E2 and E1cb irreversible mechanisms, *J Org Chem*. 68 (2003) 718–725. <https://doi.org/10.1021/jo020603o>
- [3] H. Wang, C. Fliedel, E. Manoury, R. Poli, Core-crosslinked micelles with a poly-anionic poly(styrene sulfonate)-based outer shell made by RAFT polymerization, *Polymer (Guildf)*. 243 (2022) 124640. <https://doi.org/10.1016/j.polymer.2022.124640>
- [4] F. Ross Hallett, Particle size analysis by dynamic light scattering, *Food Research International* 27(2) (1994) 195-198 [https://doi.org/10.1016/0963-9969\(94\)90162-7](https://doi.org/10.1016/0963-9969(94)90162-7)
- [5] M. Instruments, Dynamic Light Scattering Common Terms Defined, 2011. www.malvern.com/contact
- [6] K. Kanamura, Next Generation Batteries: Realization of High Energy Density Rechargeable Batteries, Springer Singapore, 2021 ISBN: 978-981-33-6667-1. <https://doi.org/10.1007/978-981-33-6668-8>

- [7] M. Korvela, M. Andersson, J. Pettersson, Internal standards in inductively coupled plasma mass spectrometry using kinetic energy discrimination and dynamic reaction cells, *J Anal At Spectrom.* 33 (2018) 1770–1776. <https://doi.org/10.1039/c8ja00171e>
- [8] M.A. Isaacs, J. Davies-Jones, P.R. Davies, S. Guan, R. Lee, D.J. Morgan, R. Palgrave, Advanced XPS characterization: XPS-based multi-technique analyses for comprehensive understanding of functional materials, *Mater Chem Front.* 5 (2021) 7931–7963. <https://doi.org/10.1039/d1qm00969a>
- [9] R. Rabinowitz, R. Marcus, J. Pellon, Synthesis, polymerization, and copolymerization of diphenyl-p-styrylphosphine, phosphine oxide, and phosphine sulfide, *J Polym Sci A.* 2 (1964) 1241–1249. <https://doi.org/10.1002/pol.1964.100020321>
- [10] C.J. Abou-Fayssal, C. Fliedel, R. Poli, A. Riisager, K. Philippot, E. Manoury, Confinement of Rh nanoparticles in triphenylphosphine oxide-2 functionalized core-crosslinked micelles for aqueous biphasic hydrogenation catalysis. In Revision
- [11] H. Wang, C.J. Abou-Fayssal, C. Fliedel, E. Manoury, R. Poli, Phosphine-Functionalized Core-Crosslinked Micelles and Nanogels with an Anionic Poly(styrenesulfonate) Shell: Synthesis, Rhodium(I) Coordination and Aqueous Biphasic Hydrogenation Catalysis, *Polymers (Basel).* 14 (2022) 4937. <https://doi.org/10.3390/polym14224937>
- [12] M. Boudart, A. Aldag, J.E. Benson, N.A. Dougharty, C. Girvin Harkins, On the specific activity of platinum catalysts, *J Cat* 6(1) (1966) 92-99, [https://doi.org/10.1016/0021-9517\(66\)90113-8](https://doi.org/10.1016/0021-9517(66)90113-8)

Chapter III: Confinement of Rh nanoparticles in core-crosslinked micelles functionalized with triphenylphosphine oxide for aqueous biphasic hydrogenation catalysis

III.1. Introduction

In previous work within the LCC team *Ligands, Complex Architectures and Catalysis* (LAC₂) triphenylphosphine was covalently bound to the core of core-crosslinked micelles (TPP@CCM) and then used as a stabilizer for Rh^I or Rh⁰ to yield catalytic nanoreactors, namely RhNP-TPP@CCMs, based on both CCM-N and CCM-C [1–3]. The RhNPs were formed *in situ* after loading the CCMs with the [Rh(COD)(μ-Cl)]₂ molecular precursors, followed by reduction of the resulting core-anchored [RhCl(COD)(TPP@CCM)] with H₂. The obtained RhNP-TPP@CCM were then applied for the aqueous biphasic hydrogenation of model substrates such as 1-octene, styrene, and acetophenone. Despite very good catalytic performances, two unexpected issues arose. When using the TPP@CCM-N nanoreactors, migration of the RhNPs towards the outer shell was observed under catalytic conditions, likely due to a competition between the shell PEO chains and the core TPP ligands for the interaction with the RhNPs surface. Conversely, the RhNPs remained well-confined in the TPP@CCM-C nanoreactors and could be efficiently recycled in catalytic hydrogenation, provided toluene was used as extraction solvent at the end of each reaction run. When using diethyl ether as an extraction solvent, on the other hand, the RhNPs were also extracted from the core of the TPP@CCM-C nanoreactors during the work-up procedure for the catalyst recovery and recycling. This result suggested that the oxygen-containing diethyl ether, like the PEO in the CCM-N shell, has a greater affinity for binding to the RhNPs surface than TPP, whereas the opposite is true in the coordination chemistry of Rh^I. Based on this hypothesis, it was decided to develop

new L@CCM nanoreactors with oxidized triphenylphosphine (TPPE, with E = S, O) as specific ligands for the RhNP anchoring in the CCM core.

The present chapter describes the syntheses and characterization of novel TPPE@CCM-C polymer latexes. Special attention is given to TPPO@CCM-C, to its loading with preformed RhNPs, and to the application of the resulting RhNP-TPPO@CCM-C nanoreactors in the catalytic hydrogenation of model substrates under aqueous biphasic conditions. Note that this chapter is related to article No. 2 in the list of publications, reported earlier, and has been accepted in *Materials Today Chemistry*.

III.2. Polymer synthesis and characterization

Two strategies were envisaged for the preparation of the CCM with oxidized phosphines. One is to oxidize the core-anchored TPP functions in the pre-synthesized TPP@CCM (section III.2.1.). The other one is to use the oxidized monomers in the polymer synthesis (section III.2.2.).

III.2.1. Attempts to oxidize TPP in the core of the CCM-C

Within the first approach, a polymer with composition $R_0-(4VPMe^+I^-)_{140}-b-St_{50}-b-(St_{0.9}-co-SDPP_{0.1})_{300}-b-(St_{0.9}-co-DEGDMA_{0.1})_{140}-SC(S)SPr$ (CCM-C 10%), made according to the published procedure [2], was treated for oxidation in two different ways: either with S_8 for the generation of core-anchored TPP sulfide (TPPS) functions (section III.2.1.1.), or with air in the presence of $[Rh(COD)(\mu-Cl)]_2$ (in catalytic amounts) for the generation of core-anchored TPP oxide (TPPO) functions (section III.2.1.2.).

III.2.1.1. Oxidation by S_8

A preliminary investigation using the molecular TPP ligand was first carried out for the optimization of the conditions needed for the oxidation within the CCM-C cores. For that, 10 equivalents of S_8 were added at room temperature to a solution of TPP in

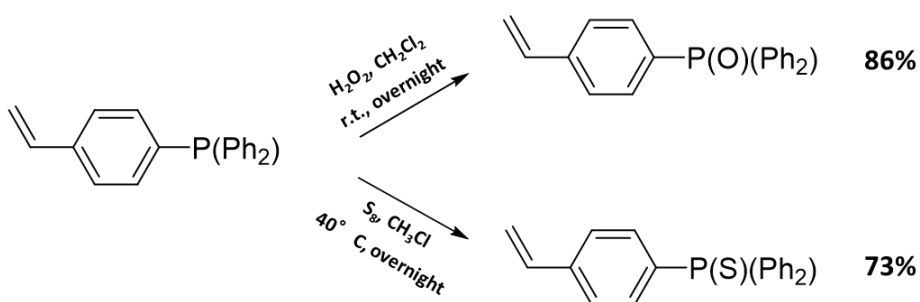
toluene- d_8 . After 0.5 h, the ^{31}P NMR spectrum showed only one peak at $\delta = 42$ ppm, indicating the total conversion of TPP to TPPS [4]. Thus, similar conditions were applied to the oxidation of TPP@CCM-C latex (using toluene as a solvent at 40 °C and stoichiometric ratio of S_8). The ^{31}P NMR spectrum in toluene- d_8 , recorded after stirring overnight, revealed only one peak at $\delta = 42$ ppm, indicating the quantitative oxidation of TPP to generate a TPPS@CCM-C latex. However, an unexpected problem occurred during the loading of the nanoreactors with the $[\text{Rh}(\text{COD})(\mu\text{-Cl})_2]$ complex. Using the previously optimized protocol for metal complexation, the toluene phase containing the metal precursor turned brown instead of colorless, while the aqueous latex phase remained turbid milky. This showed that the Rh complex did not migrate toward the TPPS@CCM-C core and suggested that some residual free sulfur remained in the organic phase, even after washing the CCM with toluene, resulting in an unwanted side reaction with $[\text{Rh}(\text{COD})(\mu\text{-Cl})_2]$. Control experiments, carried out using $[\text{Rh}(\text{COD})(\mu\text{-Cl})_2]$ in CDCl_3 and an excess of S_8 , led to a color change of the solution to brown similar to the color change observed in the organic phase during the addition of $[\text{Rh}(\text{COD})(\mu\text{-Cl})_2]$ to the TPPS@CCM-C latex. This might result partly from a possible side reaction leading to $[\text{RhCl}(\text{COD})(\text{TPPS})]$ complex formed in the organic phase by the interaction of free arms of TPPS@CCM-C (possibly, because of an incomplete crosslinking) with $[\text{Rh}(\text{COD})(\mu\text{-Cl})_2]$. ^1H NMR done in CDCl_3 of the organic brown phase revealed the presence of a quadruplet at $\delta = 3.9$ ppm and a triplet at $\delta = 5.30$ ppm characteristics of $[\text{RhCl}(\text{COD})(\text{TPPS})]$, as previously reported in the literature by Dutta and coworkers [4] (Appendix B, Figure B1). Likewise, ^{31}P NMR revealed the presence of a signal at $\delta = 25$ ppm corresponding to the $[\text{RhCl}(\text{COD})(\text{TPPS})]$ complex, but the signal was broadened which may result from a rapid dynamic exchange between coordinated and non-coordinated TPPS@CCM-C at neutral pH [5,6].

III.2.1.2. Oxidation by air

To a suspension of TPP@CCM-C in water was added $[\text{Rh}(\text{COD})(\mu\text{-Cl})_2]$ (Rh/P = 0.1, catalytic amount), and the suspension was stirred in air for 72 h at 40 °C. Under these conditions, the oxidation of the TPP in the core was not evident, since the reaction monitoring by ^{31}P NMR was prevented by line broadening due to a chemical exchange (interparticle metal migration), as previously described [6]. Despite this uncertainty, the generation of RhNPs inside the core was attempted using the previously published conditions[3] in the presence of an excess of NEt_3 [3], but no RhNP formation was revealed by the TEM analysis, suggesting that the loading of Rh^{I} in the core of the TPP@CCM-C was too low.

III.2.2. Synthesis of TPPE@CCM-C (E = S, O) by copolymerization using oxidized monomers

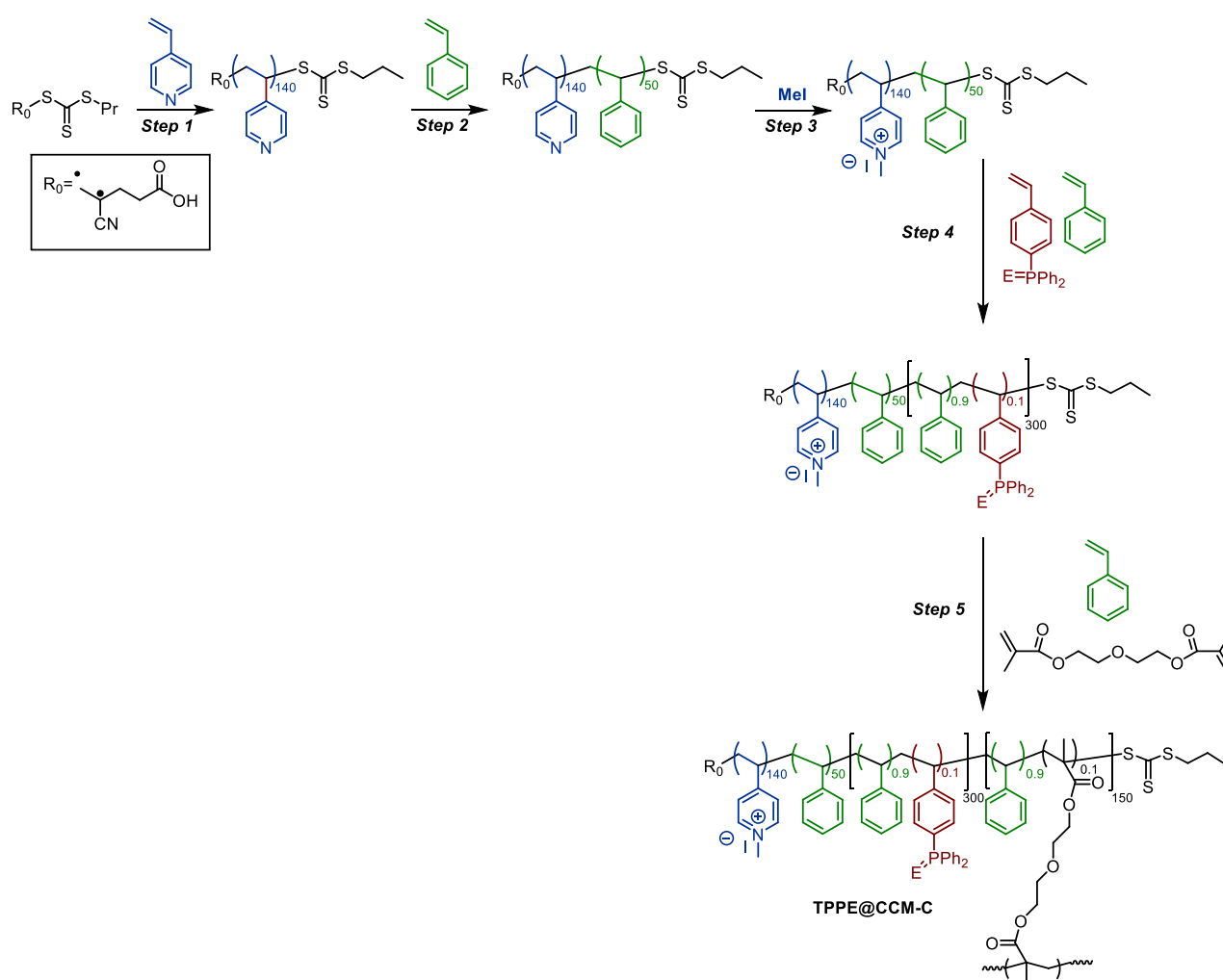
For the second approach, the oxidized monomers were first synthesized and the resulting compounds were compared to literature [7,8] (see Experimental Part, section II.3.1. Synthesis of monomers) (Scheme III.1).



Scheme III.1. Syntheses of SDPPO and SDPPS.

The syntheses of the new TPPE@CCM-C polymers were performed following the same strategy as for the preparation of the closely related TPP@CCM-C polymer (Scheme III.2). The target degrees of polymerization of each block were kept identical to those of TPP@CCM-C, as they were already optimized to provide stable latexes with

a narrow particle size distribution [2,9]. Thus, the first three steps leading to the synthesis of the amphiphilic diblock macroRAFT agent, R_0 -(VPMe⁺I)₁₄₀-*b*-St₅₀-SC(S)SnPr, isolated as a stable solid and redispersed in water, were the same as in the TPP@CCM-C synthesis [9]. They involved the homogeneous RAFT polymerization of 4-vinylpyridine (4VP) with 4-cyano-4-thiothiopropylsulfanyl pentanoic acid (CTPPA), R_0 SC(S)SnPr where $R_0 = \text{CMe}(\text{CN})\text{CH}_2\text{CH}_2\text{COOH}$, as transfer agent, forming R_0 -4VP₁₄₀-SC(S)SnPr (step 1), then chain extension with a short polystyrene block (average degree of polymerization of 50) forming an R_0 -VP₁₄₀-*b*-St₅₀-SC(S)SnPr diblock copolymer (step 2), and quaternization of the pyridine N-atoms with MeI (step 3).



Scheme III.2. Synthesis route of the TPPE@CCM-C polymer (E = S, O).

Further chain extension (step 4) was completed of the $R_0\text{-(VPMe}^+\text{I)}_{140}\text{-}b\text{-St}_{50}\text{-SC(S)SnPr}$ macroRAFT agent with a longer hydrophobic block (average degree of polymerization of 300) consisting of a statistical copolymer of styrene and a TPPE-functionalized styrene, namely SDPPO (4-styryl)diphenylphosphine oxide [10–12] (90/10 ratio), obtained by oxidation of (4-styryl)diphenylphosphine (SDPP) with H_2O_2 , or (4-styryl)diphenylphosphine sulfide (SDPPS) that was synthesized using SDPP with an excess of S_8 in chloroform. The former monomer has previously been homopolymerized [10–12] and copolymerized with styrene [13] and 9-(4-vinylphenyl)-9H-carbazole [14] by free radical polymerization, but never using the RAFT approach. The latter monomer has as well been homopolymerized and copolymerized with styrene [7].

All the polymerization steps were followed to completion (full consumption of monomers) by ^1H NMR (see section below), and the generated $R_0\text{-(VPMe}^+\text{I)}_{140}\text{-}b\text{-St}_{50}\text{-}b\text{-(St}_{0.9}\text{-co-SDPPE}_{0.1})_{300}\text{-SC(S)SnPr}$ ($E = \text{O, S}$) amphiphilic macromolecules were characterized by TEM and DLS (see section below).

III.2.2.1 Characterization of TPPS@CCM-C

Full consumption of the monomers was reached in 7.5 h, as indicated by ^1H NMR in $\text{DMSO-}d_6$ (Figure III.1).

The generated $R_0\text{-(VPMe}^+\text{I)}_{140}\text{-}b\text{-St}_{50}\text{-}b\text{-(St}_{0.9}\text{-co-SDPPS}_{0.1})_{300}\text{-SC(S)SnPr}$ amphiphilic macromolecules self-assembled in the form of micelles. The spherical micelles of the amphiphilic diblock copolymer produced by step 4 had an average size of *ca.* 38 nm, as shown by DLS (Figure III.2 a) and TEM (Figure III.2 b) analyses. These micelles were then crosslinked in a final step with DEGDMA (15 equiv. per chain), diluted with additional styrene (135 equiv. per chain), to yield the final product, $R_0\text{-(VPMe}^+\text{I)}_{140}\text{-}b\text{-St}_{50}\text{-}b\text{-(St}_{0.9}\text{-co-SDPPS}_{0.1})_{300}\text{-}b\text{-(St}_{0.9}\text{-co-DEGDMA}_{0.1})_{150}\text{-SC(S)SnPr}$ (TPPS@CCM-C), with a 10% crosslink density in the inner crosslinked cores. The final TPPS@CCM-C micelles

had spherical morphology and a larger diameter (92 nm) than the intermediate micelles, as also shown by DLS (Figure III.2 c) and TEM (Figure III.2 d) analyses.

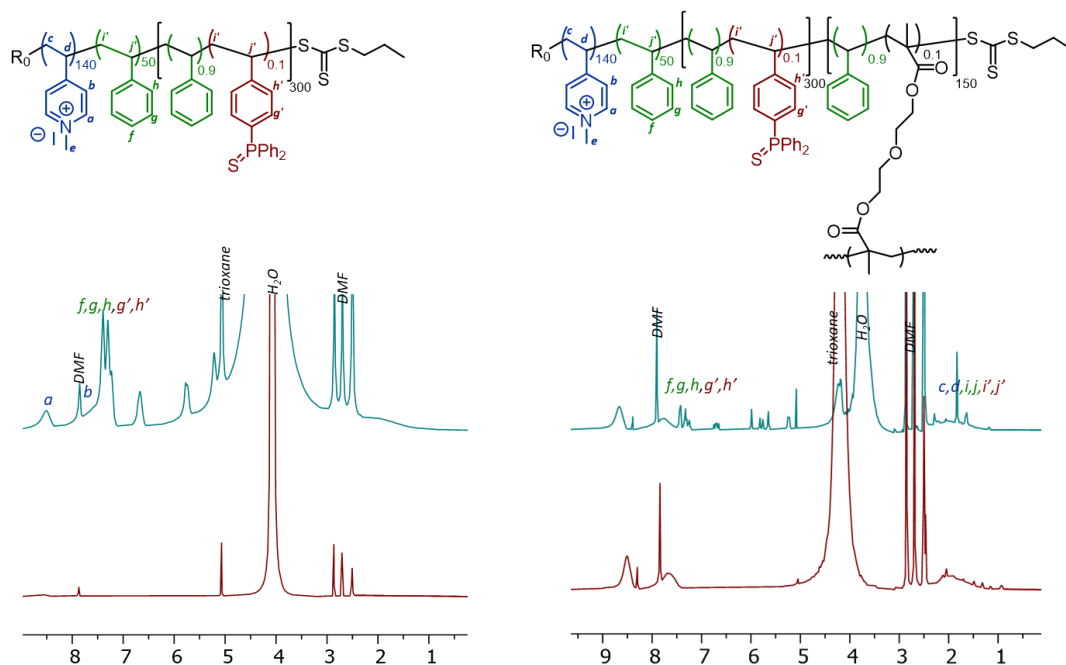


Figure III.1. ^1H NMR of the diblock (left) and the micelles (right), at $t = 0$ h (blue) and $t = 7.5$ h (red).

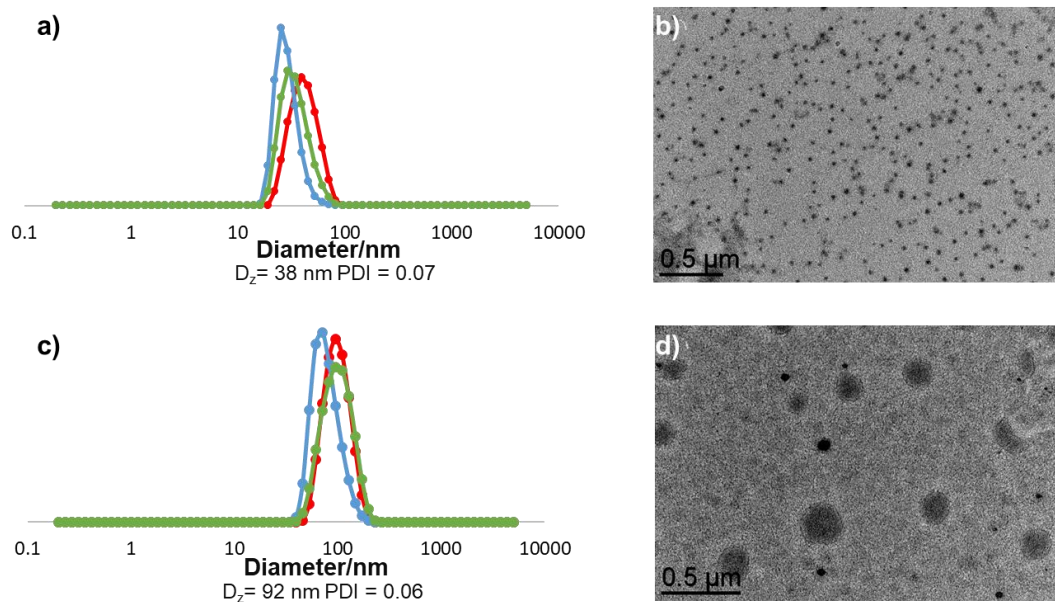


Figure III.2. DLS size distributions of aqueous dispersions of (a) the diblock $R_0\text{-(VPMe}^+\text{I)}_{140}\text{-}b\text{-St}_{50}\text{-}b\text{-(St}_{0.9}\text{-}co\text{-SDPPS}_{0.1})_{300}\text{-}b\text{-SC(S)SnPr}$ micelles and (c) TPPS@CCM-C. Color coding: number (blue), volume (green), and intensity (red). TEM images of (b) the diblock TPPS@CCM-C, and (d) TPPS@CCM-C.

II.2.2.2 Characterization of TPPO@CCM-C

The amphiphilic diblock copolymer produced by step 4, resulted in spherical micelles with an average size of *ca.* 65 nm, as shown by DLS analysis (Figure III.3 a). Following the same procedure described above for SDPPS, these micelles were then crosslinked with DEGDMA (15 equiv. per chain) to yield the final product, $R_0\text{-(VPMe}^+\text{I)}_{140}\text{-}b\text{-St}_{50}\text{-}b\text{-(St}_{0.9}\text{-}co\text{-SDPPO}_{0.1})_{300}\text{-}b\text{-(St}_{0.9}\text{-}co\text{-DEGDMA}_{0.1})_{150}\text{-SC(S)SnPr}$ (TPPO@CCM-C), with a 10% crosslink density in the inner crosslinked cores. The final TPPO@CCM-C micelles had a spherical morphology and a slightly larger diameter (98 nm) than the intermediate micelles (65 nm), as shown by DLS (Figure III.3 c) and TEM (Figure III.3 f) analyses. The size distribution was found narrower and the D_z of the distribution was slightly reduced after swelling with CHCl_3 . This was also observed for the related TPP@CCM-A and is attributed to the dominant effect of micelles disaggregation rather than core swelling, which would cause an increase in average size [15]. Accordingly, the intensity profile in Figure III.3 c, which is more sensitive to the larger size micelles, became significantly narrower and shifted to lower values upon swelling. A stability experiment was to redisperse the micelles in a mixture of THF/water (Figure III.3) to study the possibility of the latex to disassemble into single chains (as it happens for the $\text{P(4VPMe}^+\text{I)-}b\text{-PSt}$ diblock copolymers). However, it was shown that the introduction of TPPO does not allow this disassembly, and this was also the case with TPP@CCM-C [15]. The resulting latex remained well-dispersed over more than five months (Appendix B, Figure B2).

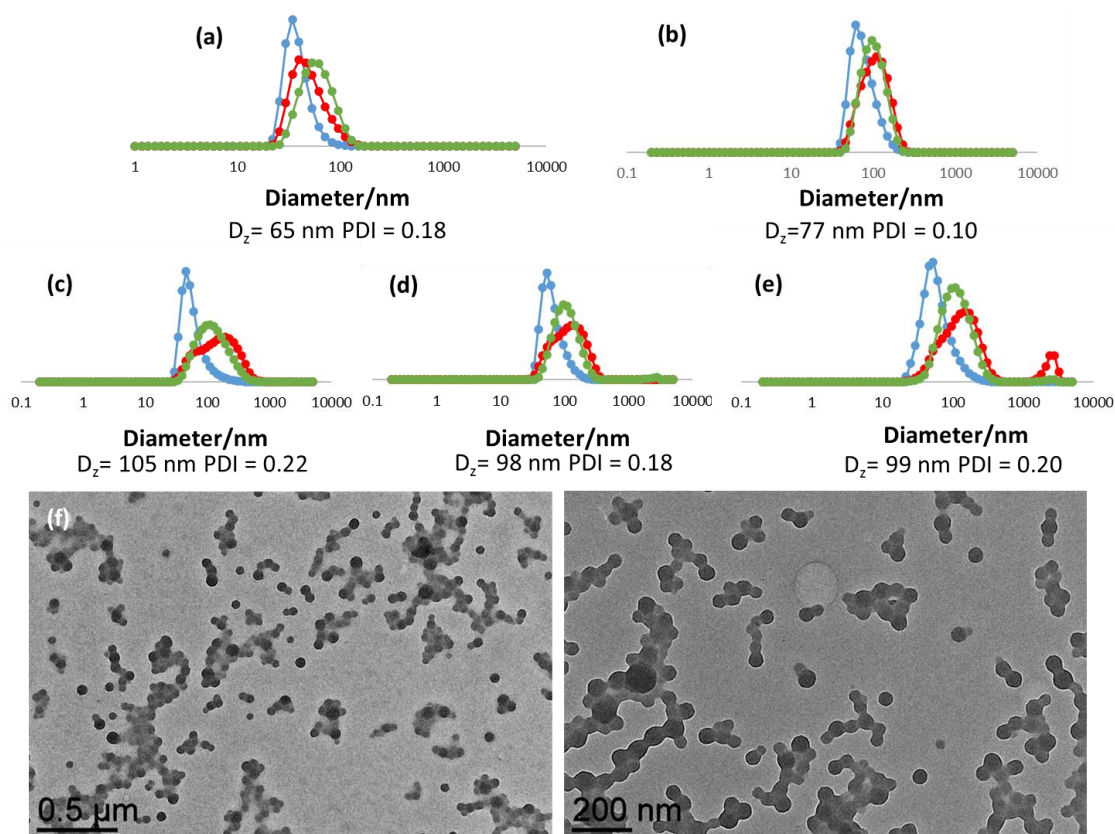


Figure III.3. DLS size distributions of aqueous dispersions of diblock $R_0\text{-(VPMe}^+\text{I)}_{140}\text{-b-St}_{50}\text{-b-(St}_{0.9}\text{-co-SDPPO}_{0.1})_{300}\text{-b-SC(S)SnPr}$ in (a) water and (b) THF/H₂O (60/40 v/v) and of TPPO@CCM-C (c) before and after swelling with (d) CHCl₃ and (e) THF/H₂O (60/40 v/v). Color coding: number (blue), volume (green), and intensity (red). f) TEM images of TPPO@CCM-C.

III.2.2.3. Choice of CCM-C for Rh nanoparticle confinement for catalytic hydrogenation

The main objective of this work was to find a ligand leading to a more effective confinement of the RhNPs within the core of micelles while also affording small nanoparticles to be used in aqueous biphasic hydrogenation. For this reason, two series of experiments were conducted in toluene for the generation of RhNPs from $[\text{Rh}(\text{COD})(\mu\text{-Cl})_2]$ as precursor using TPPS and TPPO as stabilizers and NEt₃ as a base, under the same reaction conditions as those previously used in the generation of RhNP in the core of TPP@CCM-C [3] (Figure III.4). This led to a black colloidal suspension whose TEM images (Figure III.4.) revealed the formation of RhNPs of quite different sizes.

The use of TPPO as stabilizer yielded small and defined nanoparticles with ($d_m = 2.1 \pm 0.3$ nm), whereas TPPS yielded larger and more undefined nanoparticles ($d_m = 31 \pm 6$ nm). As TPPO was found to be more efficient for the generation of small RhNPs, TPPO@CCM-C was selected for studying the generation and confinement of RhNPs in the polymer cores.

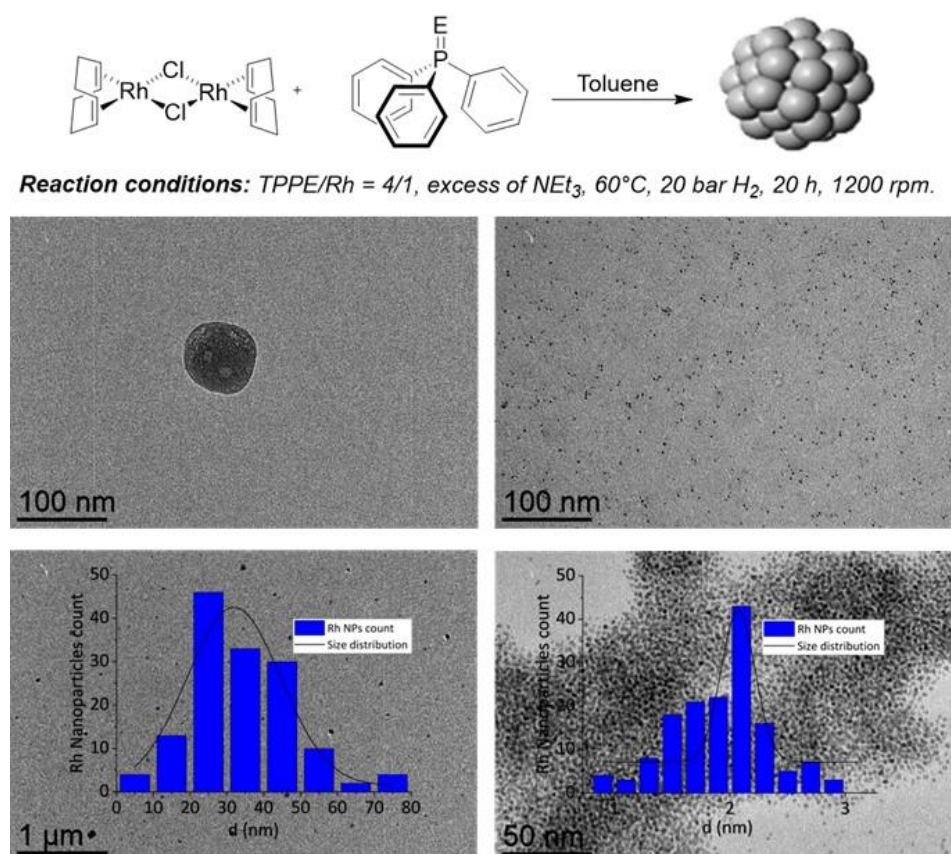


Figure III.4. TEM images and corresponding size distribution (overlaid) for RhNPs stabilized by (left) TPPS ($d_m = 31 \pm 6$ nm) and (right) TPPO ($d_m = 2.1 \pm 0.3$ nm).

III.3. Generation of Rhodium Nanoparticles

The first attempt to generate RhNP-TPPO@CCM-C followed the same procedure as previously developed to get RhNPs embedded in TPP@CCM-C, and consisted of loading the CCM-C micelles with $[Rh(COD)(\mu-Cl)]_2$ to generate a core-anchored $[RhCl(COD)(TPPO@CCM-C)]$ complex that could be reduced to RhNPs by H_2 [3]. Mononuclear complexes with the $[Rh(\eta^2:\eta^2\text{-diene})Cl(L)]$ stoichiometry (*e.g.*, diene = COD, norbornadiene) where L is an O-atom donor ligand are rare [16–19], but the

[RhCl(COD)(TPPO)] complex has been described [4,20,21]. Nevertheless, this method proved unsuccessful as the organic phase was observed to remain yellow-colored even after heating the reaction mixture at 60 °C for 1 h or after stirring at room temperature for 24 h. This indicated that the formation of a Rh^I-TPPO@CCM-C complex by cleavage of the di- μ -Cl-bridge moiety in [Rh(COD)(μ -Cl)]₂ was not favorable in the polymer core under the applied conditions. For this reason, an alternative strategy involving *ex-situ* synthesis of RhNPs and their subsequent transfer to the TPPO@CCM-C nanoreactors was envisaged (see below).

III.3.1. Kinetic study on the decomposition of [Rh(COD)(μ -Cl)]₂

The synthesis of RhNPs in toluene by the reduction of [Rh(COD)(μ -Cl)]₂ with H₂ (20 bar) in the presence of pyridine and TPP as stabilizing ligands is an alternative synthesis strategy. This ligand combination was inspired by previous work: TPP was found to be an effective stabilizer for producing ultras-small RhNPs [22–26] and pyridine was used for the formation of RhNPs in ionic liquids [24]. A screening was conducted to find the most suitable conditions for the generation of the RhNPs (Table III.1). Here, a Fisher-Porter tube was used to visually follow the color change of the [Rh(COD)(μ -Cl)]₂ solution, which is an indication of the reduction of the dimer complex under H₂ pressure. Reduction was favored at higher temperature (60 °C) with 3 bar of H₂, where a color-change of the solution containing the dimer and the stabilizers started within 10 min (Table III.1, entry 2) and resulted in a black suspension after 72 h (Table III.1, entry 4). In the UV-vis graph of the solution, the peak corresponding to the [Rh(COD)(μ -Cl)]₂ dimer at $\lambda = 408$ nm (Figure III.5, left) disappeared after the 72 h reaction at 60 °C, suggesting quantitative conversion of the Rh^I complex to RhNPs under these conditions. To confirm the formation of the RhNPs and determine their size, a TEM analysis was carried out on an aliquot withdrawn at the end of the experiment applied to Entry 4 (Figure III.5, right). This TEM image revealed the presence of small RhNPs with an average diameter of $d_m = 1.9 \pm 0.9$ nm.

Table III.1. Generation of RhNPs by the reduction of $[\text{Rh}(\text{COD})(\mu\text{-Cl})_2]_2$.^a

Entry	T (°C)	Time	Color of the reaction medium ^b
1	30	10 min	Yellow
2	60	10 min	Dark Yellow
3	30	72 h	Brown
4	60	72 h	Black

^a Toluene solution of $[\text{Rh}(\text{COD})(\mu\text{-Cl})_2]_2$ ($[\text{Rh}] = 14.2 \text{ mmol/L}$) with TPP and pyridine stabilizers ($\text{Rh/TPP/Pyridine} = 1/1/1$) and 3 bar H_2 in a Fisher-Porter tube. ^b Followed by UV-vis spectrophotometry.

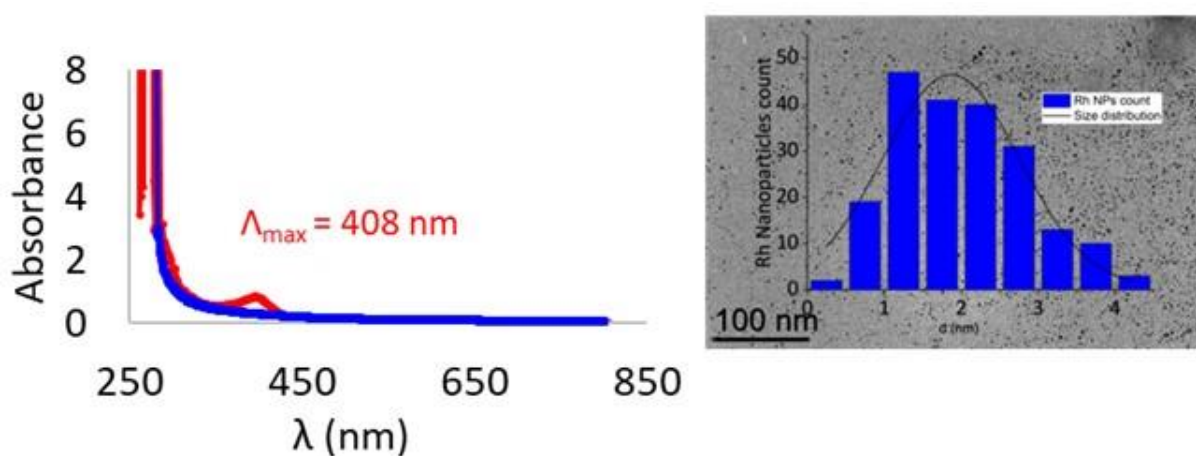


Figure III.5. UV-vis graphs of a toluene solution of $[\text{Rh}(\text{COD})(\mu\text{-Cl})_2]_2$ at $t = 0$ h (red) and $t = 72$ h (blue) after heating at 60°C (left), and TEM image with the corresponding size distribution (overlaid) of the RhNPs obtained after $t = 72$ h ($d_m = 1.9 \pm 0.9 \text{ nm}$) (right). Reaction conditions as reported in Table III.1, entries 2 and 4.

III.3.2. Generation of RhNPs under optimized conditions

To study the influence of the stabilizing ligands on the size control of RhNPs, the synthesis of the nanoparticles was also conducted in the presence of either a) pyridine alone ($\text{pyridine/Rh} = 1/1$), b) pyridine and TPP ($\text{TPP/Pyridine/Rh} = 0.5/0.5/1$), and c) TPP alone ($\text{TPP/Rh} = 1/1$) (Figure III.6). All experiments were conducted in toluene at 60°C , 20 bar H_2 , and 20 h, similar to the reaction conditions previously employed for the generation of RhNPs in the core of CCM-C [3].

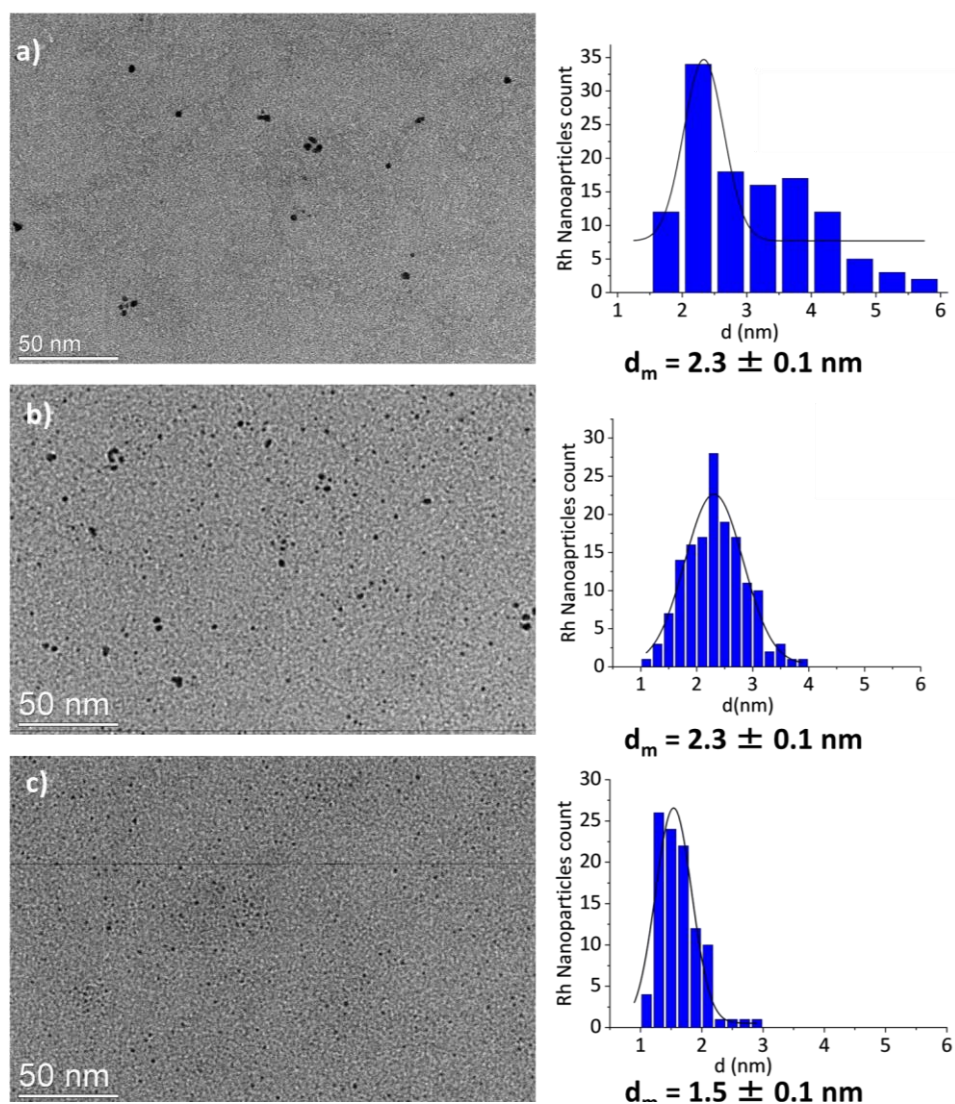


Figure III.6. TEM images and the corresponding size distribution of RhNPs stabilized by a) pyridine (Pyridine/Rh = 1/1), $d_m = 2.3 \pm 0.1$ nm; b) pyridine and TPP (TPP/Pyridine/Rh = 0.5/0.5/1), $d_m = 2.3 \pm 0.1$ nm and c) TPP (TPP/Rh = 1/1), $d_m = 1.5 \pm 0.1$ nm. Reaction conditions: 60 °C, 20 bar H_2 , 20 h, [Rh] = 14.2 mmol/L in toluene.

The generated RhNPs stabilized by TPP alone had the smallest mean diameter ($d_m = 1.5 \pm 0.1$ nm), whereas the NPs generated by pyridine stabilizer alone ($d_m = 2.3 \pm 0.1$ nm) or by pyridine and TPP stabilizers ($d_m = 2.3 \pm 0.1$ nm) were considerably larger but similar sized. These results clearly indicated the capacity of TPP to induce the formation of very small RhNPs. The RhNPs obtained with the ligand ratio TPP/Pyridine/Rh = 1/1/1 (Entry 4 in Table III.1) had an intermediate size (*ca.* 1.8 nm). Inspired by this result, nanoparticles were also generated with this ligand ratio with a higher H_2 pressure of 20 bar instead of 3 bar. Under these conditions (TPP/Pyridine/Rh

= 1/1/1, 60 °C, 20 bar H₂), a stable and black colloidal suspension of RhNPs in toluene was also formed after 20 h. TEM analysis of an aliquot of the suspension showed the presence of very small RhNPs displaying a mean diameter of 1.2 ± 0.4 nm and a symmetrical size distribution (Figure III.7). This result indicated that the combination of pyridine and TPP in a ratio TPP/Pyridine/Rh = 1/1/1 had a more efficient effect on the size control of the RhNPs than the TPP alone. These RhNPs synthesis conditions were therefore applied for the rest of the study.

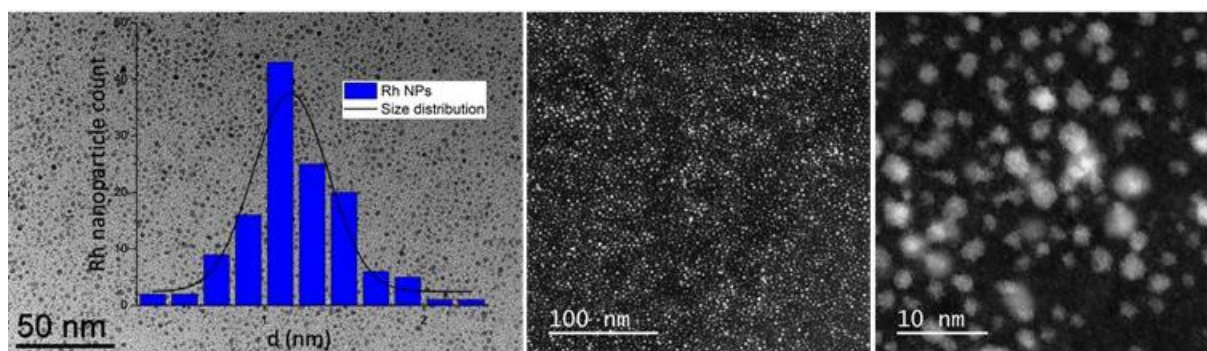


Figure III.7. TEM images of RhNPs synthesized with TPP and pyridine stabilizers (TPP/Pyridine/Rh = 1/1/1, 60 °C, 20 bar H₂) and (overlaid) the corresponding size distribution histogram ($d_m = 1.2 \pm 0.4$ nm).

III.4. Transfer of the RhNPs to the CCM-C core

Addition of the RhNPs colloidal suspension generated under optimized conditions in section III.3.2 (TPP/Pyridine/Rh = 1/1/1, 60 °C, 20 bar H₂) to the TPPO@CCM-C latex (P/Rh = 4/1), led to a fast and complete discoloration of the toluene phase while the latex became grey. This indicated the successful transfer of the RhNPs across the P(4VPMe⁺I) hydrophilic shell of the CCM-C and their anchoring to the TPPO functions in the polymer cores. This was further corroborated by DLS and TEM characterization of the final RhNP-TPPO@CCM-C (Figure III.8). The DLS analysis showed that the CCM-C polymer particles had very similar average size and size distribution before and after the loading with the RhNPs. The TEM analysis confirmed that the RhNPs were located inside the polymer particles and indicated an average size of *ca.* 1.5 ± 0.4 nm. Despite the presence of the polymer that renders the

measurement more difficult, it can be concluded that the RhNPs had quite similar sizes to the as-synthesized RhNPs (Figure III.8). This result indicates that the RhNPs are not significantly altered by the ligand exchange in the CCM-C core. Given these positive results, the final latex RhNP-TPPO@CCM-C could then be applied in biphasic hydrogenation catalysis (see below).

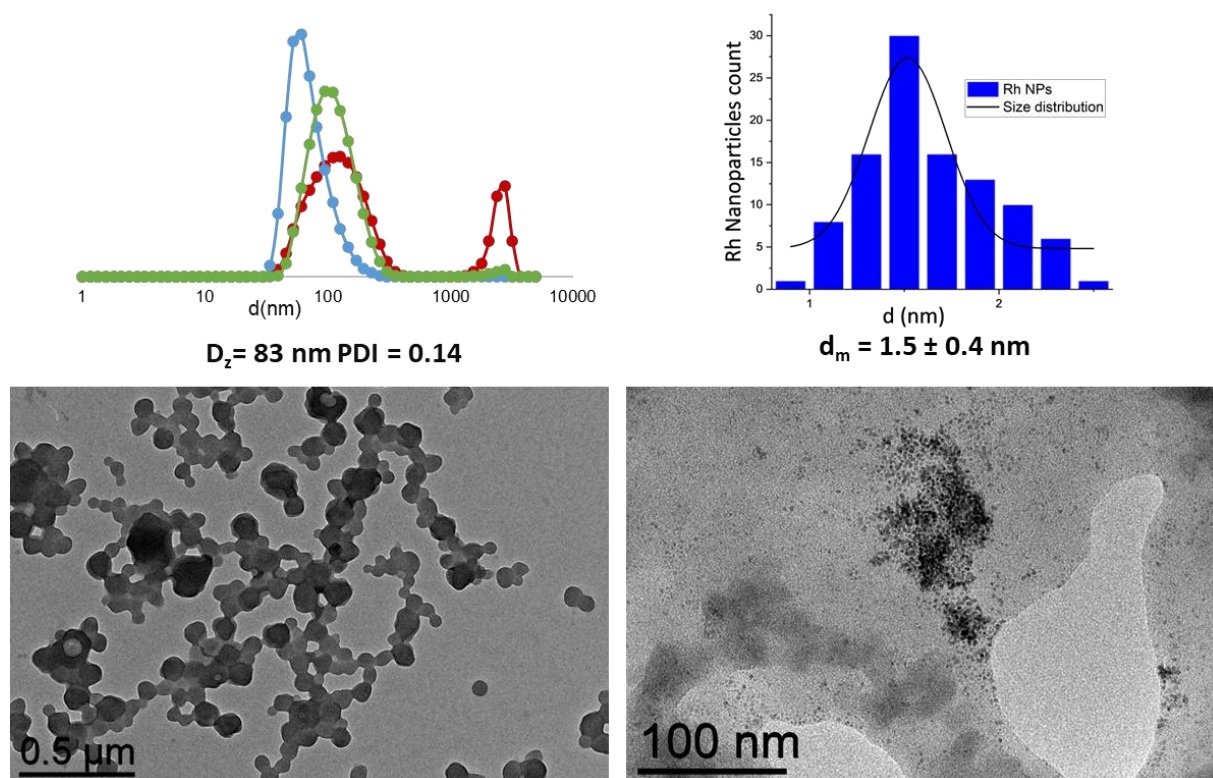


Figure III.8. DLS and TEM analysis of RhNP-TPPO@CCM-C (P/Rh = 4/1) showing the micelle size distribution (top left) and TEM images (bottom) with the corresponding size distribution of RhNPs (top right).

III.5. Catalytic hydrogenation with RhNP-TPPO@CCM-C (at LCC)

Catalytic hydrogenation (See Experimental Part) of 1-octene with the RhNP-TPPO@CCM-C nanoreactors (Rh/TPPO molar ratio of 1/4), was carried out under aqueous biphasic conditions for different reaction times using a 1-octene/Rh ratio of 200/1 with nonanol as vectorizing solvent (1-octene/nonanol = 1/9 v/v) and decane as internal standard (decane/1-octene molar ratio 1/4. Full substrate conversion was

reached after 0.5 h of vigorous stirring (1200 rpm) with 20 bar of H₂ at 25 °C (Figure III.9).

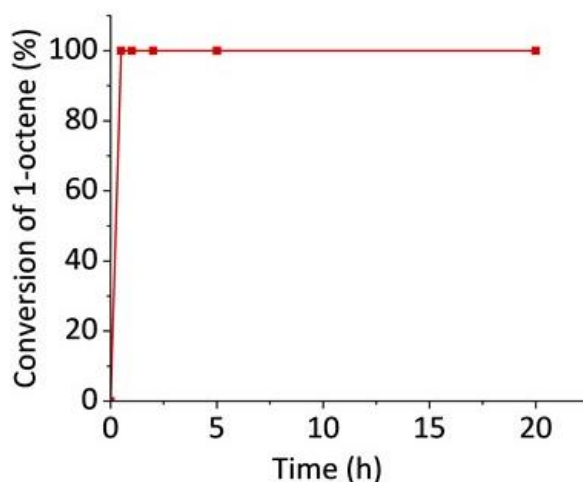


Figure III.9. Time plot for the aqueous biphasic hydrogenation of 1-octene with RhNP-TPPO@CCM-C nanoreactors (Rh/TPPO = 1/4) with nonanol as vectorizing solvent. Reaction conditions: 1-octene/Rh = 200/1, 1-octene/nonanol = 1/9 v/v, decane as internal standard (decane/1-octene = 1/4), 20 bar of H₂, 25 °C, 1200 rpm.

The recycling of the RhNP-TPPO@CCM-C latex was then evaluated using a 1-octene/Rh ratio of 2000/1 under otherwise identical conditions. At the set reaction time, the stirring was stopped leading to a neat phase separation within <3 min. The catalyst phase was then extracted and washed with diethyl ether and the combined diethyl ether phases were analyzed by GC. To pursue the catalysis, a fresh substrate solution (the same amount as in the initial run) was added followed by reaction under the same conditions and product separation using the same protocol as before. The hydrogenation of 1-octene was thus conducted over five consecutive runs (Figure III.10). Unlike the previously published results with the RhNP-TPP@CCM-C nanoreactors where the activity decreased because of RhNP extraction from the CCM-C cores[3], the RhNP-TPPO@CCM-C latex showed an essentially constant 1-octene conversion over the five runs. In addition, the TEM analysis of the recovered latex showed that the RhNPs remained confined in the CCM cores after the five catalytic runs, thus indicating the stability of the RhNP-TPPO@CCM-C latex in the recycling conditions applied conditions (Figure III.10).

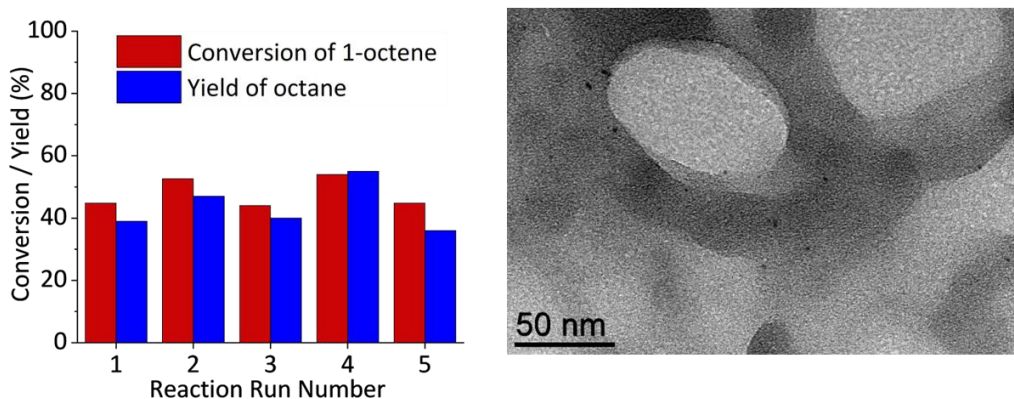


Figure III.10. Recycling study of RhNP-TPPO@CCM-C in 1-octene hydrogenation with intermediate product extraction by diethyl ether (left), and TEM image of the spent catalyst after the fifth reaction run (right). Reaction conditions: 1-octene/Rh = 2000/1, 1-octene/nonanol = 1/9 v/v, decane as internal standard (decane/1-octene = 1/4), 20 bar H₂, 25 °C, 0.25 h, 1200 rpm.

Given the successful recycling results obtained, the study was extended to the hydrogenation of styrene using the same reaction conditions with neat styrene and a substrate/Rh ratio of 2000/1 (decane as internal standard). Styrene is an interesting model substrate for studying chemoselectivity, as it contains an external C=C bond and an aromatic ring. Styrene is also a good solvent for the CCM polystyrene cores, and therefore, no vectorizing solvent was needed during catalysis. Full styrene conversion was achieved in 20 h at 20 bar H₂ and 60 °C with high selectivity (>99%) towards hydrogenation of the vinyl group, leading to ethylbenzene as the major product. Catalyst recycling was done using the same procedure as above, with no particular loss of catalyst activity over five recycling runs (Figure III.11). TEM and DLS analysis indicated no significant change in the morphology or the size of the micelles, respectively (*cf.* Figure III.12, $D_z = 68$ nm, with Figure. III.8, $D_z = 83$ nm).

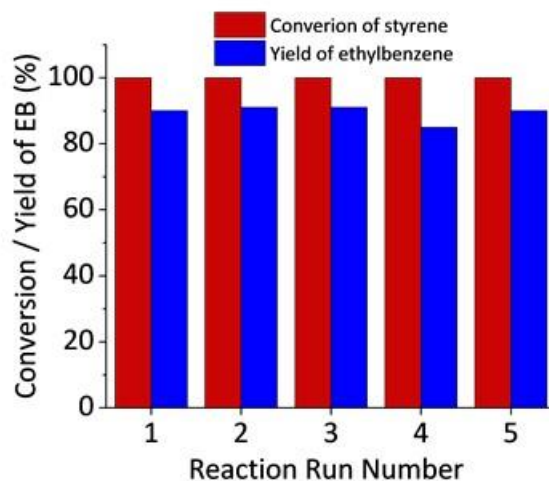


Figure III.11. Recycling study of RhNP-TPPO@CCM-C in styrene hydrogenation with intermediate product extraction by diethyl ether. Reaction conditions: styrene/Rh = 2000/1, decane as internal standard (decane/styrene = 1/4), 20 bar H₂, 60 °C, 20 h, 1200 rpm.

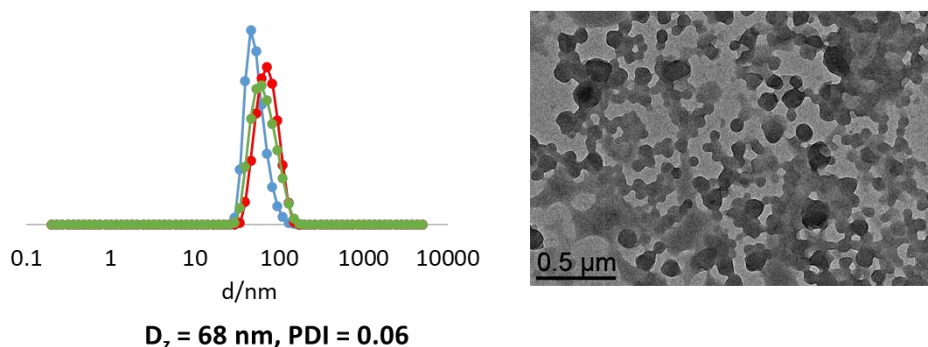


Figure III.12. DLS size distributions (PDI = 0.06; D_z = 68 nm) (left) and TEM image of the spent RhNP-TPPO@CCM-C catalyst after the fifth recycling run for styrene hydrogenation (right). Color coding: number (blue), volume (green), and intensity (red).

A recovery and recycling experiment was also carried out at a lower temperature (25 °C) and shorter reaction time (1.5 h) under otherwise identical conditions, in order to ensure partial conversion of styrene. The results looked promising as no significant loss of activity was observed and the system was recyclable in the five runs (Figure III.13).

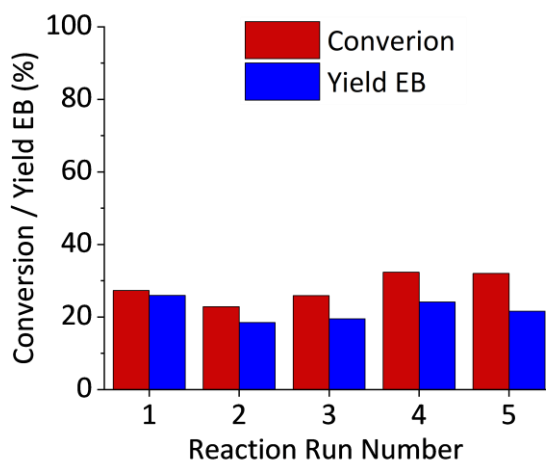


Figure III.13 Recycling study of RhNP-TPPO@CCM-C in styrene hydrogenation with intermediate product extraction by diethyl ether. Reaction conditions: styrene/Rh = 2000/1, decane as internal standard (decane/styrene = 1/4), 20 bar H₂, 25 °C, 1.5 h, 1200 rpm.

III.6. Catalytic studies of the hydrogenation of styrene (at DTU)

A reproducibility study for styrene hydrogenation was carried out at DTU, but unfortunately the results were not identical to the result obtained at LCC (Figure III.14). Under the identical reaction conditions (St/Rh ratio of 2000/1, 25 °C, 20 bar H₂, 1200 rpm) complete styrene conversion was obtained after only 0.25 h at DTU against 15 h at LCC. The disparity of the results led to further investigations to understand the source of the reproducibility issues.

The initial catalytic studies at LCC were completed in 100 mL autoclave (45 x 15 mm reactor vessel), and the stirring was ensured by a standard cylindrical magnetic stir bar. At DTU, on the other hand, the equipment consisted of a 15 mL autoclave (40 x 20 mm vial), and a magnetic cross stir bar. These differences alerted us about the possible presence of different diffusion properties in the two systems (See Experimental Part). To learn more about this issue, the RhNP-TPPO@CCM-C latex was evaluated in the hydrogenation of styrene without stirring in the DTU equipment under the same conditions as applied with stirring. In the absence of stirring, a conversion of *ca.* 63% was obtained after 5 h (*vs* a complete conversion after only 0.25 h under stirring). This result clearly indicated that when doing the biphasic hydrogenation at LCC the

system was in a diffusion domain rather than a kinetic domain, and explains also the disparity in the obtained results.

It is important to highlight at this point, that all catalytic experiments reported ahead in this manuscript (unless stated otherwise), were performed at DTU.

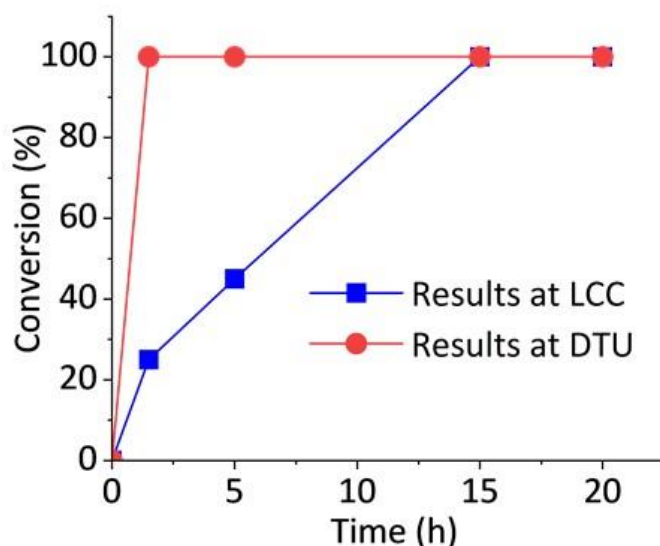


Figure III.14. Time plot for the aqueous biphasic hydrogenation of styrene using RhNP-TPPO@CCM-C done at (blue) LCC and at (red) DTU. Reaction conditions: styrene/Rh = 2000/1, decane as internal standard (decane/styrene = 1/4), 20 bar H₂, 25 °C, 1200 rpm.

III.6.1. Hydrogenation of styrene with colloidal RhNP/toluene suspension and RhNP-TPPO@CCM-C latex under optimized conditions

The catalytic activity of the colloidal toluene suspension of TPP/pyridine-stabilized RhNPs was evaluated for the hydrogenation of styrene under the mild reaction conditions defined above (20 bar H₂, 25 °C, 0.25 h) with styrene/Rh = 10000/1. A styrene conversion of ~90% was obtained, corresponding to an average TOF of ~36000 h⁻¹ (*c*TOF ~40700 h⁻¹) with complete selectivity towards EB. This catalytic performance is superior to those previously described for styrene hydrogenation with RhNPs stabilized by TPP (TOF of ~6000 h⁻¹) or diphosphate ligands (TOF of ~24000 h⁻¹) in heptane at room temperature with 40 bar H₂ and 0.25 h [22].

III.6.2. Hydrogenation of styrene with RhNP-TPPO@CCM-C

Next, the RhNP-TPPO@CCM-C latex was applied for the aqueous biphasic hydrogenation of styrene under the same temperature and pressure conditions as with the colloidal toluene RhNPs suspension (20 bar H₂, 25°C), with a styrene/Rh ratio of 2000/1, at different reaction times (Figure III.15). A nearly complete styrene conversion (~94%) was obtained in only 0.25 h, corresponding to a TOF of 7733 h⁻¹ (*c*TOF of 9850 h⁻¹), with excellent selectivity (>99%) towards EB (Table III.2, entry 1).

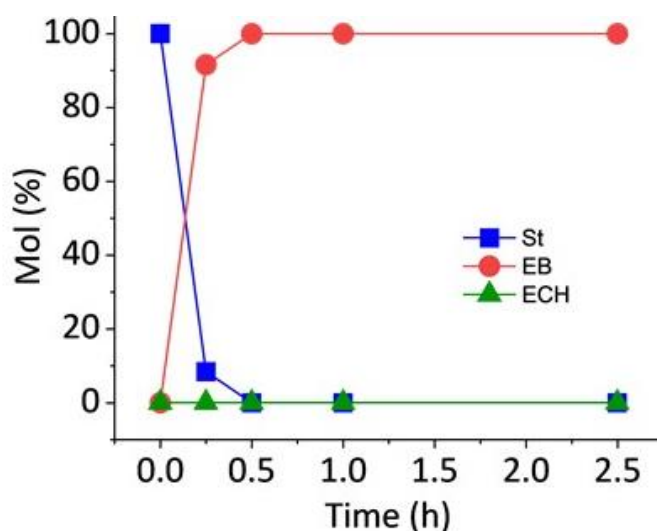


Figure III.15. Time plot for the aqueous biphasic hydrogenation of styrene using the RhNP-TPPO@CCM-C latex. Reaction conditions: styrene/Rh = 2000/1, decane as internal standard (decane/styrene = 1/4), 20 bar H₂, 25 °C, 1200 rpm.

Table III.2. Hydrogenation of styrene using RhNP-TPPO@CCM-C.^a

Entry	Molar styrene/Rh ratio	Conversion (%)	Product Yield (%)		TOF (<i>c</i> TOF) (h ⁻¹) ^b
			EB	ECH	
1	2000/1	94	94	<0.1	7733 (9850)
2	5000/1	53	52	<0.1	10547 (14300)
3	10000/1	24	23	<0.1	9062 (12440)

^a Reaction conditions: 20 bar H₂, 25°C, 0.25 h. ^b Average values over the duration of the reaction, expressed as moles of substrate converted per moles of Rh in the catalyst per hour (TOF) or as moles of substrate converted per moles of surface Rh atoms per hour (*c*TOF, in parenthesis). EB = ethylbenzene, ECH = ethylcyclohexane.

This catalytic performance was superior to that previously achieved with RhNPs embedded in the TPP@CCM-C and some other systems reported in the literature

[3,22,25,27] (Table III.3). This difference may be related to the smaller size of the *ex-situ* synthesized TPP/pyridine-stabilized RhNPs used to get RhNP-TPPO@CCM-C compared to the *in-situ* synthesized TPP@CCMC-stabilized RhNPs in RhNP-TPP@CCM-C (1.2 nm *vs.* < 5 nm). However, additional experiments indicated that the adsorbed TPP and pyridine stabilizers in the RhNP-TPPO@CCM-C catalyst also played a role (*vide infra*). An increase of the styrene/Rh ratio resulted in good and reproducible conversions within 0.25 h of 53% (styrene/Rh = 5000/1) and 24% (styrene/Rh = 10000/1), corresponding to TOFs of 10547 and 9062 h⁻¹ (*c*TOFs of 14300 and 12440 h⁻¹), respectively, again with full selectivity towards EB (Table III.2, entries 2 and 3).

Table III.3. Catalytic performance of different RhNP systems for the hydrogenation of styrene.

Stabilizer	RhNPs size (nm)	TOF (h ⁻¹)	Ref.
Triphenylphosphine	1.5	5842 ^a	[22]
Triphenylphosphite	1.52	3354 ^a	[22]
1,4-Bis(diphenylphosphino)butane	1.57	4414 ^a	[22]
TPP@CCM-C	3.7	1000 ^b	[3]
(2-(Diphenylphosphino)ferrocenyl)methane	1.3	32 ^c	[25]
(2-(diphenylphosphino)ferrocenyl)methane	1.5	18 ^c	[25]
Ion-exchange Resin Rh@D100H ⁺	2.5	270 ^d	[27]

Reaction conditions: ^a 40 bar H₂, RT, 0.25 h, heptane. ^b 20 bar H₂, RT, 20 h, neat styrene. ^c 30 bar H₂, RT, 24 h, iPrOH. ^d 1 bar H₂, RT, 1.6 h, methanol.

The recycling of the catalytic RhNP-TPPO@CCM-C latex was evaluated in two series of experiments at a fixed styrene/Rh ratio of 5000/1, by extracting the reaction products with diethyl ether or toluene, respectively, prior to the addition of a new batch of substrate for the next catalytic run. The extraction protocol was identical to that used in the previously reported recycling studies with the RhNP-TPP@CCM-C [3] and with the molecular Rh^I-TPP@CCM [2] catalytic systems. Upon stopping the stirring, a rapid phase separation (< 3 min) was observed in all reactions, thus facilitating the product separation and catalyst recovery, as already reported for the RhNP-TPP@CCM-C nanoreactors featuring the same outer shell [3]. The first catalytic runs yielded styrene

conversion of 53% in 0.25 h. However, a gradual decrease in conversion, from 53% to *ca.* 9-15%, was witnessed after the fifth run for both series of recycles, using either toluene or diethyl ether for product extraction (Figure III.16). The ICP-MS analyses showed only a cumulative loss of ~2% of the catalyst inventory after the five catalytic runs when using diethyl ether as extraction solvent, indicating that the activity decrease was not caused by metal leaching and mechanical loss of latex (Table III.4).

Table III.4. ICP-MS data for the leaching of Rh metal after each catalytical run with diethyl ether used as the washing solvent.

Run no.	$^{103}\text{Rh(LR)}^*$	IF cor RSD**	[Rh] (ppt)	[Rh] (ppm)	$\Sigma[\text{Rh}]$ (ppm)	[Rh] _{initial} (ppm)	RhNPs leached (mol %) ^{***}
1	1435618.1	1.32	283.3447	1.03			
2	1466627.8	1.10	278.5785	1.06			
3	1579747.4	1.07	560.6121	1.14	4.42	217	2.04
4	543900.5	1.64	735.1959	0.39			
5	1117440.4	0.73	91.3278	0.80			

* Low Resolution (LR). ** Relative standard deviation (RSD) was calculated for all the runs separately. *** Rh (mol%) cumulative loss.

Moreover, after catalyst separation, whether toluene or diethyl ether was used as the extraction solvent, the organic phase was completely transparent and colorless while the aqueous phase remained grey, thus indicating the retention of the RhNPs in the CCM-C latex. In both cases, the TEM images obtained for the RhNP-TPPO@CCM-C catalyst after the fifth run evidenced a preserved confinement of the RhNPs in the CCM-C cores with well-dispersed RhNPs. These results indicate that the interaction of the RhNPs with the core-linked TPPO ligands is sufficiently strong to retain them within the hydrophobic CCM-C cores, validating the initial hypothesis of the superior efficiency of oxygen-coordinating ligands. Though an artifact cannot be ruled out due to the less defined polymer-embedded RhNPs, a notable change was an increase in the particle size (from 1.5 ± 0.4 nm to 2.2 ± 0.9 nm after the fifth catalytic run) (Figure

III.17). This may indicate a slight growth or aggregation of the NPs. However, given that the standard deviation value is larger than the size change (0.9 nm *vs.* 0.7 nm), the NPs can also be considered as to be in a similar size range, thus the interpretation of the activity drop as a result of a size change does not appear satisfactory.

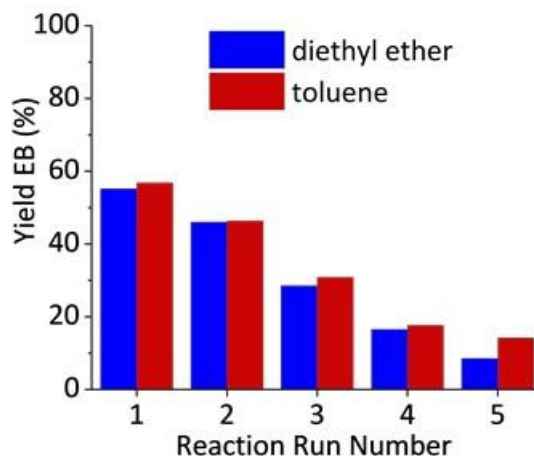


Figure III.16. Recycling study of RhNP-TPPO@CCM-C in styrene hydrogenation with intermediate product extraction by diethyl ether (blue) and toluene (red). Reaction conditions: Styrene/Rh = 5000/1, decane as internal standard (decane/styrene = 1/4), 20 bar H₂, 25 °C, 0.25 h, 1200 rpm.

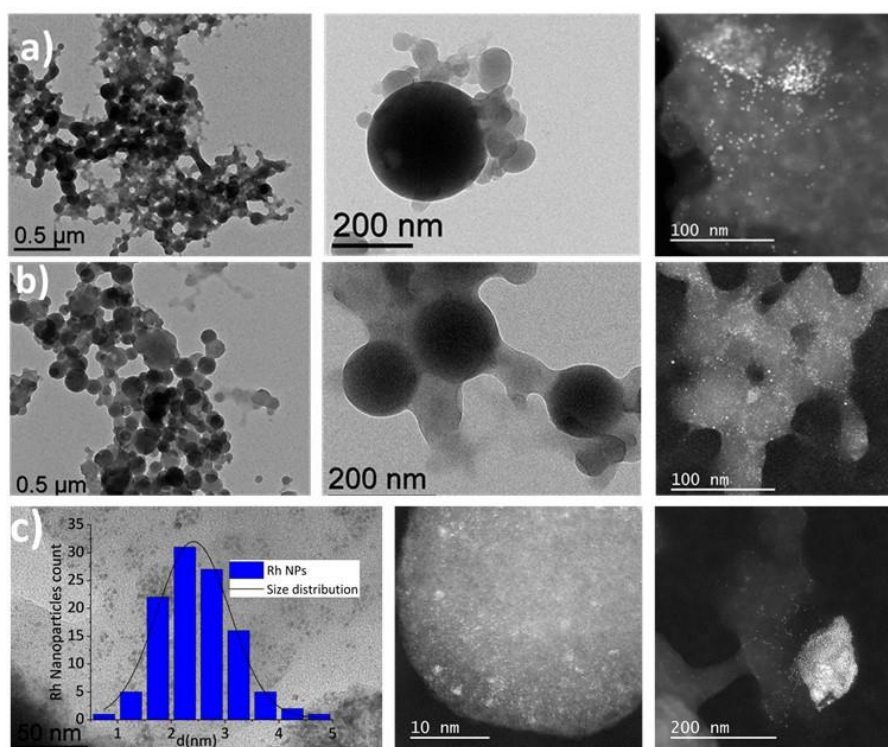


Figure III.17. TEM images of the spent RhNP-TPPO@CCM-C catalyst after the fifth catalytic run of styrene hydrogenation with intermediate product extraction by (a) diethyl ether and (b) toluene. Reaction conditions: Styrene/Rh = 5000/1, decane as internal standard (decane/styrene = 1/4), 20 bar H₂, 25 °C, 15 min, 1200 rpm. (c) TEM image and corresponding size distribution of RhNPs after washing with diethyl ether ($d_m = 2.2 \pm 0.9$ nm).

Given that, no significant metal leaching was detected and that no substantial NP agglomeration that may lead to loss of active surface was observed, progressive passivation of the RhNPs surface by rhodium oxide formation could be responsible for the decrease in catalytic performance over subsequent cycles. To verify this hypothesis, the catalyst recycling with product extraction by diethyl ether was completed under an inert argon atmosphere. In addition, the recovered RhNP-TPPO@CCM-C phase was treated with H₂ (20 bar H₂, 25°C, 1 h) prior to each catalytic run, to remove any rhodium oxide layer. Despite these precautions in the recycling experiments, the styrene conversion still decreased to 10% along the five runs (Figure III.18). The similarity of these results to those achieved without an inert atmosphere and reductive treatment (Figure III.16), suggests that passivation of the RhNPs was not the unique reason behind the decrease in the activity.

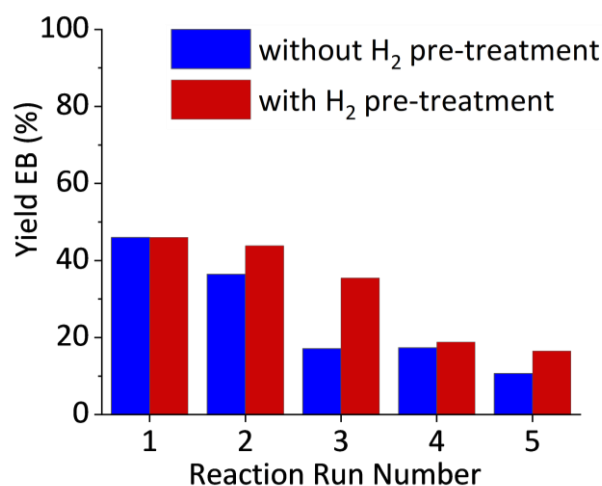


Figure III.18. Reuse of RhNP-TPPO@CCM-C in five catalytic runs of styrene hydrogenation with product extraction by diethyl ether under argon with and without intermediate H₂ treatment (20 bar H₂, 25°C, 1 h). Reaction conditions: Styrene/Rh = 5000/1, decane as internal standard (decane/styrene = 1/4), 20 bar H₂, 25°C, 0.25 h, 1200 rpm.

Another hypothesis that was considered for the activity decrease is a progressive catalyst poisoning by the 4-*tert*-butylcatechol used as a stabilizer for styrene. To probe this hypothesis, a new recycling investigation was carried out using purified styrene, but the same drop of activity was still observed, thus excluding this hypothesis. A reduction of the anchoring TPPO ligands to TPP by H₂, catalyzed by the RhNPs, is another possible hypothesis to explain the observed activity decrease, assuming a lower activity for RhNP-TPP relative to RhNP-TPPO. To assess this hypothesis, a toluene solution of TPPO- and TPP/pyridine-stabilized RhNPs (TPPO/Rh = 8/1) was exposed to H₂ (20 bar) at 60°C for 22 h. A ³¹P NMR monitoring of the solution revealed no detectable TPPO reduction. This result seems to indicate that the TPPO ligands in the CCM-C core most likely remained unchanged under the conditions of the aqueous biphasic styrene reduction catalysis. The absence of TPPO reduction to TPP is also indirectly indicated by the demonstrated ability of diethyl ether to extract the RhNPs from the RhNP-TPP@CCM-C [19], whereas the TEM analysis (*vide supra*) shows that the RhNPs are well-retained in the micellar core. A final working hypothesis is that the stabilizers used for the *ex-situ* synthesis of RhNPs (TPP/pyridine) partially remained in the TPPO@CCM-C core after loading and promoted the catalytic activity

of the RhNPs, and that the activity gradually decreased as these stabilizers/promoters were continuously washed out during the work-up for catalyst recovering and recycling. This hypothesis was tested by washing the fresh RhNP-TPPO@CCM-C latex, after RhNPs loading, three times with diethyl ether prior to use in catalysis. A GC-MS analysis of the diethyl ether extracts showed two peaks with MS spectra yielding molecular ions at m/z 112 and 83, respectively (Appendix B, Figure B3). These peaks matched cyclooctane and tetrahydropyridine, respectively, resulting from the hydrogenation of the COD ligand from $[\text{Rh}(\text{COD})(\mu\text{-Cl})_2]$ and of pyridine during the *ex-situ* synthesis of the RhNPs [28–30]. Subsequently, five subsequent catalytic runs (all reproduced three times) were carried out (20 bar H_2 , 25°C, 1 h) (Figure III.19). The first catalytic run provided a low conversion of styrene (~6%), whereas a constant styrene conversion of *ca.* 25% was achieved in the following four runs, corresponding to an average TOF of $\sim 1025 \text{ h}^{-1}$ (*c*TOF $\sim 1440 \text{ h}^{-1}$). The low conversion in the first run might indicate that an induction time would be necessary to deblock the active sites and/or the RhNPs experienced significant changes under catalytic conditions.

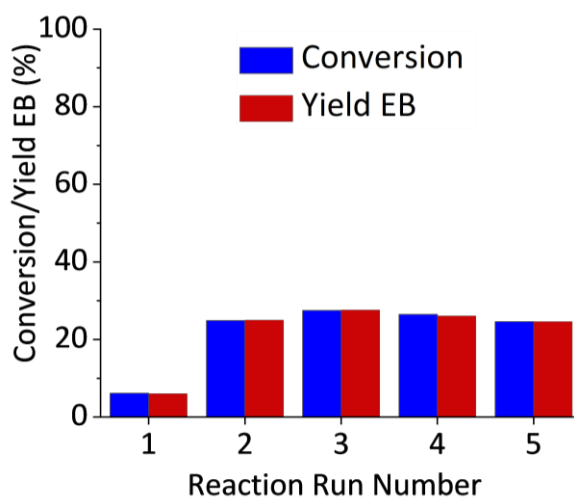


Figure III.19. Hydrogenation of styrene with RhNP-TPPO@CCM-C after three washings with diethyl ether (run 1) and recycling of the catalyst in four additional reaction runs with product extraction by diethyl ether and intermediate H_2 treatment (20 bar H_2 , 25°C, 1 h). Reaction conditions: Styrene/Rh = 5000/1, decane as internal standard (decane/styrene = 1/4), 20 bar H_2 , 25°C, 1 h, 1200 rpm.

Comparison of a series of TEM measurements performed with the diethyl ether-washed catalyst (prior to catalysis) before/after H₂ treatment and after the first and fifth catalytic runs (Figure III.20), confirmed that the RhNPs mean size indeed changed from 4.2 ± 0.2 nm to 2.2 ± 0.2 nm before and after H₂ treatment, respectively, and was further reduced to a static size of $1.8 \pm 0.1-0.3$ nm after the first catalytic run. Thus, the removal of the stabilizers likely induced a slight size increase or agglomeration of the RhNPs, resulting in lower catalytic activity, as also previously reported for RhNPs in styrene hydrogenation [22,29], while the successive H₂ treatment prompted reconstruction [26,31] of the NPs possibly aided by the presence of TPPO@CCM-C. Notably, although a different reaction time was applied (1 h *vs.* 0.25 h), the styrene conversion value of *ca.* 25% obtained after the initial run is comparable to that obtained in the fourth and fifth recycles (Appendix B, Table B1), performed with intermediate product extraction by diethyl ether (Figure III.16). This suggests that the diethyl ether washings performed between the consecutive catalytic runs (Figure III.16) have a similar effect to those carried out on the fresh RhNP-TPPO@CCM-C prior to its implementation in catalysis. This indicates a possible role of the RhNP stabilizers (TPP, pyridine and tetrahydropyridine, see GC-MS results above) on the hydrogenation of styrene when they are not eliminated by solvent washings [32–35]. It is also to be noted that, as shown above, the RhNP-catalyzed styrene hydrogenation in toluene yields a much higher TOF for the RhNPs stabilized by TPP and pyridine (~ 36000 h⁻¹) with respect to other RhNPs synthesized using other stabilizers, under similar experimental conditions [26]. This highlights that a careful choice of stabilizers to pre-synthesized RhNPs for their transfer in the CCM-C, or the integration of co-ligands in the cores of CCM-C could be a way to boost the catalytic performance, but this is out of the scope of the present work.

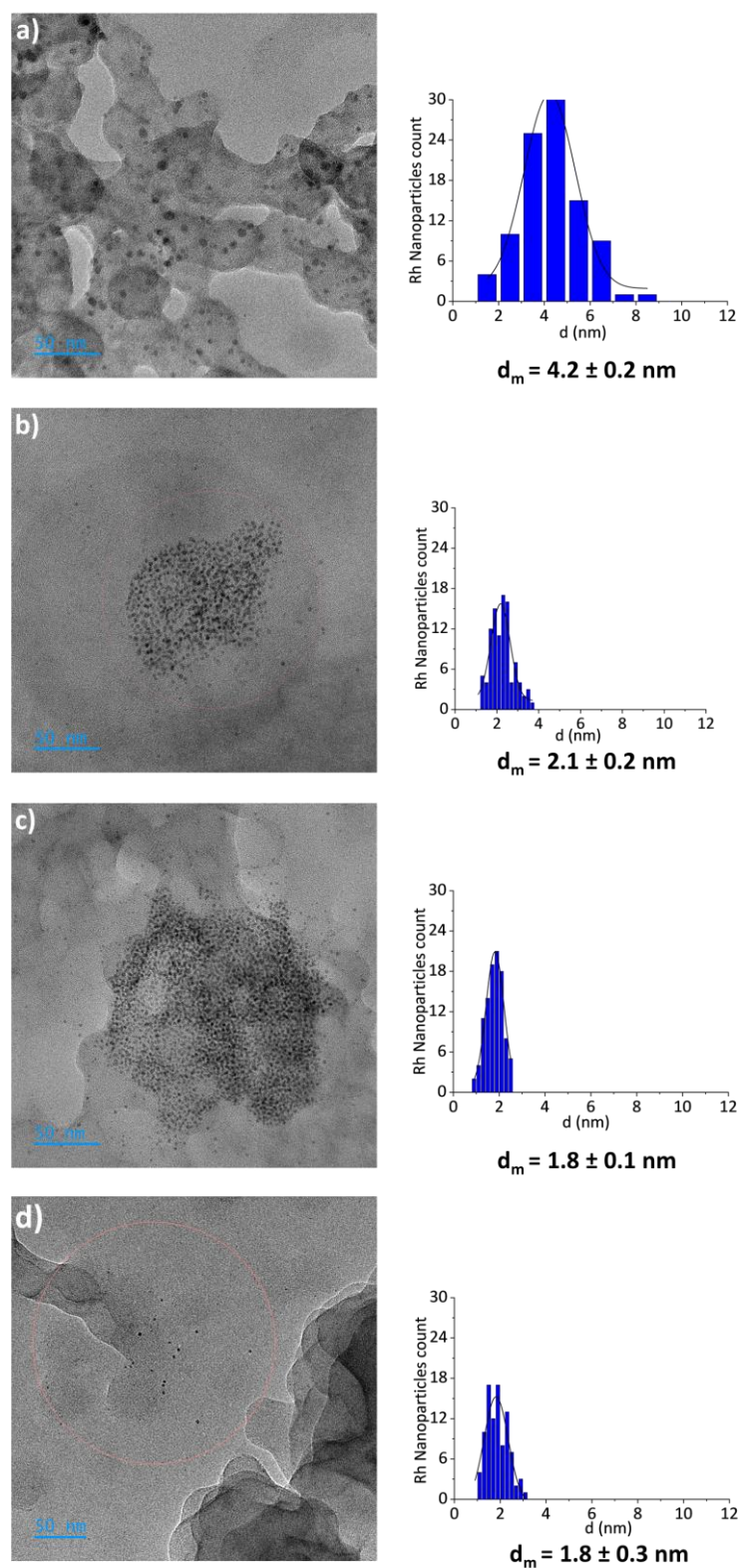


Figure III.20. HR-TEM analysis of withdrawn aliquots with RhNP-TPPO@CCM-C catalyst after a) washing with ether prior to regeneration ($d_m = 4.2 \pm 0.2$ nm), b) regeneration with 20 bar H_2 , 1h, 25 °C ($d_m = 2.1 \pm 0.2$ nm), c) first hydrogenation run ($d_m = 1.8 \pm 0.1$ nm), and d) fifth hydrogenation run ($d_m = 1.8 \pm 0.3$ nm).

III.7. Summary and Outlook

Ultrasmall TPP/pyridine-stabilized RhNPs demonstrated excellent catalytic activity (average TOF of $\sim 36000\text{ h}^{-1}$, c TOF of $\sim 40700\text{ h}^{-1}$) and complete selectivity in the hydrogenation of styrene to EB under mild conditions ($25\text{ }^{\circ}\text{C}$, 20 bar of H_2) in toluene. These NPs were successfully transferred to the TPPO-functionalized core of a novel CCM-C polymer with a cationic shell synthesized by RAFT polymerization. The resulting RhNP-TPPO@CCM-C latex proved effective in the aqueous biphasic hydrogenation of styrene. Contrarily to the similar TPP core ligand-containing polymer (RhNP-TPP@CCM-C), the RhNPs remain anchored to the polymer core by diethyl ether extraction of the hydrogenation product. This shows that the nature of the core functional ligands of the polymer micelles is a key parameter to improve the stability and the recycling of the catalytic latex. Even though the extraction of the TPP and pyridine ligands used for the *ex-situ* RhNP synthesis during the work-up between recycles, induced a gradual decrease of the catalytic activity, a stable catalyst phase was obtained after preliminary extensive washing and an initial reaction run, yielding a TOF of $\sim 1025\text{ h}^{-1}$ (c TOF $\sim 1440\text{ h}^{-1}$), over several recycles. Further investigations could focus on improving the catalytic performance of the CCM nanoreactors and on extending their application to the hydrogenation of other substrates, including carbonyl compounds. Furthermore, RhNP-TPPO@CCM-C exhibited superior efficiency in the hydrogenation of 1-octene when compared to its counterparts featuring TPP@CCM-C. Nevertheless, it is important to utilize the optimized system described herein, for subsequent comparative analyses and research endeavors.

This chapter has also presented the synthesis of a well-dispersed latex of TPPS@CCM-C. Although TPPS ligands proved ineffective for the generation of small RhNPs, TPPS is a good ligand for Au^{III} , Pd^{I} and Pd^{II} and these molecular systems could successfully be used in other catalyzed reactions like thia-Michael additions [36], allylic alkylations

[37] or cross-coupling reactions [4,38], opening new perspectives on the catalytic application of these nanoreactors.

III.8. References

- [1] A. Joumaa, S. Chen, S. Vincendeau, F. Gayet, R. Poli, E. Manoury, Rhodium-catalyzed aqueous biphasic hydrogenation of alkenes with amphiphilic phosphine-containing core-shell polymers, *Molecular Catalysis*. 438 (2017) 267–271. <https://doi.org/10.1016/j.mcat.2017.06.005>
- [2] H. Wang, L. Vendrame, C. Fliedel, S. Chen, F. Gayet, F. D'Agosto, M. Lansalot, E. Manoury, R. Poli, Triphenylphosphine-Functionalized Core-Cross-Linked Micelles and Nanogels with a Polycationic Outer Shell: Synthesis and Application in Rhodium-Catalyzed Biphasic Hydrogenations, *Chemistry - A European Journal*. 27 (2021) 5205–5214. <https://doi.org/10.1002/chem.202004689>
- [3] H. Wang, A.M. Fiore, C. Fliedel, E. Manoury, K. Philippot, M.M. Dell'Anna, P. Mastrorilli, R. Poli, Rhodium nanoparticles inside well-defined unimolecular amphiphilic polymeric nanoreactors: Synthesis and biphasic hydrogenation catalysis, *Nanoscale Adv.* 3 (2021) 2554–2566. <https://doi.org/10.1039/d1na00028d>
- [4] P. Das, P. Chutia, D. Kumar Dutta, Efficient Carbonylation of Methanol Catalyzed by Rhodium(I) Cyclooctadiene Complexes with Triphenylphosphinechalcogenide Ligands, *Chem Lett* 7 (2002) 766–767, <https://doi.org/10.1246/cl.2002.766>
- [5] S. Chen, E. Manoury, F. Gayet, R. Poli, Coordination chemistry inside polymeric nanoreactors: Metal migration and cross-exchange in amphiphilic core-shell polymer latexes, *Polymers (Basel)*. 8(2) (2016) 26 <https://doi.org/10.3390/polym8020026>
- [6] S. Chen, F. Gayet, E. Manoury, A. Joumaa, M. Lansalot, F. D'Agosto, R. Poli, Coordination Chemistry Inside Polymeric Nanoreactors: Interparticle Metal Exchange and Ionic Compound Vectorization in Phosphine-Functionalized Amphiphilic Polymer Latexes, *Chemistry - A European Journal*. 22 (2016) 6302–6313. <https://doi.org/10.1002/chem.201504923>
- [7] R. Rabinowitz, R. Marcus, J. Pellon, Synthesis, polymerization, and copolymerization of diphenyl-p-styrylphosphine, phosphine oxide, and phosphine sulfide, *J Polym Sci A*. 2 (1964) 1241–1249. <https://doi.org/10.1002/pol.1964.100020321>.

- [8] N. Li, F. Chen, G. Wang, Q. Zeng, Copper-catalyzed C–P cross-coupling of arylmethyl quaternary ammonium salts via C–N bond cleavage, *Monatsh Chem.* 151 (2020) 99–106. <https://doi.org/10.1007/s00706-019-02535-y>
- [9] H. Wang, L. Vendrame, C. Fliedel, S. Chen, F. Gayet, E. Manoury, X. Zhang, F. D'agosto, M. Lansalot, R. Poli, Core-Cross-Linked Micelles Made by RAFT Polymerization with a Polycationic Outer Shell Based on Poly(1-methyl-4-vinylpyridinium), *Macromolecules.* 53 (2020) 2198–2208. <https://doi.org/10.1021/acs.macromol.9b02582>
- [10] R. el Abed, F. Aloui, J.P. Genêt, B. ben Hassine, A. Marinetti, Synthesis And Resolution Of 2-(Diphenylphosphino)Heptahelicene, *J Organomet Chem.* 692 (2007) 1156–1160, <https://doi.org/10.1016/j.jorganchem.2006.11.022>
- [11] J. Sanmartín, M.R. Bermejo, C.A. Mcauliffe, A. Sousa, M. Fondo, E. Gómez-Fórneas, Synthesis Of Polymer-Supported Triphenylphosphine Oxide Complexes Of Divalent Copper And Cobalt. A Study On Their Reactivity With Sulfur Dioxide *Inorg Chim Acta* 255 (1997) 269-278, [https://doi.org/10.1016/S0020-1693\(96\)05373-X](https://doi.org/10.1016/S0020-1693(96)05373-X)
- [12] R.K. O'reilly, C.J. Hawker, K.L. Wooley, Cross-linked block copolymer micelles: Functional nanostructures of great potential and versatility, *Chem Soc Rev.* 35 (2006) 1068–1083. <https://doi.org/10.1039/b514858h>
- [13] S. Kondo, K. Furukawa, K. Tsuda. Polymeric analogues of triphenylphosphine oxide as stable phase transfer catalysts. *J Polym Sci Part A* 30 (1992) 1503-1506 <https://doi.org/10.1002/POLA.1992.080300731>
- [14] C. Li, Y. Wang, D. Sun, H. Li, X. Sun, D. Ma, Z. Ren, S. Yan, Thermally Activated Delayed Fluorescence Pendant Copolymers with Electron- and Hole-Transporting Spacers, *ACS Appl Mater Interfaces.* 10 (2018) 5731–5739. <https://doi.org/10.1021/acsami.8b00136>
- [15] H. Wang, C.J. Abou-Fayssal, C. Fliedel, E. Manoury, R. Poli, Phosphine-Functionalized Core-Crosslinked Micelles and Nanogels with an Anionic Poly(styrenesulfonate) Shell: Synthesis, Rhodium(I) Coordination and Aqueous Biphasic Hydrogenation Catalysis, *Polymers (Basel).* 14 (2022) 14224937 <https://doi.org/10.3390/polym14224937>
- [16] S. Vanicek, M. Podewitz, J. Stubbe, D. Schulze, H. Kopacka, K. Wurst, T. Müller, P. Lippmann, S. Haslinger, H. Schottenberger, K.R. Liedl, I. Ott, B. Sarkar, B. Bildstein, Highly Electrophilic, Catalytically Active and Redox-Responsive Cobaltoceniumyl and Ferrocenyl Triazolylidene Coinage Metal Complexes, *Chemistry - A European Journal.* 24 (2018) 3742–3753. <https://doi.org/10.1002/chem.201705051>

- [17] M. Deimling, M. Kirchhof, B. Schwager, Y. Qawasmi, A. Savin, T. Mühlhäuser, W. Frey, B. Claasen, A. Baro, T. Sottmann, S. Laschat, Asymmetric Catalysis in Liquid Confinement: Probing the Performance of Novel Chiral Rhodium–Diene Complexes in Microemulsions and Conventional Solvents, *Chemistry - A European Journal*. 25 (2019) 9464–9476. <https://doi.org/10.1002/chem.201900947>
- [18] J. Nowakowski, S. Nowakowska, G. Srivastava, M. Baljovic, J. Girovsky, N. Ballav, T.A. Jung, Probing the Reactivity of Functionalized Surfaces by Porphyrin Metalation, *ChemistrySelect*. 1 (2016) 891–895. <https://doi.org/10.1002/slct.201600215>
- [19] T. Nishimura, Y. Maeda, T. Hayashi, Asymmetric cyclopropanation of alkenes with dimethyl diazomalonate catalyzed by chiral diene-rhodium complexes, *Angewandte Chemie - International Edition*. 49 (2010) 7324–7327. <https://doi.org/10.1002/anie.201003775>
- [20] F.H. Hu, L.S. Wang, S.F. Cai, Solubilities of triphenylphosphine oxide in selected solvents, *J Chem Eng Data*. 54 (2009) 1382–1384. <https://doi.org/10.1021/je800842z>
- [21] R. Bonnaire, D. Diavoust, N. Platzner, Rh NMR Studies of Organometallic Rhodium(I) Derivatives, *Org Mag Reson* 22, (1984) 80–85, <https://doi.org/10.1002/mrc.1270220205>
- [22] J.L. Castelbou, A. Gual, E. Mercadé, C. Claver, C. Godard, Ligand effect in the Rh-NP catalyzed partial hydrogenation of substituted arenes, *Catal Sci Technol*. 3 (2013) 2828–2833. <https://doi.org/10.1039/c3cy00388d>
- [23] J.L. Castelbou, E. Bresó-Femenia, P. Blondeau, B. Chaudret, S. Castellón, C. Claver, C. Godard, Tuning the selectivity in the hydrogenation of aromatic ketones catalyzed by similar ruthenium and rhodium nanoparticles, *ChemCatChem*. 6 (2014) 3160–3168. <https://doi.org/10.1002/cctc.201402524>
- [24] A. Serrano-Maldonado, E. Martin, I. Guerrero-Ríos, Pyridine-Stabilized Rhodium Nanoparticles in Ionic Liquids as Selective Hydrogenation and Transfer Hydrogenation Catalysts, *Eur J Inorg Chem*. 2019 (2019) 2861. <https://doi.org/10.1002/ejic.201900575>
- [25] M. Ibrahim, M.M. Wei, E. Deydier, E. Manoury, R. Poli, P. Lecante, K. Philippot, Rhodium nanoparticles stabilized by ferrocenyl-phosphine ligands: Synthesis and catalytic styrene hydrogenation, *Dalton Transactions*. 48 (2019) 6777–6786. <https://doi.org/10.1039/c9dt01006h>
- [26] S.A. Stratton, K.L. Luska, A. Moores, Rhodium nanoparticles stabilized with phosphine functionalized imidazolium ionic liquids as recyclable arene

hydrogenation catalysts, *Catal Today*. 183 (2012) 96–100. <https://doi.org/10.1016/j.cattod.2011.09.016>

[27] C. Moreno-Marrodan, F. Liguori, E. Mercadé, C. Godard, C. Claver, P. Barbaro, A mild route to solid-supported rhodium nanoparticle catalysts and their application to the selective hydrogenation reaction of substituted arenes, *Catal Sci Technol*. 5 (2015) 3762–3772. <https://doi.org/10.1039/c5cy00599j>

[28] F. Martinez-Espinar, P. Blondeau, P. Nolis, B. Chaudret, C. Claver, S. Castellón, C. Godard, NHC-stabilised Rh nanoparticles: Surface study and application in the catalytic hydrogenation of aromatic substrates, *J Catal*. 354 (2017) 113–127. <https://doi.org/10.1016/j.jcat.2017.08.010>

[29] M.L. Buil, M.A. Esteruelas, S. Niembro, M. Oliván, L. Orzechowski, C. Pelayo, A. Vallribera, Dehalogenation and hydrogenation of aromatic compounds catalyzed by nanoparticles generated from rhodium bis(imino)pyridine complexes, *Organometallics*. 29 (2010) 4375–4383. <https://doi.org/10.1021/om1003072>

[30] M. Guerrero, N.T.T. Chau, S. Noël, A. Denicourt-Nowicki, F. Hapiot, A. Roucoux, E. Monflier, K. Philippot, About the Use of Rhodium Nanoparticles in Hydrogenation and Hydroformylation Reactions, *Curr Org Chem* 17 (2013) 364–399, <https://doi.org/10.2174/1385272811317040006>

[31] C. Vollmer, E. Redel, K. Abu-Shandi, R. Thomann, H. Manyar, C. Hardacre, C. Janiak, Microwave irradiation for the facile synthesis of transition-metal nanoparticles (NPs) in ionic liquids (ILs) from metal-carbonyl precursors and Ru-, Rh-, and Ir-NP/IL dispersions as biphasic liquid-liquid hydrogenation nanocatalysts for cyclohexene, *Chem Eur J* 16 (2010) 3849–3858. <https://doi.org/10.1002/chem.200903214>

[32] E. Baralt, Z.J. Sandra Smith, Z. Jamie Hurwitz, Z.T. István Horváth, R.H. Fish, Homogeneous Catalytic Hydrogenation. 6. Synthetic and Mechanistic Aspects of the Regioselective Reductions of Model Coal Nitrogen, Sulfur, and Oxygen Heteroaromatic Compounds Using the (η^5 -Pentamethylcyclopentadienyl)rhodium Tris(acetonitrile) Dication Complex as the Catalyst Precursor. *J Am Chem Soc* 114, (1992) 5187–5196, <https://doi.org/10.1021/ja00039a033>

[33] H. Imai, T. Nishiguchi, K. Fukuzumi, Transfer Hydrogenation and Transfer Hydrogenolysis. 13. Hydrogen Transfer from Cyclic Amines to Aromatic Nitro Compounds Catalyzed by Noble Metal Salts, *J Org Chem* 42 (1977) 431–434, <https://doi.org/10.1021/jo00433a024>

[34] E. Baráth, Hydrogen Transfer Reactions Of Carbonyls, Alkynes, And Alkenes With Noble Metals In The Presence Of Alcohols/Ethers And Amines As Hydrogen Donors, *Catalysts* 8 (2018) 671, <https://doi.org/10.3390/catal8120671>

- [35] M. Studer, C. Wedemeyer-Exl, F. Spindler, H.-U. Blaser, Enantioselective Homogeneous Hydrogenation of Monosubstituted Pyridines and Furans, *Monatsh Chem* 131 (2000) 1335–1343, [https://doi.org/10.1016/S1381-1169\(98\)00200-3](https://doi.org/10.1016/S1381-1169(98)00200-3)
- [36] D.P. Nair, M. Podgórski, S. Chatani, T. Gong, W. Xi, C.R. Fenoli, C.N. Bowman, The Thiol-Michael addition click reaction: A powerful and widely used tool in materials chemistry, *Chemistry of Materials*. 26 (2014) 724–744. <https://doi.org/10.1021/cm402180t>
- [37] H. Sugama, Hi. Saito, H. Danjo, T. Imamoto. P-Chirogenic Phosphine/Sulfide Hybrid Ligands. *Synthesis* 15 (2001) 2348-2353. <https://doi.org/10.1055/s-2001-18433>
- [38] P. Das, U. Bora, A. Tairai, C. Sharma, Triphenylphosphine chalcogenides as efficient ligands for room temperature palladium(II)-catalyzed Suzuki-Miyaura reaction, *Tetrahedron Lett.* 51 (2010) 1479–1482. <https://doi.org/10.1016/j.tetlet.2010.01.032>

Chapter IV: Aqueous biphasic hydrogenation with one-pot-synthesized Rh nanoparticles in polycationic-shell and triphenylphosphine oxide-functionalized core-cross-linked micelles

IV.1. Introduction

In the previous chapter, it was demonstrated that the *in-situ* generation of the RhNPs in TPPO@CCM-C failed because the TPPO ligands did not provide sufficiently stable core-anchored Rh^I-TPPO precursor complexes after reaction with [Rh(COD)(μ -Cl)]₂. Instead, the RhNPs were synthesized by an *ex-situ* step employing stabilizers (TPP/pyridine mixture) to obtain small-sized RhNPs [1,2], followed by their successive transfer to the CCM cores. The resulting RhNP-TPPO@CCM-C nanoreactors were very active in styrene hydrogenation and withstood RhNP extraction by diethyl ether, but the activity of the catalyst decreased gradually, converging to a constant value after four to five recycles. This phenomenon was attributed to the removal of the surface-bound RhNP stabilizers by the diethyl ether extractions, which altered the stability and activity of the RhNPs. Accordingly, a similar moderate, but unchanged upon recycling, activity was also obtained when the pristine RhNP-TPPO@CCM-C catalyst was extensively pre-washed with diethyl ether prior to the first catalytic run (see Chapter III).

In this chapter, a novel one-pot synthesis approach is described for the RhNP-TPPO@CCM-C catalyst which does not require the use of additional stabilizers. The resulting catalyst was thoroughly characterized and applied in the aqueous biphasic hydrogenation of styrene as well as of other selected alkene, alkyne, and carbonyl substrates. Note that this chapter is related to article No. 4 in the list of publications and has been submitted for publication.

IV.2. One-pot synthesis and characterization of RhNP-TPPO@CCM-C

RhNPs embedded in the hydrophobic cores of a stable latex of TPPO@CCM-C were synthesized in a single step by heating a biphasic mixture containing the aqueous TPPO@CCM-C latex and a toluene solution of $[\text{Rh}(\text{COD})(\mu\text{-Cl})_2]$ under H_2 pressure. This could be performed without any additional stabilizer or base additive (Table IV.1, Entry 1) and without the need for a preliminary *ex-situ* synthesis of the RhNPs (as previously reported). Comparative syntheses were also carried out in the presence of a base such as pyridine or NEt_3 (Table IV.1, Entries 2 and 3, respectively), which can assist the reaction by trapping the HCl produced during the reduction of Rh^{I} to Rh^0 , in addition to potentially contribute to the RhNP stabilization [3]. After the synthesis and phase separation, all three produced RhNP-TPPO@CCM-C latexes were black, signaling the successful formation and confinement of RhNPs in the core of the CCMs.

Table IV.1. Synthesis of RhNP-TPPO@CCM-C.^a

Entry	Base	Molar TPPO/Rh/Base ratio	RhNPs average size (nm)	
			Before catalysis	After catalysis
1	-	4/1/0	1.7 ± 0.2	1.9 ± 0.6
2	Pyridine	4/1/4	2.9 ± 0.6	3.1 ± 0.1
3	NEt_3	4/1/4	2.1 ± 0.1	1.8 ± 0.2

^aReaction conditions: 20 bar H_2 , 20 h, 60 °C, toluene, 1200 rpm.

TEM analyses confirmed the successful incorporation of the RhNPs in the TPPO@CCM-C in all cases (Figure IV.1). The RhNPs synthesized without base (Entry 1) showed a particularly narrow size distribution with a mean diameter (d_m) of 1.7 ± 0.2 nm. On the other hand, the RhNPs produced in the presence of pyridine or NEt_3 (Table IV.1, Entries 2 and 3, respectively), were found agglomerated and with slightly larger average diameters of 2.9 ± 0.6 nm and 2.1 ± 0.1 nm, respectively (Figure IV.1).

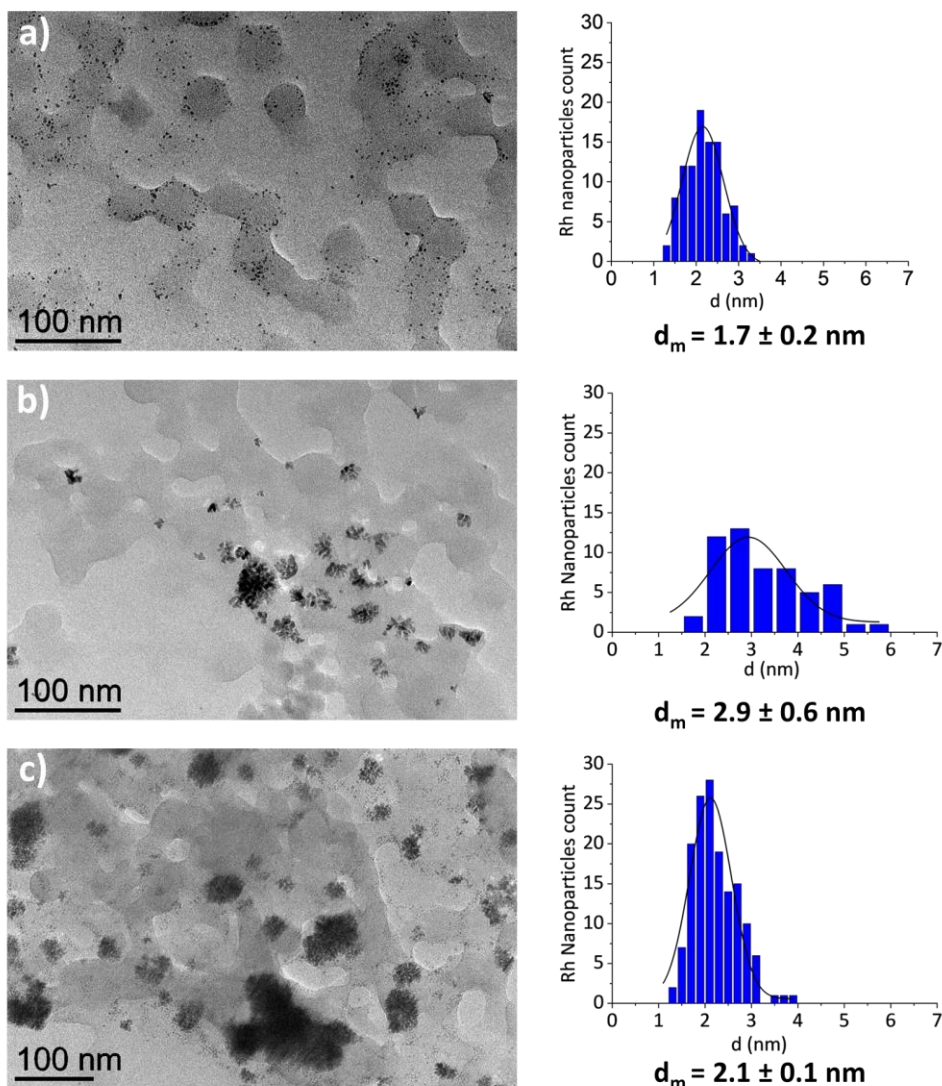


Figure IV.1. TEM images of the three one-pot-synthesized RhNP-TPPO@CCM-C latexes (left), and corresponding RhNP size distributions (right), obtained (a) without base, (b) with pyridine and (c) with NEt₃.

When using only molecular TPPO (*i.e.* not linked to the CCM support) as a stabilizer under the same reaction conditions (toluene, TPPO/Rh = 4/1, 20 bar H₂, 60 °C, 1200 rpm, 20 h) and no base additive, a black colloidal suspension of RhNPs was also obtained. These RhNPs were also found to have a slightly larger average diameter than those embedded in the TPPO@CCM-C latex generated without a base ($d_m = 2.4 \pm 0.2$ nm *vs.* 1.7 ± 0.2 nm) and were relatively well dispersed (Figure IV.2).

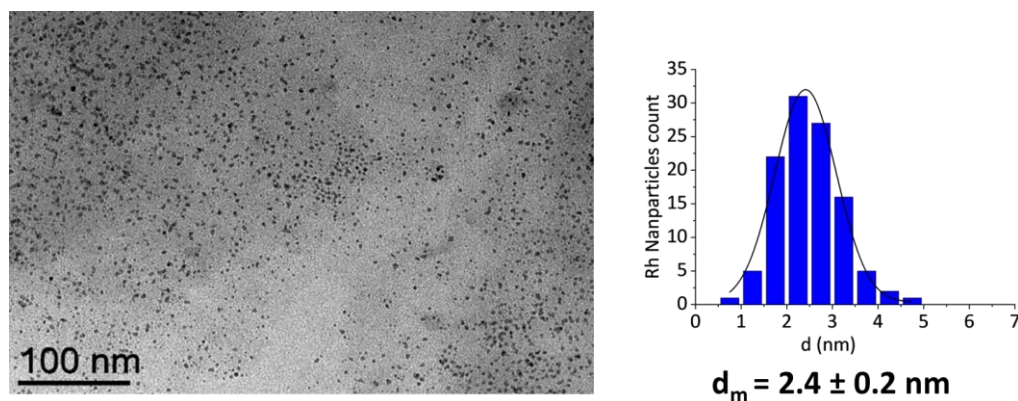


Figure IV.2. TEM image of RhNPs obtained using only molecular TPPO as a stabilizer (TPPO/Rh = 4/1) with the corresponding size distribution ($d_m = 2.4 \pm 0.2$ nm). Reaction conditions: toluene solution, 20 bar H_2 , 60 °C, 20 h.

Furthermore, when treating a $[Rh(COD)(\mu-Cl)]_2$ solution in toluene under H_2 pressure in the absence of any polymer, stabilizer, and base, only large agglomerates were produced under the same reaction conditions as for the three one-pot-synthesized RhNP-TPPO@CCM-C latexes (Figure IV.3).

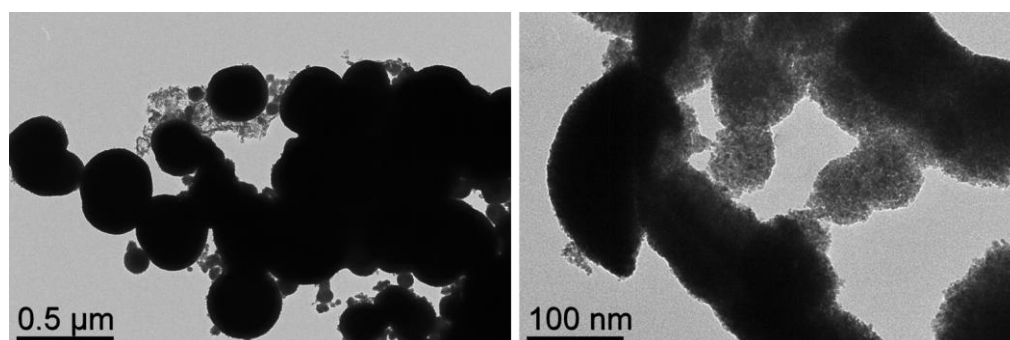


Figure IV.3. TEM image of Rh agglomerates generated in the absence of stabilizers. Reaction conditions: toluene solution, 20 bar H_2 , 60 °C, 20 h.

The smaller size of the RhNPs in the TPPO@CCM-C obtained from the base-free one-pot procedure may result from a more efficient stabilization in the polymer, due to the combined interaction with the oxygen lone pairs of TPPO ligands in the CCM-C core and π -electrons of the phenyl groups in the styrene monomers. The confinement effect may also provide an improved rate of nucleation, resulting in a greater number of NPs and a consequent decrease in their average size [2,4–11]. In principle, the nucleation may predominantly occur either within the CCM cores or in the bulk toluene phase, followed by migration and anchoring within the CCM cores. Since small-sized NPs

($d_m = 2.4 \pm 0.2$ nm) were generated in the presence of molecular TPPO in the toluene phase, even without base, whereas large agglomerates were generated in toluene without stabilizer, it seems likely that faster nucleation occurred within the CCM-C cores that contain TPPO ligands.

TG/DSC analyses of the TPPO@CCM-C and RhNP-TPPO@CCM-C polymers were performed under N_2 to examine their relative thermal stability (Figure IV.4). TPPO@CCM-C showed an initial decomposition phase at 239 °C (*ca.* 20 wt.% loss), followed by a gradual weight loss at higher temperatures with a peak at 413 °C (total weight loss *ca.* 88 wt.%). RhNP-TPPO@CCM-C, on the other hand, exhibited an initial degradation phase at a higher temperature (264 °C, *ca.* 50 wt.% loss) with a second peak at 403 °C and a lower total weight loss (77 wt.%), suggesting an effect of the RhNPs on the decomposition of the Rh loaded polymer. The thermal stability of the RhNP-TPPO@CCM-C latex was insufficient to perform further investigations of the RhNPs active sites by conventional techniques such as carbon monoxide temperature-programmed desorption (CO-TPD), which requires high temperatures for the CO desorption [12,13] and may be affected by the polymer degradation.

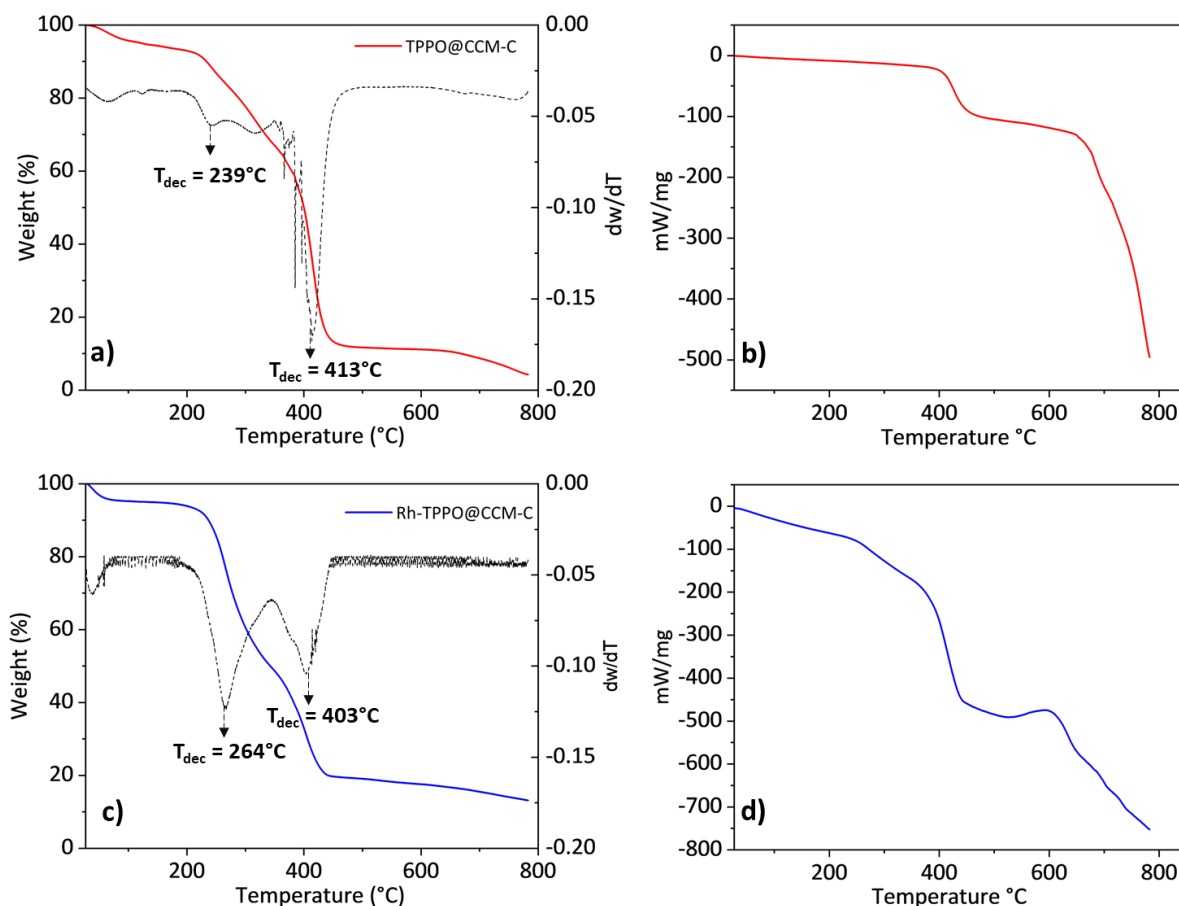


Figure IV.4. TGA (a,c) and DSC (b,d) profiles of TPPO@CCM-C (red, top) and RhNP-TPPO@CCM-C (blue, bottom).

In line with this, XPS analyses performed on the TPPO@CCM-C and RhNP-TPPO@CCM-C systems (Appendix C, Figure C1-C3, Table C1) indicated a shift in binding energy in the presence of RhNPs in the core of the TPPO@CCM-C polymer, which is particularly notable for the O1s excitation ($\Delta E = 0.58$ eV), supporting the existence of RhNPs-polymer interaction in RhNP-TPPO@CCM-C. To further corroborate the interaction between the TPPO ligand in the CCM-C and the RhNPs, ATR-FTIR spectra of TPPO@CCM-C and RhNP-TPPO@CCM-C were compared to that of molecular TPPO (Figure IV.5). The strong P-C stretching band of TPPO at 1120 cm^{-1} [14] was visible in both TPPO@CCM-C and in the broad envelope band ($1120\text{--}1182\text{ cm}^{-1}$) for RhNP-TPPO@CCM-C. The strong P=O stretching band of TPPO (1182 cm^{-1}) [14] was also quite evident in TPPO@CCM-C and for the TPPO in the RhNP-TPPO@CCM (TPPO/Rh = 4/1). However, a new signal at (1156 cm^{-1}) was also observed

in the case of RhNP-TPPO@CCM-C, likely corresponding to a redshifted P=O stretching band of the TPPO bound to the RhNPs surface as also previously observed for other metal-coordinated TPPO compounds [15,16].

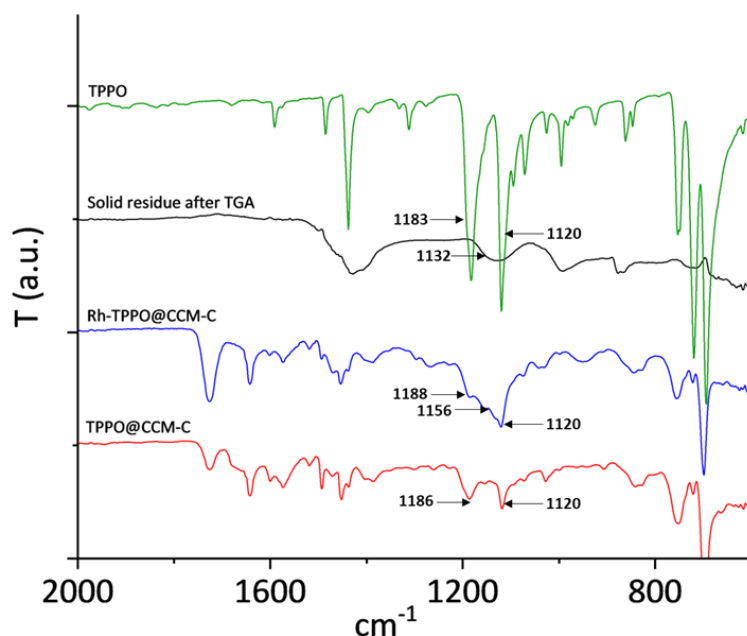


Figure IV.5. ATR-FTIR spectra of TPPO@CCM-C (red), RhNP-TPPO@CCM-C (blue), solid residue after TGA (black), and molecular TPPO (green), in the range of 700-2000 cm⁻¹

IV.3. Aqueous biphasic hydrogenation with RhNP-TPPO@CCM-C

IV.3.1. Hydrogenation of styrene without base additive

Using the RhNP-TPPO@CCM-C latex produced in the absence of base, an initial series of catalytic runs with different reaction times were carried out at 25 °C, under 20 bar of H₂ pressure and stirring of 1200 rpm to limit external mass transfer, with a styrene/Rh ratio of 5000/1 (Figure IV.6). A complete conversion of styrene was reached after 2 h corresponding to an average TOF of 3000 h⁻¹ (*c*TOF 4300 h⁻¹).

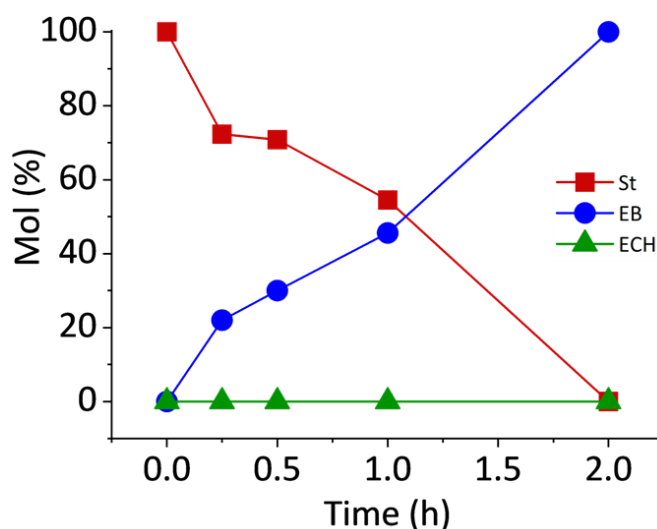


Figure IV.6. Time plot for the aqueous biphasic hydrogenation of styrene using RhNP-TPPO@CCM-C prepared without base. Reaction conditions: styrene/Rh = 5000/1, 20 bar H₂, 25 °C, 1200 rpm.

Additional catalytic runs with a fixed reaction time of 0.25 h and different styrene/Rh ratios yielded the results reported in Table IV.2, Entries 1-3. The system showed excellent selectivity (>99%) towards the formation of ethylbenzene (EB) with the formation of only trace amounts of the fully saturated product ethylcyclohexane (ECH), as also previously described for styrene hydrogenation using other RhNP-CCM catalysts [3] and in Chapter III. Moreover, phase separation was fast in all reactions (< 3 min), facilitating product separation and catalyst recovery, as already observed for other aqueous biphasic catalytic applications of nanoreactors featuring the same outer shell (CCM-C) [3,17].

Hydrogenation of styrene was also performed with the same RhNP-TPPO@CCM-C latex at higher temperatures (30 °C-55 °C) with a styrene/Rh ratio of 5000/1 (Table IV.2, Entries 4-7). At 55 °C, a conversion of 83% was obtained after 0.25 h, yielding a very high average TOF of 16100 h⁻¹ (cTOF 23600 h⁻¹).

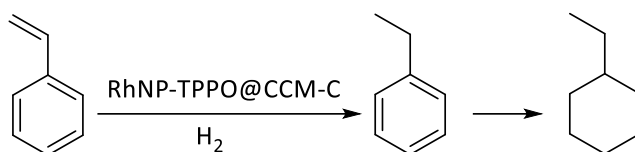


Table IV.2. Hydrogenation of styrene using RhNP-TPPO@CCM-C prepared without base.^a

Entry	Molar styrene/Rh ratio	T (°C)	Conversion (%)	Selectivity (%)		TOF (<i>c</i> TOF) ^b (h ⁻¹)
				EB	ECH	
1	2000/1	25	82	>99	<0.1	7800 (11500)
2	5000/1	25	21	>99	<0.1	4500 (6500)
3	10000/1	25	8	>99	<0.1	3000 (4450)
4	5000/1	30	35	>99	>0.1	8000 (11600)
5	5000/1	35	58	>99	<0.1	11200 (16400)
6	5000/1	45	65	>99	<0.1	12900 (19000)
7	5000/1	55	83	>99	<0.1	16100 (23600)

^a Reaction conditions: 20 bar H₂, 25 °C, 0.25 h, 1200 rpm. ^b Corrected TOF (*c*TOF) calculated by considering only the surface Rh atoms (see Experimental Part). EB: ethylbenzene, ECH: ethylcyclohexane.

The more moderate conversions obtained in the 25-35 °C range allowed to estimate an apparent reaction activation energy (E_a) of 69 ± 6 kJ/mol from an Arrhenius plot (Figure IV.7), which is comparable to the E_a obtained for the gas-phase hydrogenation of styrene [18]. However, at higher reaction temperatures the apparent E_a decreased to 4 ± 1 kJ/mol, indicating diffusion limitations (internal mass transfer)[19,20].

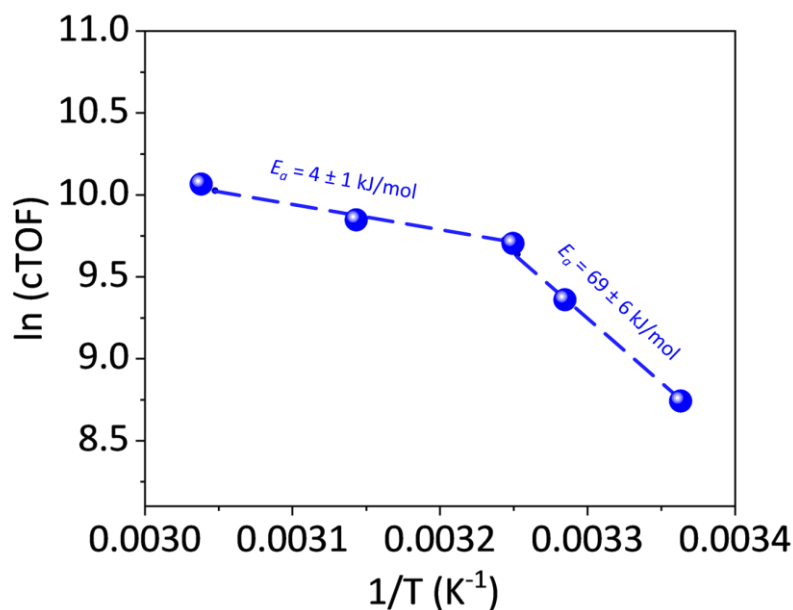


Figure IV.7. Arrhenius plot of the hydrogenation of styrene using RhNP-TPPO@CCM-C prepared without base. Reaction conditions: styrene/Rh = 5000/1, 20 bar H₂, 0.25 h, 1200 rpm, accuracy of temperature measured with ± 0.5 -1 °C.

The RhNP-TPPO@CCM-C latex recycling was further evaluated for a series of catalytic runs with a styrene/Rh ratio of 5000/1 and 0.25 h of reaction time with intermediate product extraction by diethyl ether (Figure IV.8). The extraction procedure was similar to that previously applied to recycle the RhNP-TPP@CCM-C [3] and RhNP-TPPO@CCM-C latexes (see Chapter III), as well as the latex of the molecular Rh^I-TPP@CCM [3,17]. A rather constant styrene conversion of *ca.* 21%, corresponding to an average TOF of ~ 4500 h⁻¹ (cTOF of 6500 h⁻¹), was obtained over the six consecutive reaction runs, but only when the recovered catalyst system was reactivated with H₂ (20 bar, 1 h, 25 °C) prior to addition of new batch of substrate. A recycling experiment without this reactivation treatment gave erratic results, possibly because of the passivation of the RhNPs by surface oxide layer [2,21] formation during the recycling procedures as also discussed in Chapter III. A TEM analysis on the recovered latex after run six (Figure IV.9) showed that the RhNPs remained well-dispersed, with a similar size distribution (1.9 ± 0.6 nm) as prior to catalysis (see Table IV.1).

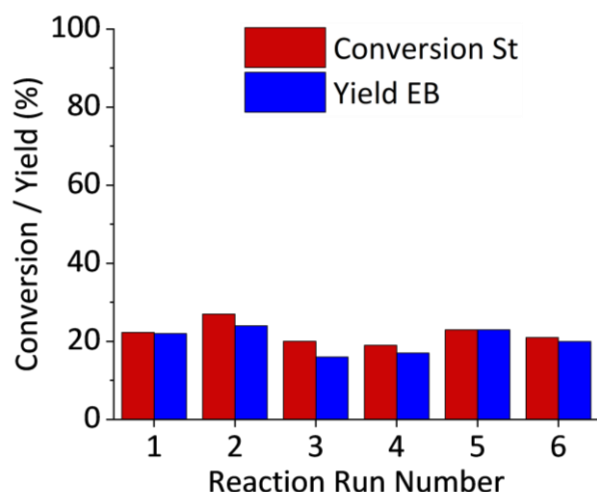


Figure IV.8. Reuse of RhNP-TPPO@CCM-C catalyst in six catalytic runs of styrene hydrogenation with product extraction by diethyl ether and intermediate H₂ treatment (20 bar H₂, 25 °C, 1 h, 1200 rpm) and product extraction by diethyl ether. Reaction conditions: Styrene/Rh = 5000/1, 20 bar H₂, 25 °C, 0.25 h, 1200 rpm.

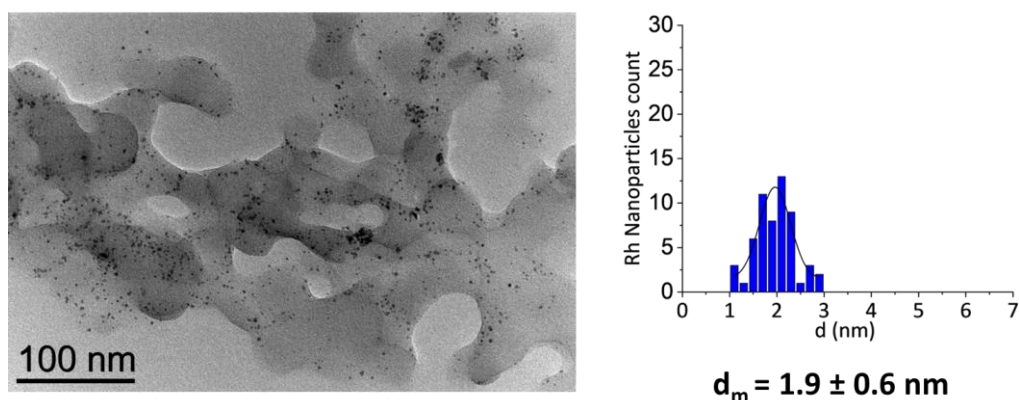


Figure IV.9. TEM image of RhNP-TPPO@CCM-C recording from an aliquot during recycling after run six (left) and corresponding size distribution ($d_m = 1.9 \pm 0.6$ nm) (right).

A reference hydrogenation experiment was carried out under the same conditions using a toluene phase of the TPPO-stabilized RhNPs as catalyst (20 bar H₂, 25 °C, styrene/Rh = 10000/1, 0.25 h). This resulted in a styrene conversion of 53% (average TOF ~20000 h⁻¹, *c*TOF 21500 h⁻¹) with >99% of EB selectivity. Using EB as substrate under the same reaction conditions yielded only 0.6% of ECH, confirming the high selectivity of the TPPO-stabilized RhNPs under the mild reaction conditions applied. The *c*TOF decreased from ~21500 h⁻¹ for the reaction carried out with the RhNP-TPPO/toluene catalytic system to ~6500 h⁻¹ for that conducted with the RhNP-

TPPO@CCM-C/biphasic system, which indicates that the latter was influenced by internal mass transport restrictions of the styrene substrate and/or the EB product.

IV.3.2. Hydrogenation of styrene with base additive

The RhNP-TPPO@CCM-C latexes obtained in the presence of pyridine (Table IV.1, Entry 2) or NEt_3 (Table IV.1, Entry 3) were also evaluated for styrene hydrogenation, after extensive prewashing with diethylether prior to the first catalytic run (Figure IV.10).

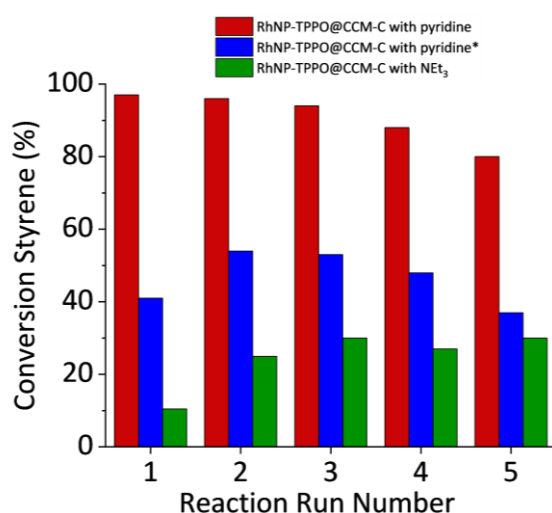


Figure IV.10. Reuse of the RhNP-TPPO@CCM-C latexes prepared with base additives in styrene hydrogenation with intermediate H_2 treatment (20 bar H_2 , 25 °C, 0.25 h, 1200 rpm) and product extraction by diethyl ether. Reaction conditions: Styrene/Rh = 5000/1 (*6500/1), 20 bar H_2 , 25 °C, 0.25 h, 1200 rpm.

When using the RhNP-TPPO@CCM-C latex prepared with NEt_3 , the first catalytic run yielded a styrene conversion of ~10%, but the subsequent runs converged to a stable conversion of *ca.* 25-30%. Similar differences between the first and consecutive reaction runs were reported for the RhNP-TPPO@CCM-C latex obtained by transfer of *ex-situ* synthesized RhNPs (see Chapter III) as well as other studies using NEt_3 [3]. This can be explained by an induction time, possibly resulting from restructuring of the RhNP surface under catalytic conditions (see Chapter III) which produced more catalytically active sites and consecutive higher conversion [2,21]. On the other hand, the RhNP-TPPO@CCM-C latex prepared with pyridine showed much higher activity

(conversion of *ca.* 97%), with an average TOF of $\sim 18200 \text{ h}^{-1}$ (*c*TOF 40000 h^{-1}) in the first run. However, the activity steadily decreased over the subsequent runs, most likely as a consequence of the continuous removal of adsorbed pyridine from the RhNP surface during the successive recycling treatments that involve diethyl ether extractions. This result is analogous to that shown by the RhNP-TPPO@CCM-C latex obtained by incorporating the *ex-situ* synthesized RhNPs with stabilization by TPP and pyridine as stabilizers (see Chapter III). It thus confirms that the presence of pyridine has a beneficial effect on the RhNP catalytic activity which might be due to a cleaner Rh surface as the result of less chlorides, present in the organometallic dimer, that may be better eliminated. The intimate reason for this promotion effect is currently unknown. Interestingly, when the catalyst recyclability was performed with a higher styrene/Rh ratio of 6500/1, the activity dropped in the first run (as expected) to an average TOF of $\sim 10000 \text{ h}^{-1}$ (*c*TOF 23000 h^{-1}), and the system proved less stable compared to the RhNP-TPPO@CCM-C synthesized in one-pot without base (Figure IV.8). A potential factor that influences the activity may be alteration in internal mass transfer limitations, which are likely to be more significant when the St/Rh ratio is higher (St/Rh = 5000/1 *vs* 6500/1). Additionally, TEM analyses of the recovered latexes synthesized in the presence of pyridine or NEt_3 showed similar RhNP dispersion and size distributions after the fifth catalytic runs ($3.1 \pm 0.1 \text{ nm}$ and $1.8 \pm 0.2 \text{ nm}$, for pyridine and NEt_3 respectively, Figure IV.11) as prior to the first catalytic runs ($2.9 \pm 0.6 \text{ nm}$ and $2.1 \pm 0.1 \text{ nm}$ for pyridine and NEt_3 , respectively (see Figure IV.1).

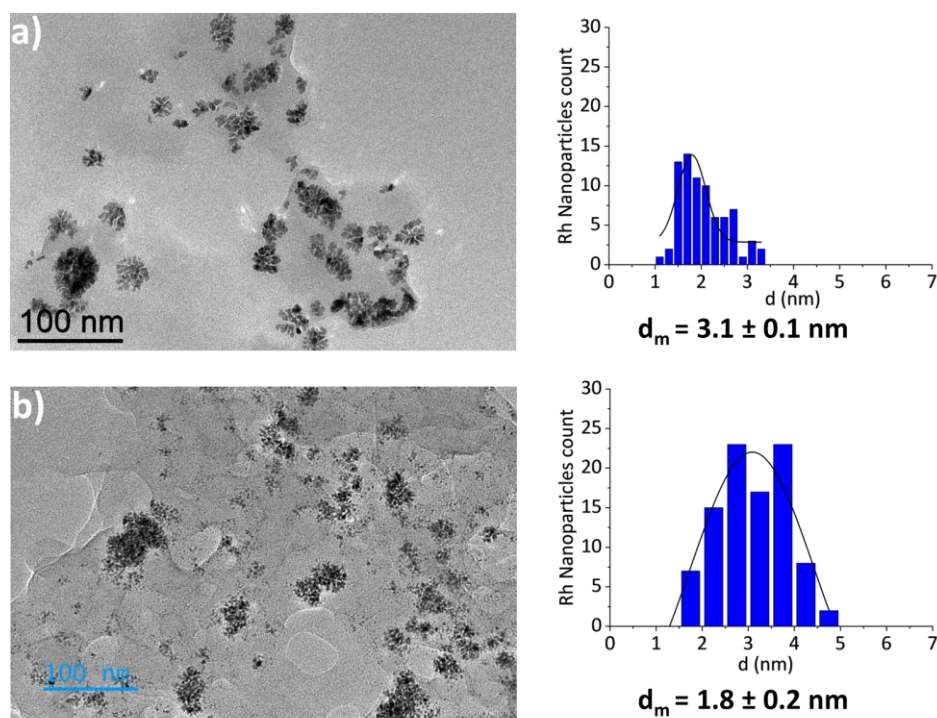


Figure IV.11. TEM images and corresponding size distributions of spent RhNP-TPPO@CCM-C prepared with (a) pyridine (Table IV.1, Entry 2) and with (b) NEt₃ (Table IV.1, Entry 3).

IV.3.3. Hydrogenation of styrene in the presence of Hg

To examine whether the RhNP-TPPO@CCM-C latex (synthesized without base) also contained catalytically active Rh^I species in addition to RhNPs, a styrene hydrogenation experiment (styrene/Rh = 5000/1) was carried out in the presence of a large excess of Hg (Hg/Rh = 500/1), which is known to poison and deactivate the RhNPs [22]. No significant styrene conversion was observed (<0.1%) after 0.25 h of reaction, suggesting that no active Rh^I is present in the TPPO@CCM-C core. A control TEM analysis of the recovered latex after the catalytic run with Hg (Figure IV.12) still showed the presence of small RhNPs in the polymer, but with a larger average diameter (*ca.* 2.7 ± 0.1 nm *vs.* 1.7 ± 0.2 nm) than prior to catalysis, along with much larger particles (average size *ca.* 16 ± 5 nm) that can be attributed to nanoscopic Hg droplets. HR-TEM analyses coupled with energy-dispersive X-ray spectroscopy (EDX) were done on the spent latex after Hg poisoning and indicated the presence of Hg along with RhNPs. The EDX analysis showed a clear signal for elemental Rh as well as well-identified signals for Hg, P, and I atoms coming from the TPPO@CCM-C

polymer that embeds the particles (Appendix C, Figure C4). The increase in the apparent size of the RhNPs could result from the formation of a Hg-Rh amalgam at the surface of the RhNPs [23,24]. This result indicates that Hg is able to cross the CCM hydrophilic shell.

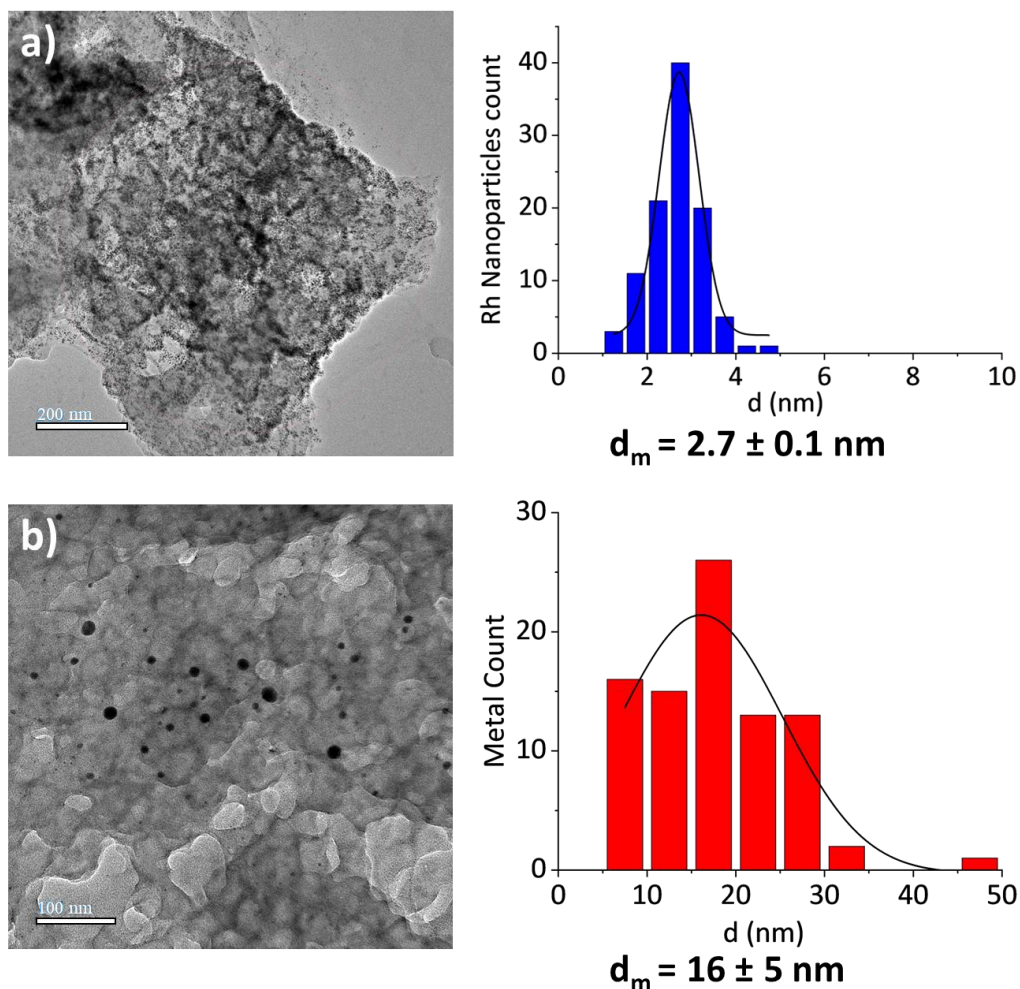


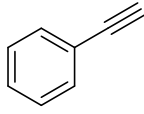
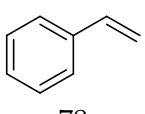
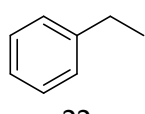
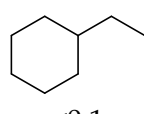
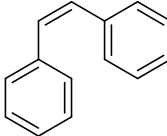
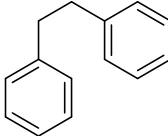
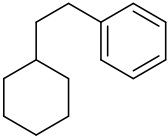
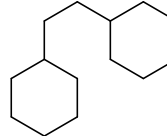
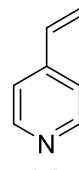
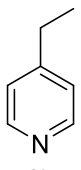
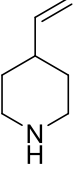
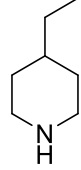
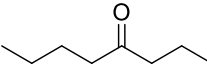
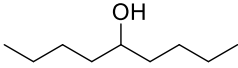
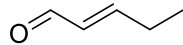
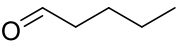
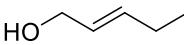
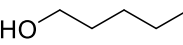
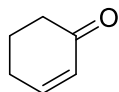
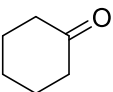
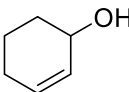
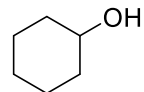
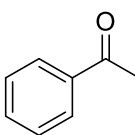
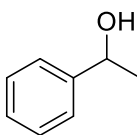
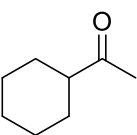
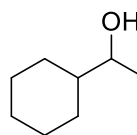
Figure IV.12. TEM images (left) of a) RhNPs and b) Hg particles and the corresponding size distributions (right) RhNPs ($d_m = 2.7 \pm 0.1$ nm; left) and Hg particles ($d_m = 16 \pm 5$ nm; right) in RhNP-TPPO@CCM-C.

IV.3.4. Hydrogenation of other substrates

Lastly, the applicability of the RhNP-TPPO@CCM-C latex synthesized without base was screened for the aqueous biphasic hydrogenation of other substrates, including selected aromatics, alkenes, alkynes, and carbonyl compounds (substrate/Rh = 5000/1; performed with neat substrate and not optimized) (Table IV.3). The results confirmed a rather high hydrogenation activity (average TOFs of 1000-1100 h^{-1}) and high

selectivity towards the reduction of both double and triple carbon-carbon bonds in phenylacetylene (Entry 1) and 4-vinylpyridine (Entry 3). The catalytic activity was, however, significantly lower than for styrene under similar reaction conditions ($cTOF$ 4500 h^{-1} ; see Table IV.2). Highly sterically hindered *Z*-stilbene (Entry 2) and the aliphatic α,β -unsaturated substrate (*E*)-hex-2-enal (Entry 5) were only hydrogenated to a low extent under the applied conditions. Also, the carbonyl group of the aliphatic compound 5-nonanone (Entry 4) was hardly hydrogenated, whereas the cyclic (and activate) α,β -unsaturated substrate 2-cyclohexen-1-one (Entry 6) yielded a good conversion ($cTOF$ of 1000 h^{-1}) with high selectivity (63.7%) to cyclohexanol, and acetophenone (Entry 7) showed an even higher conversion ($cTOF$ of 3000 h^{-1}), with a nearly quantitative selectivity toward phenylethanol (>99%). Notably, no significant hydrogenation of the aromatic ring was observed in any of the reactions. Overall, the non-optimized results achieved during the catalytic screening clearly indicate the potential of the RhNP-TPPO@CCM-C catalyst synthesized without base for the hydrogenation of other types of unsaturated substrates than styrene.

Table IV.3. Aqueous biphasic hydrogenation of selected aromatics, alkenes, alkynes, and carbonyl substrates using Rh-TPPO@CCM-C.^a

Entry	Substrate / Conversion (%) ^b	Products / Selectivity (%) ^b	Average c_{TOF} (h ⁻¹)		
1	 30	 78	 22	 <0.1	1100
2	 <0.1	 nd	 nd	 nd	2.5
3	 79	 97	 nd	 nd	3200
4	 <0.1		 nd		2.5
5	 <0.1	 nd	 nd	 nd	2.5
6	 27	 1	 35	 64	1000
7	 86	 >99	 <0.1	 <0.1	3000

^a Reaction conditions: Substrate/Rh = 5000/1, 20 bar H₂, 25 °C, 0.25 h, 1200 rpm. ^b Conversions and selectivities determined by GC-FID. Product identification confirmed by ¹H NMR (Entries 4 and 5) and GC-MS (Entry 3). nd = not detected.

IV.4. Summary and Outlook

A RhNP-TPPO@CCM-C latex was successfully synthesized by one-pot reduction of [Rh(COD)(μ -Cl)]₂/toluene in the presence of an aqueous TPPO@CCM-C latex and in the absence of additional stabilizers and base. The produced RhNPs were smaller in size (1.7 \pm 0.2 nm) than their analogs synthesized under similar conditions in the presence of only TPPO as stabilizer (2.4 \pm 0.2 nm). This difference underlines the

positive confinement effect on the RhNP size, which leads to smaller NPs. The new catalyst demonstrated very good catalytic activity (c TOFs of 4500-16000 h⁻¹) and quantitative selectivity in the hydrogenation of neat styrene to ethylbenzene under mild conditions (20 bar H₂, 25-55 °C). The catalyst was also applicable to hydrogenation of other unsaturated substrates under similar reaction conditions, including alkynes and carbonyl compounds. The facile one-pot synthesis procedure and the stable anchoring of the RhNPs to the core TPPO ligands circumvented the RhNP leaching during the diethyl ether extractions (as also reported earlier in Chapter III), making the RhNP-TPPO@CCM-C latex highly attractive for aqueous biphasic catalysis with catalyst recycling. Further investigations may focus on understanding and improving the hydrogenation performance of this RhNP-TPPO@CCM-C catalytic system (*e.g.*, by employing vectorizing solvents). Also, a dedicated study could focus on the variation of the Rh precursor, aiming to systematically explore its influence on the generation of well-defined RhNPs and, consequently, its implications for catalytic activity. The scope will be further extended to encompass the confinement of other metal NPs and probe their catalytic efficacy in the hydrogenation of diverse substrates.

IV.5. References

- [1] J.L. Castelbou, E. Bresó-Femenia, P. Blondeau, B. Chaudret, S. Castellón, C. Claver, C. Godard, Tuning the selectivity in the hydrogenation of aromatic ketones catalyzed by similar ruthenium and rhodium nanoparticles, *ChemCatChem*. 6 (2014) 3160–3168. <https://doi.org/10.1002/cctc.201402524>
- [2] S.A. Stratton, K.L. Luska, A. Moores, Rhodium nanoparticles stabilized with phosphine functionalized imidazolium ionic liquids as recyclable arene hydrogenation catalysts, *Catal Today*. 183 (2012) 96–100. <https://doi.org/10.1016/j.cattod.2011.09.016>
- [3] H. Wang, A.M. Fiore, C. Fliedel, E. Manoury, K. Philippot, M.M. Dell'Anna, P. Mastrorilli, R. Poli, Rhodium nanoparticles inside well-defined unimolecular amphiphilic polymeric nanoreactors: Synthesis and biphasic hydrogenation catalysis, *Nanoscale Adv.* 3 (2021) 2554–2566. <https://doi.org/10.1039/d1na00028d>

- [4] M.A. Gelesky, S. S. X. Chiaro, F. A. Pavan, J. H. Z. dos Santos, J Dupont, Supported ionic liquid phase rhodium nanoparticle hydrogenation catalysts, Dalton Trans. (2007) 5546–5548. <https://doi.org/10.1039/B708111A>
- [5] L.M. Rossi, L.L.R. Vono, M.A.S. Garcia, T.L.T. Faria, J.A. Lopez-Sanchez, Screening of soluble rhodium nanoparticles as precursor for highly active hydrogenation catalysts: The effect of the stabilizing agents, Top Catal. 56 (2013) 1228–1238. <https://doi.org/10.1007/s11244-013-0089-z>
- [6] C. Chaudhari, H. Imatome, Y. Nishida, K. Sato, K. Nagaoka, Recyclable Rh-PVP nanoparticles catalyzed hydrogenation of benzoic acid derivatives and quinolines under solvent-free conditions, Catal Commun. 126 (2019) 55–60. <https://doi.org/10.1016/j.catcom.2019.02.019>
- [7] F. Martinez-Espinar, P. Blondeau, P. Nolis, B. Chaudret, C. Claver, S. Castellón, C. Godard, NHC-stabilised Rh nanoparticles: Surface study and application in the catalytic hydrogenation of aromatic substrates, J Catal. 354 (2017) 113–127. <https://doi.org/10.1016/j.jcat.2017.08.010>
- [8] M. Ibrahim, M.A.S. Garcia, L.L.R. Vono, M. Guerrero, P. Lecante, L.M. Rossi, K. Philippot, Polymer: Versus phosphine stabilized Rh nanoparticles as components of supported catalysts: Implication in the hydrogenation of cyclohexene model molecule, Dalton Trans. 45 (2016) 17782–17791. <https://doi.org/10.1039/c6dt03104h>
- [9] G. Vitulli, C. Evangelisti, P. Pertici, A.M. Caporusso, N. Panziera, P. Salvadori, M.G. Faga, C. Manfredotti, G. Martra, S. Coluccia, A. Balerna, S. Colonna, S. Mobilio, Supported rhodium nanoparticles in catalysis: The role of stabilizers on catalytic activity and structural features, J Organomet Chem. 681 (2003) 37–50. [https://doi.org/10.1016/S0022-328X\(03\)00529-1](https://doi.org/10.1016/S0022-328X(03)00529-1)
- [10] H. Bin Pan, C.M. Wai, One-step synthesis of size-tunable rhodium nanoparticles on carbon nanotubes: A study of particle size effect on hydrogenation of xylene, J Phys Chem C. 114 (2010) 11364–11369. <https://doi.org/10.1021/jp101368p>
- [11] T.T. Nguyen, P. Serp, Confinement of metal nanoparticles in carbon nanotubes, ChemCatChem. 5 (2013) 3595–3603. <https://doi.org/10.1002/cctc.201300527>
- [12] M.M.M. Jansen, J. Gracia, B.E. Nieuwenhuys, J.W. Niemantsverdriet, Interactions between co-adsorbed CO and H on a Rh(100) single crystal surface, Phys Chem Chem Phys. 11 (2009) 10009–10016. <https://doi.org/10.1039/b910497f>
- [13] S. Murphy, C. Streb, S.B. Vendelbo, C. Conradsen, Y. Tison, K. Nielsen, L. Bech, R.M. Nielsen, M. Johansson, I. Chorkendorff, J.H. Nielsen, Probing the crossover in CO desorption from single crystal to nanoparticulate Ru model catalysts, Phys Chem Chem Phys. 13 (2011) 10333–10341. <https://doi.org/10.1039/c1cp20371a>

- [14] G.B. Deacon, J.H.S. Green, Vibrational spectra of ligands and complexes-II I&ared spectra ($3650\text{--}375\text{ cm}^{-1}$) of triphenyl-phosphine, triphenylphosphine oxide, and their complexes, *Spectrochim. Acta A: Mol. Spectrosc.* 24 (1968) 845-852. [https://doi.org/10.1016/0584-8539\(68\)80183-7](https://doi.org/10.1016/0584-8539(68)80183-7)
- [15] K. Senevirathne, A.W. Burns, M.E. Bussell, S.L. Brock, Synthesis and characterization of discrete nickel phosphide nanoparticles: Effect of surface ligation chemistry on catalytic hydrodesulfurization of thiophene, *Adv Funct Mater.* 17 (2007) 3933–3939. <https://doi.org/10.1002/adfm.200700758>
- [16] S. Carencio, C. Boissière, L. Nicole, C. Sanchez, P. Le Floch, N. Mézailles, Controlled design of Size-tunable monodisperse nickel nanoparticles, *Chem Mat.* 22 (2010) 1340–1349. <https://doi.org/10.1021/cm902007g>
- [17] H. Wang, L. Vendrame, C. Fliedel, S. Chen, F. Gayet, F. D'Agosto, M. Lansalot, E. Manoury, R. Poli, Triphenylphosphine-Functionalized Core-Cross-Linked Micelles and Nanogels with a Polycationic Outer Shell: Synthesis and Application in Rhodium-Catalyzed Biphasic Hydrogenations, *Chemistry - A European Journal.* 27 (2021) 5205–5214. <https://doi.org/10.1002/chem.202004689>
- [18] C. Betti, J. Badano, C. Lederhos, M. Maccarrone, N. Carrara, F. Coloma-Pascual, M. Quiroga, C. Vera, Kinetic study of the selective hydrogenation of styrene over a Pd egg-shell composite catalyst, *Reaction Kinetics, Mechanisms and Catalysis.* 117 (2016) 283–306. <https://doi.org/10.1007/s11144-015-0910-8>
- [19] Z.A. Piskulich, O.O. Mesele, W.H. Thompson, Removing the barrier to the calculation of activation energies: Diffusion coefficients and reorientation times in liquid water, *J Chem Phys* 147 (2017) 134103. <https://doi.org/10.1063/1.4997723>
- [20] H. Rafatijo, D.L. Thompson, General application of Tolman's concept of activation energy, *J Chem Phys* 147 (2017) 224111. <https://doi.org/10.1063/1.5009751>
- [21] C. Vollmer, E. Redel, K. Abu-Shandi, R. Thomann, H. Manyar, C. Hardacre, C. Janiak, Microwave irradiation for the facile synthesis of transition-metal nanoparticles (NPs) in ionic liquids (ILs) from metal-carbonyl precursors and Ru-, Rh-, and Ir-NP/IL dispersions as biphasic liquid-liquid hydrogenation nanocatalysts for cyclohexene, *Chem Eur J.* 16 (2010) 3849–3858. <https://doi.org/10.1002/chem.200903214>
- [22] J.A. Widegren, R.G. Finke, A review of the problem of distinguishing true homogeneous catalysis from soluble or other metal-particle heterogeneous catalysis under reducing conditions, *J Mol Catal A Chem.* 198 (2003) 317–341. [https://doi.org/10.1016/S1381-1169\(02\)00728-8](https://doi.org/10.1016/S1381-1169(02)00728-8)
- [23] C. Guminski, The Hg-Rh (Mercury-Rhodium) System *J. Phase Equil.* 23 (2002) 537–540. <https://doi.org/10.1361/105497102770331280>

[24] J.A. Widegren, R.G. Finke, A review of the problem of distinguishing true homogeneous catalysis from soluble or other metal-particle heterogeneous catalysis under reducing conditions, *J Mol Catal A Chem.* 198 (2003) 317–341. [https://doi.org/10.1016/S1381-1169\(02\)00728-8](https://doi.org/10.1016/S1381-1169(02)00728-8)

Chapter V: Synthesis and characterization of novel cross-linked micelles with polycationic shell and pyridine/triphenylphosphine-functionalized core

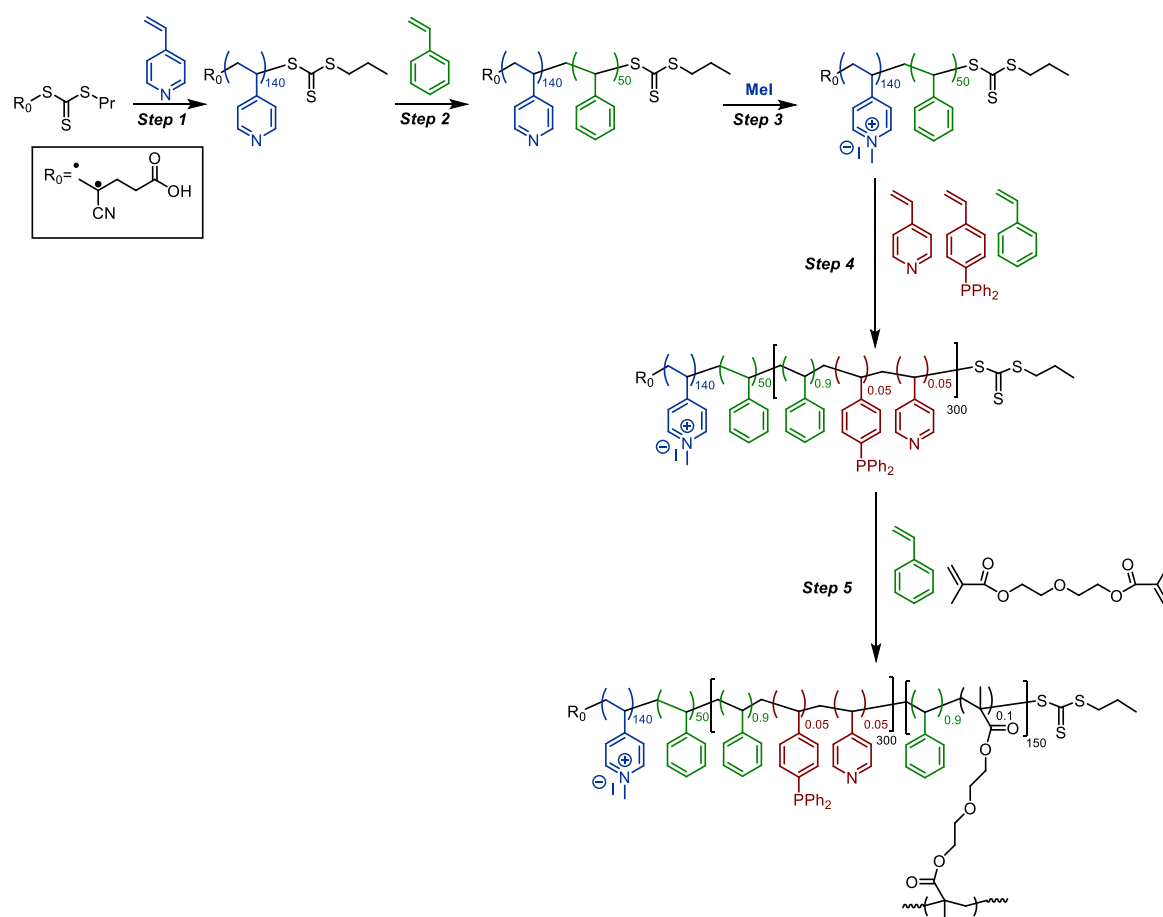
V.1. Introduction

In the previous chapter, the synthesis of TPPO@CCM-C and its successful use to anchor RhNPs in the polymer cores, which avoided extraction of the NPs with diethyl ether, was described. In parallel work, another ligand-functionalized core CCM-C was developed as a possible solution for anchoring the RhNPs in the core. The purpose was to imitate the role of chelating ligands that afford better stabilization for metals and thus to build an efficient nanoreactor system to improve the catalyst recycling. Inspired by the effectiveness of the RhNPs synthesis in the presence of pyridine and TPP, polymerizable analogs of these stabilizers (namely, vinylpyridine or VP and styryldiphenylphosphine or SDPP) were therefore used to prepare a modified CCM-C where both stabilizers are covalently bound to the core. In the present chapter, the synthesis and characterization of these new core cross-linked micelles are described along with initial catalytic results obtained at LCC using Rh^I as catalyst. Note that this chapter is derived from the draft of article No. 6 in the list of publications reported earlier.

V.2. Polymer synthesis and characterization

The synthesis of the new VP-SDPP@CCM-C polymer was performed following the same strategy as for the preparation of the closely related polymers, namely TPP@CCM-C [1,2], TPPO@CCM-C and TPPS@CCM-C (Chapter III) (Scheme V.1). The target degrees of polymerization of each block were kept identical to those of TPPO@CCM-C, as they were already optimized to provide stable latexes with a narrow particle size distribution [1,2]. Thus, the first three steps leading to the

synthesis of the amphiphilic diblock macroRAFT agent, $R_0\text{-(VPMe}^+\text{I)}_{140}\text{-}b\text{-St}_{50}\text{-SC(S)SnPr}$, isolated as a stable solid and redispersed in water, were once again the same as in the TPP@CCM-C synthesis [2]. They involved the homogeneous RAFT polymerization of 4-vinylpyridine (4VP) with 4-cyano-4-thiothiopropylsulfanyl pentanoic acid (CTPPA), $R_0\text{SC(S)SnPr}$ where $R_0 = \text{CMe(CN)CH}_2\text{CH}_2\text{COOH}$, as transfer agent, forming $R_0\text{-4VP}_{140}\text{-SC(S)SnPr}$ (step 1), then chain extension with a short polystyrene block (average degree of polymerization of 50) forming a $R_0\text{-VP}_{140}\text{-}b\text{-St}_{50}\text{-SC(S)SnPr}$ diblock copolymer (step 2), and quaternization of the pyridine N-atoms with MeI (step 3).



Scheme V.1. Synthesis route of the VP-SDPP@CCM-C polymer.

The fourth step was a further chain extension of the $R_0\text{-(VPMe}^+\text{I)}_{140}\text{-}b\text{-St}_{50}\text{-SC(S)SnPr}$ macroRAFT agent with a longer hydrophobic block (average degree of polymerization of 300) consisting of a statistical copolymer of styrene, SDPP and VP

(90/5/5 ratio). These micelles were then crosslinked in a final step with DEGDMA (15 equiv. per chain), diluted with additional styrene (135 equiv. per chain), to yield the final product, R_0 -(VPMe⁺I⁻)₁₄₀-*b*-St₅₀-*b*-(St_{0.9}-*co*-SDPP_{0.05}-4VP_{0.05})₃₀₀-*b*-(St_{0.9}-*co*-DEGDMA_{0.1})₁₅₀-SC(S)SnPr (VP-SDPP@CCM-C). All the polymerization steps were followed to completion (full consumption of monomers) by ¹H NMR (Figure V.1).

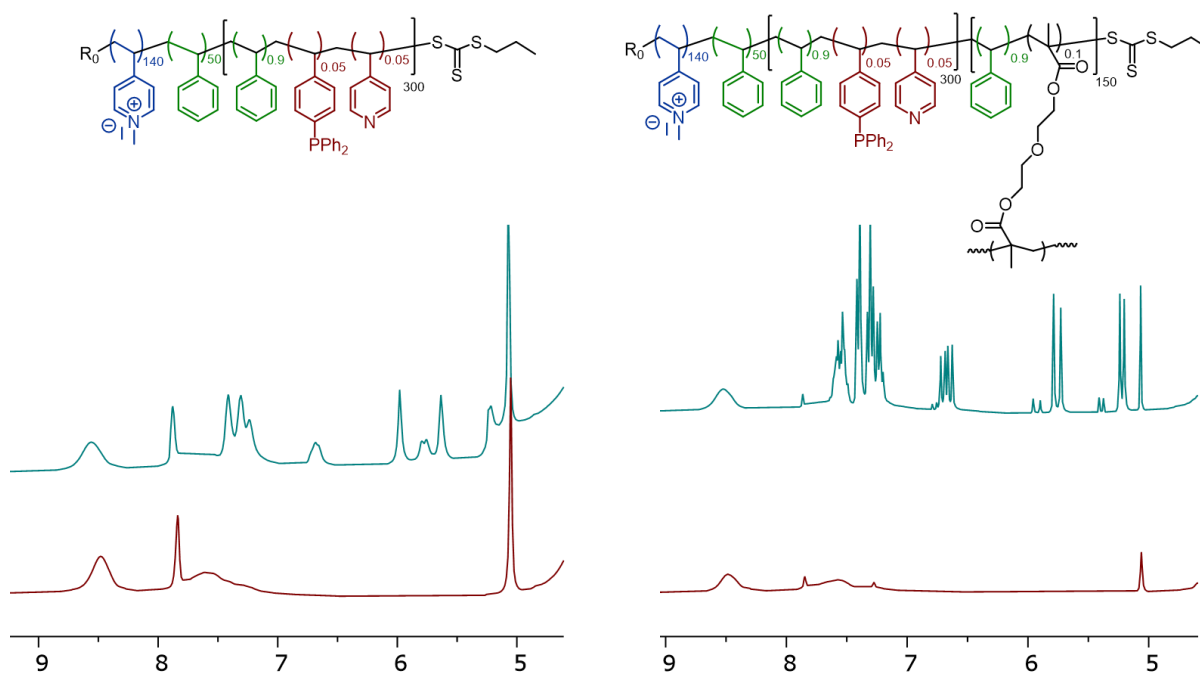


Figure V.1. ¹H NMR of the diblock (left) and the micelles (right), at t_0 (blue) and $t = 4.5$ h (red).

The final VP-SDPP@CCM-C micelles had a larger average diameter (108 nm) than the intermediate micelles (69 nm), as shown by DLS (Figure V.2b and 2a, respectively). TEM revealed that these newly CCMs are well dispersed with spherical morphology (Figure V.2 c).

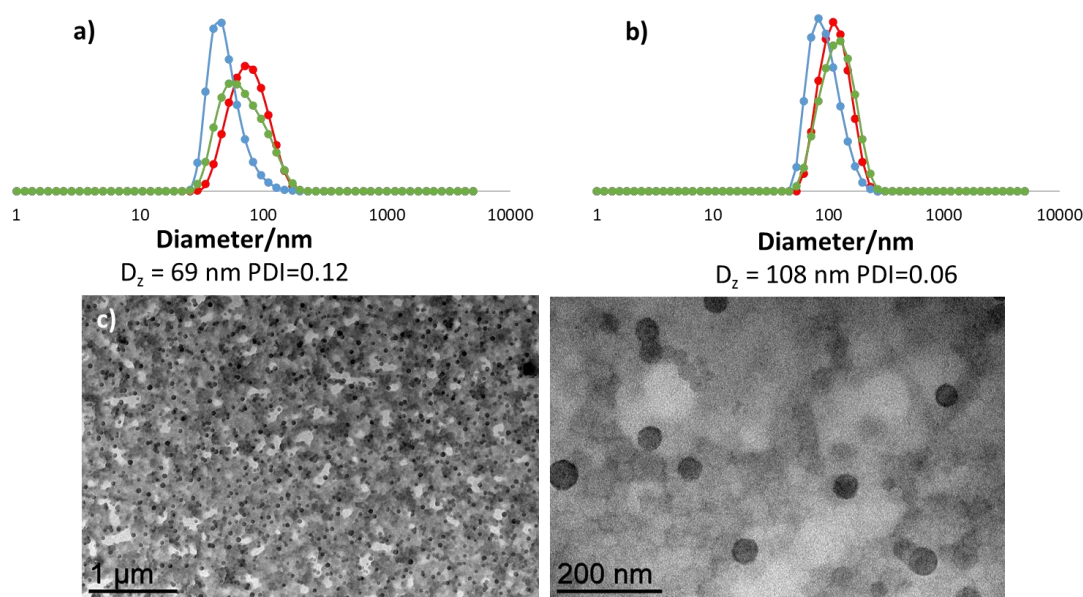


Figure V.2. DLS size distributions of aqueous dispersions of (a) the diblock R_0 -(VPMe⁺I)₁₄₀-*b*-St₅₀-*b*-(St_{0.9}-*c*O-SDPPS_{0.05}-4VP_{0.05})₃₀₀-*b*-SC(S)SnPr micelles and (b) VP-TPP@CCM-C. Color coding: number (blue), volume (green) and intensity (red). c) TEM image of VP-TPP@CCM-C.

Since 4VP was observed to be a very good solvent for SDPP, the chain extension of the R_0 -(VPMe⁺I)₁₄₀-*b*-St₅₀-SC(S)SnPr macroRAFT agent was also attempted without the use of additional styrene. For that purpose, the fourth step was a statistical copolymerization of 4VP and SDPP with a 95/5 ratio, maintaining a target degree of polymerization of 300. The average diameter of the resulting diblock copolymer micelles was 73 nm, with a broad size distribution and a higher polydispersity index that clearly indicates that the resulting latex is more polydispersed, with the presence of large particles (PDI > 0.3), than the micelles obtained by chain extension with styrene (Figure V.3a). These micelles were then crosslinked in a final step with DEGDMA (150 equiv. per chain), to yield the final product, R_0 -(VPMe⁺I)₁₄₀-*b*-St₅₀-*b*-(4VP_{0.95}-*c*O-SDPP_{0.05})₃₀₀-*b*-DEGDMA₁₅₀-SC(S)SnPr (VP-SDPP@CCM-C) with a broad size distribution and an average diameter of 139 nm (Figure V.3 b).

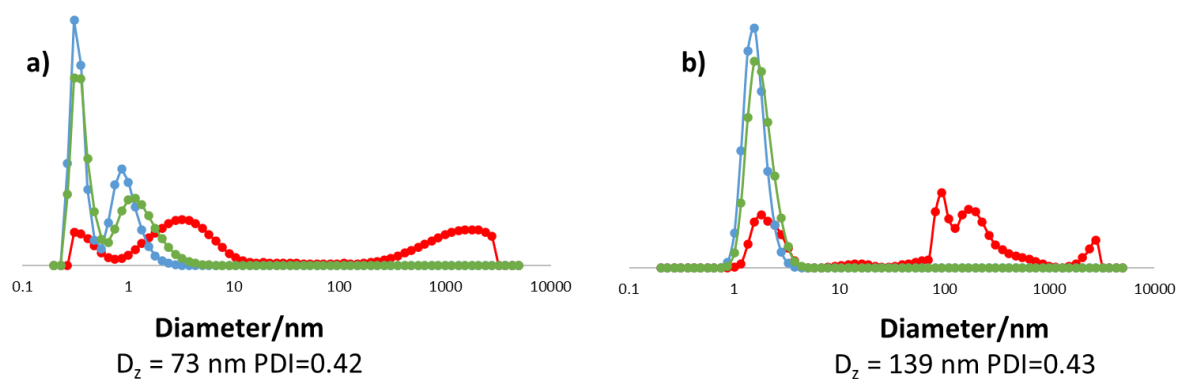


Figure V.3. DLS size distributions of aqueous dispersions of (a) the diblock $R_0-(VPMe^+I)_{140}-b-St_{50}-b-(VP_{0.95}-CO-SDPP_{0.05})_{300}-b-SC(S)SnPr$ micelles and (b) VP-TPP@CCM-C. Color coding: number (blue), volume (green) and intensity (red).

The surface composition and structure of nanomaterials play a crucial role in dictating their response to interactions with their surroundings. Several key factors associated with the surface properties include the surface charge, the surface energy and the pH. Each one of these can individually influence the performance of the nanomaterial [3]. Further experiments are needed to understand the reason behind the resulting large particles with a high polydispersity index. However, the lower quality of the VP-SDPP@CCM-C obtained without the use of styrene in the fourth step underlines the importance of its use for the chain extension. All subsequent catalytic studies were carried out with the $R_0-(VPMe^+I)_{140}-b-St_{50}-b-(St_{0.9}-CO-SDPP_{0.05}-4VP_{0.05})_{300}-b-(St_{0.9}-CO-DEGDMA_{0.1})_{150}-SC(S)SnPr$ polymer.

V.3. $[Rh(COD)(\mu-Cl)]_2$ precatalyst coordination

Using a previously optimized protocol [1], the complex $[Rh(COD)(\mu-Cl)]_2$ was added to the CCM-C cores after swelling the polymer particles with toluene ($P/Rh = 4/1$). By stirring the latex phase with a toluene solution of the metal complex at room temperature, the Rh complex was efficiently transferred into the CCM-C cores within 0.25 h. The transfer was visually confirmed by the disappearance of the yellow coloration of the organic phase and by the slight coloration of the latex in the aqueous phase. Thus, the polycationic nature of the outer shell did not hinder the migration of

the metal complex, as previously shown and extensively studied in the group [1,4] (Figure V.4). The corresponding latex contains $[\text{RhCl}(\text{COD})(\text{L@CCM-C})]$, where the ligand bonded to the Rh^{I} center may either be TPP or pyridine. It is named Rh-VP-SDPP@CCM-C.



Figure V.4. Photographs of the mixture of the VP-SDPP@CCM-C latex with a $[\text{Rh}(\text{COD})(\mu\text{-Cl})_2]$ /toluene solution ($P/\text{Rh} = 4:1$) before (left) and after stirring (right).

As studied before [4], RhNPs can be generated in the core of the nanoreactors without the need for a base, and this occurs at lower temperatures when the P/Rh^{I} ratio is lower. Accordingly, the CCM-C was loaded using a P/Rh ratio of 2/1. As shown in Figure V.5, the organic phase remained yellow after 0.5 h, but turned limpid and white after 24 h.



Figure V.5. Photographs of the mixture of the VP-SDPP@CCM-C latex with a $[\text{Rh}(\text{COD})(\mu\text{-Cl})_2]$ /toluene solution ($P/\text{Rh} = 2:1$) before stirring (left) and after stirring for 0.5 h (middle) and 24 h (right).

V.4. Aqueous biphasic catalysis with Rh^I-VP-SDPP@CCM-C

V.4.1 Aqueous biphasic hydrogenation with Rh^I

The Rh^I-VP-SDPP@CCM-C latex, obtained as described in the previous section (P/Rh = 4/1), was applied to the aqueous biphasic hydrogenation of 1-octene to octane (1-octene/Rh = 200:1; 20 bar H₂; 60 °C; 20h) in a steel autoclave, using nonanol as vectorizing solvent (1-octene/nonanol = 1:9 v/v) and decane as internal standard (decane/1-octene = 1:4). After loading the latex and substrate into the autoclave, the latter was charged with 20 bar H₂ and stirred at 60 °C for 20 h, 1200 rpm. After the set reaction time, the latex was extracted with diethyl ether, and the combined organic phases were analyzed by GC. The analysis confirmed the formation of octane with a 1-octene conversion of 91% (and total selectivity towards octane, with no observation of isomerization products), which is a similar result to that obtained with Rh^I-TPP@CCM-C [1]. No further catalytic experiments were carried out with the molecular Rh system, and the focus was instead shifted toward the generation of core-anchored RhNPs in the modified nanoreactors.

V.4.2 Attempts to generate RhNP-VP-SDPP@CCM-C

The first attempts to reduce the Rh^I-VP-SDPP@CCM-C latex and generate CCM-Cs with core-anchored RhNPs were carried out without added base since the core ligands of the polymer that are pyridine based and TPP have already proved efficient for generating RhNPs [5]. The latex was first core-swollen with toluene, then loaded with [Rh(COD)(μ-Cl)]₂ as described above (Section V.4.1) and transferred to an autoclave, which was subsequently pressurized with 20 bar of H₂ and kept stirring for 20 h at 60 °C [4]. After the set reaction time, the polymer had surprisingly maintained its initial color, signaling the absence of any metal reduction to RhNPs. As this could be explained by a lack of decomposition of the Rh^I anchored complex, a higher temperature was then probed (80 °C), but again, no color change was observed. These

results suggest that the combination of TPP and pyridine ligands in the core (TPP:py:Rh = 4:4:1) provides improved stabilization to the Rh^I center, compared to TPP alone [4] and TPPO (as seen in Chapter IV), blocking its reduction to Rh⁰ under the employed conditions. Other attempts to promote the Rh^I reduction, including the addition of a base, NEt₃ or pyridine, which should further help by trapping the HCl that would be generated by the H₂ reduction, and thus facilitate the generation of RhNPs, as it was previously demonstrated in the reduction of Rh^I-TPP@CCM-C [4], was again unsuccessful for this system.

V.5. Summary and Outlook

The introduction of a combination of TPP and pyridine as anchoring groups in the hydrophobic core of amphiphilic star-block copolymers led to well-dispersed CCMs with a narrow size distribution. The use of the mentioned combination of ligands proved efficient in the generation of nanoreactors with a core-anchored molecular catalyst, Rh^I-VP-SDPP@CCM-C, which demonstrated good catalytic activity in the hydrogenation of 1-octene. However, this Rh^I-VP-SDPP@CCM-C latex could not be used as a precursor for the generation of core-anchored RhNPs under the operating conditions that we have so far explored. Therefore, further investigations on the generation of RhNPs in the core of the developed VP-SDPP@CCM-C could be envisaged as future work. These CCMs will be also used for the confinement of other *d*-block metals and their application in aqueous biphasic hydrogenation. The synthesis of new CCMs with 4-vinylpyridine and 4-styryldiphenylphosphine oxide ligands bonded within the core could also be planned as new nanoreactors for the confinement of RhNPs.

V.6. References

[1] H. Wang, L. Vendrame, C. Fliedel, S. Chen, F. Gayet, F. D'Agosto, M. Lansalot, E. Manoury, R. Poli, Triphenylphosphine-Functionalized Core-Cross-Linked Micelles and Nanogels with a Polycationic Outer Shell: Synthesis and Application in Rhodium-

Catalyzed Biphasic Hydrogenations, *Chem Eur J* 27 (2021) 5205–5214.
<https://doi.org/10.1002/chem.202004689>

[2] H. Wang, L. Vendrame, C. Fliedel, S. Chen, F. Gayet, E. Manoury, X. Zhang, F. D'agosto, M. Lansalot, R. Poli, Core-Cross-Linked Micelles Made by RAFT Polymerization with a Polycationic Outer Shell Based on Poly(1-methyl-4-vinylpyridinium), *Macromolecules* 53 (2020) 2198–2208.
<https://doi.org/10.1021/acs.macromol.9b02582>

[3] A. Singer, Z. Barakat, S. Mohapatra, S.S. Mohapatra, Nanoscale Drug-Delivery Systems: In Vitro and In Vivo Characterization, in *Nanocarriers for Drug Delivery: Nanoscience and Nanotechnology in Drug Delivery*, Elsevier Science Ltd., (2018) 395–419. <https://doi.org/10.1016/B978-0-12-814033-8.00013-8>

[4] H. Wang, A.M. Fiore, C. Fliedel, E. Manoury, K. Philippot, M.M. Dell'Anna, P. Mastrorilli, R. Poli, Rhodium nanoparticles inside well-defined unimolecular amphiphilic polymeric nanoreactors: Synthesis and biphasic hydrogenation catalysis, *Nanoscale Adv.* 3 (2021) 2554–2566. <https://doi.org/10.1039/d1na00028d>

[5] M. Guerrero, N.T.T. Chau, S. Noël, A. Denicourt-Nowicki, F. Hapiot, A. Roucoux, E. Monflier, K. Philippot, About the Use of Rhodium Nanoparticles in Hydrogenation and Hydroformylation Reactions *Curr Org Chem* 17(4) (2013) 364 – 399
<https://doi.org/10.2174/1385272811317040006>

Chapter VI: Rh nanoparticles confined in novel polyanionic core-crosslinked micelles with triphenylphosphine oxide-functionalization: Synthesis, characterization, and application in aqueous biphasic hydrogenation

VI.1. Introduction

In a recent contribution, a CCM with a polyanionic shell (CCM-A) of homopolymer blocks of poly(sodium styrenesulfonate) and triphenylphosphine as core-ligands has been reported [1,2]. The formation of these CCM-A requires fewer synthetic steps compared to their CCM-C cationic counterparts, making them easier to prepare. Moreover, another interest of CCM with a polyanionic outer shell is the limitation of polymer particle interpenetration owing to the repulsion caused by Coulombic forces. This phase separation in aqueous biphasic hydrogenation compared to the other CCM-N and CCM-C systems. However, when using CCM-A as nanoreactor for Rh catalyst confinement [1], an unexpected complication at the catalyst loading stage was faced as the result of the polyanionic shell interaction with the Rh precursor, which prevented effective catalyst loading. This issue led us to envisage an alternative route to confine RhNPs in the core of CCM-A micelles by adjusting the nature of the core-ligands to allow interaction with the RhNPs.

In this chapter, the synthesis of the new TPPO@CCM-A polymer by RAFT polymerization, and a RhNP-TPPO@CCM-A latex by introduction of *ex-situ* synthesized RhNPs into the core using a previously optimized method are reported. In contrast to earlier attempts, this method proved successful by overcoming the challenges posed by the polyanionic nature of the shell. Additionally, the RhNP-TPPO@CCM-A latex was also prepared by a one-pot synthesis approach by reducing $[\text{Rh}(\text{COD})(\mu\text{-Cl})_2]$ /toluene directly in the presence of an aqueous TPPO@CCM-A latex

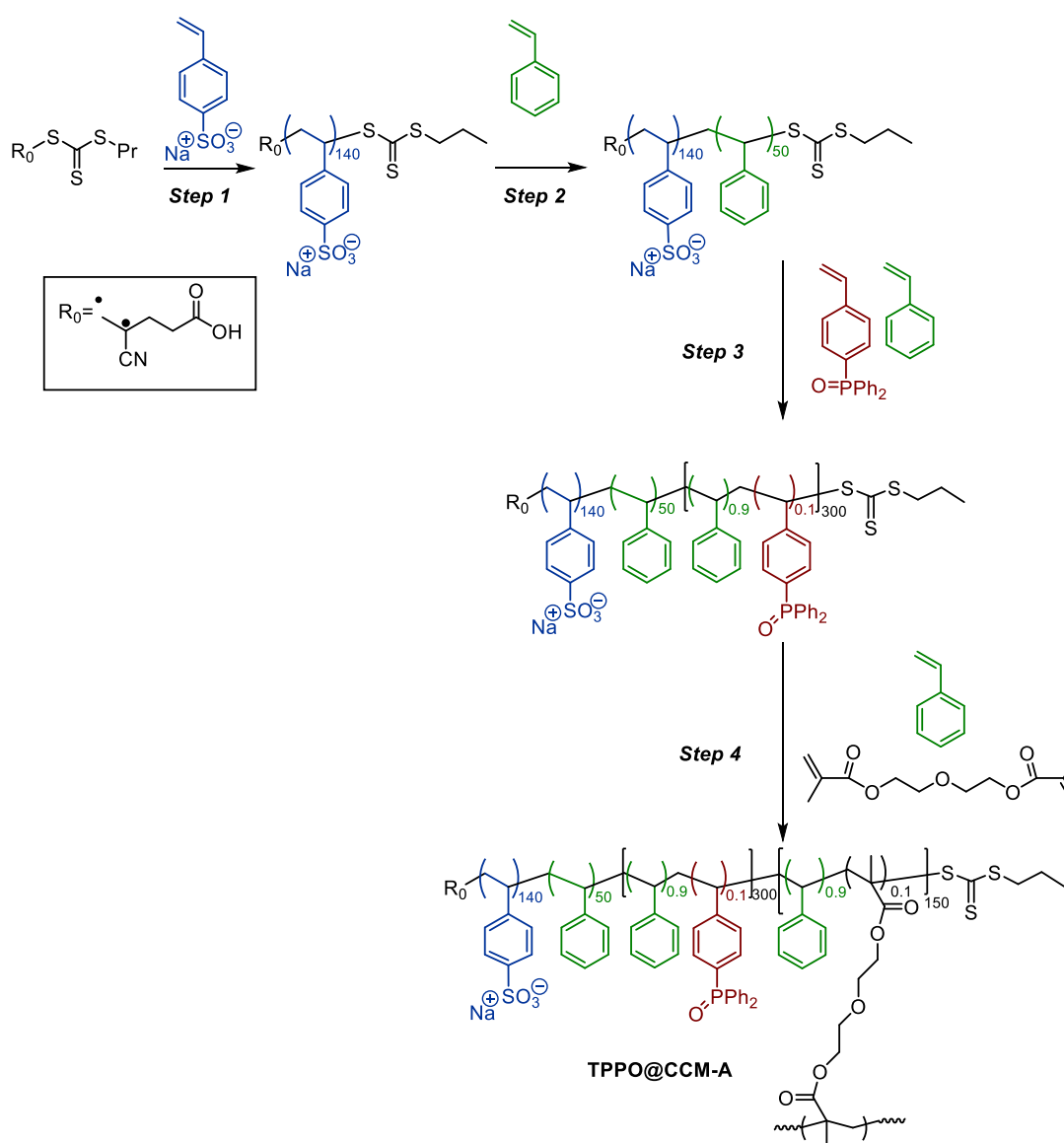
without the need of auxiliary stabilizers or bases. Note that this chapter is related to article No. 5 in the list of publications reported earlier.

VI.2. Polymer synthesis and characterization

The synthesis of the CCM with a TPPO-functionalized CCM-A core (TPPO@CCM-A) followed the same convergent strategy previously optimized for the preparation of the other CCMs [1,2], with the α - and ω -chain ends of the macromolecule provided by the RAFT chain transfer agent CTPPA ($R_0 = -C(CH_3)(CN)CH_2CH_2COOH$). The optimized synthetic route was reported and published previously using SDPP as core monomer, while the use of SDPPO in RAFT polymerization for the synthesis of CCM-Cs has been shown previously in Chapter III. The final latexes contain up to 14.4 wt% of polymer and have low viscosity, as expected for suspensions of spherical micelles, and proved stable over several months with no evidence of coagulation.

The synthesis of the TPPO@CCM-A was carried out by fixing the degrees of polymerization to 140 for the outer hydrophilic $P(SSNa^+)$ shell and to 300 for the polystyrene (PSt) core (Scheme VI.1). The fraction of SDPPO (a solid monomer) in the St/SDPPO mixture is limited by the SDPPO solubility in styrene (*ca.* 25 mol%). CCMs were initially developed by extending the $R_0-(SSNa^+)_{140}-SC(S)SnPr$ macromolecules with a short PSt block (50 monomer units), yielding an amphiphilic diblock copolymer, which self-assembles (Step 2). Further chain extension of the $R_0-(SSNa^+)_{140}-b-St_{50}-SC(S)SnPr$ macroRAFT agent with the St/SDPPO (90/10) mixture was performed directly as an emulsion polymerization, ensuring full incorporation of the SDPPO monomer in the CCM core, as confirmed by 1H NMR, and leading to $R_0-(SSNa^+)_{140}-b-St_{50}-b-(St_{0.9}-CO-SDPPO_{0.1})_{300}-SC(S)SnPr$ (Step 3). The spherical micelles of the amphiphilic diblock copolymer thus produced in step 4 had an average size of *ca.* 32 nm, as shown by DLS analysis (Figure VI.1a). The final crosslinking step was carried out with DEGDMA (15 equiv. per chain), diluted with additional styrene (135 equiv. per chain), leading to CCM-A of composition $R_0-(SSNa^+)_{140}-b-St_{50}-b-(St_{0.9}-CO-$

SDPPO_{0.1})₃₀₀-*b*-(St_{0.9}-*co*-DEGDMA_{0.1})₁₅₀-SC(S)SnPr (Step 4), with a 10% crosslink density in the inner crosslinked core.



Scheme VI.1. Synthesis route of the TPPO@CCM-A polymer.

The final TPPO@CCM-A polymer particles had spherical morphology and a slightly larger diameter (45 nm) than the intermediate micelles, as shown by DLS (Figure VI.1 b) and TEM (Figure VI.1 d) analyses, and narrower than their analogs synthesized in the presence of SDDP [1]. After swelling with CHCl₃ (Figure VI.1c), the distribution was relatively unchanged. This phenomenon upon swelling can be attributed to the dominant effect of micelles disaggregation rather than core swelling which would

cause an increase in average size, similar to what was seen before with TPP@CCM-A[1,2] as well as TPP@CCM-C [3] and TPPO@CCM-C (see Chapter III).

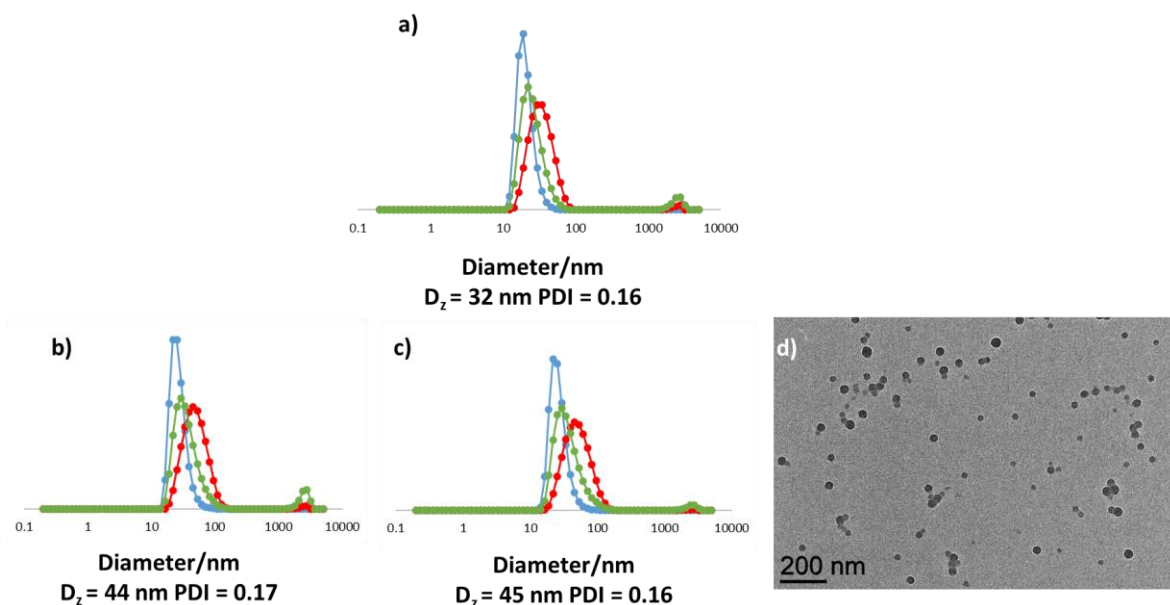


Figure VI.1. DLS size distributions of (a) the diblock $R_0-(SS-Na^+)_{140}-b-St_{50}-b-(St_{0.9}-co-SDPPO_{0.1})_{300}-SC(S)SnPr$ dispersed in $NaCl_{(aq)}$ and of the aqueous dispersions of TPPO@CCM-A (b) in $NaCl_{(aq)}$, (c) after core swelling with $CHCl_3$. Color coding: number (blue), volume (green) and intensity (red). d) TEM image of the TPPO@CCM-A.

VI.3. Synthesis and characterization of RhNPs-TPPO@CCM-A

The synthesis of RhNPs-TPPO@CCM-A systems was performed following two different methods; 1) loading the TPPO@CCM-A latex with *ex-situ* synthesized RhNPs in the presence of stabilizing ligands and, 2) direct synthesis of RhNPs in the presence of TPPO@CCM-A, as described hereafter.

VI.3.1. *Ex-situ* synthesis of RhNPs and transfer to TPPO@CCM-A

A colloidal suspension of RhNPs in toluene ($ca\ 1.2 \pm 0.4\ nm$, see Chapter III) was synthesized following a previously applied *ex-situ* protocol, where $[Rh(COD)(\mu-Cl)]_2$ was reduced under H_2 pressure (20 bar) in the presence of pyridine and TPP as stabilizing ligands. Toluene was used as solvent for the RhNP synthesis due to its high swelling power for the polystyrene-based CCM-A core [4], and the pyridine/TPP

ligand combination was chosen given our previous work on TPPO@CCM-C where it showed to effectively stabilize RhNPs (see Chapter III). The addition of the RhNPs colloidal suspension to the TPPO@CCM-A latex ($P/Rh = 4/1$) led to a fast and complete discoloration of the toluene phase, while the latex became grey. This indicated the successful transfer of the RhNPs across the $P(SS^-Na^+)$ hydrophilic shell of the CCM-A particles and, attributed, to their anchoring to the TPPO core functions. TEM analysis of the final RhNP-TPPO@CCM-A confirmed that the RhNPs were located inside the polymer particles, displaying a mean size of 2.1 ± 0.1 nm (Figure VI.2). No other characterization nor catalytic application were done on this system given the easiest single step protocol further developed (VI.3.2 section).

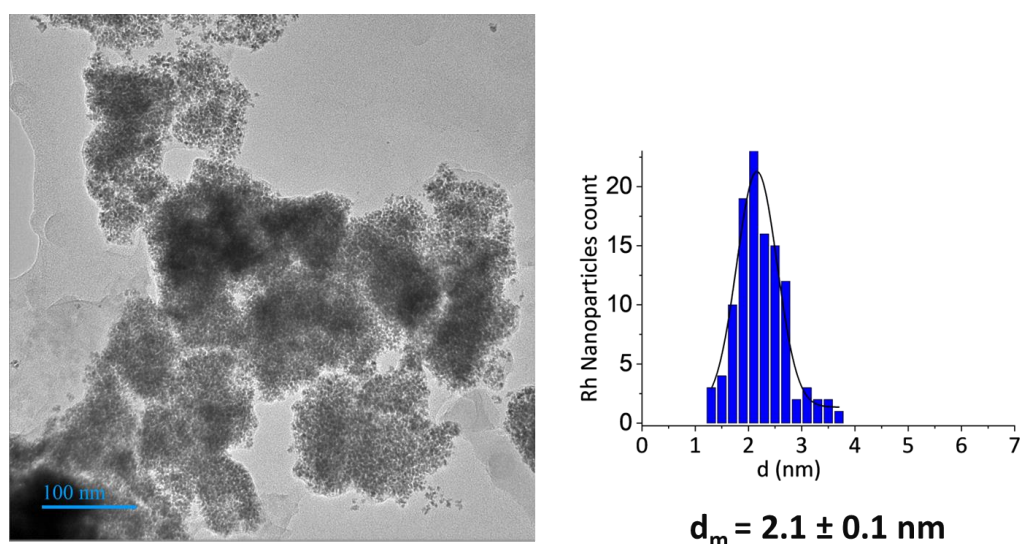


Figure VI.2. TEM images of RhNP-TPPO@CCM-A synthesized by RhNPs transfer and the corresponding size distribution of RhNPs ($d_m = 2.1 \pm 0.1$ nm).

VI.3.2. One-pot synthesis of RhNPs-TPPO@CCM-A

A stable latex of RhNP-TPPO@CCM-A was also synthesized in a single step by heating (60 °C) a biphasic mixture containing aqueous TPPO@CCM-A latex and a toluene solution of $[Rh(COD)(\mu-Cl)]_2$ under H_2 pressure (20 bar), without additives (base or ligand). The obtained latex showed to be black while the toluene phase was colorless and transparent, signaling successful formation and confinement of RhNPs in the core of the CCMs. TEM analysis of the so-obtained RhNP-TPPO@CCM-A latex evidenced

the presence of RhNPs in the polymer core that display a larger mean size of 3.1 ± 0.6 nm compared to the polymer prepared in the two-step procedure (Figure VI.3).

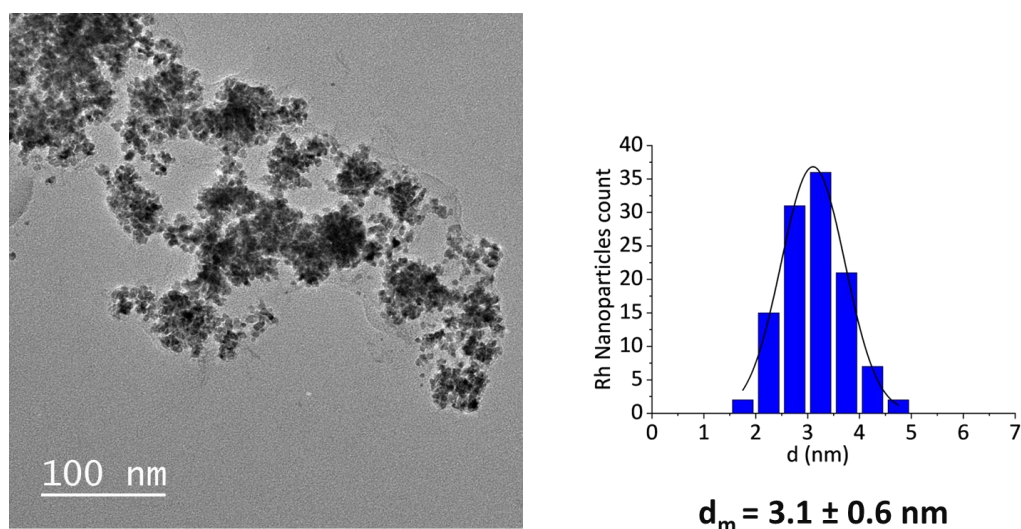


Figure VI.3. TEM images of one-pot synthesized RhNP-TPPO@CCM-A and the corresponding size distribution of RhNPs ($d_m = 3.1 \pm 0.6$ nm).

VI.3.2.1. Characterization of one-pot synthesized RhNPs-TPPO@CCM-A

The stability of the one-pot synthesized RhNP-TPPO@CCM-A was studied by TGA performed under N_2 (Figure VI.4). The RhNP-TPPO@CCM-A polymer proved thermally stable up to $T_{dec} = 254$ °C (temperature of decomposition) that led to the initial weight loss. A gradual weight loss was then observed, attributed to the decomposition of the polymer chain with a 60 wt.% at 418 °C, evidencing the total decomposition of the polymeric chains. Overall, the results obtained by TGA indicate that the polymer is stable up to 200 °C, however beyond this temperature, it started to decompose.

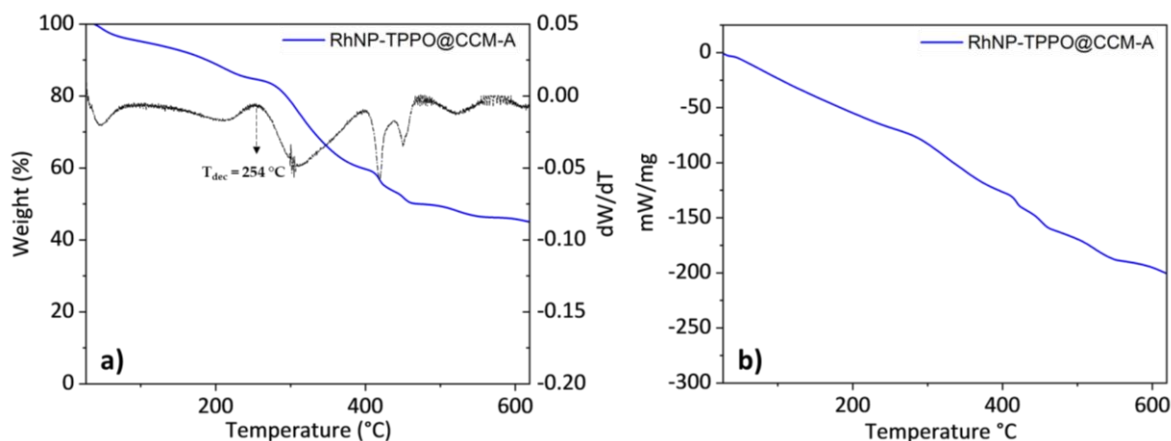


Figure VI.4. TGA (a) and DSC (b) profiles of RhNP-TPPO@CCM-A.

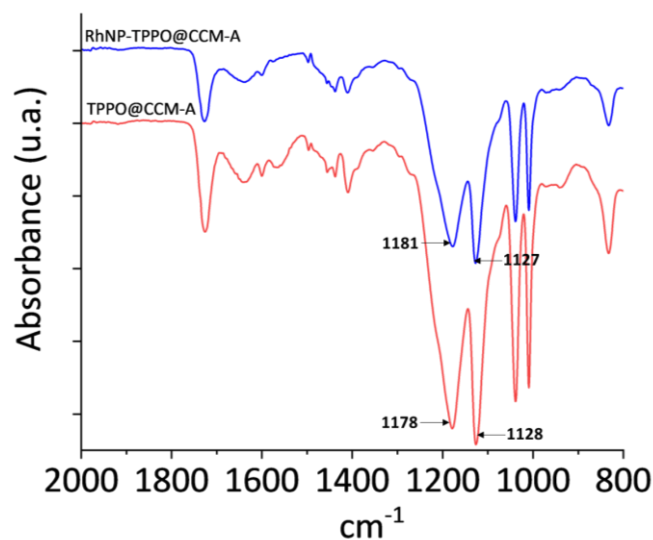
The interaction between the polymer and the RhNPs was analyzed by XPS analyses performed on the two systems (Appendix D Figure D1-D3) that revealed a shift in binding energy of TPPO in the presence of RhNPs in the core of the polymer, which was particularly notable for the O1s excitation ($\Delta E = 2.6$ eV (Scan A) and 4.6 eV (Scan C)), further supporting the presence of RhNPs-polymer interactions in the RhNP-TPPO@CCM-A latex (Table VI.1), in accordance with the results obtained in Chapter IV.

To further corroborate the interaction, ATR-FTIR spectra of TPPO@CCM-A and RhNP-TPPO@CCM-A were compared to those of TPPO (Chapter IV). The strong P=O stretching band of TPPO (1178 cm^{-1}) [5] was quite evident in TPPO@CCM-A, but less intense and slightly blueshifted ($\sim 1181\text{ cm}^{-1}$) in RhNP-TPPO@CCM-C (Figure VI.5) which is different from that found for RhNP-TPPO@CCM-C (Chapter IV) [6,7]. This indicates that the RhNP-polymer interaction might be different from that of the CCM-C. To elucidate this difference more detailed characterization is needed to probe the interaction of RhNPs with other potential anchoring groups in the polymer, including the polyanionic shell.

Table VI.1. Binding energies (eV) of the chemical states of the C, S, O atoms in TPPO@CCM-A and RhNP-TPPO@CCM-A.

Atom	Binding Energy TPPO@CCM-A (eV)	FWHM (eV)	Atomic ratio (%)	Binding Energy RhNP-TPPO@CCM-A (eV)	FWHM (eV)	Atomic ratio (%)	ΔE (eV) ^a
C _{1s} Scan A	283.5	0.97	4.11	283.5	0.95	6.1	0
C _{1s} Scan B	284.7	1.27	91.6	284.7	1.5	69.5	0.05
C _{1s} Scan C	286	0.92	1.94	286	1.4	16.5	0
C _{1s} Scan D	286.7	0.72	1.75	287.2	1.11	2.1	0.52
C _{1s} Scan E	288.86	0.7	0.59	288.78	1.39	5.82	0.08
S _{2p} Scan A	168.3	1.5	81.77	168.07	1.9	41.13	0.23
S _{2p} Scan B	169.6	0.94	18.23	169.47	2.21	58.87	0.13
P _{2p} Scan A	132.43	1.28	66.21	132.59	1.66	66.38	0.16
P _{2p} Scan B	133.29	1.22	33.79	133.45	2.78	33.62	0.16
O _{1s} Scan A	530.8	1.93	80.16	533.4	1.89	19.33	2.6
O _{1s} Scan B	532.29	1.78	14.3	532.09	2.17	77.2	0.2
O _{1s} Scan C	535.4	2.27	5.54	530.72	1.3	3.47	4.68

^a $\Delta E = |\text{Binding energy (TPPO@CCM-A)} - \text{binding energy (RhNP-TPPO@CCM-A)}|$.

**Figure VI.5.** ATR-FTIR spectra of TPPO@CCM-A (red) and RhNP-TPPO@CCM-C (blue) in the range of 700-2000 cm⁻¹.

VI.4. Hydrogenation catalysis with one-pot synthesized RhNPs-TPPO@CCM-A

VI.4.1. Styrene hydrogenation

The RhNP-TPPO@CCM-C latex prepared by transfer of *ex-situ* synthesized RhNPs in the presence of TPP/pyridine previously showed to provide high activity in aqueous biphasic styrene hydrogenation (see Chapter III). However, upon recycling process involving intermediate product extraction by diethyl ether, the catalyst gradually lost activity over consecutive catalytic runs explained by the removal of the initial stabilizers from the RhNPs surface (as also described in Chapter III). Conversely, the RhNP-TPPO@CCM-C latex prepared in one-pot synthesis condition without additives, showed a good recyclability for up to six consecutive runs with unchanged activity as described in Chapter IV.

The hydrogenation of styrene study with the one-pot synthesized RhNP-TPPO@CCM-A latex was performed at a high stirring rate (1200 rpm) to limit external mass transport limitation. The reaction was performed under 20 bar H₂ pressure for 0.25 h at a temperature range of 27-44 °C and using a St/Rh ratio of 2000/1 and 5000/1 (Table VI.2). The RhNPs-TPPO@CCM-A catalyst proved moderately active; a conversion up to 39% at 44 °C for a St/Rh ratio of 2000/1 (Entry 3, Table VI.2), corresponding to average TOF values up to 3080 h⁻¹ (*c*TOF, values up to 7050 h⁻¹). However, a full selectivity (>99%) towards ethyl benzene (EB) was observed, indicating that in the conditions applied this catalyst was not able to catalyze the hydrogenation of the aromatic ring to provide ethyl cyclohexane (ECH). In the case of St/Rh 2000/1 ratio, when the reaction time was prolonged, full styrene conversion (>99%) was reached after 2 h at 25 °C, corresponding to a TOF of 1100 h⁻¹ (*c*TOF of 2500 h⁻¹) still with full selectivity (>99%) towards EB (Figure VI.6).

**Table VI.2:** Hydrogenation of styrene with one-pot synthesized RhNPs-TPPO@CCM-A.^a

Entry	Molar styrene/Rh ratio	T (°C)	Conversion (%)	Selectivity (%)		TOF (<i>c</i> TOF) (h ⁻¹)
				EB	ECH	
1	2000/1	27	18	>99	<0.1	1500 (3240)
2	2000/1	35	32	>99	<0.1	2515 (5760)
3	2000/1	44	39	>99	<0.1	3080 (7050)
4	5000/1	27	11	>99	<0.1	2015 (4600)
5	5000/1	35	25	>99	<0.1	4425 (10125)
6	5000/1	43	27	>99	<0.1	4560 (10440)

^a Reaction conditions: 20 bar H₂, 0.25 h, 1200 rpm. EB: ethylbenzene, ECH : ethylcyclohexane.

The quantitative selectivity towards EB with both the RhNPs-TPPO@CCM-A and its analogous RhNPs-TPPO@CCM-C (see Chapter IV), denotes this selectivity is apparently independent of the size of the core-confined RhNPs (1.7 and 3.1 nm, respectively) as well as the composition of the outer CCM shell (cationic or anionic) and CCM sizes (98 and 44 nm, respectively). Nevertheless, as elucidated in Chapter I, it is well-established that both the nature of the support and the RhNPs surface-bound ligands can alter selectivity. Thus, it will be important to scrutinize the impact of ligand surface coverage in forthcoming catalysis investigations.

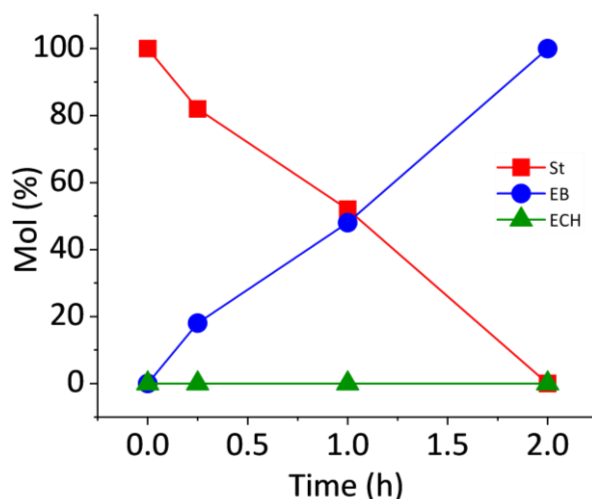


Figure VI.6. Time plot for the aqueous biphasic hydrogenation of styrene using one-pot synthesized RhNPs-TPPO@CCM-A latex. Reaction conditions: Styrene/Rh = 2000/1, 20 bar H₂, 25 °C.

The apparent activation energy (E_a) of the reaction conducted with the RhNPs-TPPO@CCM-A latex, at St/Rh ratios of 2000/1 and 5000/1, was further estimated *via* Arrhenius plots (Figure VI.7). Focusing on the two lowest reaction temperatures for the reaction with St/Rh ratio of 5000/1 (Table VI.2, Entries 4 and 5), the E_a was estimated as 57 ± 0.3 kJ/mol. This value is significantly lower than for the analogous reaction (69 ± 6 kJ/mol) conducted with RhNP-TPPO@CCM-C (see Chapter IV), thus pointing to more severe internal mass transport limitation with the RhNP-TPPO@CCM-C catalytic system. Conversely, the E_a was estimated to be 71 ± 0.4 kJ/mol for the reaction with a St/Rh ratio of 2000/1 (Table VI.2, Entries 1 and 2), which is notably consistent with the values previously reported for styrene hydrogenation in the gas phase [8] and the reaction with RhNP-TPPO@CCM-C under aqueous biphasic conditions using a St/Rh ratio of 5000/1. Hence, it is likely that part of limitation in the reaction conducted with St/Rh ratio of 5000/1 arises from the use of a significantly higher volume of substrate (St/latex volume ratio *ca.* 2), compared to the reaction performed with a St/Rh ratio of only 2000/1. Moreover, when considering the two highest sets of reaction temperatures (Table VI.2, Entries 2 and 3, Entries 5 and 6), the corresponding E_a values tend toward 0 and 2.4 kJ/mol, respectively. These low values reflect that the catalytic activities (*i.e.*, *c*TOFs) were almost the same at different

temperatures (35 – 44 °C), thus corroborating increased mass transport restriction [9–11] at higher reaction temperatures as also found with the RhNP-TPPO@CCM-C system (see Chapter IV). It is important to mention that these preliminary findings should be reinforced by catalytic activity measurements performed at more temperatures to further validate the estimated E_a values.

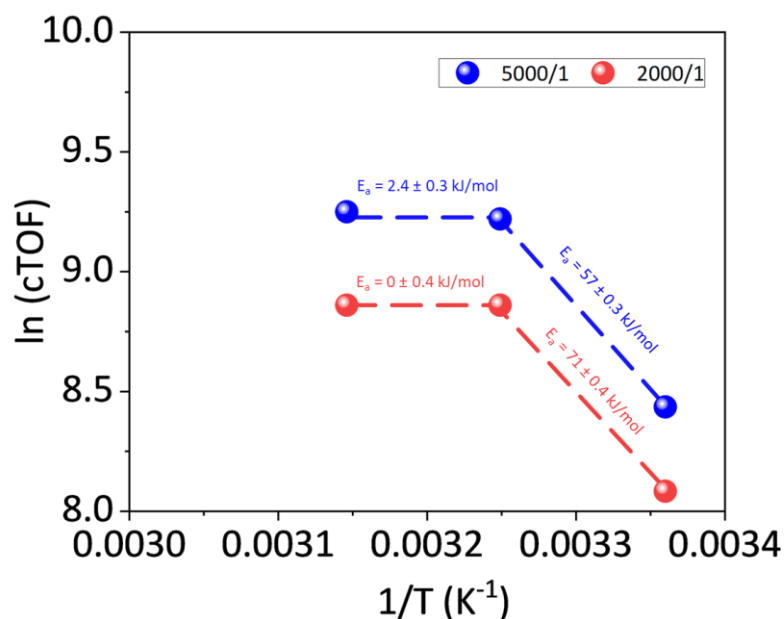


Figure VI.7. Apparent activation energy of the hydrogenation of styrene using one-pot synthesized RhNPs-TPPO@CCM-A latex. Reaction conditions: Styrene/Rh = 2000/1 (red) and 5000/1 (blue), 20 bar H_2 , 0.25 h, 1200 rpm.

Recycling of the RhNP-TPPO@CCM-A latex was also evaluated for a series of catalytic runs with a St/Rh ratio of 2000/1 (20 bar H_2 , 25 °C, 0.25 h) with intermediate product extraction by diethyl ether (Figure VI.8). This extraction procedure is similar as was applied to recycle the RhNP-TPPO@CCM-C and RhNP-TPPO@CCM-C latexes [3,12] as well as the latex of the molecular Rh^I -TPPO@CCM [3,12]. A constant styrene conversion of *ca.* 18%, corresponding to an average TOF of ~ 1500 h^{-1} (*c*TOF of 3240 h^{-1}), was obtained over the five reaction runs, but only when the catalyst system was reactivated with H_2 (20 bar, 1 h, 25 °C) prior to addition of a new batch of substrate. The ICP-MS analyses showed only a cumulative loss of $\sim 1.9\%$ of the catalyst inventory after the five catalytic runs (Appendix D, Table D1). Although the system showed good recyclability and selectivity towards EB, it showed a much lower *c*TOF (6500 h^{-1})

compared to the previously examined RhNP-TPPO@CCM-C system (Chapter IV). This disparity in average *c*TOFs of about 100% for the two systems with the different CCM shells confirms that the activity of the RhNP-TPPO@CCM-A catalyst is limited to a greater extent by mass transport of the substrate/product between the CCM core and the organic bulk phase [9].

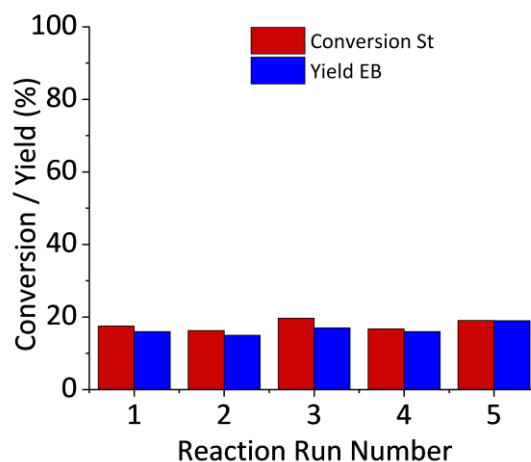


Figure VI.8. Reuse of one-pot synthesized RhNPs-TPPO@CCM-A catalyst in six reaction runs of styrene hydrogenation with intermediate H₂ treatment (20 bar H₂, 25 °C, 1 h) and product extraction by diethyl ether. Reaction conditions: Styrene/Rh = 2000/1, 20 bar H₂, 25 °C, 0.25 h.

Furthermore, TEM analysis on the recovered latex after the fifth run (Figure VI.9), showed that the RhNPs remained well dispersed with the similar mean diameter of (3.1 ± 0.6 nm) as prior to catalysis, but with a broader size distribution, that might result from the presence of some agglomeration due to the intermediate washing with diethylether.

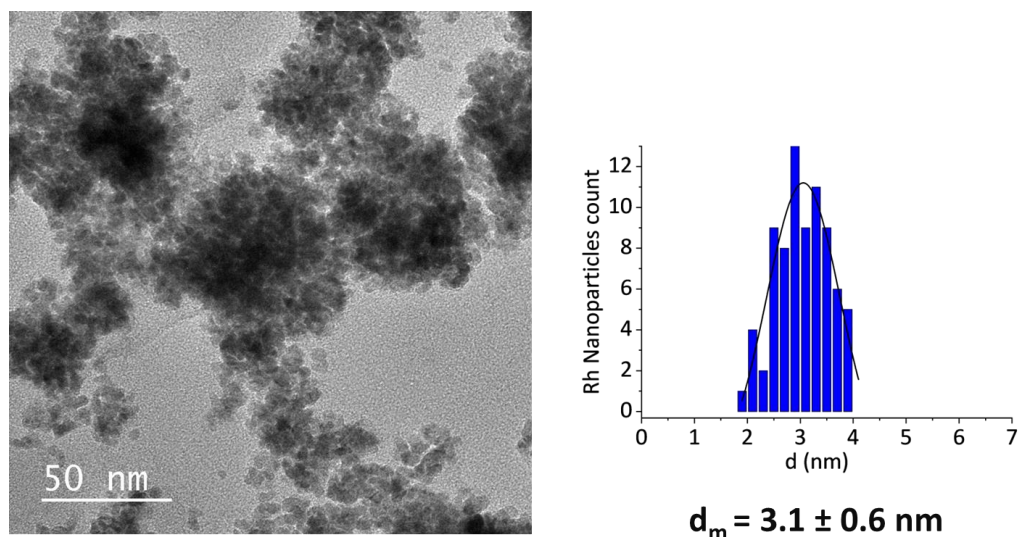
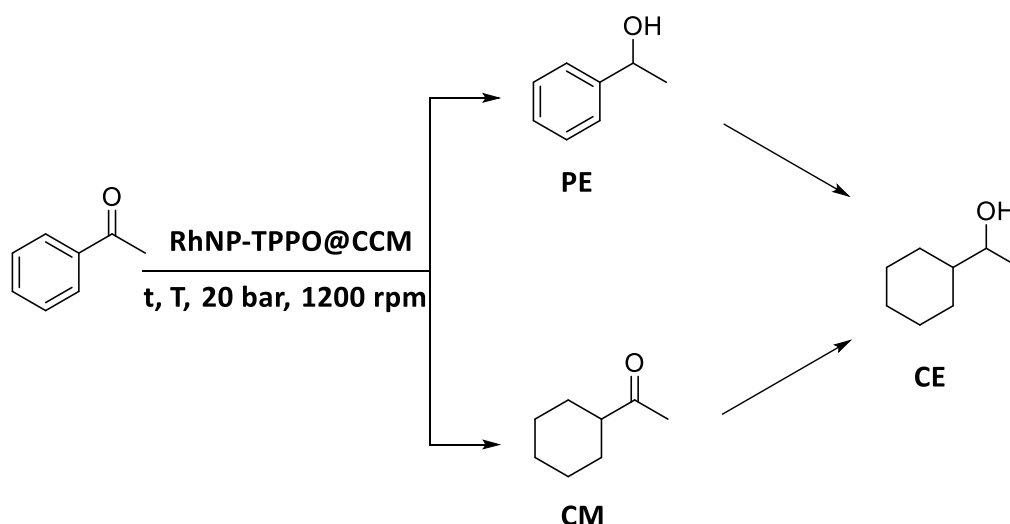


Figure VI.9. TEM images of one-pot synthesized RhNP-TPPO@CCM-A after the fifth reaction run and the corresponding size distribution of RhNPs ($d_m = 3.1 \pm 0.6 \text{ nm}$).

VI.4.2. Acetophenone hydrogenation

In a previous study, the RhNP-TPP@CCM-C catalyst was shown to perform poorly in aqueous biphasic hydrogenation of acetophenone (TOF of 0.5 h^{-1} with 20 bar H_2 , $25 \text{ }^\circ\text{C}$ over 20 h) in comparison to styrene [12]. This was attributed to severe mass transport limitation for acetophenone substrate, which was interpreted as resulting from a possible interaction of the carbonyl group with the polycationic shell of the CCM-C. Recently, however, the hydrogenation of acetophenone was successively conducted using RhNPs-TPPO@CCM-C with an average $c\text{TOF}$ of 3000 h^{-1} vs 6500 h^{-1} for styrene hydrogenation under similar reaction conditions as for styrene hydrogenation (Chapter IV). To further explore the possible effect of the outer CCM shell on the acetophenone mass transport, a series of hydrogenation reaction were conducted at different temperatures to compare the performance of one-pot synthesized RhNP-TPPO@CCM-C and RhNPs-TPPO@CCM-A catalyst with acetophenone (Scheme VI.2).



Scheme VI.2. Products resulting from the hydrogenation of acetophenone catalyzed by RhNP-TPPO@CCMs.

Interestingly, the hydrogenation of acetophenone using RhNPs-TPPO@CCM-C proceeded with higher average c TOFs of 3000 and 3880 h^{-1} at temperatures of 25 and 60 $^{\circ}\text{C}$, respectively (Table VI.3, Entries 1 and 2), compared to that with the RhNPs-TPPO@CCM-A which led to average c TOFs of 2240 and 3110 h^{-1} (Table VI.2, Entries 3 and 4) under the same conditions (acetophenone/Rh = 5000/1, 20 bar H_2 , 2 h, 1200 rpm). This suggests that the smaller size of the CCM-A micelles and different shell structure compared to that of CCM-C, induced additional limitation for the transport of acetophenone towards the RhNPs sites, leading to lower overall reaction rates and lower conversion efficiencies. Hence, the disparity in activity does not necessarily imply that the interaction between the carbonyl group and the polycationic or polyanionic shell is different. To further elucidate that, a series of FTIR analyses is envisaged, to probe the interaction of the carbonyl function with the polycharged shells.

Table VI.3. Aqueous biphasic hydrogenation of acetophenone with one-pot synthesized RhNP-TPPO@CCM-C and RhNPs-TPPO@CCM-A^a

Entry	Catalyst	T (°C)	Conv. (%)	Selectivity (%)			TOF (<i>c</i> TOF) (h ⁻¹)
				PE	CM	CE	
1	RhNP-TPPO@CCM-C	25	86	>99	<0.1	<0.1	2120 (3000)
2	RhNP-TPPO@CCM-C	60	>99	>99	<0.1	<0.1	2600 (3880)
3	RhNP-TPPO@CCM-A	25	45	>99	<0.1	<0.1	979 (2240)
4	RhNP-TPPO@CCM-A	60	60	>99	<0.1	<0.1	2045 (3110)

^a Reaction conditions: Acetophenone/Rh = 5000/1, 20 bar H₂, 2 h, 1200 rpm.

Another important factor that may also contribute to the disparity of the results is the confinement effect caused by the differing chemical compositions and physical properties of the two types of nanoreactors (*vide supra*) (Chapter IV). Such effect can alter the local concentration of reactants inside the CCMs and influence the nucleation rates of RhNPs, leading to different NP sizes (*cf.* Figure VI.3, $d_m = 3.1 \text{ nm} \pm 0.6 \text{ nm}$, with Figure IV.1.a, $d_m = 1.7 \pm 0.2 \text{ nm}$) and size distributions, as well as the accessibility of active sites for catalysis within the nanoreactors.

VI.5. Summary and Outlook

Novel CCMs with a polyanionic shell and TPPO-functionalized core (TPPO@CCM-A) were synthesized by RAFT polymerization. Nano-sized RhNPs synthesized by an *ex-situ* protocol using a previously optimized method were then successfully introduced into the TPPO@CCM-A. Remarkably, a one-pot synthesis approach also yielded a RhNP-TPPO@CCM-A latex by reducing [Rh(COD)(μ -Cl)]₂/toluene without requiring auxiliary stabilizers or bases, thus providing an easiest synthesis method. This catalyst proved efficient and recyclable in the aqueous biphasic hydrogenation of both styrene and acetophenone, but yielded a lower activity compared to its CCM-C counterpart, primarily due to internal mass transfer limitations. Addressing the disparities in results caused by confinement effects may require in-depth kinetic and mechanistic studies. Understanding the factors contributing to the results is key to tailoring the CCM polymeric systems and optimizing their catalytic performance, and such investigations will be a focal point of future work.

VI.6. References

- [1] H. Wang, C.J. Abou-Fayssal, C. Fliedel, E. Manoury, R. Poli, Phosphine-Functionalized Core-Crosslinked Micelles and Nanogels with an Anionic Poly(styrenesulfonate) Shell: Synthesis, Rhodium(I) Coordination and Aqueous Biphasic Hydrogenation Catalysis, *Polymers (Basel)* 14 (2022) 14224937 <https://doi.org/10.3390/polym14224937>
- [2] H. Wang, C. Fliedel, E. Manoury, R. Poli, Core-crosslinked micelles with a poly-anionic poly(styrene sulfonate)-based outer shell made by RAFT polymerization, *Polymer (Guildf)*. 243 (2022) 124640 <https://doi.org/10.1016/j.polymer.2022.124640>
- [3] H. Wang, L. Vendrame, C. Fliedel, S. Chen, F. Gayet, F. D'Agosto, M. Lansalot, E. Manoury, R. Poli, Triphenylphosphine-Functionalized Core-Cross-Linked Micelles and Nanogels with a Polycationic Outer Shell: Synthesis and Application in Rhodium-Catalyzed Biphasic Hydrogenations, *Chem Eur J*. 27 (2021) 5205–5214. <https://doi.org/10.1002/chem.202004689>
- [4] X. Zhang, A.F. Cardozo, S. Chen, W. Zhang, C. Julcour, M. Lansalot, J.F. Blanco, F. Gayet, H. Delmas, B. Charleux, E. Manoury, F. D'Agosto, R. Poli, Core-Shell Nanoreactors for Efficient Aqueous Biphasic Catalysis, *Chem Eur J*. 20 (2014) 15505–15517. <https://doi.org/10.1002/chem.201403819>
- [5] Deacon, Glen B. and J.H.S. Green. "Vibrational spectra of ligands and complexes—II Infra-red spectra (3650–375 cm⁻¹ of triphenyl-phosphine, triphenylphosphine oxide, and their complexes." *Spectrochimica Acta Part A: Molecular and Biomolecular Spectroscopy* 24 (1968) 845-852 [https://doi.org/10.1016/0584-8539\(69\)80031-0](https://doi.org/10.1016/0584-8539(69)80031-0)
- [6] S. Carencio, C. Boissière, L. Nicole, C. Sanchez, P. Le Floch, N. Mézailles, Controlled design of Size-tunable monodisperse nickel nanoparticles, *Chem Mat*. 22 (2010) 1340–1349. <https://doi.org/10.1021/cm902007g>
- [7] K. Senevirathne, A.W. Burns, M.E. Bussell, S.L. Brock, Synthesis and characterization of discrete nickel phosphide nanoparticles: Effect of surface ligation chemistry on catalytic hydrodesulfurization of thiophene, *Adv Funct Mater*. 17 (2007) 3933–3939. <https://doi.org/10.1002/adfm.200700758>
- [8] C. Betti, J. Badano, C. Lederhos, M. Maccarrone, N. Carrara, F. Coloma-Pascual, M. Quiroga, C. Vera, Kinetic study of the selective hydrogenation of styrene over a Pd egg-shell composite catalyst, *Reaction Kinetics, Mechanisms and Catalysis*. 117 (2016) 283–306. <https://doi.org/10.1007/s11144-015-0910-8>

- [9] A Borsla, A.M Wilhelm, H Delmas, Hydrogenation of olefins in aqueous phase, catalyzed by polymer-protected rhodium colloids: kinetic study, *Catalysis Today*, 66(2–4) (2001) 389-395, [https://doi.org/10.1016/S0920-5861\(00\)00635-0](https://doi.org/10.1016/S0920-5861(00)00635-0)
- [10] Z.A. Piskulich, O.O. Mesele, W.H. Thompson, Removing the barrier to the calculation of activation energies: Diffusion coefficients and reorientation times in liquid water, *J Chem Phys.* 147 (2017). <https://doi.org/10.1063/1.4997723>
- [11] H. Rafatijo, D.L. Thompson, General application of Tolman’s concept of activation energy, *J Chem Phys* 147 (2017). <https://doi.org/10.1063/1.5009751>
- [12] H. Wang, A.M. Fiore, C. Fliedel, E. Manoury, K. Philippot, M.M. Dell’Anna, P. Mastrorilli, R. Poli, Rhodium nanoparticles inside well-defined unimolecular amphiphilic polymeric nanoreactors: Synthesis and biphasic hydrogenation catalysis, *Nanoscale Adv.* 3 (2021) 2554–2566. <https://doi.org/10.1039/d1na00028d>

Chapter VII: Synthesis and characterization of nickel nanoparticles and their application in catalysis

VII.1. Introduction

The hydrogenation of alkynes to produce (E)- or (Z)-alkenes holds significant importance in the field of fine chemistry and for the polymerization industry [1]. One particular interest involves the elimination of phenylacetylene from styrene feedstocks, as it is relevant to industrial practices and scientific research [2]. The industrial significance stems from the polymerization of styrene, which requires pure feedstocks to maintain the performance of the catalyst. Typical catalysts employed for the hydrogenation of alkynes are supported by Pd-based and Pt-based systems. The catalysts often rely on the use of toxic lead salts as inhibitors [3]. The catalyst performance depends on several factors, such as the interactions between the active metal nanoparticles and their environment, which can be governed through alloys [4], additives [5], and metal supports [6], ultimately affecting the reaction's outcome. One widely utilized industrial catalyst is Lindlar's catalyst Pd/CaCO₃ (doped with Pb(OAc)₂ [5,7], or modified with lead acetate and quinoline). This catalyst, established in 1952, is a benchmark for alkyne hydrogenations. Recent research, employing Density Functional Theory (DFT) [4], has shown that adding lead (Pb) as a secondary metal to Pd not only prevents the formation of overly reactive hydride phases but also obstructs alkene adsorption, preventing overhydrogenation. Furthermore, the inclusion of quinoline improves selectivity by enhancing site separation and inhibiting the formation of unwanted oligomers [5]. Additionally, the properties of the support material, as in the case of supported Pt/ γ -Al₂O₃ [6], can also influence the catalytic performance. For instance, factors like texture, pore size, and crystal phase can impact reactant diffusion and adsorption. The former catalyst demonstrates good selectivity in the semi-hydrogenation of internal alkynes but lacks selectivity with

monosubstituted alkynes and may partially isomerize (Z)-alkenes into (E)-alkenes [8]. In addition to the cost of Pd and Pt, the limited catalyst reuse and robustness, catalyst passivation – which is mainly caused by the presence of toxic leads/salts – and the need for the addition of an amine modifier are the main drawbacks of this catalytic system [9]. The development of efficient, chemoselective, and eco-friendly catalysts, namely that contain earth-abundant and low-cost metals while being recyclable, is challenging, especially for industrial and big-scale applications. Well-defined NiNPs proved successful in the selective hydrogenation of alkynes into alkenes with better catalytic activity than conventional heterogeneous catalysts, because of their higher active surface areas [1,10]. These properties have garnered significant attention as attractive substitutes in the field of alkyne hydrogenation [1,10–15]. In addition to that, NiNPs present several advantages such as high reactivity and selectivity, but also, based on their magnetic properties, the ability to be easily separated from the reaction medium through magnetic precipitation in the presence of an external magnet. This enables them to be recovered and reused, thus fulfilling the eco-friendly character of recyclability. Magnetic recovery is well recognized as an efficient and speedy technique for catalyst separation [16,17].

It is well known in the literature, and this has been already mentioned in all the previous chapters, that the characteristics and catalytic properties of metal nanoparticles can be tuned by the use of suitable stabilizers. Stabilizing agents can be ligands, surface active agents, solid supports, polymers including polymeric core crosslinked micelles (CCMs), *etc.* The latter systems can provide stability, solubility, and recyclability of the MNPs [10]. As part of my PhD project, an industrial secondment was performed at IFPEN (Institut Français du Pétrole, Energies Nouvelles) in Solaize, France. To this end, the use of NiNPs, confined in core cross-linked micelles was considered for the selective hydrogenation of alkynes. This project was based on the potential use of nickel to decrease the use of noble metals and the

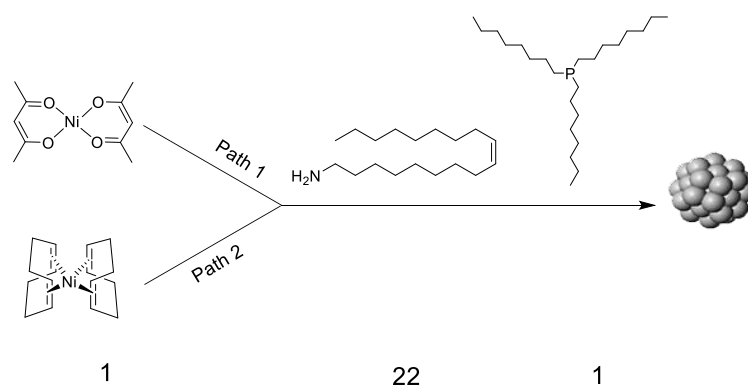
cost of the catalyst for industrial applications, in combination with the advantages of biphasic catalysis conditions as offered by the CCMs systems.

In the present chapter, the synthesis of nickel nanoparticles (NiNPs) stabilized with P- and N-based ligands as well as the one-pot synthesis of NiNP-TPPO@CCM-A latex that contains confined NiNPs are reported. The application of the colloidal suspension of NiNPs in the hydrogenation of alkynes will also be described. The initial plan was to test the NiNPs embedded in the CCM-A polymer micelles for aqueous biphasic hydrogenation of alkynes and to study the recovery of the catalyst. However, due to the size of the reactors used for the catalytic hydrogenation experiments that needed a large scale-up of the synthesis of the CCM-A polymer and of the NiNP-TPPO@CCM-A latex, the catalyses were performed using only the unconfined NiNPs. Note that this chapter is derived from the draft of article No. 6 in the list of publications, reported earlier.

VII.2. NiNPs synthesis and characterization

The first NiNPs synthesis was carried out by following the high-temperature procedure using $[\text{Ni}(\text{acac})_2]$ as a precursor reported by Carencio *et al.* [18].

$[\text{Ni}(\text{acac})_2]$ (Path 1) or $[\text{Ni}(\text{COD})_2]$ (Path 2) were used as precursors in the presence of oleylamine (N-ligand) and tri-*n*-octylphosphine (P-ligand) as stabilizers (Ni/N/P = 1/22/1) (Scheme VII.1). The reaction mixture was heated up to 215 °C for 2 h, without hydrogen (See Chapter II, Section II.10.1). After the set reaction time, samples were withdrawn for TEM analyses.



Scheme VII.1. Synthesis of NiNPs from $[\text{Ni}(\text{acac})_2]$ (Path 1) or $[\text{Ni}(\text{COD})_2]$ (Path 2) in the presence of oleylamine and tri-n-octylphosphine as stabilizers

Under these synthesis conditions, using $[\text{Ni}(\text{acac})_2]$ as precursor led to the formation of NiNPs with a mean diameter of 11.3 ± 2.3 nm while $[\text{Ni}(\text{COD})_2]$ provided nanoparticles with a lower mean diameter (3.4 ± 0.3 nm) and a narrower size distribution (Figure VII.1). Since the temperature, the supersaturation of solutions, the molar volumes, and the stabilizers were identical and only the nickel precursor differed for the two syntheses protocols of NiNPs, one can speculate that the NP growth mechanism was not identical due to the nature of the precursor. Two limitation factors can be considered: either the diffusion of the two precursor monomers to the growing NP surface was not identical, or the reaction of these monomers on the NP surface did not follow the same kinetics [19]. However, this alone cannot explain the large difference observed in the NP size. The mechanism of growth is caused by the change in solubility of the NPs depending on their size. Above a certain critical radius, the particles will form and grow whereas below this radius the particles will redissolve. Indeed, due to the high solubility and the surface energy of smaller particles within the solution, this can lead to their redissolution and in turn, allow the larger particles to grow even more. This phenomenon is referred to as the Ostwald ripening [20] and might explain the formation of large NiNPs under the reaction conditions of Path 1. Contrarily, digestive ripening [19] which is actually the inverse of Ostwald ripening where smaller particles grow at the expense of larger ones could explain the formation of the smaller NiNPs observed when applying the Path 2

reaction conditions. In the case of inverse Ostwald ripening, the NP formation is also controlled by the surface energy of the particles within the solution but it is the larger particles that redissolve in favor of the growth of smaller particles. In addition, the generation of NiNPs by decomposition of the Ni(0) complex $[\text{Ni}(\text{COD})_2]$ might be more thermodynamically favored than that from $[\text{Ni}(\text{acac})_2]$, which requires the reduction of Ni(II) to Ni(0), which takes place in the presence of amine. This could also explain the formation of smaller and better-sized-controlled (narrower size distribution) Ni NPs when starting from $[\text{Ni}(\text{COD})_2]$ compared to $[\text{Ni}(\text{acac})_2]$.

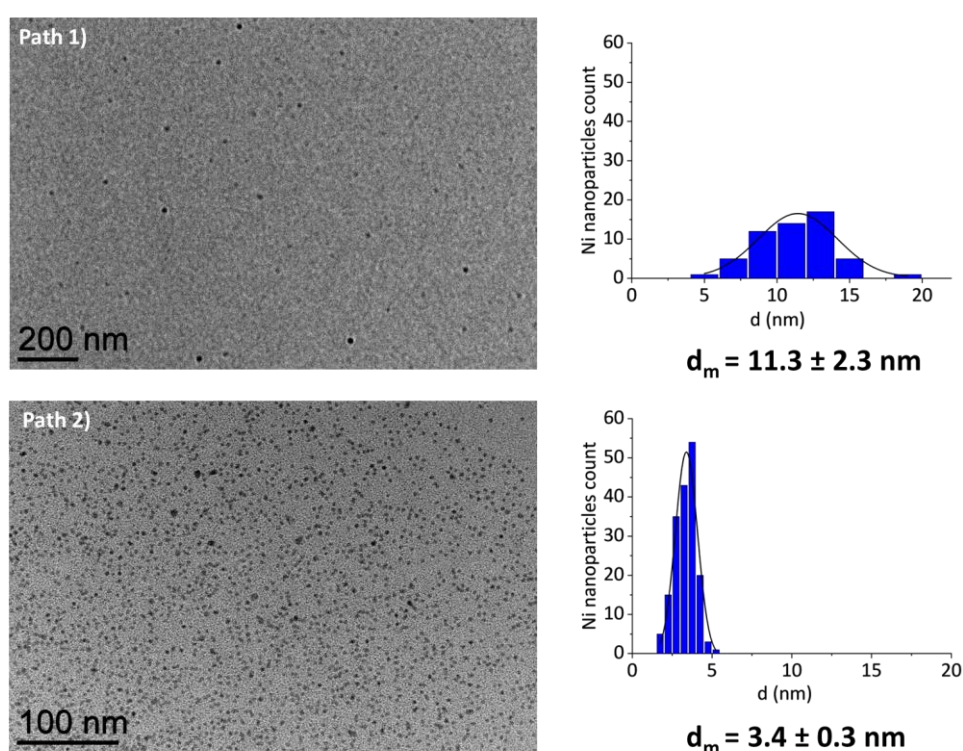
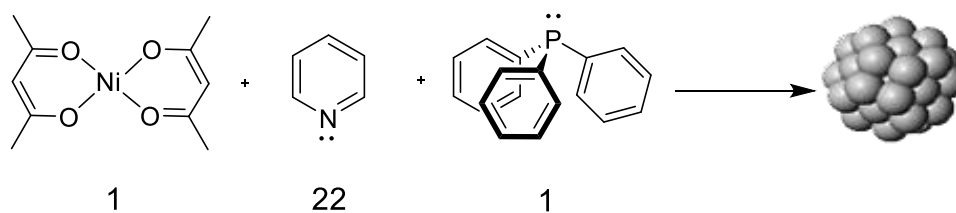


Figure VII.1. TEM images and corresponding size distribution histograms of NiNPs obtained by Path 1 ($d_m = 11.3 \pm 2.3 \text{ nm}$) and Path 2 ($d_m = 3.4 \pm 0.3 \text{ nm}$). Reaction conditions: 215 °C, 2 h, P = 1 atm, 1200 rpm.

The influence of different stabilizing ligands and reaction conditions on the formed NiNPs was subsequently studied. Concerning the stabilizing ligands, those previously used to *ex-situ* synthesize RhNPs, namely pyridine and triphenylphosphine (TPP) (see Chapter III), were considered with the aim to explore their capacity to also stabilize NiNPs. $[\text{Ni}(\text{acac})_2]$ was chosen as the precursor for this study, due to its solubility in both toluene and H_2O , which renders it important for

further applications in CCMs. The reaction was performed either in neat pyridine or in the presence of toluene as diluting solvent using a Ni/N/TPP molar ratio of 1/22/1 (Scheme VII.2), which was also applied for the synthesis of RhNPs. After 20 h of reaction under 20 bar of H₂ at 110 °C (temperature limited by the boiling point of pyridine), the NiNPs synthesized in neat pyridine displayed an average size of $d_m = 2.8 \pm 0.2$ nm and a narrow size distribution. Conversely, when the reaction was conducted in the presence of toluene, the formed NiNPs presented an average diameter of $d_m = 7.4 \pm 4.0$ nm and a broader size distribution (Figure VII.2). The observed difference in size may be linked to the dilution of the Ni species in the medium with toluene compared to the synthesis in neat pyridine. In principle, diluted conditions are expected to favor the formation of smaller NPs as the concentration of metal atoms is lower, thus limiting their attraction, but this is not the case here. Ostwald ripening is another hypothesis that is favored in the case of a broad-size distribution. It could also be an effect of dilution of the stabilizing ligands that would tend to decrease their adsorption at the growing NP surface in the presence of toluene compared to neat pyridine conditions. This would limit the NP growth, thus leading to larger particles.



Scheme VII.2. Synthesis of NiNPs from [Ni(acac)₂] in the presence of pyridine and triphenylphosphine in a) neat pyridine (Ni/N/TPP = 1/22/1) and b) toluene (Ni/N/TPP = 1/1/1). Reaction conditions: H₂ (20 bar), 20 h, 110 °C, 1200 rpm.

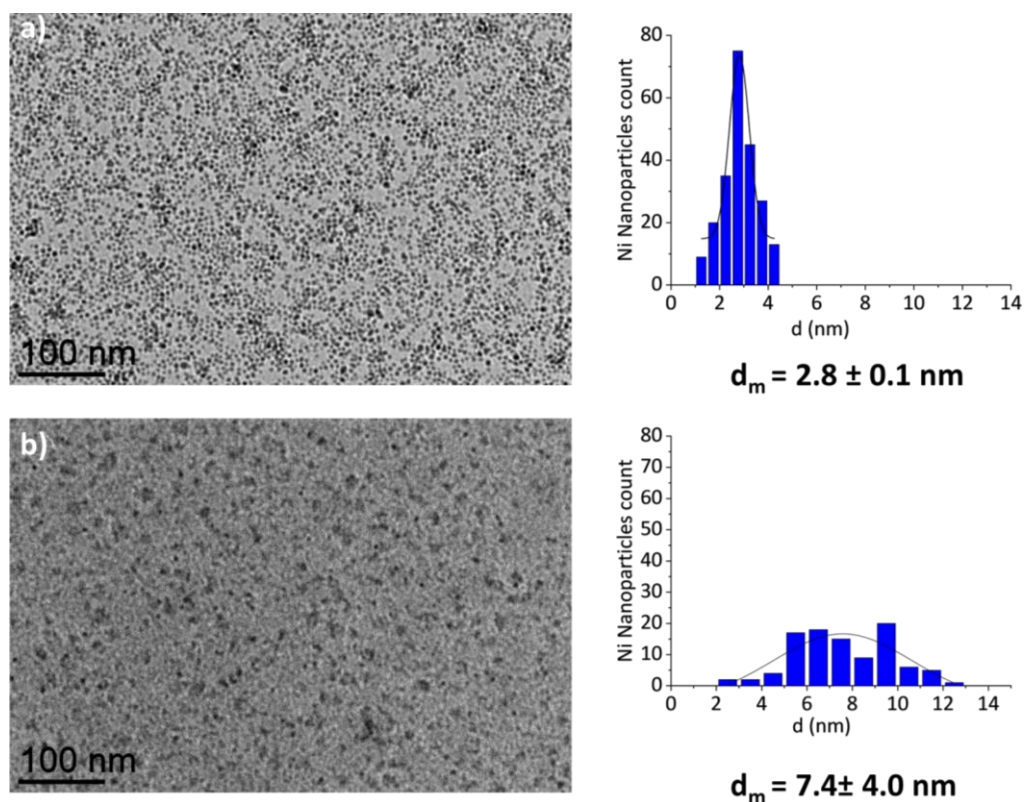


Figure VII.2. TEM images and corresponding size distribution histograms of NiNPs prepared in a) neat pyridine (Ni/N/TPP = 1/22/1) with $d_m = 2.8 \pm 0.1$ nm and b) toluene (Ni/N/TPP = 1/1/1) with $d_m = 7.4 \pm 4.0$ nm.

As mentioned in Chapter II (section II.1.5.), the size of the reactors used at IFPEN for catalytic studies imposed the use of a larger reaction volume for an optimized mechanical stirring. Although the presence of toluene had provided NiNPs with a higher average diameter and a broader size distribution, as indicated above, the syntheses of NiNPs performed at IFPEN were first conducted using 22 equivalents of pyridine diluted in 10 mL of cyclohexane. However, under these conditions, no formation of NPs was observed. A set of experiments were then conducted with the [Ni(acac)₂] and [Ni(COD)₂] complexes for comparison purposes. When using only TPP as a stabilizing ligand, diluted in 10 mL of cyclohexane (Ni/TPP = 1/1), the formation of NiNPs with an average diameter of 5.7 ± 1.9 nm (Table VII.1 Entry 1) and 3.8 ± 0.7 nm (Table VII.1 Entry 2) was observed for [Ni(acac)₂] and [Ni(COD)₂], respectively. However, when the synthesis was carried out without solvent (Ni/TPP/Pyridine = 1/1/121) (the amount of pyridine was governed by the size of the reactor used, see

Experimental Section), the resulting NiNPs had an average diameter of 2.8 ± 0.2 nm when $[\text{Ni}(\text{acac})_2]$ was used as precursor and 1.6 ± 0.7 nm with $[\text{Ni}(\text{COD})_2]$ as precursor (Table VII.1, Entries 3 and 4) (Appendix E, Figure E1). Hence, as previously observed, the $[\text{Ni}(\text{COD})_2]$ precursor led to smaller NiNPs than the $[\text{Ni}(\text{acac})_2]$ complex.

Table VII.1. Synthesis of NiNPs^a.

Entry	Precursor	Molar Ni/TPP/N ratio	Condition	NiNPs average size diameter (nm)
1	$[\text{Ni}(\text{acac})_2]$	1/1/0	Cyclohexane	5.7 ± 1.9
2	$[\text{Ni}(\text{COD})_2]$	1/1/0	Cyclohexane	3.8 ± 0.7
3	$[\text{Ni}(\text{acac})_2]$	1/1/121	Neat	2.8 ± 0.2
4	$[\text{Ni}(\text{COD})_2]$	1/1/121	Neat	1.6 ± 0.7

^aReaction Conditions: 20 bar H_2 , 110 °C, 1200 rpm, 20 h.

An additional experiment was conducted to investigate the effect of washing on the NiNP size. To achieve this, NiNPs synthesized from $[\text{Ni}(\text{COD})_2]$ under neat conditions (Table VII.1, Entry 4) were washed 4 times with cyclohexane. As a result, the washed nanoparticles displayed an important increase in the average size, yielding a mean diameter of $d_m = 4.9 \pm 1.3$ nm (Appendix E, Figure E2) against a $d_m = 1.6 \pm 0.7$ nm when no washing was performed (an increase of *ca.* 3.3 nm). This difference in size can be explained by the elimination of the stabilizing ligands that dissolved in cyclohexane during the washing treatment. Such a ligand elimination may have led to a decrease in stabilization followed by agglomeration or even coalescence of the initial nanoparticles into larger ones. After this result, no further variation of synthesis conditions was done and the retained conditions to prepare NiNPs for application in the semi-hydrogenation of alkynes were those of Entry 4 in Table VII.1, namely $[\text{Ni}(\text{COD})_2]$, neat conditions, 20 bar H_2 , 110 °C, 1200 rpm, 20 h, and no washing with cyclohexane.

VII.3. Semi-hydrogenation of 3-hexyne with NiNPs

It is important to note that in all the catalytic experiments performed, a volume of 10 mL of cyclohexane was used, as imposed by the size of the reactors. Using the NiNPs synthesized by the procedure described in Table VII.1, Entry 4 (average diameter of *ca.* 1.6 nm) as catalyst, a first series of runs for the hydrogenation of 3-hexyne (3-hexyne/Ni ratio = 33/1) were carried out with different reaction times at 60 °C, 20 bar of H₂ and a stirring rate of 1200 rpm to limit external mass transfer (Figure VI.3). A complete conversion of 3-hexyne was reached after 10 h of reaction corresponding to an average TOF of 3 h⁻¹ (*c*TOF 4.8 h⁻¹). However, an induction period of 2 h was observed from the time plot. As the NiNPs were synthesized with a large excess of stabilizing ligands (Ni/TPP/Pyridine = 1/1/121), it can be expected that the surface of the NPs would be more accessible when these ligands are displaced by the substrate to be transformed. The time needed for ligand displacement and substrate adsorption may explain the induction period that is observed from the kinetic experiment. Concerning the selectivity obtained, it was found to be quantitative for (*Z*)-hex-3-ene, whatever the reaction time. These results clearly indicate that 3-hexyne did not undergo any further hydrogenation to hexane or isomerization to (*E*)-hex-3-ene.

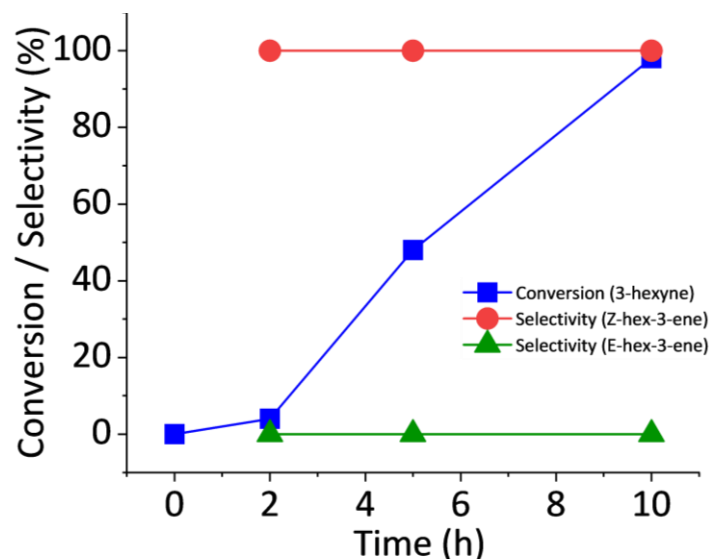


Figure VII.3. Time plot for the hydrogenation of 3-hexyne using the colloidal suspension of NiNPs synthesized in neat conditions (Ni/TPP/Pyridine = 1/1/121). Reaction conditions: 3-hexyne/Ni = 33/1, 20 bar H₂, 60 °C.

Although the selectivities toward (Z)-hex-3-ene were remarkable, the low TOF and *c*TOFs (respectively 3 and 4.8 h⁻¹) constitute a major drawback. One explanation for the slow conversion could be the dilution factor due to the addition of cyclohexane, which may have affected the reaction kinetics. To check the effect of dilution, a series of experiments was carried out by increasing the substrate/Ni ratio, namely using a 3-hexyne/Ni ratio of 100 and 200 in comparison to 33, while keeping the same catalytic conditions (20 bar H₂, 60 °C, 1200 rpm, 5 h). This provided a series of *c*TOFs of 4.8 h⁻¹, 10.5 h⁻¹ and 45 h⁻¹ with 3-hexyne/Ni ratios of 33, 100 and 200, respectively, with a total selectivity towards (Z)-alkene in all reactions. Thus, whereas not changing the selectivity of the reaction, the increase of the 3-hexyne/Ni ratio allowed to reach better conversions, thus confirming the role of the substrate in the performance of the NiNPs. A higher substrate concentration may favor the displacement of the stabilizing ligands (pyridine and TPP) from the metal surface, thus increasing the NP surface reactivity for the hydrogenation of the 3-hexyne.

Regarding the total selectivity observed for the semi-hydrogenation of 3-hexyne to (Z)-hex-3-ene, a control experiment was performed using the latter compound as substrate under the same catalytic conditions (20 bar H₂, 60 °C, 1200 rpm, 22 h,

substrate/Ni = 33). Remarkably, no conversion to the corresponding alkane was observed, thus confirming the total selectivity of the catalyst for the semi-hydrogenation of 3-hexyne into (Z)-hex-3-ene only. This performance can be corroborated by the inability of (Z)-hex-3-ene, which is less nucleophilic than 3-hexyne, to interact with the NiNPs surface, which likely also explains why the consecutive reduction of (Z)-hex-3-ene did not occur (Appendix E, Figure E3).

VI.4. One-pot synthesis of NiNP-TPPO@CCM-A latex

Following a one-step process, NiNPs could be synthesized within a stable TPPO@CCM-A latex. The synthesis process consisted of heating a biphasic mixture of an aqueous TPPO@CCM-A latex and a toluene solution of $[\text{Ni}(\text{COD})_2]$ under H_2 pressure (20 bar) for 20 h, without adding an auxiliary stabilizing agent or base additive, in accordance to Chapters IV and VI. It is important to clarify that, unlike what was mentioned earlier when $[\text{Ni}(\text{acac})_2]$ was used for further research because it is soluble in toluene and water, we opted for the $[\text{Ni}(\text{COD})_2]$ as NiNP precursor. This choice was driven by two main reasons. First, a desire to minimize the release of potential stabilizing molecules for the particles (namely acacH). Second, as demonstrated in previous research with the one-pot synthesis of RhNP-TPPO@CCM-C and RhNP-TPPO@CCM-A, it is possible to generate metal nanoparticles without the need for an additional step, namely, the transfer to the core then the reduction of the metal precursor. After stopping the stirring of the reaction mixture, it spontaneously phase-separated into a black latex and a colorless, transparent toluene phase. This result suggested that the confinement of the NiNPs in the TPPO@CCM-A core was successful, which was confirmed by the TEM analysis (Figure VII.4). Indeed, TEM images revealed the presence of small-sized NiNPs ($d_m = 2.8 \pm 0.3$ nm) with a narrow size distribution inside the polymer matrix.

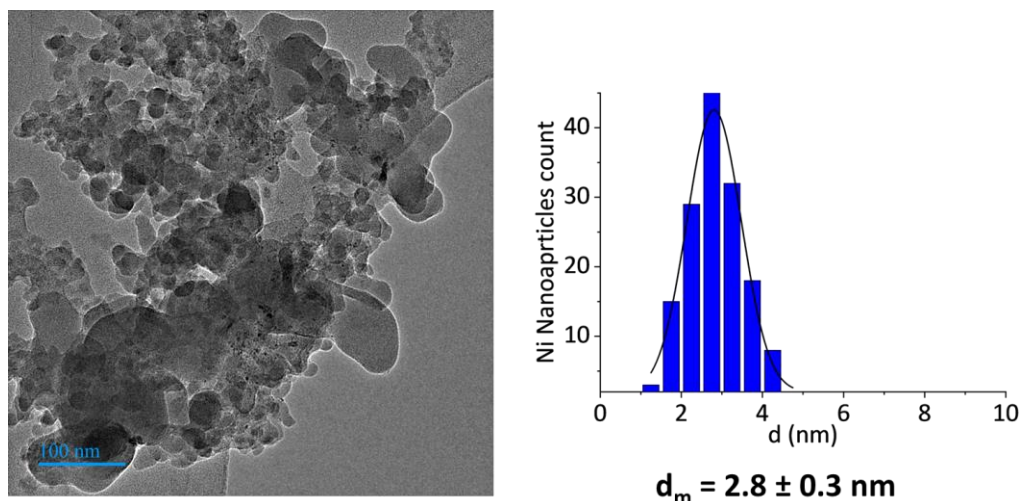


Figure VII.4. TEM images of the one-pot-synthesized NiNP-TPPO@CCM-A and the corresponding size distribution of NiNPs ($d_m = 2.8 \pm 0.3$ nm).

The small size and narrow size distribution of the NiNPs formed from the base-free one-pot procedure may result from a more efficient stabilization in the polymer, due to the combined interaction with the oxygen lone pairs of TPPO and the π -electrons of the phenyl groups in the styrene monomers [21]. Even though a confinement effect may also improve the nucleation rate, leading to a greater number of NPs and a consequent decrease in their average size, it is more likely that the nucleation occurred within the CCM-A. Note that such confinement in the polymer cores was already reached in the case of RhNPs (see previous Chapters IV and VI and studies [22–30]). Unfortunately, during the IFPEN secondment, it was not possible to test the catalytic performance of the NiNP-TPPO@CCM-A latex for the hydrogenation of 3-hexyne in comparison to ligand-stabilized NiNPs.

VII.5. Summary and Outlook

This chapter has outlined the synthesis of NiNPs with different stabilizers (TOP, oleylamine, TPP, pyridine and TPPO@CCM-A) and has explored how these ligands may influence the size and size dispersion of the obtained nanoparticles. The NiNPs stabilized using TPP and pyridine were evaluated as catalysts for the hydrogenation of 3-hexyne. While the NPs exhibited low performance in terms of c TOFs, the system

exhibited a total selectivity for the thermodynamically less stable (Z)-hex-3-ene in the semi-hydrogenation of 3-hexyne.

Furthermore, a one-pot synthesis has allowed the preparation of a NiNP-TPPO@CCM-A latex, following a previously optimized procedure for RhNPs, that has the advantage of not requiring additional stabilizers. The reported preliminary results highlight the potential of this newly developed one-pot synthesis approach to generate MNPs in the cores of polymeric micelles. Also, a variety of metal complexes may be utilized to tailor the application of diverse metal-containing CCM-A nanoreactors in catalysis. This could help to overcome a previously observed challenge involving the interaction between complexes and the polyanionic shell of CCMs.

Overall, the results presented in this chapter are encouraging, considering that the performance and specificity of the supported Ni catalysts are significantly affected by various factors [31,32]. These factors include the quantity of Ni metal loaded [33], the size of the dispersed Ni metal particles [21,34], the interactions between the metal and the CCM polymer, as well as the composition of the CCM [35–38]. It is crucial to comprehend the role of all these elements to tailor the synthesis of encapsulated NiNPs using CCMs to fine-tune the reactivity, activity, and selectivity of these nanoreactors. In addition to that, this study has paved the way for new perspectives in the catalytic application of CCM-A nanoreactors, and an evaluation of the catalytic performance of the NiNP-TPPO@CCM-A latex for the hydrogenation of 3-hexyne, in comparison to ligand-stabilized NiNPs, would certainly be warranted. In future work, the extension of the synthesis protocol to the formation of CCM-C nanoreactors with other *d*-block metals could further expand the scope of the work.

VII.6. References

[1] S. Carencó, A. Leyva-Pérez, P. Concepción, C. Boissire, N. Mézailles, C. Sanchez, A. Corma, Nickel phosphide nanocatalysts for the chemoselective

hydrogenation of alkynes, *Nano Today*. 7 (2012) 21–28. <https://doi.org/10.1016/j.nantod.2011.12.003>

[2] B.A. Wilhite, M.J. McCreedy, A. Varma, Kinetics of phenylacetylene hydrogenation over Pt/ γ -Al₂O₃ catalyst, *Ind Eng Chem Res*. 41 (2002) 3345–3350. <https://doi.org/10.1021/ie0201112>

[3] M. Crespo-Quesada, F. Cárdenas-Lizana, A.L. Dessimoz, L. Kiwi-Minsker, Modern trends in catalyst and process design for alkyne hydrogenations, *ACS Catal*. 2 (2012) 1773–1786. <https://doi.org/10.1021/cs300284r>

[4] M. García-Mota, J. Gómez-Díaz, G. Novell-Leruth, C. Vargas-Fuentes, L. Bellarosa, B. Bridier, J. Pérez-Ramírez, N. López, A density functional theory study of the “mythic” Lindlar hydrogenation catalyst, *Theor Chem Acc*. 128 (2011) 663–673. <https://doi.org/10.1007/s00214-010-0800-0>

[5] M. Crespo-Quesada, A. Yarulin, M. Jin, Y. Xia, L. Kiwi-Minsker, Structure sensitivity of alkynol hydrogenation on shape- and size-controlled palladium nanocrystals: Which sites are most active and selective?, *J Am Chem Soc*. 133 (2011) 12787–12794. <https://doi.org/10.1021/ja204557m>

[6] D.R. Kennedy, G. Webb, S.D. Jackson, D. Lennon, Propyne hydrogenation over alumina-supported palladium and platinum catalysts, *Appl Catal A Gen*. 259 (2004) 109–120. <https://doi.org/10.1016/j.apcata.2003.09.018>

[7] J. Stachurski, J.M. Thomas, Structural aspects of the Lindlar catalyst for selective hydrogenation. *Catal. Lett*. 1 (1988) 67–72 <https://doi.org/10.1007/BF00765356>

[8] C. Oger, L. Balas, T. Durand, J.M. Galano, Are alkyne reductions chemo-, regio-, and stereoselective enough to provide pure (Z)-olefins in polyfunctionalized bioactive molecules?, *Chem Rev*. 113 (2013) 1313–1350. <https://doi.org/10.1021/cr3001753>

[9] A. Jung, A. Jess, T. Schubert, W. Schütz, Performance of carbon nanomaterial (nanotubes and nanofibres) supported platinum and palladium catalysts for the hydrogenation of cinnamaldehyde and of 1-octyne, *Appl Catal A Gen*. 362 (2009) 95–105. <https://doi.org/10.1016/j.apcata.2009.04.026>

[10] A.M. López-Vinasco, L.M. Martínez-Prieto, J.M. Asensio, P. Lecante, B. Chaudret, J. Cámpora, P.W.N.M. Van Leeuwen, Novel nickel nanoparticles stabilized by imidazolium-amidinate ligands for selective hydrogenation of alkynes, *Catal Sci Technol*. 10 (2020) 342–350. <https://doi.org/10.1039/c9cy02172h>

[11] D. Bouzouita, J.M. Asensio, V. Pfeifer, A. Palazzolo, P. Lecante, G. Pieters, S. Feuillastre, S. Tricard, B. Chaudret, Chemoselective H/D exchange catalyzed by nickel

nanoparticles stabilized by N-heterocyclic carbene ligands, *Nanoscale*. 12 (2020) 15736–15742. <https://doi.org/10.1039/d0nr04384b>

[12] A. Reina, I. Favier, C. Pradel, M. Gómez, Stable Zero-Valent Nickel Nanoparticles in Glycerol: Synthesis and Applications in Selective Hydrogenations, *Adv Synth Catal*. 360 (2018) 3544–3552. <https://doi.org/10.1002/adsc.201800786>

[13] F. Alonso, P. Riente, M. Yus, Alcohols for the α -alkylation of methyl ketones and indirect aza-Wittig reaction promoted by nickel nanoparticles, *Eur J Org Chem*. (2008) 4908–4914. <https://doi.org/10.1002/ejoc.200800729>

[14] H. Konnerth, M.H.G. Prechtel, Selective partial hydrogenation of alkynes to (Z)-alkenes with ionic liquid-doped nickel nanocatalysts at near ambient conditions, *Chem Com* 52 (2016) 9129–9132. <https://doi.org/10.1039/c6cc00499g>

[15] L. Zaramello, B.L. Albuquerque, J.B. Domingos, K. Philippot, Kinetic investigation into the chemoselective hydrogenation of α,β -unsaturated carbonyl compounds catalyzed by Ni(0) nanoparticles, *Dalton Trans*. 46 (2017) 5082–5090. <https://doi.org/10.1039/c7dt00649g>

[16] L. Wu, A. Mendoza-Garcia, Q. Li, S. Sun, Organic Phase Syntheses of Magnetic Nanoparticles and Their Applications, *Chem Rev*. 116 (2016) 10473–10512. <https://doi.org/10.1021/acs.chemrev.5b00687>

[17] L.M. Rossi, N.J.S. Costa, F.P. Silva, R. Wojcieszak, Magnetic nanomaterials in catalysis: Advanced catalysts for magnetic separation and beyond, *Green Chem*. 16 (2014) 2906–2933. <https://doi.org/10.1039/c4gc00164h>

[18] S. Carencio, C. Boissière, L. Nicole, C. Sanchez, P. Le Floch, N. Mézailles, Controlled design of Size-tunable monodisperse nickel nanoparticles, *Chem Mat*. 22 (2010) 1340–1349. <https://doi.org/10.1021/cm902007g>

[19] N.T.K. Thanh, N. Maclean, S. Mahiddine, Mechanisms of nucleation and growth of nanoparticles in solution, *Chem Rev*. 114 (2014) 7610–7630. <https://doi.org/10.1021/cr400544s>

[20] P. Rein ten Wolde, D. Frenkel, Homogeneous nucleation and the Ostwald step rule, *Phys. Chem. Chem. Phys.*, 1999,1, 2191–2196 <https://doi.org/10.1039/A809346F>.

[21] W.L. Vrijburg, J.W.A. Van Helden, A.J.F. Van Hoof, H. Friedrich, E. Groeneveld, E.A. Pidko, E.J.M. Hensen, Tunable colloidal Ni nanoparticles confined and redistributed in mesoporous silica for CO₂ methanation, *Catal Sci Technol*. 9 (2019) 2578–2591. <https://doi.org/10.1039/c9cy00532c>

- [22] M. A. Gelesky, S. S. X. Chiaro, F. A. Pavan, J. H. Z. dos Santos, J. Dupont, Supported ionic liquid phase rhodium nanoparticle hydrogenation catalysts, *Dalton Trans.* (2007) 5549–5553 <https://doi.org/10.1039/B708111A>
- [23] L.M. Rossi, L.L.R. Vono, M.A.S. Garcia, T.L.T. Faria, J.A. Lopez-Sanchez, Screening of soluble rhodium nanoparticles as precursor for highly active hydrogenation catalysts: The effect of the stabilizing agents, *Top Catal.* 56 (2013) 1228–1238. <https://doi.org/10.1007/s11244-013-0089-z>
- [24] C. Chaudhari, H. Imatome, Y. Nishida, K. Sato, K. Nagaoka, Recyclable Rh-PVP nanoparticles catalyzed hydrogenation of benzoic acid derivatives and quinolines under solvent-free conditions, *Catal Commun.* 126 (2019) 55–60. <https://doi.org/10.1016/j.catcom.2019.02.019>
- [25] F. Martinez-Espinar, P. Blondeau, P. Nolis, B. Chaudret, C. Claver, S. Castellón, C. Godard, NHC-stabilised Rh nanoparticles: Surface study and application in the catalytic hydrogenation of aromatic substrates, *J Catal.* 354 (2017) 113–127. <https://doi.org/10.1016/j.jcat.2017.08.010>
- [26] M. Ibrahim, M.A.S. Garcia, L.L.R. Vono, M. Guerrero, P. Lecante, L.M. Rossi, K. Philippot, Polymer: Versus phosphine stabilized Rh nanoparticles as components of supported catalysts: Implication in the hydrogenation of cyclohexene model molecule, *Dalton Trans.* 45 (2016) 17782–17791. <https://doi.org/10.1039/c6dt03104h>
- [27] G. Vitulli, C. Evangelisti, P. Pertici, A.M. Caporusso, N. Panziera, P. Salvadori, M.G. Faga, C. Manfredotti, G. Martra, S. Coluccia, A. Balerna, S. Colonna, S. Mobilio, Supported rhodium nanoparticles in catalysis: The role of stabilizers on catalytic activity and structural features, *J Organomet Chem.* 681 (2003) 37–50. [https://doi.org/10.1016/S0022-328X\(03\)00529-1](https://doi.org/10.1016/S0022-328X(03)00529-1)
- [28] H. Bin Pan, C.M. Wai, One-step synthesis of size-tunable rhodium nanoparticles on carbon nanotubes: A study of particle size effect on hydrogenation of xylene, *J Phys Chem C.* 114 (2010) 11364–11369. <https://doi.org/10.1021/jp101368p>
- [29] T.T. Nguyen, P. Serp, Confinement of metal nanoparticles in carbon nanotubes, *ChemCatChem.* 5 (2013) 3595–3603. <https://doi.org/10.1002/cctc.201300527>
- [30] S.A. Stratton, K.L. Luska, A. Moores, Rhodium nanoparticles stabilized with phosphine functionalized imidazolium ionic liquids as recyclable arene hydrogenation catalysts, *Catal Today.* 183 (2012) 96–100. <https://doi.org/10.1016/j.cattod.2011.09.016>
- [31] R.A. Van Santen, Complementary structure sensitive and insensitive catalytic relationships, *Acc Chem Res.* 42 (2009) 57–66. <https://doi.org/10.1021/ar800022m>

- [32] C. Vogt, E. Groeneveld, G. Kamsma, M. Nachtegaal, L. Lu, C.J. Kiely, P.H. Berben, F. Meirer, B.M. Weckhuysen, Unravelling structure sensitivity in CO₂ hydrogenation over nickel, *Nat Catal.* 1 (2018) 127–134. <https://doi.org/10.1038/s41929-017-0016-y>
- [33] S. Hwang, J. Lee, U.G. Hong, J.G. Seo, J.C. Jung, D.J. Koh, H. Lim, C. Byun, I.K. Song, Methane production from carbon monoxide and hydrogen over nickel-alumina xerogel catalyst: Effect of nickel content, *Jof Indus and Eng Chem.* 17 (2011) 154–157. <https://doi.org/10.1016/j.jiec.2010.12.015>
- [34] P. Munnik, M.E.Z. Velthoen, P.E. de Jongh, K.P. de Jong, C.J. Gommers, Nanoparticle Growth in Supported Nickel Catalysts during Methanation Reaction- Larger is Better, *Angew Chem.* 126 (2014) 9647–9651. <https://doi.org/10.1002/ange.201404103>
- [35] M.A. Vannice, R.L. Garten, Metal-support effects on the activity and selectivity of Ni catalysts in COH₂ synthesis reactions, *J. of Catalysis* 56(2) (1979) 236–248, [https://doi.org/10.1016/0021-9517\(79\)90110-6](https://doi.org/10.1016/0021-9517(79)90110-6)
- [36] J. Gao, Q. Liu, F. Gu, B. Liu, Z. Zhong, F. Su, Recent advances in methanation catalysts for the production of synthetic natural gas, *RSC Adv.* 5 (2015) 22759–22776. <https://doi.org/10.1039/c4ra16114a>
- [37] L. He, Q. Lin, Y. Liu, Y. Huang, Unique catalysis of Ni-Al hydrotalcite derived catalyst in CO₂ methanation: Cooperative effect between Ni nanoparticles and a basic support, *J of En Chem* 23 (2014) 587–592. [https://doi.org/10.1016/S2095-4956\(14\)60144-3](https://doi.org/10.1016/S2095-4956(14)60144-3)
- [38] N. Yao, H. Ma, Y. Shao, C. Yuan, D. Lv, X. Li, Effect of cation-oligomer interactions on the size and reducibility of NiO particles on NiRu/SiO₂ catalysts, *J Mater Chem.* 21 (2011) 17403–17412. <https://doi.org/10.1039/c1jm13029c>

Chapter VIII: Conclusions and Perspectives

The aim of this PhD project was to develop new methods for efficient confinement of metal nanoparticles (MNPs) in polymeric core-crosslinked micelle (CCM) nanoreactors, with both cationic and anionic shells, for application of the resulting MNP@CCMs latexes in aqueous biphasic hydrogenation. To this end, novel core-crosslinked micelles functionalized with triphenylphosphine oxide and a polycationic shell were developed by extension of a previously optimized RAFT polymerization approach.

The first attempt to produce RhNP-TPPO@CCM-C consisted in loading the TPPO@CCM-C micelles with $[\text{Rh}(\text{COD})(\mu\text{-Cl})_2]$, in order to generate a core-anchored $[\text{RhCl}(\text{COD})(\text{TPPO@CCM-C})]$ complex that could be reduced to RhNPs by H_2 , following the same procedure as previously developed to get RhNPs embedded in TPP@CCM-C. This proved unsuccessful, indicating that the formation of a Rh^{I} -TPPO@CCM-C complex by cleavage of the di- $\mu\text{-Cl}$ -bridge moiety in $[\text{Rh}(\text{COD})(\mu\text{-Cl})_2]$ was not favorable in the polymer core under the applied conditions. Given that, an alternative strategy involving *ex-situ* synthesis of RhNPs using TPP and pyridine as stabilizers, affording ultrasmall RhNPs, and their subsequent transfer to the TPPO@CCM-C nanoreactors was envisaged. This strategy allowed the successful transfer of the RhNPs to the TPPO-functionalized cores. Although the resulting RhNP-TPPO@CCM-C latex proved effective in the aqueous biphasic hydrogenation of styrene, with only 2% of catalyst leaching, a gradual extraction of the TPP and pyridine ligands used for the *ex-situ* RhNPs synthesis during the work-up between recycles, induced a steady decrease of the catalytic activity. Nevertheless, a stable catalyst phase was obtained after preliminary extensive washing and an initial reaction run, yielding a TOF of $\sim 1025 \text{ h}^{-1}$ (*c*TOF $\sim 1440 \text{ h}^{-1}$), over several recycles.

To improve the system, a new approach has been developed consisting of a one-pot synthesis of RhNP-TPPO@CCM-C catalyst, which does not require the use of

additional stabilizers. The produced RhNPs were smaller in size (1.7 ± 0.2 nm) than their analogs synthesized under similar conditions in the presence of only TPPO as stabilizer (2.4 ± 0.2 nm). This difference underlines the positive confinement effect on the RhNPs size, which leads to smaller NPs. The new catalyst demonstrated very good catalytic activity (c TOFs of 4500-16000 h^{-1}) and full selectivity in the hydrogenation of neat styrene to ethylbenzene under mild conditions (20 bar H_2 , 25-55 $^\circ\text{C}$). The catalyst was also applicable for the hydrogenation of other unsaturated substrates under similar reaction conditions, including alkynes and carbonyl compounds, making the RhNP-TPPO@CCM-C latex highly attractive for aqueous biphasic catalysis including catalyst recycling. The overall obtained catalytic results with RhNP-TPPO@CCM-C showed that the nature of the core-functional ligands of the polymer micelles is a key parameter to improving the stability and the recycling of the catalytic latex.

Inspired by the effectiveness of the RhNPs synthesis in the presence of pyridine and TPP, polymerizable analogs of these stabilizers (vinylpyridine or VP and styryldiphenylphosphine or SDPP) were hereafter used to prepare a modified CCM-C, where both stabilizers were covalently bound to the core leading to well-dispersed CCMs with a narrow size distribution. The use of the mentioned combination of ligands proved efficient in the generation of nanoreactors with a core-anchored molecular catalyst, Rh^I-VP-SDPP@CCM-C, which demonstrated good catalytic activity in the hydrogenation of 1-octene. However, this Rh^I-VP-TPP@CCM-C latex could not be used as a precursor for the generation of core-anchored RhNPs under the operating conditions that have been so far been explored. Therefore, further investigations on the generation of RhNPs in the core of the developed VP-SDPP@CCM-C, and other *d*-block metals are envisaged as future work. In addition, the synthesis of new CCMs with VP and SDPP oxide ligands bonded within the core could be targeted as a new generation of nanoreactors for the confinement of RhNPs, as TPPO proved very efficient in overcoming the problem of RhNPs extraction by diethyl ether upon catalyst recycling.

On the other hand, previously developed CCMs with a polyanionic shell (CCM-A) and TPP ligands have proven synthetically less demanding, as the formation of this polymer system required fewer synthetic steps compared to its cationic counterparts thus making it easier to prepare than the previous CCM generations. However, when the CCM-A were used as nanoreactors for Rh^I catalyst confinement, an unexpected complication at the catalyst loading stage was encountered owing to a possible interaction of the polyanionic shell with the Rh precursor, which prevented effective catalyst loading. Since TPPO proved efficient in anchoring RhNPs and resisted diethyl ether extraction (*vide supra*), novel CCM-A with TPPO-functionalization has been developed by RAFT polymerization. Subsequently, nano-sized and well-dispersed RhNPs were synthesized by an *ex-situ* protocol using the previously optimized method and introduced successfully into the TPPO@CCM-A. Additionally, a one-pot synthesis approach was also found to yield a RhNPs-TPPO@CCM-A latex by reducing [Rh(COD)(μ -Cl)]₂/toluene without the need for auxiliary stabilizers or bases. This catalyst proved efficient and recyclable in the aqueous biphasic hydrogenation of both styrene and acetophenone, with total selectivity towards ethylbenzene and phenylethanol, respectively, but lower activity compared to its CCM-C counterparts primarily due to significant internal mass transfer limitations. To mitigate these limitations various strategies may be employed, including increasing the Rh loading to enhance the availability of active sites, thus improving reaction rates and overall reactor performance. The complete selectivity towards EB with both the RhNP-TPPO@CCM-A and the analogous RhNP-TPPO@CCM-C denotes selectivity to be apparently independent of both the sizes of the embedded RhNPs (within the size range 1.7 - 3.1 nm) as well as the composition of the outer CCM shells and CCM sizes. It will be important to scrutinize the impact of the RhNPs surface coverage by ligand in forthcoming investigations.

During this PhD project, an industrial secondment was also performed at IFPEN (*Institut Français du Pétrole, Energies Nouvelles*) in Solaize, France. To this end, the use of NiNPs confined in CCMs was considered for the selective hydrogenation of

alkynes. This project was based on the interest of Ni to decrease the use of noble metals and the cost of the catalyst for industrial applications, in combination with the advantages of biphasic catalysis conditions as offered by the CCMs systems. Preliminary results outlined the feasibility of the synthesis of NiNPs with different stabilizers, and how these ligands may influence the size and dispersion of the obtained NPs. The NiNPs stabilized using TPP and pyridine were evaluated as catalysts for the hydrogenation of 3-hexyne. While the NPs exhibited low performance in terms of catalytic activity, the system exhibited a total selectivity for the thermodynamically less stable (Z)-hex-3-ene in the semi-hydrogenation of 3-hexyne. Furthermore, a one-pot synthesis allowed the preparation of a NiNP-TPPO@CCM-A latex, following the previously optimized procedure for RhNPs, which has the advantage of not requiring additional stabilizers. The reported results highlight the potential of this newly developed one-pot synthesis approach to generate MNPs in the cores of polymeric micelles. In future work, the NiNPs core anchoring will be extended to other synthesized CCMs, namely VP-SDPP@CCM-C and TPPO@CCM-C, and the resulting catalysts will be used in aqueous biphasic hydrogenation with an aim to compare the effect of the CCMs on both the activity and selectivity towards alkynes and α,β -unsaturated compounds. Application of similar strategies to develop new systems with other *d*-block metals could further expand the scope of the work.

Appendix A for Chapter II

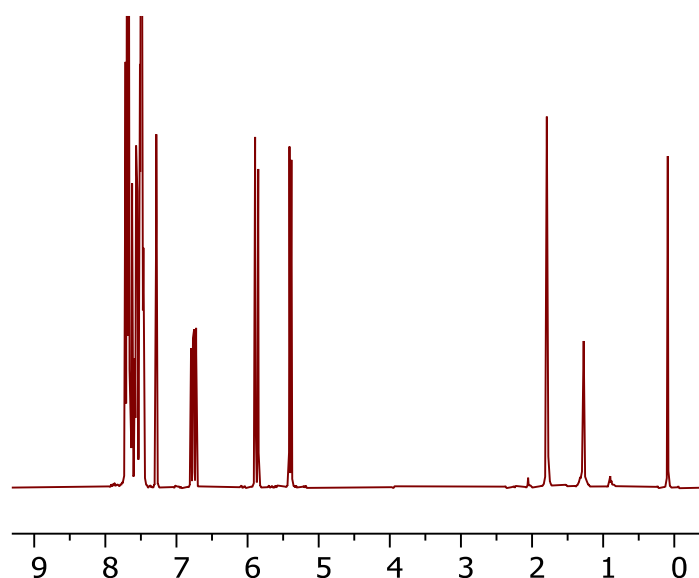


Figure A1. ¹H NMR of SDPPO δ/ppm (CDCl₃): 7.73-7.62 (m, 6H, Ph); 7.60-7.52 (m, 2H, Ph); 7.52-7.45 (m, 6H, Ph); 6.76 (dd, $J_{\text{HH}} = 17.6$ Hz, $J_{\text{HH}} = 10.9$ Hz, 1H, $\underline{\text{C}}\text{H}$ vinyl); 5.87 (d, $J_{\text{HH}} = 17.6$ Hz, 1H, $\underline{\text{C}}\text{H}$ vinyl); 5.40 (d, $J_{\text{HH}} = 10.9$ Hz, 1H, $\underline{\text{C}}\text{H}$ vinyl).

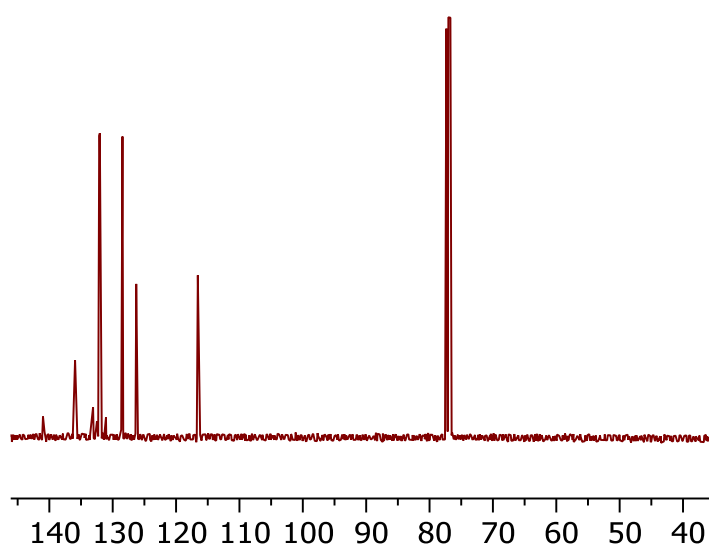


Figure A2. ¹³C{¹H} NMR of SDPPO δ/ppm (CDCl₃): 141.01 (d, $J_{\text{CP}}=2.9$ Hz , quat Ph $\underline{\text{C}}$ -vinyl); 135.93 (d, $J_{\text{CP}}= 1.7$ Hz, CH vinyl); 132.58 (d, $J_{\text{CP}}=104$ Hz , quat Ph); 132.41 (d, $J_{\text{CP}}=10.2$ Hz, CH Ph); 132.08 (d, $J_{\text{CP}}= 9.9$ Hz, CH Ph); 131.95 (d, $J_{\text{CP}}= 2.8$ Hz, CH Ph); 131.57 (d, $J_{\text{CP}}= 101$ Hz,

quaternaryPh); 128.52 (d, $J_{CP}=12.1\text{Hz}$, CH Ph); 128.22 (d, $J_{CP}=12.4\text{Hz}$, CH Ph); 116.57 (s, CH_2 vinyl).

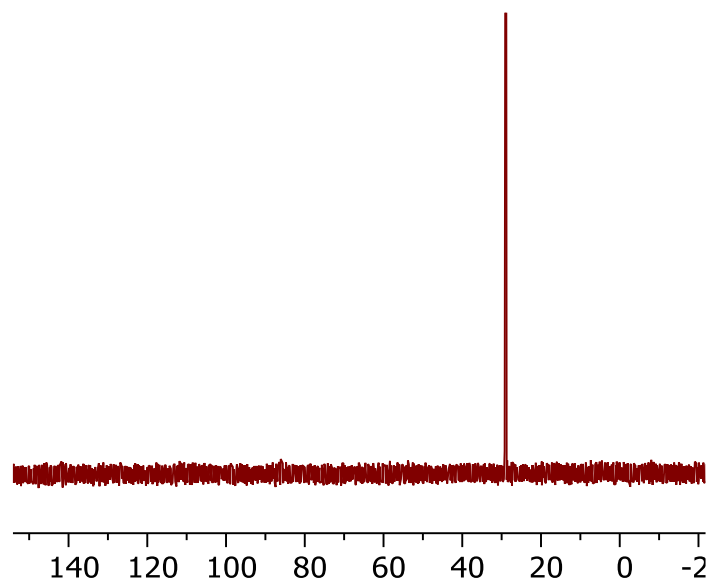


Figure A3. $^{31}\text{P}\{^1\text{H}\}$ NMR of SDPPO δ/ppm (CDCl_3): 28.91.

Elemental Composition Report

Page 1

Single Mass Analysis

Tolerance = 1.4 mDa / DBE: min = -1.5, max = 80.0

Element prediction: Off

Monoisotopic Mass, Odd and Even Electron Ions

47 formula(e) evaluated with 1 results within limits (all results (up to 1000) for each mass)

Elements Used:

C: 0-100 H: 0-100 O: 0-5 P: 0-1

DCI-CH4

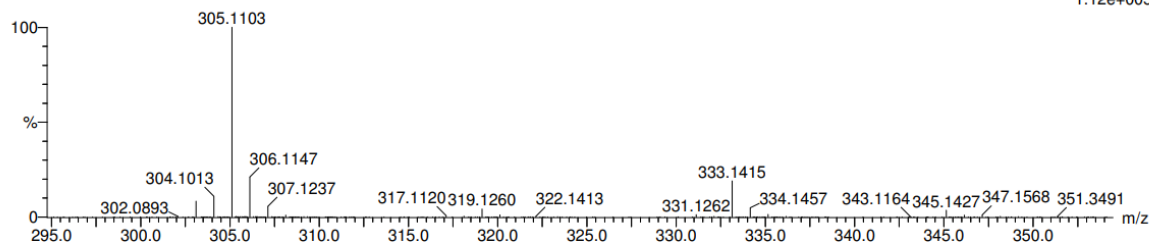
20210623-CAF-DPPSO 63 (1.050) Cm (63:68-143:148x5.000)

GCT Premier CAB109

23-Jun-202110:34:17

TOF MS Cl+

1.12e+005



Minimum: -1.5
Maximum: 1.4 10.0 80.0

Mass	Calc. Mass	mDa	PPM	DBE	i-FIT	Formula
305.1103	305.1095	0.8	2.6	12.5	919.2	C20 H18 O P

Figure A4. HR-MS analysis of SDPPO (calculated monoisotopic mass for SDPPO+H⁺ (C₂₀H₁₈PO): 305.1095).

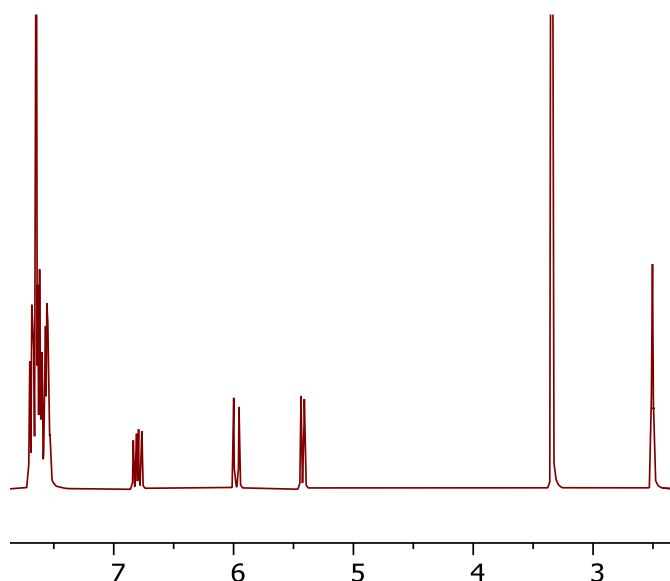


Figure A5. ¹H NMR of SDPPS δ/ppm (CDCl₃): 7.73-7.62 (m, 6H, Ph); 7.60-7.52 (m, 2H, Ph); 7.52-7.45 (m, 6H, Ph); 4.49 (m, 1H, subst. Cp); 6.76 (dd, J_{HH}= 17.6Hz, J_{HH}= 10.9Hz, 1H, CH₂ vinyl); 5.85 (d, J_{HH}= 17.6Hz, 1H, CH vinyl) 5.40 (d, J_{HH}= 10.9Hz, 1H, CH vinyl)

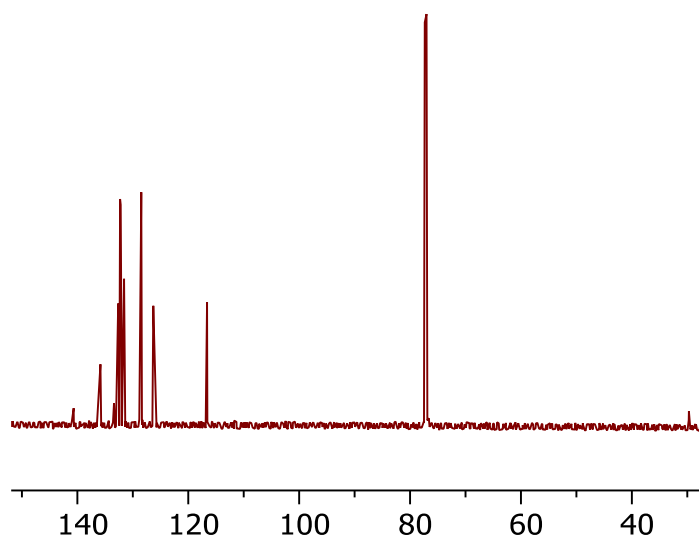


Figure A6. ¹³C{¹H} NMR of SDPPS δ/ppm (CDCl₃): 141.01 (d, J_{CP}=2.9Hz, quat? Ph C-vinyl); 135.93 (d, J_{CP}=1.7Hz, CH vinyl); 132.58 (d, J_{CP}=104Hz, quat Ph); 132.41 (d, J_{CP}=10.2Hz, CH Ph); 132.08 (d, J_{CP}=9.9Hz, CH Ph); 131.95 (d, J_{CP}=2.8Hz, CH Ph); 131.57 (d, J_{CP}=101Hz, quat Ph); 128.52 (d, J_{CP}=12.1Hz, CH Ph); 128.22 (d, J_{CP}=12.4Hz, CH Ph); 116.57 (s, CH₂ vinyl)

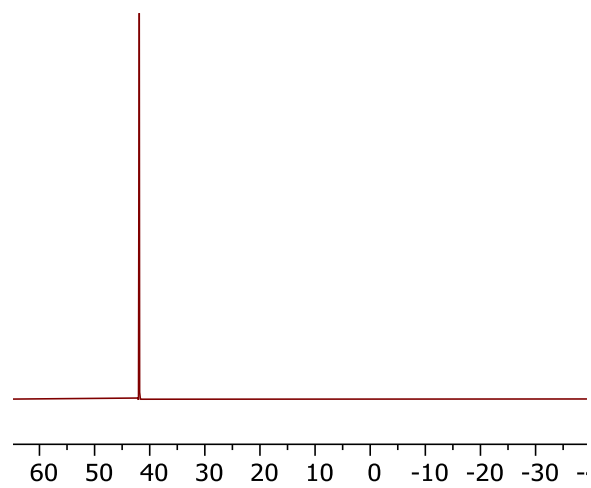


Figure A7. $^{31}\text{P}\{^1\text{H}\}$ NMR of SDPPS δ/ppm (CDCl_3): 42.9

Appendix B for Chapter III

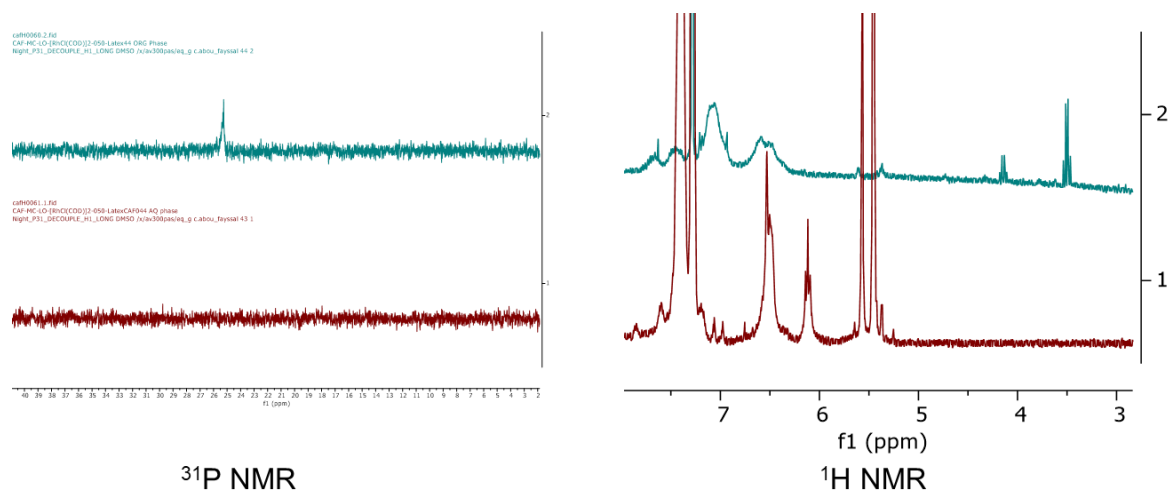


Figure B1. ^1H NMR (CDCl_3) (right) of the organic brown phase after loading $[\text{Rh}(\text{COD})(\mu\text{-Cl})_2]$ to TPPS@CCM-C, showing a quadruplet at 3.9 ppm and a triplet at 5.3 ppm (blue) and of $[\text{Rh}(\text{COD})(\mu\text{-Cl})_2]$ reference (red). ^{31}P NMR (left) of the aqueous phase (red), organic phase (blue) $\delta = 25$ ppm corresponding to the $[\text{RhCl}(\text{COD})(\text{TPPS})]$ complex.

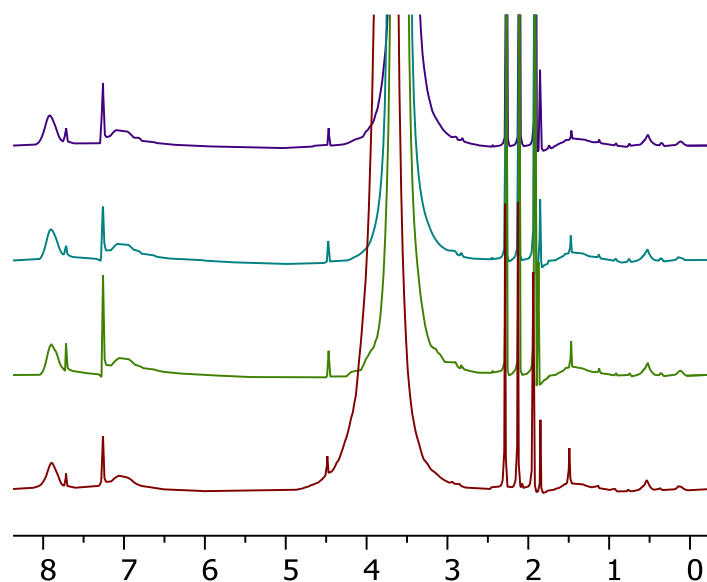


Figure B2. ^1H spectra ($\text{DMSO-}d_6$) of TPPO@CCM right after synthesis (red), after 1 week (green), after 2 weeks (blue) and after 5 months (purple).

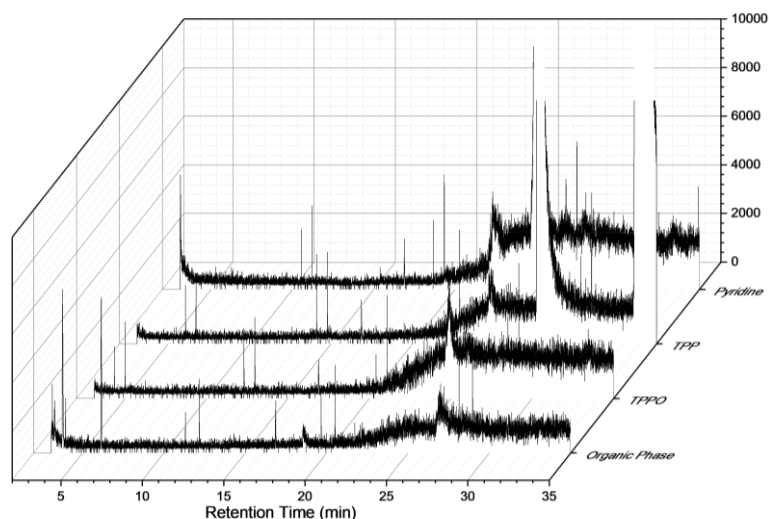


Figure B3. GC-MS of the organic phase extracted prior to the aqueous biphasic hydrogenation of styrene using diethyl ether as solvent indicating the presence of TPP (m/z 253) and tetrahydropyridine (m/z 83).

Table B1. Comparison of TOF and cTOFs of the washed latex prior to catalysis (Figure III.19) and the untreated latex (Figure III.16), both after the 5th Run, indicating that the diethyl ether washings performed between the consecutive catalytic runs (Figure III.16) have a similar effect to those carried out on the fresh RhNP-TPPO@CCM-C prior to its implementation in catalysis (Figure III.19)

Entry	TOF (h ⁻¹)	RhNPs average size (nm)	cTOF ^a (h ⁻¹)
Figure III.19 – fifth run	1025	1.8 ± 0.1 nm	1440
Figure III.16 – fifth run	1300	1.5 ± 0.4 nm	1700

^a Based on the mean diameter of RhNPs measured after the transfer of RhNPs to the CCM-C. ^b Based on the mean diameter of RhNPs measured after the first catalytic run.

Appendix C for Chapter IV

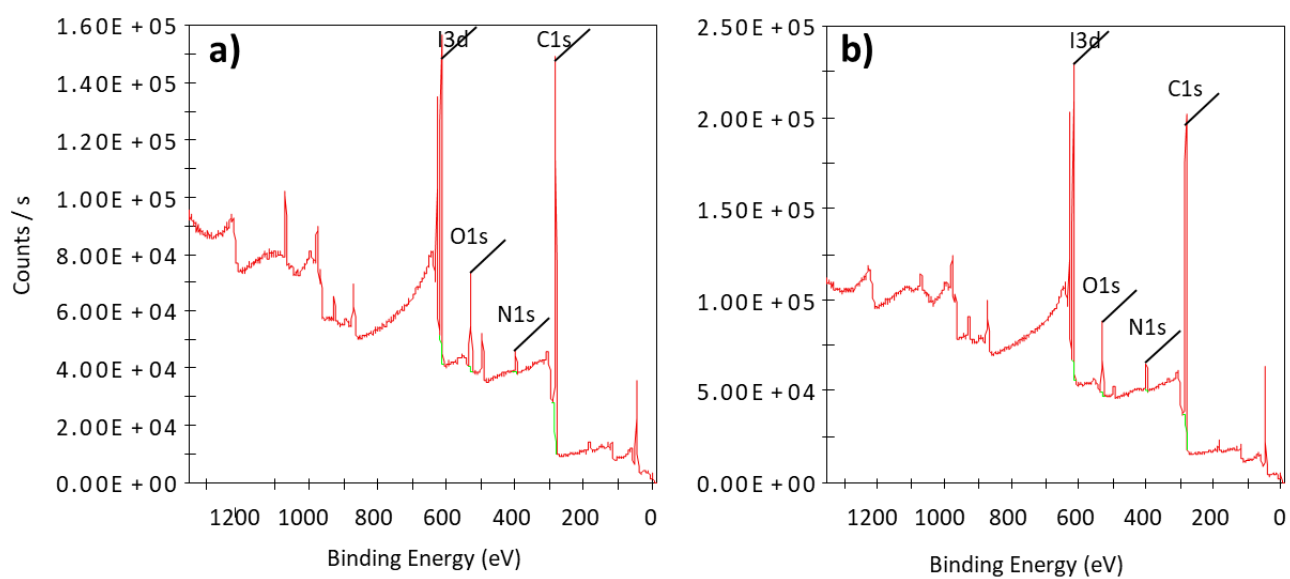


Figure C1. XPS survey spectra of a) TPPO@CCM-C and b) RhNP-TPPO@CCM-C.

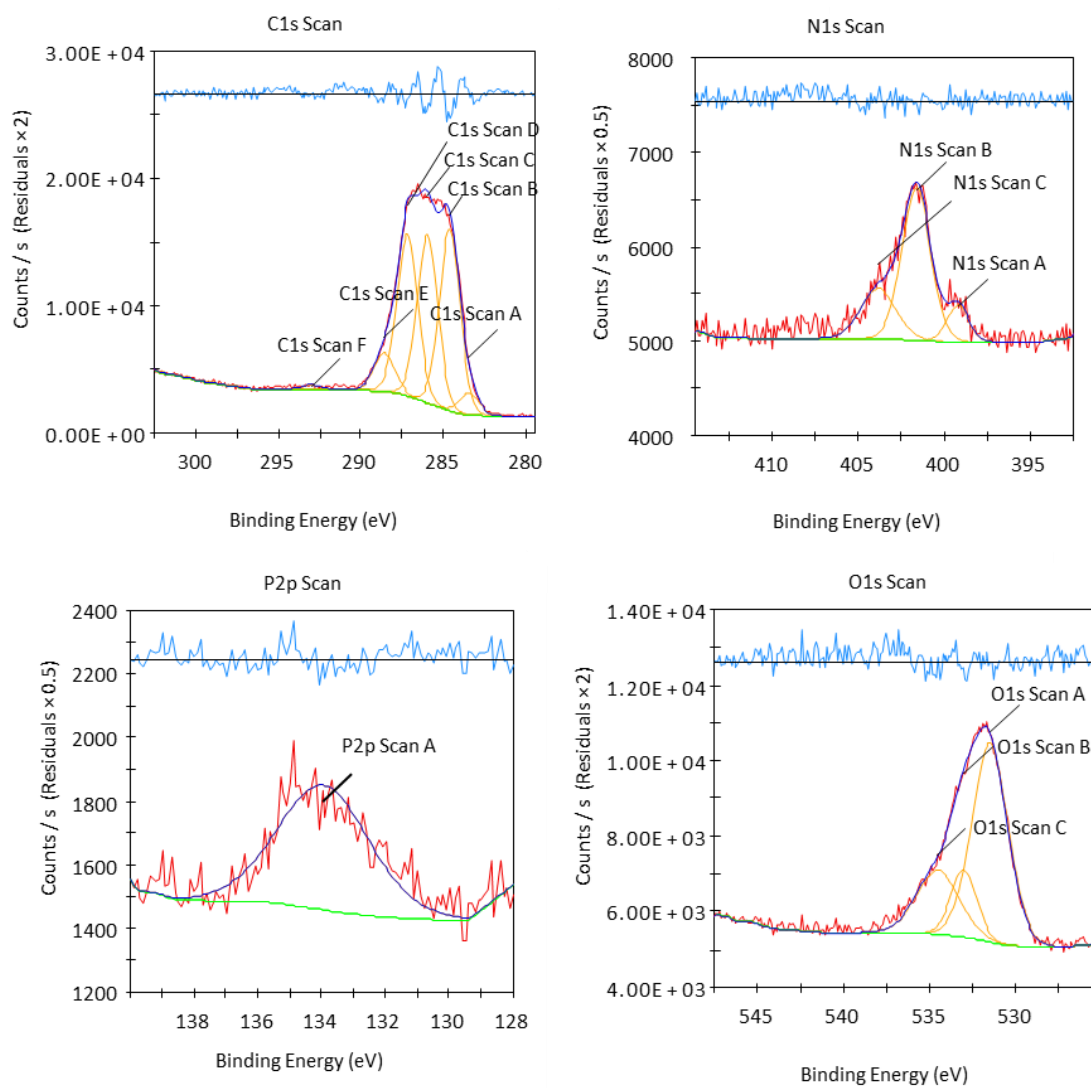


Figure C2. High-resolution XPS scan spectra of TPPO@CCM-C.

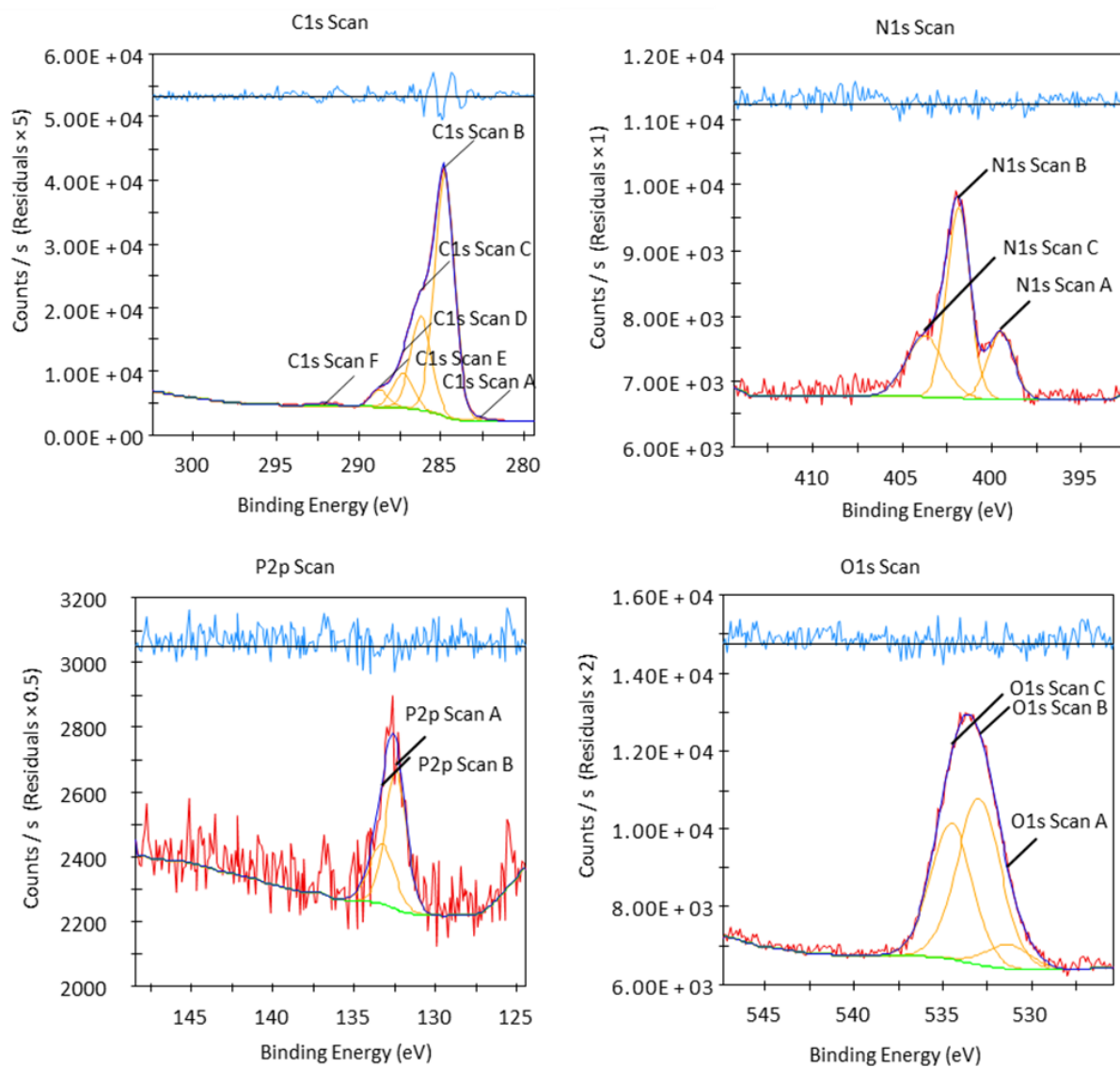


Figure C3. High-resolution XPS scan spectra of Rh-TPPO@CCM-C.

Table C1. Binding energies (eV) of the chemical states of the C, N, and O atoms in TPPO@CCM-C and RhNP-TPPO@CCM-C.

Atom	Binding Energy TPPO@CCM-C	FWHM (eV)	Atomic ratio (%)	Binding Energy RhNP-TPPO@CCM-C	FWHM (eV)	Atomic ratio (%)	ΔE (eV) ^a
C_{1s} Scan A	283.50	1.44	3.65	282.64	1.44	0.85	0.86
C_{1s} Scan B	284.69	1.44	53.41	284.81	1.4	61.14	0.12
C_{1s} Scan C	286.00	1.44	32.37	286.25	1.44	24.41	0.25
C_{1s} Scan D	287.24	1.33	7.48	287.31	1.44	9.06	0.07
C_{1s} Scan E	288.50	1.27	1.90	288.71	1.26	3.81	0.21
C_{1s} Scan F	292.28	1.44	1.19	292.00	1.44	0.73	0.28
N_{1s} Scan A	399.17	1.50	11.45	399.47	1.71	21.04	0.30
N_{1s} Scan B	401.59	1.94	62.63	401.85	1.51	52.22	0.26
N_{1s} Scan C	403.80	2.40	25.91	403.74	2.4	26.74	0.06
P_{2p} Scan A	132.36	2.64	66.21	132.39	1.55	66.21	0.03
P_{2p} Scan B	133.22	2.43	33.79	133.25	1.82	33.79	0.03
O_{1s} Scan A	531.22	1.92	46.96	531.28	2.88	7.69	0.06
O_{1s} Scan B	532.84	1.92	41.31	532.93	2.88	51.98	0.09
O_{1s} Scan C	535.05	1.92	11.72	534.47	2.74	40.34	0.58

^a ΔE = Binding energy (TPPO@CCM-C) – binding energy (RhNP-TPPO@CCM-C).

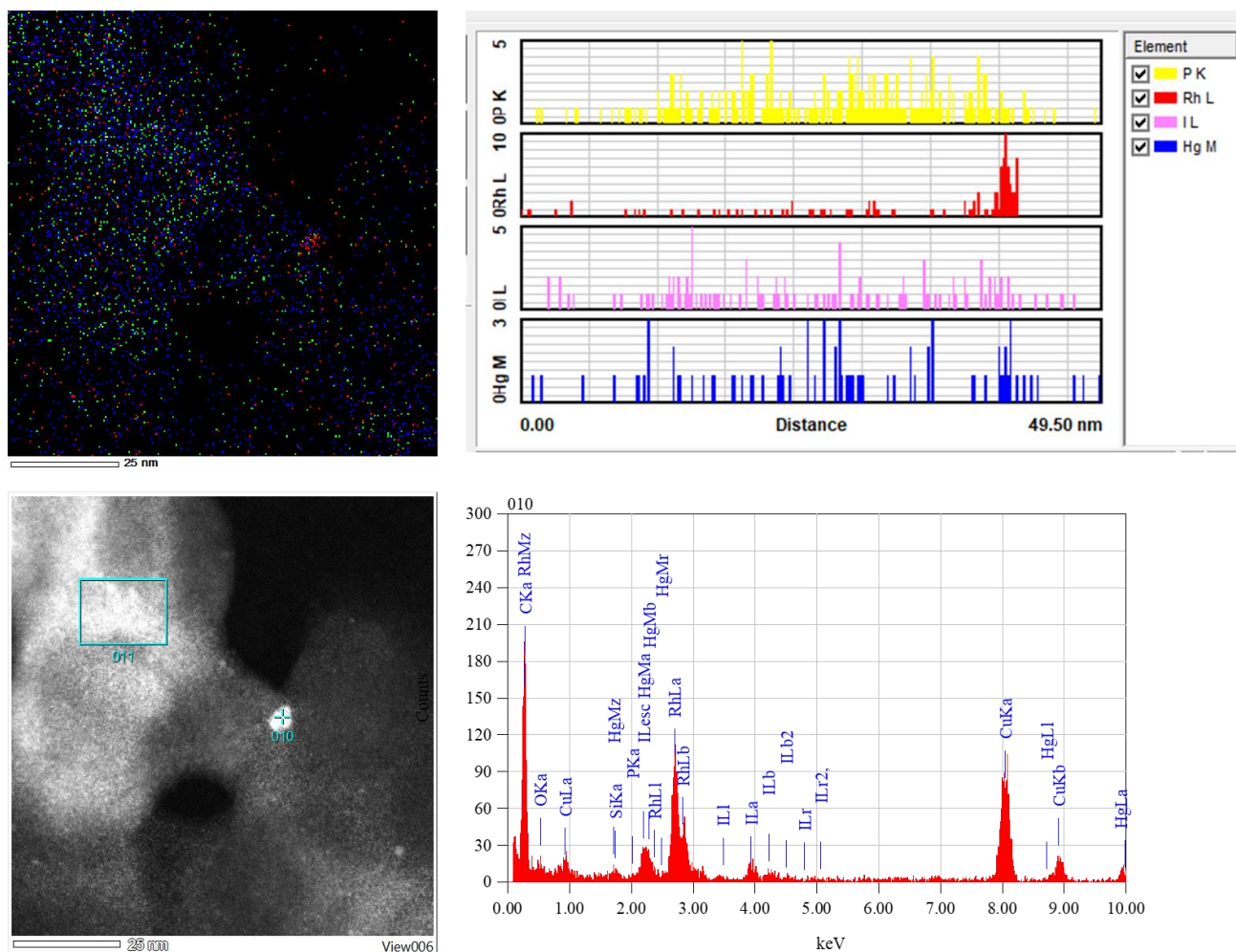


Figure C4. HR-TEM images coupled with energy-dispersive X-ray spectroscopy (EDX) after Hg poisoning, indicating the presence of Hg along with RhNPs. The EDX analysis showed a clear signal for elemental Rh as well as well-identified signals for Hg, P, and I atoms coming from the TPPO@CCM-C polymer that embeds the particles.

Appendix D for Chapter VI

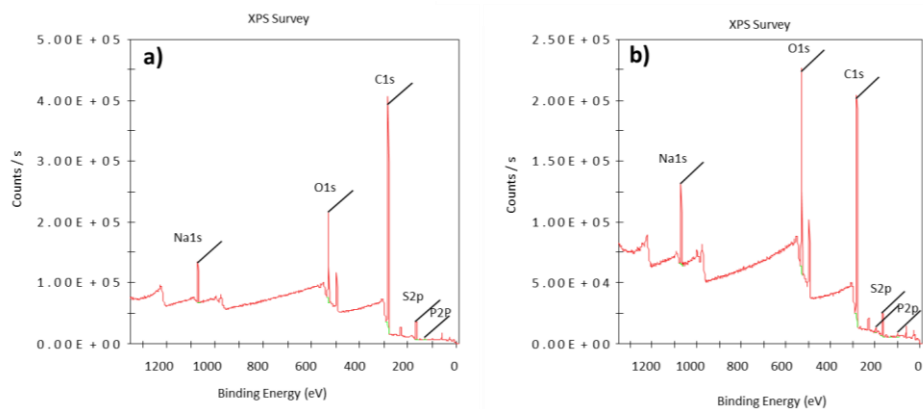


Figure D1. XPS survey spectra of a) TPPO@CCM-A and b) RhNP-TPPO@CCM-A.

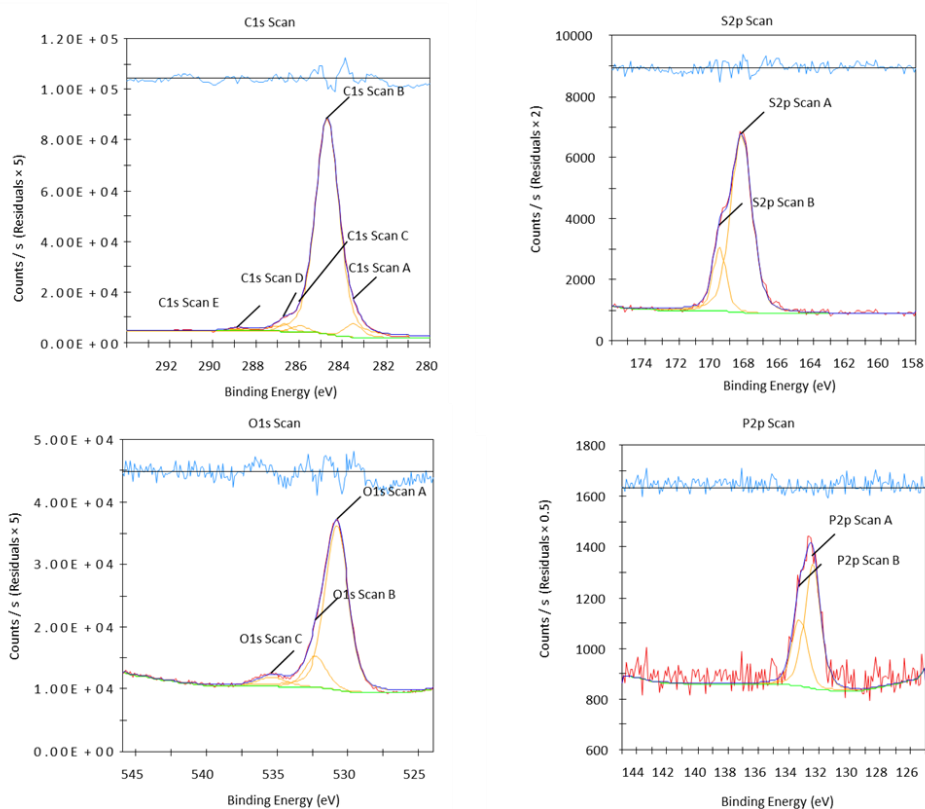


Figure D2. High-resolution XPS scan spectra of TPPO@CCM-A.

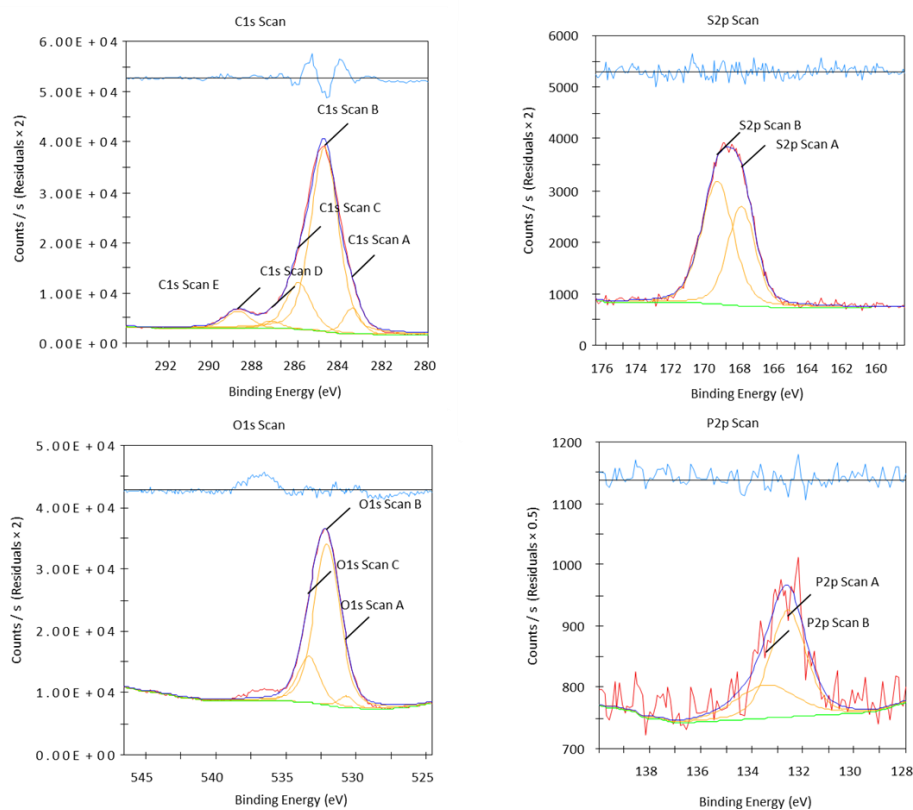


Figure E3. High-resolution XPS scan spectra of RhNP-TPPO@CCM-A.

Table D1. ICP-MS data for the leaching of Rh metal after each catalytic run with diethyl ether used as the washing solvent between recycles.

Run no.	^{103}Rh (LR)*	IF cor RSD**	[Rh] (ppt)	[Rh] (ppm)	$\Sigma[\text{Rh}]$ (ppm)	[Rh] _{initial} (ppm)	RhNPs leached (mol %)***
1	717366.0	0.78	51.6462	0.52			
2	1100850.1	1.52	79.2549	0.79			
3	678649.8	1.03	48.8589	0.49	3.1	161	1.93
4	788315.9	1.34	56.7542	0.57			
5	1013990.8	0.83	73.0015	0.73			

* Low Resolution (LR). ** Relative standard deviation (RSD) was calculated for all the run separately.

*** Rh (mol%) cumulative loss.

Appendix E for Chapter VII

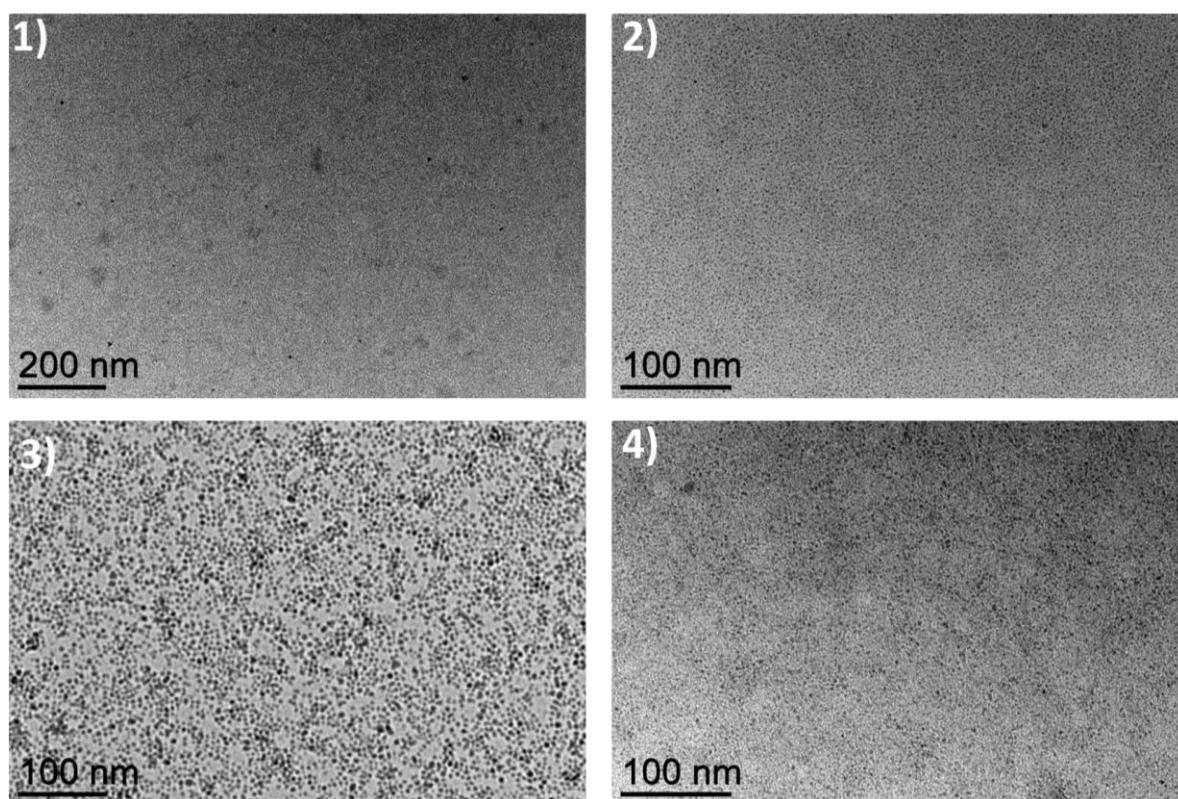


Figure E1. TEM images of NiNPs presented in Table VII.1. 1) synthesized from $[\text{Ni}(\text{acac})_2]$ in cyclohexane (Ni/TPP/N ratio = 1/1/0; entry 1), 2) Entry 2, synthesized from $[\text{Ni}(\text{COD})_2]$ in cyclohexane (Ni/TPP/N ratio = 1/1/0; entry 2), 3) synthesized from $[\text{Ni}(\text{acac})_2]$ in neat conditions (Ni/TPP/N ratio = 1/1/121; entry 3) and 4) synthesized from $[\text{Ni}(\text{COD})_2]$ in neat conditions (Ni/TPP/N ratio = 1/1/121; entry 4). Reaction conditions: 20 bar H_2 , 110 °C, 1200 rpm, 20 h.

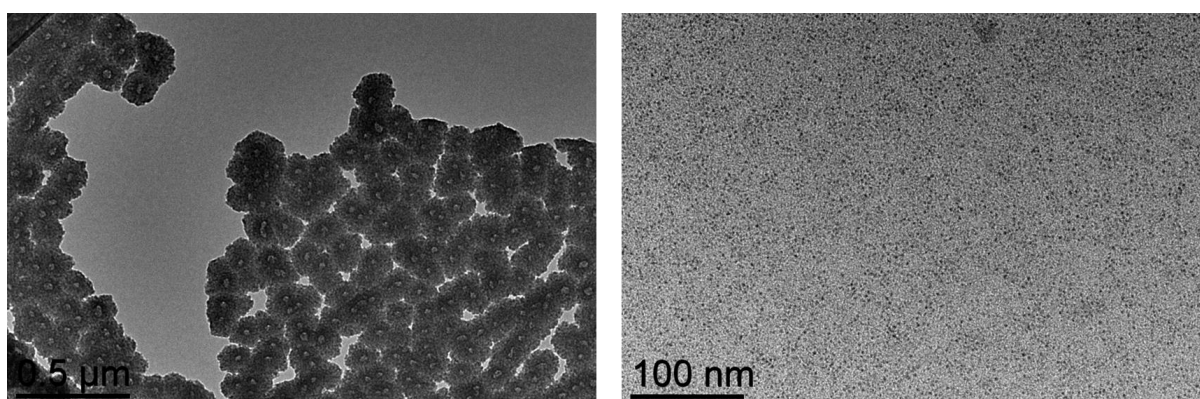


Figure E2. TEM images of NiNPs after the 4th washing with cyclohexane

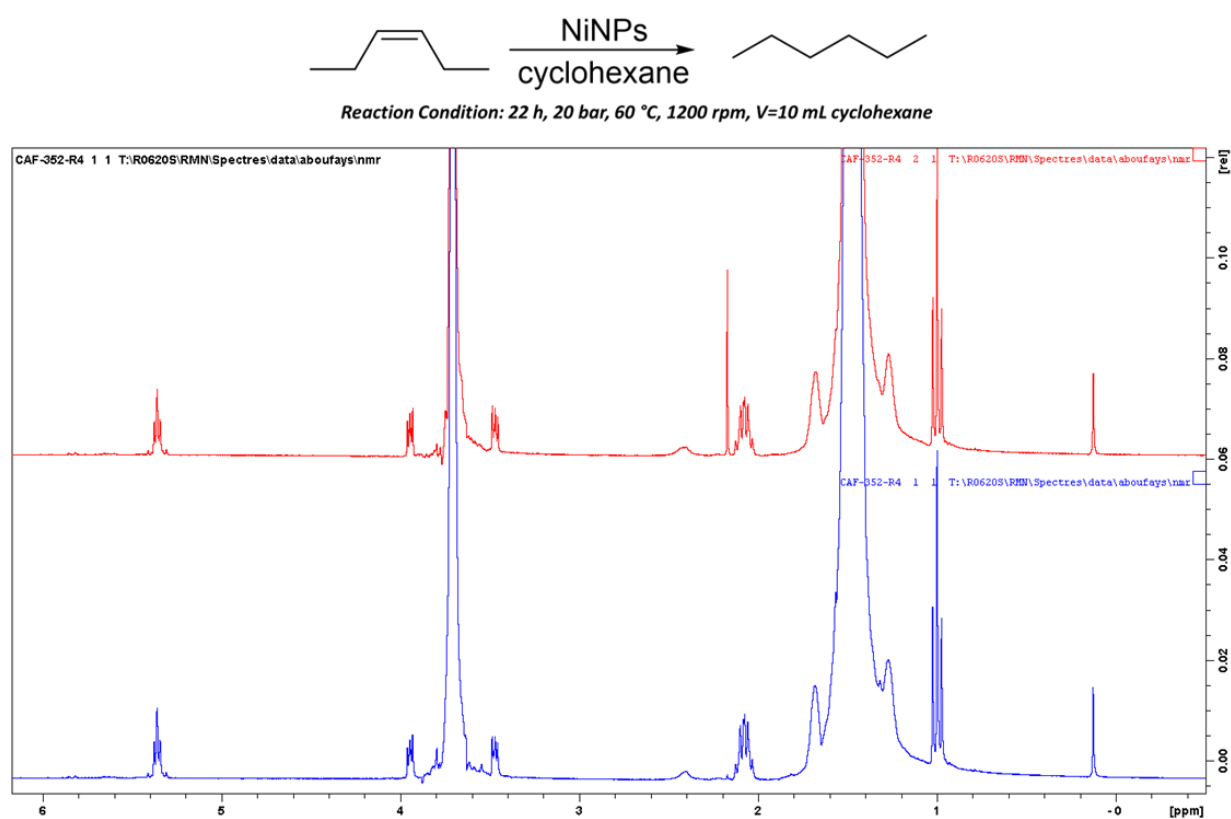


Figure E3. Control experiment of the hydrogenation of (Z)-hex-2-ene in the presence of NiNPs. Reaction conditions: V=10 mL of cyclohexane, 20 bar, 60 °C, 1200 rpm, 22 h,

Résumé de la thèse

Synthèse et confinement de nanoparticules métalliques dans des polymères amphiphiles à coeur-coquille pour application en catalyse biphasique

I. Introduction

La transformation catalytique de composés organiques avec des nanoparticules métalliques (MNPs) [1] dans des micelles [2,3] combine les avantages de la catalyse homogène et hétérogène, notamment une haute activité, sélectivité et durabilité [4]. La nanocatalyse [1,2] avec des catalyseurs à base de nanoparticules métalliques (NPMs) bien définies en taille, est un pont qui relie entre la catalyse homogène et hétérogène. Les dimensions nanométriques des catalyseurs confèrent des propriétés distinctives injoignable avec des matériaux en vrac, permettant une réactivité spécifique et des propriétés avantageuses telles que l'efficacité, la sélectivité, la stabilité prononcée en milieu réactionnel, ainsi que la facilité de récupération du catalyseur, et du recyclage [3–6]. Dans les dispersions colloïdales de NPMs ultrafines, les énergies de surface et les morphologies sont influencées par la taille des particules, conduisant à une réactivité de surface intrinsèque accrue [6]. Pour les nanoparticules à base de rhodium (NPRh), plusieurs méthodes de synthèse ont été développées pour le contrôle de la taille [7,8], comprenant des méthodes basées sur la réduction de sels métalliques et l'approche organométallique avec la décomposition des précurseurs de Rh. Généralement, le contrôle de la taille est réalisé en utilisant divers types d'agents de contrôle qui empêchent la croissance ultérieure des RhNPs, tandis que la stabilisation ultérieure des NPs en solution est assurée par l'ajout d'agents stabilisants tels que des surfactants (sels d'ammonium) [9–11], des polymères [12–15], des dendrimères [5] ou des ligands [8,16–22]. Ces stabilisateurs facilitent également la bonne recyclabilité des NPs lorsqu'ils sont utilisés en catalyse. Les MNPs offrent un rapport surface/volume élevé, résultant en un grand nombre de sites catalytiques

potentiels [5], et la surface métallique peut être stabilisée par des ligands appropriés, de manière similaire aux complexes moléculaires. Le confinement des MNPs à l'intérieur d'une matrice (par exemple, des oxydes métalliques, des matériaux carbonés ou polymères) peut améliorer davantage la stabilité et les performances catalytiques. En particulier, les MNPs supportées par polymère [6] ont suscité un intérêt significatif en catalyse en raison de la récupération facile et de la réutilisation du catalyseur. Avec de tels systèmes, l'utilisation de l'eau comme solvant ou dispersant produit des systèmes biphasiques aqueux [4,7,8] où la simple séparation de phases facilite la récupération et le recyclage du catalyseur et permet de réduire l'utilisation de solvants organiques volatils et des distillations énergivores, avec un impact positif sur l'environnement dans l'esprit de la chimie verte. Cependant, lorsque le catalyseur a une faible solubilité dans la phase réactant/produit organique et que le réactant a une faible solubilité dans l'eau, la réaction peut être limitée à l'interface organique/eau et souffrir de restrictions de transfert de masse. L'utilisation de surfactants ou de systèmes micellaires peut améliorer la cinétique de transfert de masse dans les réactions biphasiques aqueuses/organiques en augmentant les concentrations du catalyseur et du substrat dans la zone de réaction. Ancrer le catalyseur dans les cœurs hydrophobes des micelles permet d'augmenter la concentration locale du catalyseur et du substrat et de réduire l'impact du transfert de masse, à condition que le transport de masse entre les cœurs micellaires et la phase organique en vrac soit aisé. Lorsque les micelles sont cinétiquement inertes (échange lent avec le surfactant libre en solution) ou lorsqu'elles sont rendues unimoléculaires par réticulation de la coquille ou de cœur, elles fonctionnent comme des nanoréacteurs catalytiques individuels. Certains d'entre nous ont développé des protocoles synthétiques vers des micelles cœurs-réticulées hautement modulaires (CCMs) [23–33] en tant que dispersions aqueuses stables avec une teneur élevée en polymère (> 20% en poids), par polymérisation de transfert d'addition-fragmentation réversible (RAFT) [34]. La première génération de CCMs présentait une coque neutre (CCM-N) [30,31] composée de blocs de copolymères aléatoires de méthacrylate de poly(éthylène

glycol) (PEO) et d'acide méthacrylique. Des CCMs analogues avec une coquille polycationique (CCM-C) de blocs d'homopolymère d'iodure de 4-vinyl-N-méthylpyridinium (4VPMe⁺I⁻) ont également été préparés [15] ainsi que des analogues avec une coque polyanionique de type (CCM-A) de blocs d'homopolymère de poly(sodium styrenesulfonate) (P(SSNa⁺)) (Figure 1).

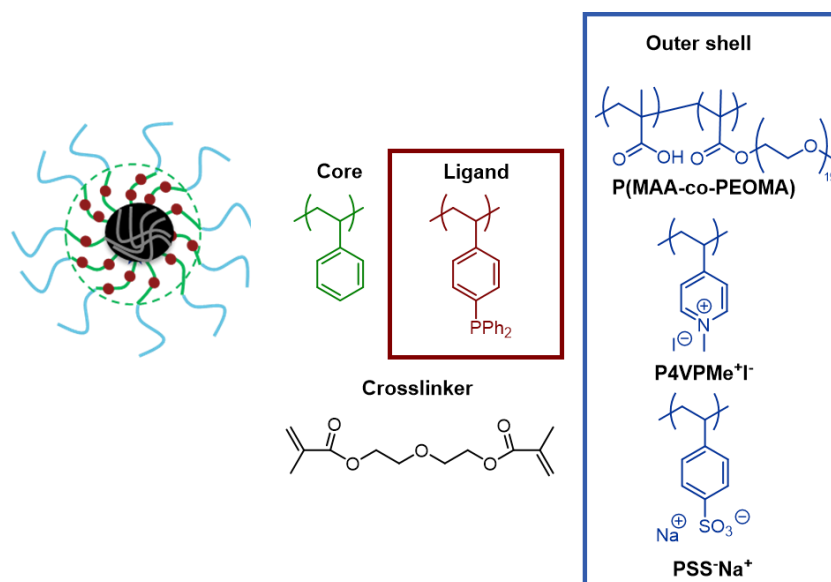


Figure 1. Micelles réticulées de base fonctionnée par TPP (TPP@CCM) et différentes coquilles.

Tous les CCMs développés jusqu'à présent ont un cœur à base de polystyrène avec du diméthacrylate de diéthylène glycol (DEGDMA) comme réticulant, mais ont été fonctionnalisés avec différents ligands liés au cœur, fournissant des nanoréacteurs L@CCM avec L = triphénylphosphine (TPP) [13,16,19,22], bis(4-méthoxyphényl)phénylphosphine [12], nixantphos [14] et carbène N-hétérocyclique [18]. Des pré-catalyseurs moléculaires (par exemple, [Rh(acac)(CO)₂] ou [Rh(COD)(μ-Cl)]₂; acac = acétylacétonate, COD = 1,5-cyclooctadiène) ont été fixés avec succès dans les cœurs de CCM par coordination de ligands, générant des nanoréacteurs catalytiques pour l'hydroformylation d'oléfines biphasiques aqueuses [25,30,31,33] et l'hydrogénation [23,28,35,36].

II. MNPs confinés dans CCM-C pour application en catalyse d'hydrogénation biphasique aqueuse

Lors d'investigations sur la portée du substrat, où l'hydrogénation catalytique de l'acétophénone a été tentée, le latex [RhCl(COD)(TPP@CCM-C)] est devenu noir[35], suggérant la réduction du complexe Rh^I moléculaire en métal Rh⁰. Rétrospectivement, cette méthode s'est avérée très efficace pour générer des RhNPs au sein du noyau des CCMs, suscitant ainsi des investigations plus approfondies sur l'hydrogénation biphasique impliquant des RhNPs[35]. Cet objectif était au cœur du projet de thèse actuel, abordant spécifiquement les défis importants rencontrés lors du travail précédent. RhNP-TPP@CCM-C a montré une excellente performance dans l'hydrogénation de 1-octène et du styrène, avec une conversion complète et une sélectivité totale vers l'hydrogénation de la fonction oléfinique. Notamment, l'activité catalytique était supérieure à celle du système moléculaire Rh^I. RhNP-TPP@CCM-C s'est également avéré recyclable pour l'hydrogénation du styrène en quatre cycles sans perte d'activité, les RhNPs restant bien dispersés lorsque le toluène était utilisé pour la récupération du produit/recyclage du catalyseur. Cependant, lors de l'utilisation de l'éther diéthylique comme solvant d'extraction, une perte dramatique d'activité a été observée. Ce phénomène a été attribué à une extraction des RhNPs du noyau CCM-C induite par l'éther diéthylique, un solvant à base d'oxygène.

III. Portée du travail de thèse

La découverte décrite ci-dessus de la formation de RhNPs catalytiquement actifs dans le système TPP@CCM-C constitue la base du travail de recherche mené dans le cadre de cette thèse de doctorat. L'objectif général de la recherche était de développer des solutions innovantes pour améliorer le confinement de MNPs, principalement des RhNPs, dans le CCM-C, afin d'obtenir des systèmes catalytiques performants, stables et recyclables pour la catalyse d'hydrogénation liquide-liquide biphasique aqueuse en tant que domaine d'application. Pour atteindre cet objectif, des outils de synthèse issus de la chimie des polymères CCM et de la nanochimie organométallique ont été combinés, et plusieurs approches pour atteindre les sous-objectifs décrits ci-dessous ont été explorées. Les principaux résultats de la recherche sont présentés dans les

paragrapes suivants. De nouvelles synthèses de polymères incorporant des ligands TPPO et des coquilles polycationiques ont été développées pour améliorer le confinement des RhNPs dans le but de raffiner leur activité, leur sélectivité et leur portée.

IV. Confinement des nanoparticules de Rh dans des micelles réticulées au cœur fonctionnalisées par l'oxyde de triphénylphosphine pour la catalyse d'hydrogénation biphasique aqueuse

Sur la base de l'hypothèse présentée dans la section précédente, de nouveaux nanoréacteurs L@CCM avec des ligands d'oxyde de triphénylphosphine (TPPO) en tant que fonctions centrales d'ancrage des RhNP basées sur l'oxygène ont été développés. En ce qui suit la synthèse et la caractérisation du nouveau latex type polymère TPPO@CCM-C, son chargement avec des RhNPs préformées, et l'application des nanoréacteurs résultants RhNP-TPPO@CCM-C dans l'hydrogénation catalytique du styrène dans des conditions biphasiques aqueuses, sont décrites.

IV.1. Synthèse et caractérisation du polymère

La synthèse du nouveau polymère TPPO@CCM-C a été réalisée en suivant la même stratégie que celle utilisée pour la préparation du polymère étroitement lié TPP@CCM-C (Schéma 1). Les degrés de polymérisation cibles de chaque bloc ont été maintenus identiques à ceux de TPP@CCM-C, car ils étaient déjà optimisés pour fournir des latex stables avec une distribution de taille de particules étroite [28,29]. Ainsi, les trois premières étapes conduisant à la synthèse de l'agent macroRAFT dibloc amphiphile, $R_0-(VPMe^+I)_{140}-b-St_{50}-SC(S)SnPr$, isolé sous forme solide stable et redispersé dans l'eau, étaient les mêmes que dans la synthèse de TPP@CCM-C [28]. Elles impliquaient la polymérisation RAFT homogène de 4VP avec CTPPA, $R_0SC(S)SnPr$ où $R_0 = CMe(CN)CH_2CH_2COOH$), en tant qu'agent de transfert, formant $R_0-4VP_{140}-SC(S)SnPr$ (étape 1), puis l'extension de chaîne avec un bloc polystyrène court (degré moyen de polymérisation de 50) formant un copolymère dibloc $R_0-VP_{140}-b-St_{50}-SC(S)SnPr$ (étape 2), et la quaternisation des atomes de pyridine avec MeI (étape

3). La quatrième étape a été une extension supplémentaire de la chaîne de l'agent macroRAFT $R_0-(VPMe^+I^-)_{140}-b-St_{50}-SC(S)SnPr$ avec un bloc hydrophobe plus long (degré moyen de polymérisation de 300) constitué d'un copolymère statistique de styrène et de styrène fonctionnalisé par TPPO, à savoir SDPPO (oxyde de 4-styryldiphénylphosphine) [37,38] (rapport 90/10), qui a été obtenu par oxydation de SDPP avec H_2O_2 .

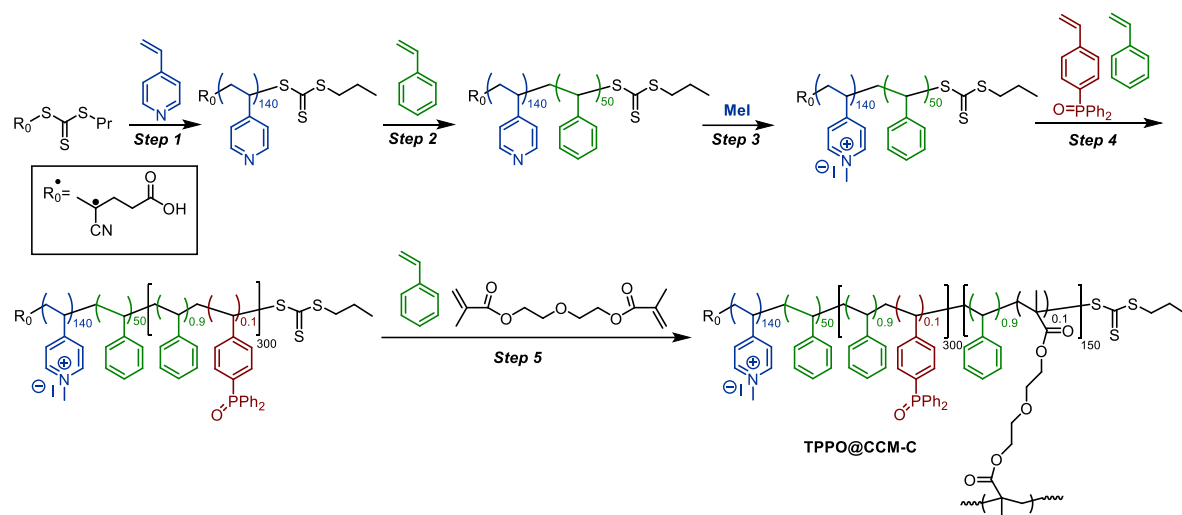


Schéma 1. Synthèse du polymère TPPO@CCM-C.

Les micelles de morphologie sphériques du copolymère dibloc amphiphile produites à l'étape 4 avaient une taille moyenne d'environ 65 nm, comme le montre l'analyse DLS (Figure 2a). Ces micelles ont ensuite été réticulées dans une dernière étape avec du DEGDMa (15 équivalents par chaîne), dilué avec du styrène supplémentaire (135 équivalents par chaîne), pour produire le produit final, $R_0-(VPMe^+I^-)_{140}-b-St_{50}-b-(St_{0.9}-co-SDPPO_{0.1})_{300}-b-(St_{0.9}-co-DEGDMa_{0.1})_{150}-SC(S)SnPr$ (TPPO@CCM-C), avec une densité de réticulation de 10% dans le noyau réticulé interne. Les particules finales du polymère TPPO@CCM-C avaient une morphologie sphérique et un diamètre légèrement plus grand (99 nm) que les micelles intermédiaires, comme le montrent les analyses DLS (Figure 2c) et TEM (Figure 2d). La distribution de taille est devenue plus étroite et la D_z de la distribution a légèrement diminué après gonflement avec du $CHCl_3$. Ce phénomène de réduction de taille lors du gonflement a également été

observé pour des CCMs apparentées avec une coquille anionique (TPP@CCM-A) et a été attribué à l'effet dominant de la désagrégation des micelles plutôt qu'au gonflement du noyau, qui provoquerait une augmentation de la taille moyenne [24]. En conséquence, le profil d'intensité dans la Figure 2b, plus sensible aux micelles de plus grande taille, est devenu significativement plus étroit et s'est déplacé vers des valeurs plus basses après le gonflement.

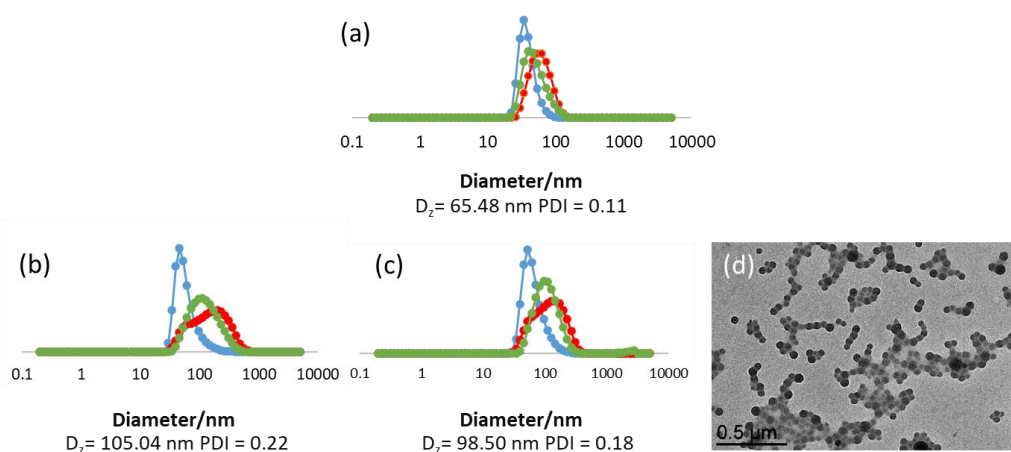


Figure 2. Distributions de taille par DLS des dispersions aqueuses (a) des micelles dibloc R₀-(VPMe⁺I)₁₄₀-b-St₅₀-b-(St_{0.9}-co-SDPPO_{0.1})₃₀₀-b-SC(S)SnPr et de TPPO@CCM-C (b) avant et (c) après gonflement avec du CHCl₃. Codage couleur : nombre (bleu), volume (vert) et intensité (rouge). d) Image TEM de TPPO@CCM-C.

IV.2. Synthèse de RhNP-TPPO@CCM-C

La première tentative de production de RhNP-TPPO@CCM-C consistait à charger le CCM-C avec $[\text{Rh}(\text{COD})(\mu\text{-Cl})_2]$, afin de générer un complexe $[\text{RhCl}(\text{COD})(\text{TPPO@CCM-C})]$ ancré au cœur qui pourrait être réduit en RhNPs par H₂, suivant la procédure précédemment développée pour générer des RhNPs incorporés dans TPP@CCM-C [35]. Les complexes mononucléaires avec la stœchiométrie $[\text{Rh}(\eta^2:\eta^2\text{-diène})\text{Cl}(\text{L})]$ (par exemple, diène = COD, norbornadiène), où L est un ligand donneur d'atome d'oxygène, sont rares [39–42], mais le complexe $[\text{RhCl}(\text{COD})(\text{Ph}_3\text{PO})]$ a été décrit [43,44]. Cependant, cette méthode s'est avérée infructueuse car la phase organique est restée de couleur jaune, même après chauffage du mélange réactionnel à 60°C pendant 1 h ou agitation à température ambiante

pendant 24 h. Cela indique que la formation d'un complexe Rh^I-TPPO@CCM-C dans le noyau polymère par clivage du groupe pont di- μ -Cl dans [Rh(COD)(μ -Cl)]₂ n'est pas favorable dans les conditions appliquées. Par conséquent, une stratégie alternative impliquant la synthèse en *ex-situ* de RhNPs et leur transfert ultérieur vers les nanoréacteurs TPPO@CCM-C a été envisagée. À cette fin, les RhNPs ont été produites par réduction de [Rh(COD)(μ -Cl)]₂ avec H₂ en présence de pyridine et de TPP en tant que ligands stabilisants. Cette combinaison de ligands a été inspirée par des rapports antérieurs, qui ont montré que le TPP était un stabilisateur efficace pour produire des RhNPs ultrapetites [12,20,45–47], tandis que la pyridine était utilisée pour la formation de RhNPs dans des liquides ioniques [46]. La synthèse des RhNPs a été réalisée dans le toluène, qui a un pouvoir de gonflement élevé pour le noyau CCM-C à base de polystyrène [32]. Les conditions optimisées (TPP/Pyridine/Rh = 1/1/1, 60°C, 20 bar H₂, 20 h) ont conduit à une suspension colloïdale stable et noire de RhNPs, qui présentait un diamètre moyen de 1.2 ± 0.4 nm et une distribution de taille étroite (Figure 3).

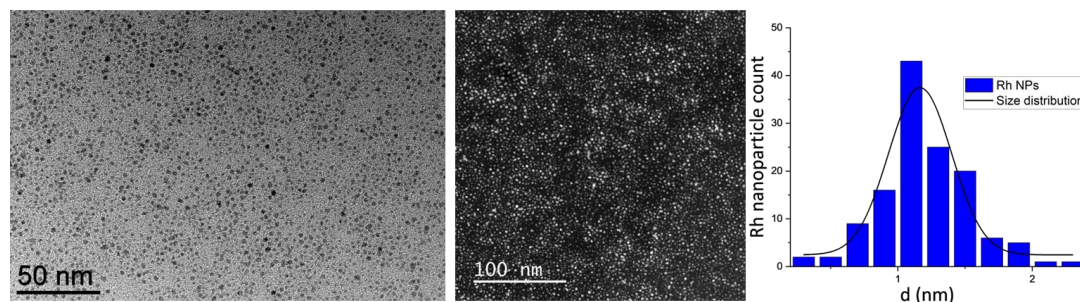


Figure 3. Images TEM des RhNPs stabilisées par TPP et pyridine (à gauche) et l'histogramme correspondant de la distribution de taille ($d_m = 1.2 \pm 0.4$ nm) (à droite).

L'addition de la suspension colloïdale de RhNPs au latex TPPO@CCM-C (P/Rh = 4/1) a entraîné une décoloration rapide et complète de la phase de toluène, tandis que le latex devenait gris. Cela indiquait le transfert réussi des RhNPs à travers la coquille hydrophile P(4VPMe⁺I) du CCM-C et leur ancrage aux fonctions TPPO dans les noyaux polymères, ce qui a été corroboré par la caractérisation DLS et TEM du RhNP-TPPO@CCM-C final. L'analyse DLS a montré que les particules de polymères CCM-C avaient une taille moyenne et une distribution de taille très similaires avant et après le

chargement avec les RhNPs. L'analyse TEM a confirmé que les RhNPs étaient situés à l'intérieur des particules polymères et indiquait une taille moyenne d'environ 1.5 ± 0.4 nm. Malgré la présence du polymère qui rend la mesure plus difficile, on peut conclure que les RhNPs avaient des tailles assez similaires aux RhNPs synthétisés (Figure 3). Ce résultat indique que les RhNPs ne sont pas significativement altérées par l'échange de ligands dans le noyau CCM-C.

IV.3. Hydrogénation du styrène avec RhNP-TPPO@CCM-C dans des conditions biphasiques

Le latex de RhNP-TPPO@CCM-C a été appliquée à l'hydrogénation biphasique aqueuse du styrène dans les mêmes conditions de température et de pression que la suspension colloïdale de RhNPs (20 bar H_2 , 25°C), avec un rapport styrène/Rh de 2000/1, à différents temps de réaction (Figure 4). Comme le styrène est un bon solvant pour le polystyrène, aucun solvant vecteur n'était nécessaire, et l'hydrogénation a été réalisée avec le substrat pur [28,35] en utilisant une agitation de 1200 tr/min pour assurer un bon transfert de masse externe.

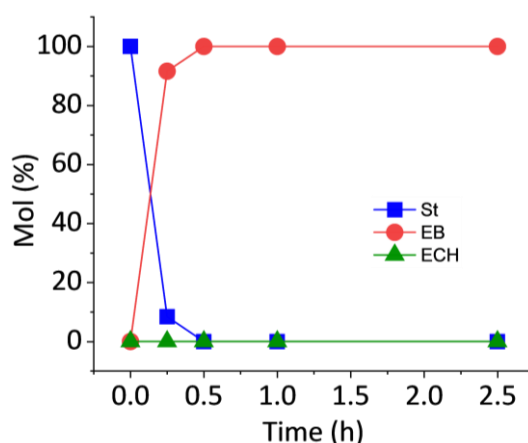


Figure 4. Profil du temps pour l'hydrogénation biphasique aqueuse du styrène en utilisant RhNPs-TPPO@CCM-C. Conditions réactionnelle : styrène/Rh = 2000/1, 20 bar H_2 , 25°C.

Une conversion presque complète du styrène (environ 94 %) a été obtenue en seulement 0.25 h, correspondant à un TOF de 7733 h^{-1} (cTOF de 9850 h^{-1}), avec une excellente sélectivité (>99 %) envers l'EB (Tableau 1, entrée 1). Cette performance catalytique est supérieure à celle obtenue précédemment avec des nanoparticules de

Rh incorporées dans le TPP@CCM-C [20,21,28]. Cette différence peut être liée à la plus petite taille des nanoparticules de Rh stabilisées ex-situ par TPP/pyridine utilisées pour l'obtention du RhNP-TPPO@CCM-C par rapport aux nanoparticules de Rh stabilisées in-situ par TPP@CCMC dans RhNP-TPP@CCM-C (1.2 nm contre < 5 nm). Cependant, des expériences supplémentaires ont indiqué que les stabilisateurs TPP et pyridine adsorbés dans le catalyseur RhNP-TPPO@CCM-C jouaient également un rôle (voir ci-dessous). Une augmentation du rapport styrène/Rh a donné des conversions bonnes et reproductibles en 0.25 h de 53 % (styrène/Rh = 5000/1) et 24 % (styrène/Rh = 10000/1), correspondant à des TOFs de 10547 et 9062 h⁻¹ (cTOFs de 14300 et 12440 h⁻¹), respectivement, toujours avec une sélectivité complète envers l'EB (Tableau 1, entrées 2 et 3). Après l'arrêt de l'agitation, une séparation de phase rapide (< 3 min) a été observée dans toutes les réactions, facilitant ainsi la séparation des produits et la récupération du catalyseur, comme déjà rapporté pour les nanoréacteurs RhNP-TPP@CCM-C présentant la même coquille [35].

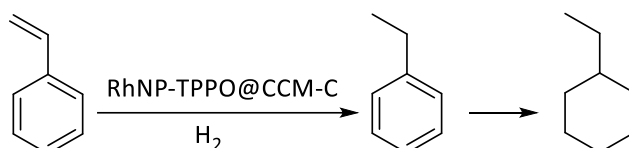


Table 1. Hydrogénation du styrène en utilisant RhNP-TPPO@CCM-C^a

Entrée	Rapport molaire styrène/Rh	Conversion (%)	Rendement (%)		TOF (h ⁻¹) ^b
			Ethylbenzene	Ethylcyclohexane	
1	2000/1	94	94	<0.1	7733 (9850)
2	5000/1	53	52	<0.1	10547 (14300)
3	10000/1	24	23	<0.1	9062 (12440)

^a Conditions réactionnelles : 20 bar H₂, 25°C, 0.25 h. ^b Valeurs moyennes sur la durée de la réaction, exprimées en moles de substrat converties par moles de Rh dans le catalyseur par heure (TOF) ou en moles de substrat converties par moles d'atomes de Rh de surface par heure (cTOF, entre parenthèses).

Le recyclage du latex catalytique RhNP-TPPO@CCM-C a été évalué dans deux séries d'expériences à un rapport styrène/Rh fixe de 5000/1, en extrayant les produits de réaction avec de l'éther diéthylique ou du toluène, respectivement, avant l'ajout d'un nouveau lot de substrat pour la réaction catalytique qui suit. Le protocole d'extraction était identique à celui utilisé dans les études de recyclage précédemment rapportées

avec le RhNP-TPP@CCM-C [35] et avec les systèmes catalytiques moléculaires Rh^I-TPP@CCM [28]. Les premières réactions catalytiques ont produit une conversion du styrène de 53 % en 0.25 h. Cependant, une diminution progressive de la conversion, de 53 % à environ 9-15 %, a été observée après la cinquième série de recyclages pour les deux séries, en utilisant soit de l'éther diéthylique, soit du toluène pour l'extraction des produits (Figure 5a). Les analyses ICP-MS ont montré une perte cumulative d'environ 2 % de l'inventaire du catalyseur après les cinq réactions catalytiques lors de l'utilisation de l'éther diéthylique comme solvant d'extraction, indiquant que la diminution de l'activité n'était pas causée par la lixiviation du métal et la perte mécanique du latex. De plus, après la séparation du catalyseur, que le toluène ou l'éther diéthylique ait été utilisé comme solvant d'extraction, la phase organique était complètement transparente et incolore, tandis que la phase aqueuse restait grise, indiquant ainsi la rétention des nanoparticules de Rh dans le latex CCM-C. Dans les deux cas, les images TEM obtenues pour le catalyseur RhNP-TPPO@CCM-C après la cinquième série de recyclages ont mis en évidence un confinement préservé des nanoparticules de Rh dans les cœurs de CCM-C avec des nanoparticules de Rh bien dispersées. Ces résultats indiquent que l'interaction des nanoparticules de Rh avec les ligands TPPO liés au cœur est suffisamment forte pour les retenir à l'intérieur des cœurs hydrophobes de CCM-C, validant l'hypothèse initiale de l'efficacité supérieure des ligands de coordination de l'oxygène. Bien qu'un artefact ne puisse pas être exclu en raison des nanoparticules de Rh moins définies incorporées dans le polymère, un changement notable était une augmentation de la taille des particules (passant de 1.5 ± 0.4 nm à 2.2 ± 0.9 nm après la cinquième réaction catalytique). Cela peut indiquer une légère croissance ou agrégation des nanoparticules. Cependant, étant donné que la valeur d'écart type est plus grande que le changement de taille (0.9 nm contre 0.7 nm), on peut également considérer que les nanoparticules sont dans une plage de taille similaire, de sorte que l'interprétation de la baisse d'activité comme résultat d'un changement de taille ne semble pas satisfaisante.

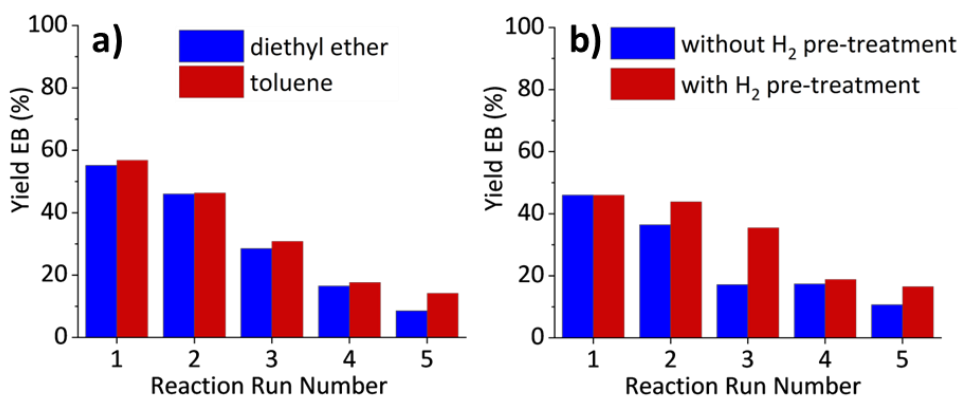


Figure 5. Réutilisation de RhNP-TPPO@CCM-C dans cinq réactions catalytiques d'hydrogénation du styrène (a) avec extraction intermédiaire du produit par l'éther diéthylique (bleu) et le toluène (rouge), (b) avec extraction du produit par l'éther diéthylique sous argon avec et sans traitement intermédiaire à l'H₂ (20 bar H₂, 25°C, 1 h). Conditions de réaction : styrène/Rh = 5000/1, 20 bar H₂, 25°C, 0.25 h.

Étant donné qu'aucune lixiviation significative du métal n'a été détectée et qu'aucune agglomération substantielle des nanoparticules qui pourrait entraîner une perte de surface active n'a été observée, une passivation progressive de la surface des nanoparticules de Rh par la formation d'oxyde de rhodium pourrait être responsable de la diminution des performances catalytiques au fil des recycles subséquents. Pour vérifier cette hypothèse, le recyclage du catalyseur avec extraction du produit par l'éther diéthylique a été réalisé sous une atmosphère d'argon inerte. De plus, la phase récupérée de RhNP-TPPO@CCM-C a été traitée avec H₂ (20 bar H₂, 25°C, 1 h) avant chaque réaction catalytique, pour éliminer toute couche d'oxyde de rhodium. Malgré ces précautions dans les expériences de recyclage, la conversion du styrène a diminué à 10 % au cours des cinq cycles (Figure 5b). La similitude de ces résultats avec ceux obtenus sans atmosphère inerte et sans traitement réducteur suggère que la passivation des nanoparticules de Rh n'était pas la seule raison de la diminution de l'activité. Une dernière hypothèse de travail est que les stabilisateurs utilisés pour la synthèse *ex-situ* des nanoparticules de Rh (TPP/pyridine) sont partiellement restés dans le noyau TPPO@CCM-C après le chargement et ont favorisé l'activité catalytique des nanoparticules de Rh, et que l'activité a diminué progressivement à mesure que ces stabilisateurs/promoteurs étaient continuellement éliminés lors des opérations de récupération et de recyclage du catalyseur. Cette hypothèse a été testée en lavant le

latex fraîche de RhNP-TPPO@CCM-C, après le chargement des nanoparticules de Rh, trois fois avec de l'éther diéthylique avant son utilisation en catalyse. Une analyse GC-MS des extraits d'éther diéthylique a montré deux pics avec des spectres de masse MS produisant des ions moléculaires à m/z 112 et 83, respectivement. Ces pics correspondent au cyclooctane et à la tétrahydropyridine résultant de l'hydrogénation du ligand COD de $[\text{Rh}(\text{COD})(\mu\text{-Cl})_2]$ et de la pyridine pendant la synthèse *ex-situ* des nanoparticules de Rh [11,22,48]. Ensuite, cinq cycles catalytiques consécutifs (tous reproduits trois fois) ont été effectués (20 bar H_2 , 25°C, 1 h) (Figure 6). La première réaction catalytique a fourni une faible conversion du styrène (environ 6%), tandis qu'une conversion constante d'environ 25 % a été obtenue lors des quatre cycles suivants, correspondant à un TOF moyen d'environ 1025 h^{-1} (cTOF d'environ 1440 h^{-1}). La faible conversion lors du premier cycle pourrait indiquer qu'un temps d'induction serait nécessaire pour débloquer les sites actifs et/ou que les nanoparticules de Rh ont subi des changements significatifs dans des conditions catalytiques. La comparaison d'une série de mesures TEM effectuées avec le catalyseur lavé à l'éther diéthylique (avant la catalyse) avant/après le traitement à l' H_2 et après le premier et le cinquième cycle catalytique a confirmé que la taille moyenne des nanoparticules de Rh a effectivement changé de $4.2 \pm 0.2 \text{ nm}$ à $2.2 \pm 0.2 \text{ nm}$ avant et après le traitement à l' H_2 , respectivement, et a été réduite à une taille statique de $1.8 \pm 0.1\text{-}0.3 \text{ nm}$ après le premier cycle catalytique. Ainsi, l'élimination des stabilisateurs a probablement induit une légère augmentation de la taille ou une agrégation des nanoparticules de Rh, entraînant une activité catalytique réduite, comme déjà rapporté pour les nanoparticules de Rh dans l'hydrogénation du styrène[49], tandis que le traitement successif à l' H_2 a favorisé la reconstruction des nanoparticules, probablement aidée par la présence de TPPO@CCM-C[47]. Notamment, bien qu'un temps de réaction différent ait été appliqué (1 h contre 0.25 h), la valeur de conversion du styrène d'environ 25% obtenue après la première réaction est comparable à celle obtenue dans les quatrième et cinquième recyclages effectués avec l'extraction intermédiaire du produit par l'éther diéthylique (Figure 5b). Cela suggère que les

lavages à l'éther diéthylique effectués entre les cycles catalytiques consécutifs (Figure 6b) ont un effet similaire à ceux réalisés sur le RhNP-TPPO@CCM-C frais avant sa mise en œuvre en catalyse. Cela indique un rôle possible des stabilisateurs des nanoparticules de Rh (TPP, pyridine et tétrahydropyridine, voir résultats GC-MS ci-dessus) dans l'hydrogénation du styrène lorsqu'ils ne sont pas éliminés par des lavages de solvant [50–53]. Il convient également de noter que, comme indiqué ci-dessus, l'hydrogénation du styrène catalysée par les nanoparticules de Rh dans le toluène donne un TOF beaucoup plus élevé pour les nanoparticules de Rh stabilisées par TPP et pyridine (environ 36000 h^{-1}) par rapport à d'autres nanoparticules de Rh synthétisées avec d'autres stabilisateurs, dans des conditions expérimentales similaires [47]. Cela souligne qu'un choix méticuleux des stabilisateurs pour les nanoparticules de Rh pré-synthétisées pour leur transfert dans le CCM-C, ou l'intégration de co-ligands dans les cœurs de CCM-C, pourrait être une façon d'améliorer les performances catalytiques, cependant cela va au-delà du champ d'étude du présent travail.

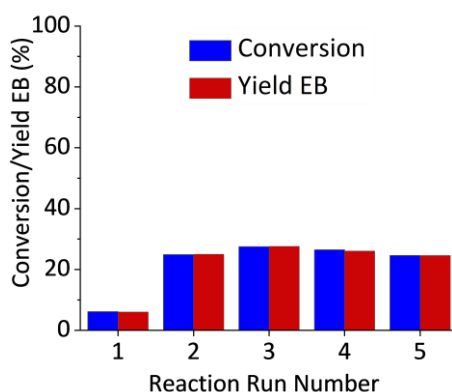


Figure 6. Hydrogénation du styrène avec RhNP-TPPO@CCM-C après trois lavages à l'éther diéthylique (cycle 1) et recyclage du catalyseur dans quatre cycles de réaction supplémentaires avec extraction du produit par l'éther diéthylique et traitement intermédiaire à l' H_2 (20 bar H_2 , 25°C , 1 h). Conditions de réaction : styrène/Rh = 5000/1, 20 bar H_2 , 25°C , 1 h.

V. Hydrogénation biphasique aqueuse avec des nanoparticules de Rh synthétisées en une seule étape dans des micelles à coque polycationique et à noyau réticulé fonctionnalisé par l'oxyde de triphénylphosphine

Vu les résultats précédents, dans la suite une nouvelle approche de synthèse en une seule étape est décrite pour le catalyseur RhNP-TPPO@CCM-C, qui ne nécessite pas l'utilisation de stabilisateurs supplémentaires. Le catalyseur résultant a été soigneusement caractérisé et appliqué dans l'hydrogénation biphasique aqueuse du styrène ainsi que d'autres substrats choisis tels que les alcènes, les alcynes et les composés carbonyles.

V.1. Synthèse en une seule étape et caractérisation de RhNP-TPPO@CCM-C

Des nanoparticules de Rh incorporées dans les cœurs hydrophobes d'un latex stable de TPPO@CCM-C ont été synthétisées en une seule étape en chauffant un mélange biphasique contenant le latex aqueux TPPO@CCM-C et une solution de toluène de $[\text{Rh}(\text{COD})(\mu\text{-Cl})]_2$ sous pression de H_2 . Cela pourrait être réalisé sans l'ajout de stabilisateur ou d'additif de base supplémentaire (Tableau 2, Entrée 1) et sans nécessiter une synthèse *ex-situ* préalable des nanoparticules de Rh (comme précédemment rapporté). Des synthèses comparatives ont également été réalisées en présence d'une base telle que la pyridine ou Et_3N (Tableau 2, Entrées 2 et 3, respectivement), qui peut aider la réaction en piégeant l'HCl produit lors de la réduction de Rh^{I} à Rh^0 , en plus de contribuer potentiellement à la stabilisation des nanoparticules de Rh[35]. Après la synthèse et la séparation des phases, tous les trois latex de RhNP-TPPO@CCM-C produits étaient noirs, indiquant la formation réussie et le confinement des nanoparticules de Rh dans le cœur des CCMs.

Table 2. Synthesis of RhNP-TPPO@CCM-C.^a

Entrée	Base	Rapport molaire TPPO/Rh/Base	Taille moyenne RhNPs (nm)	
			Avant Catalyse	Après Catalyse
1	-	4/1/0	1.7 ± 0.2	1.9 ± 0.6
2	Pyridine	4/1/4	2.9 ± 0.6	3.1 ± 0.1
3	NEt_3	4/1/4	2.1 ± 0.1	1.8 ± 0.2

^a Conditions réactionelles: 20 bar H_2 , 20 h, 60 °C, toluène, 1200 tr/min .

Les analyses TEM ont confirmé l'incorporation réussie des RhNPs dans le TPPO@CCM-C dans tous les cas. Les RhNPs synthétisées sans base (Entrée 1) ont montré une distribution de taille particulièrement étroite avec un diamètre moyen $d_m = 1.7 \pm 0.2$ nm. En revanche, les RhNPs produites en présence de pyridine ou de Et₃N (Tableau 2, Entrées 2 et 3, respectivement) étaient agglomérées et présentaient des diamètres moyens légèrement plus importants de 2.9 ± 0.6 nm et 2.1 ± 0.1 nm, respectivement.

V.2. Hydrogénation biphasique aqueuse avec RhNP-TPPO@CCM-C sans additif basique

En utilisant le latex de RhNP-TPPO@CCM-C produit en l'absence de base, une première série de réactions catalytiques avec différentes durées de réaction a été réalisée à 25 °C, sous 20 bar de pression de H₂ et agitation à 1200 tr/min pour limiter le transfert de masse externe, avec un rapport styrène/Rh de 5000/1. Une conversion complète du styrène a été atteinte après 2 heures, correspondant à un TOF moyen de 3000 h⁻¹ (cTOF 4300 h⁻¹). Des réactions catalytiques supplémentaires avec un temps de réaction fixe de 0.25 h et différents rapports styrène/Rh ont donné les résultats rapportés dans le Tableau 3, Entrées 1-3. Le système a montré une excellente sélectivité (>99%) pour la formation de l'éthylbenzène (EB) avec la formation de seulement de petites quantités du produit entièrement saturé, l'éthylcyclohexane (ECH), comme déjà décrit précédemment pour l'hydrogénation du styrène utilisant d'autres catalyseurs RhNP-CCM [35]. De plus, la séparation de phase a été rapide dans toutes les réactions (<3 min), facilitant la séparation des produits et la récupération du catalyseur, comme déjà observé pour d'autres applications catalytiques biphasiques aqueuses de nanoréacteurs présentant la même coque externe (CCM-C)[28,35] . L'hydrogénation du styrène a également été réalisée avec le même latex de RhNP-TPPO@CCM-C à des températures plus élevées (30 °C- 55 °C) avec un rapport styrène/Rh de 5000/1 (Tableau 3, Entrées 4-7). À 55 °C, une conversion de 83% a été obtenue après 0,25 h, fournissant un TOF moyen très élevé de 16100 h⁻¹ (cTOF 23600 h⁻¹). Les conversions plus modérées obtenues dans la plage de 25 à 35 °C ont permis

d'estimer une énergie d'activation apparente de la réaction (E_a) de 69 ± 6 kJ/mol à partir d'un tracé d'Arrhenius, qui est comparable à l' E_a obtenue pour l'hydrogénation du styrène en phase gazeuse [54]. Cependant, à des températures de réaction plus élevées, l' E_a apparente a diminué à 4 ± 1 kJ/mol, indiquant des limitations de diffusion (transfert de masse interne)[55,56].

Table 3. Hydrogenation du styrene en utilisant RhNP-TPPO@CCM-C préparé sans additives de base.^a

Entrée	Rapport molaire styrene/Rh	T (°C)	Conversion (%)	Selectivité (%)		TOF (cTOF) ^b (h ⁻¹)
				EB	ECH	
1	2000/1	25	82	>99	<0.1	7800 (11500)
2	5000/1	25	21	>99	<0.1	4500 (6500)
3	10000/1	25	8	>99	<0.1	3000 (4450)
4	5000/1	30	35	>99	<0.1	8000 (11600)
5	5000/1	35	58	>99	<0.1	11200 (16400)
6	5000/1	45	65	>99	<0.1	12900 (19000)
7	5000/1	55	83	>99	<0.1	16100 (23600)

^a Conditions réactionelles: 20 bar H₂, 25 °C, 0.25 h, 1200 rpm. ^b Corrected TOF (cTOF) calculé en considérant la surface d'atomes de Rh. EB: ethylbenzène, ECH : ethylcyclohexane.

Le recyclage du latex de RhNP-TPPO@CCM-C a été évalué plus avant pour une série de réactions catalytiques avec un rapport styrène/Rh de 5000/1 et un temps de réaction de 0.25 h, avec extraction intermédiaire du produit par éther diéthylique (Figure 7a). La procédure d'extraction était similaire à celle précédemment utilisée pour recycler les latex de RhNP-TPP@CCM-C [35] et RhNP-TPPO@CCM-C (voir paragraphe précédent), ainsi que le latex du Rh^I-TPP moléculaire@CCM [28]. Une conversion assez constante du styrène d'environ 21 %, correspondant à un TOF moyen d'environ 4500 h⁻¹ (cTOF de 6500 h⁻¹), a été obtenue sur les six réactions consécutives, mais uniquement lorsque le système de catalyse récupéré a été réactivé avec H₂ (20 bar, 1 h, 25 °C) avant l'ajout d'un nouveau lot de substrat. Une expérience de recyclage sans ce traitement de réactivation a donné des résultats erratiques, probablement en raison de

la passivation des RhNPs par la formation d'une couche d'oxyde en surface [47,49] pendant les procédures de recyclage, comme discuté également dans le paragraphe précédent. Une analyse TEM sur le latex récupéré après la sixième réaction (Figure 7b) a montré que les RhNPs restaient bien dispersées, avec une distribution de taille similaire (1.9 ± 0.6 nm) à celle avant la catalyse (voir Tableau 2).

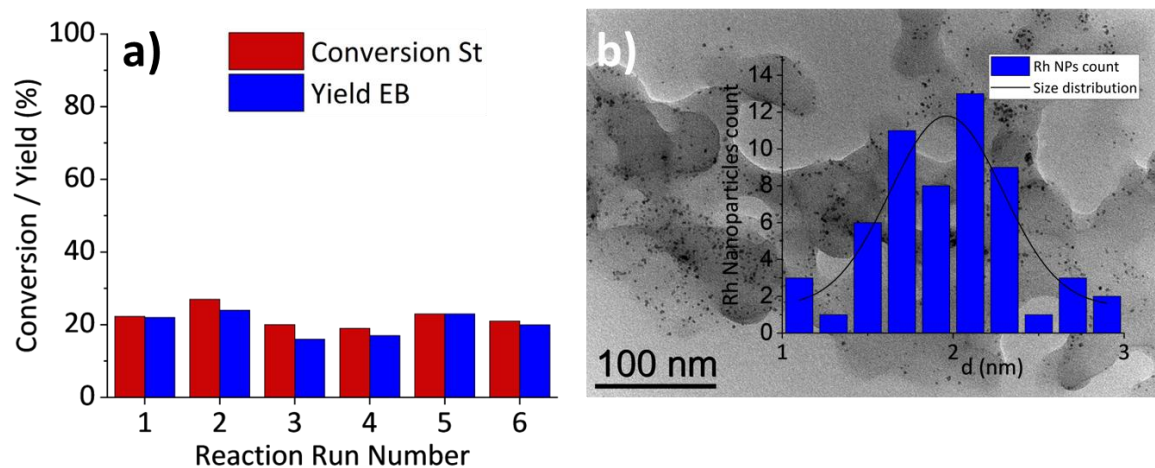


Figure 7. (a) Réutilisation du catalyseur RhNP-TPPO@CCM-C évaluée dans six réactions catalytiques d'hydrogénation du styrène avec extraction du produit par éther diéthylique et traitement intermédiaire à l' H_2 (20 bar H_2 , 25 °C, 1 h, 1200 tr/min) et extraction du produit par éther diéthylique. Conditions de réaction : Styrène/Rh = 5000/1, 20 bar H_2 , 25 °C, 0,25 h, 1200 tr/min (b) TEM du RhNP-TPPO@CCM-C après la sixième réaction avec les RhNPs bien dispersées, et la distribution de taille correspondante, plutôt à celle observée avant la catalyse (1.9 ± 0.6 nm) (superposés).

VI. Conclusion et perspectives

L'objectif de ce projet de thèse était de développer de nouvelles méthodes pour le confinement efficace de nanoparticules métalliques (MNPs) dans des nanoréacteurs micellaires à coeur-réticulés (CCM), avec des coquilles cationiques, en vue d'appliquer les latex MNP@CCMs résultants dans l'hydrogénation biphasique aqueuse. À cette fin, de nouvelles micelles à coeur-réticulés fonctionnalisées avec de l'oxyde de triphénylphosphine et une coque polycationique ont été développées par extension d'une approche de polymérisation RAFT optimisée précédemment. La première tentative de production de RhNP-TPPO@CCM-C consistait à charger les micelles

TPPO@CCM-C avec $[\text{Rh}(\text{COD})(\mu\text{-Cl})_2]$, afin de générer un complexe $[\text{RhCl}(\text{COD})(\text{TPPO@CCM-C})]$ ancré dans le coeur, qui pourrait être réduit en RhNPs par H_2 , suivant la même procédure que celle développée précédemment pour obtenir des RhNPs incorporés dans TPP@CCM-C. Cela s'est révélé infructueux, indiquant que la formation d'un complexe Rh^{I} -TPPO@CCM-C par clivage du groupement pont di- $\mu\text{-Cl}$ dans $[\text{Rh}(\text{COD})(\mu\text{-Cl})_2]$ n'était pas favorable dans le coeur polymérique dans les conditions appliquées. Étant donné cela, une stratégie alternative impliquant la synthèse *ex-situ* de RhNPs en utilisant TPP et la pyridine comme stabilisateurs, produisant des RhNPs ultrapetites, et leur transfert ultérieur dans les nanoréacteurs TPPO@CCM-C, a été envisagée. Cette stratégie a permis le transfert réussi des RhNPs vers les coeurs fonctionnalisés par TPPO. Bien que le latex résultant RhNP-TPPO@CCM-C se soit avéré efficace dans l'hydrogénation biphasique aqueuse du styrène, avec seulement 2 % de lixiviation du catalyseur, une extraction graduelle des ligands TPP et pyridine utilisés pour la synthèse *ex-situ* des RhNPs pendant le travail entre les cycles, a induit une diminution régulière de l'activité catalytique. Néanmoins, une phase de catalyseur stable a été obtenue après un lavage préliminaire approfondi et une première réaction, produisant une TOF d'environ 1025 h^{-1} (cTOF d'environ 1440 h^{-1}), sur plusieurs cycles. Pour améliorer le système, une nouvelle approche a été développée consistant en une synthèse en une seule étape du catalyseur RhNP-TPPO@CCM-C, qui ne nécessite pas l'utilisation de stabilisateurs supplémentaires. Les RhNPs produites étaient de taille plus petite ($1.7 \pm 0.2 \text{ nm}$) que leurs homologues synthétisés dans des conditions similaires en présence uniquement de TPPO comme stabilisateur ($2.4 \pm 0.2 \text{ nm}$). Cette différence souligne l'effet positif du confinement sur la taille des RhNPs, conduisant à des NPs plus petites. Le nouveau catalyseur a démontré une très bonne activité catalytique (cTOFs de 4500 à 16000 h^{-1}) et une sélectivité totale dans l'hydrogénation du styrène pur en éthylbenzène dans des conditions douces (20 bar H_2 , 25-55 °C). Les résultats catalytiques globaux avec RhNP-TPPO@CCM-C ont montré que la nature des ligands fonctionnalisant le coeur des

micelles polymères est un paramètre clé pour améliorer la stabilité et le recyclage du latex catalytique.

VII. Références

- [1] R.L. Johnston, Metal nanoparticles and nanoalloys, in: *Frontiers of Nanoscience*, Elsevier Ltd; 3 (2012) 1–42, <https://doi.org/10.1016/B978-0-08-096357-0.00006-6>
- [2] T. Shen, S. Zhou, J. Ruan, X. Chen, X. Liu, X. Ge, C. Qian, Recent advances on micellar catalysis in water, *Adv Colloid Interface Sci.* 287 (2021) 102299, <https://doi.org/10.1016/j.cis.2020.102299>
- [3] T. Kotre, M.T. Zarka, J.O. Krause, M.R. Buchmeiser, R. Weberskirch, O. Nuyken, Design And Application Of Amphiphilic Polymeric Supports For Micellar Catalysis, In: *Macromol Symp* (2004) 203–214, <https://doi.org/10.1002/masy.200451316>
- [4] Boy. Cornils, *Catalysis from A to Z : A Concise Encyclopedia*; Wiley-VCH; ISBN 352729855X (2000), [https://doi.org/10.1016/S1351-4180\(13\)70258-7](https://doi.org/10.1016/S1351-4180(13)70258-7)
- [5] P. Serp, K. Philippot Editors, *Nanomaterials in Catalysis* Wiley-VCH (2012). Online ISBN:9783527656875. <https://doi.org/10.1002/9783527656875>
- [6] D. Astruc Editor, *Nanoparticles and Catalysis*, Wiley-VCH, (2007). Online ISBN:978352762132.3 <https://doi.org/10.1002/9783527621323>
- [7] B. Chaudret, K. Philippot, Organometallic nanoparticles of metals or metal oxides, *Oil and Gas Science and Technology.* 62 (2007) 799–817. <https://doi.org/10.2516/ogst:2007062>
- [8] A. Roucoux, J. Schulz, H. Patin, Reduced transition metal colloids: A novel family of reusable catalysts?, *Chem Rev.* 102 (2002) 3757–3778. <https://doi.org/10.1021/cr010350j>
- [9] D. Astruc, F. Lu, J.R. Aranzaes, Nanoparticles as recyclable catalysts: The frontier between homogeneous and heterogeneous catalysis, *Angew Chem Int Ed* 44 (2005) 7852–7872. <https://doi.org/10.1002/anie.200500766>
- [10] C. Burda, X. Chen, R. Narayanan, M.A. El-Sayed, Chemistry and properties of nanocrystals of different shapes, *Chem Rev.* 105 (2005) 1025–1102. <https://doi.org/10.1021/cr030063a>
- [11] M. Guerrero, N.T.T. Chau, S. Noël, A. Denicourt-Nowicki, F. Hapiot, A. Roucoux, E. Monflier, K. Philippot, About the Use of Rhodium Nanoparticles in

Hydrogenation and Hydroformylation Reactions, *Curr Org Chem* 17 (2013) 364-399
<https://doi.org/10.2174/1385272811317040006>

[12] J.L. Castelbou, E. Bresó-Femenia, P. Blondeau, B. Chaudret, S. Castellón, C. Claver, C. Godard, Tuning the selectivity in the hydrogenation of aromatic ketones catalyzed by similar ruthenium and rhodium nanoparticles, *ChemCatChem*. 6 (2014) 3160–3168. <https://doi.org/10.1002/cctc.201402524>

[13] E. Guyonnet Bilé, R. Sassine, A. Denicourt-Nowicki, F. Launay, A. Roucoux, New ammonium surfactant-stabilized rhodium(0) colloidal suspensions: Influence of novel counter-anions on physico-chemical and catalytic properties, *Dalton Trans.* 40 (2011) 6524–6531. <https://doi.org/10.1039/c0dt01763a>

[14] E. Guyonnet Bilé, E. Cortelazzo-Polisini, A. Denicourt-Nowicki, R. Sassine, F. Launay, A. Roucoux, Chiral ammonium-capped rhodium(0) nanocatalysts: Synthesis, characterization, and advances in asymmetric hydrogenation in neat water, *ChemSusChem*. 5 (2012) 91–101. <https://doi.org/10.1002/cssc.201100364>

[15] E. Guyonnet-Bilé, A. Denicourt-Nowicki, R. Sassine, P. Beaunier, F. Launay, A. Roucoux, N-Methylephedrium salts as chiral surfactants for asymmetric hydrogenation in neat water with rhodium(0) nanocatalysts, *ChemSusChem*. 3 (2010) 1276–1279. <https://doi.org/10.1002/cssc.201000206>

[16] A Borsla, A.M Wilhelm, H Delmas, Hydrogenation of olefins in aqueous phase, catalyzed by polymer-protected rhodium colloids: kinetic study, *Cat Today*, 66(2–4) (2001) 389-395 [https://doi.org/10.1016/S0920-5861\(00\)00635-0](https://doi.org/10.1016/S0920-5861(00)00635-0)

[17] H. Mao, X. Liao, B. Shi, Amphiphilic tannin-stabilized Rh nanoparticles: A highly active and reusable catalyst in biphasic aqueous-organic system, *Catal Commun.* 16 (2011) 210–214. <https://doi.org/10.1016/j.catcom.2011.09.038>

[18] C. Chaudhari, H. Imatome, Y. Nishida, K. Sato, K. Nagaoka, Recyclable Rh-PVP nanoparticles catalyzed hydrogenation of benzoic acid derivatives and quinolines under solvent-free conditions, *Catal Commun.* 126 (2019) 55–60. <https://doi.org/10.1016/j.catcom.2019.02.019>

[19] H. Hirai, M. Ohtaki, M. Komiyama, Preparation of Highly Active Hydrogenation Catalyst by Immobilization of Polymer-Protected Colloidal Rhodium Particles, *Chem Lett* 16 (1987) 149-152 <https://doi.org/10.1246/CL.1987.149>

[20] J.L. Castelbou, A. Gual, E. Mercadé, C. Claver, C. Godard, Ligand effect in the Rh-NP catalysed partial hydrogenation of substituted arenes, *Catal Sci Technol.* 3 (2013) 2828–2833. <https://doi.org/10.1039/c3cy00388d>

- [21] C. Moreno-Marrodan, F. Liguori, E. Mercadé, C. Godard, C. Claver, P. Barbaro, A mild route to solid-supported rhodium nanoparticle catalysts and their application to the selective hydrogenation reaction of substituted arenes, *Catal Sci Technol.* 5 (2015) 3762–3772. <https://doi.org/10.1039/c5cy00599j>
- [22] F. Martinez-Espinar, P. Blondeau, P. Nolis, B. Chaudret, C. Claver, S. Castellón, C. Godard, NHC-stabilised Rh nanoparticles: Surface study and application in the catalytic hydrogenation of aromatic substrates, *J Catal.* 354 (2017) 113–127. <https://doi.org/10.1016/j.jcat.2017.08.010>
- [23] H. Wang, C.J. Abou-Fayssal, C. Fliedel, E. Manoury, R. Poli, Phosphine-Functionalized Core-Crosslinked Micelles and Nanogels with an Anionic Poly(styrenesulfonate) Shell: Synthesis, Rhodium(I) Coordination and Aqueous Biphasic Hydrogenation Catalysis, *Polymers (Basel)*. 14 (2022) 4937 <https://doi.org/10.3390/polym14224937>
- [24] H. Wang, C. Fliedel, E. Manoury, R. Poli, Core-crosslinked micelles with a poly-anionic poly(styrene sulfonate)-based outer shell made by RAFT polymerization, *Polymer (Guildf)*. 243 (2022) 124640 <https://doi.org/10.1016/j.polymer.2022.124640>
- [25] A. Joumaa, F. Gayet, E.J. Garcia-Suarez, J. Himmelstrup, A. Riisager, R. Poli, E. Manoury, Synthesis of nixantphos core-functionalized amphiphilic nanoreactors and application to rhodium-catalyzed aqueous biphasic 1-octene hydroformylation, *Polymers (Basel)* 12 (2020) 1107 <https://doi.org/10.3390/POLYM12051107>
- [26] S. Chen, F. Gayet, E. Manoury, A. Joumaa, M. Lansalot, F. D'Agosto, R. Poli, Coordination Chemistry Inside Polymeric Nanoreactors: Interparticle Metal Exchange and Ionic Compound Vectorization in Phosphine-Functionalized Amphiphilic Polymer Latexes, *Chem Eur J* 22 (2016) 6302–6313. <https://doi.org/10.1002/chem.201504923>
- [27] A. Joumaa, S. Chen, S. Vincendeau, F. Gayet, R. Poli, E. Manoury, Rhodium-catalyzed aqueous biphasic hydrogenation of alkenes with amphiphilic phosphine-containing core-shell polymers, *Molecular Catalysis*. 438 (2017) 267–271. <https://doi.org/10.1016/j.mcat.2017.06.005>
- [28] H. Wang, L. Vendrame, C. Fliedel, S. Chen, F. Gayet, F. D'Agosto, M. Lansalot, E. Manoury, R. Poli, Triphenylphosphine-Functionalized Core-Cross-Linked Micelles and Nanogels with a Polycationic Outer Shell: Synthesis and Application in Rhodium-Catalyzed Biphasic Hydrogenations, *Chem Eur J* 27 (2021) 5205–5214. <https://doi.org/10.1002/chem.202004689>
- [29] H. Wang, L. Vendrame, C. Fliedel, S. Chen, F. Gayet, E. Manoury, X. Zhang, F. D'agosto, M. Lansalot, R. Poli, Core-Cross-Linked Micelles Made by RAFT Polymerization with a Polycationic Outer Shell Based on Poly(1-methyl-4-

vinylpyridinium), *Macromolecules*. 53 (2020) 2198–2208. <https://doi.org/10.1021/acs.macromol.9b02582>

[30] S. Chen, A.F. Cardozo, C. Julcour, J.F. Blanco, L. Barthe, F. Gayet, M. Lansalot, F. D'Agosto, H. Delmas, E. Manoury, R. Poli, Amphiphilic core-cross-linked micelles functionalized with bis(4-methoxyphenyl)phenylphosphine as catalytic nanoreactors for biphasic hydroformylation, *Polymer (Guildf)*. 72 (2015) 327–335. <https://doi.org/10.1016/j.polymer.2015.02.024>

[31] A.F. Cardozo, C. Julcour, L. Barthe, J.F. Blanco, S. Chen, F. Gayet, E. Manoury, X. Zhang, M. Lansalot, B. Charleux, F. D'Agosto, R. Poli, H. Delmas, Aqueous phase homogeneous catalysis using core-shell nanoreactors: Application to rhodium-catalyzed hydroformylation of 1-octene, *J Catal*. 324 (2015) 1–8. <https://doi.org/10.1016/j.jcat.2015.01.009>

[32] X. Zhang, A.F. Cardozo, S. Chen, W. Zhang, C. Julcour, M. Lansalot, J.F. Blanco, F. Gayet, H. Delmas, B. Charleux, E. Manoury, F. D'Agosto, R. Poli, Core-Shell Nanoreactors for Efficient Aqueous Biphasic Catalysis, *Chem Eur J* 20 (2014) 15505–15517. <https://doi.org/10.1002/chem.201403819>

[33] E. Lobry, A.F. Cardozo, L. Barthe, J.F. Blanco, H. Delmas, S. Chen, F. Gayet, X. Zhang, M. Lansalot, F. D'Agosto, R. Poli, E. Manoury, C. Julcour, Core phosphine-functionalized amphiphilic nanogels as catalytic nanoreactors for aqueous biphasic hydroformylation, *J Catal*. 342 (2016) 164–172. <https://doi.org/10.1016/j.jcat.2016.07.023>

[34] F. D'Agosto, J. Rieger, M. Lansalot, RAFT-Mediated Polymerization-Induced Self-Assembly, *Angew Chem Int Ed* 59 (2020) 8368–8392. <https://doi.org/10.1002/anie.201911758>

[35] H. Wang, A.M. Fiore, C. Fliedel, E. Manoury, K. Philippot, M.M. Dell'Anna, P. Mastorilli, R. Poli, Rhodium nanoparticles inside well-defined unimolecular amphiphilic polymeric nanoreactors: Synthesis and biphasic hydrogenation catalysis, *Nanoscale Adv*. 3 (2021) 2554–2566. <https://doi.org/10.1039/d1na00028d>

[36] S.S. Sambou, R. Hromov, I. Ruzhylo, H. Wang, A. Allandrieu, C. Sabatier, Y. Coppel, J.C. Daran, F. Gayet, A. Labande, E. Manoury, R. Poli, Amphiphilic polymeric nanoreactors containing Rh(i)-NHC complexes for the aqueous biphasic hydrogenation of alkenes, *Catal Sci Technol*. 11 (2021) 6811–6824. <https://doi.org/10.1039/d1cy00554e>

[37] R.K. O'reilly, C.J. Hawker, K.L. Wooley, Cross-linked block copolymer micelles: Functional nanostructures of great potential and versatility, *Chem Soc Rev*. 35 (2006) 1068–1083. <https://doi.org/10.1039/b514858h>

- [38] R. El Abed, F. Aloui, J.P. Genêt, B. Ben Hassine, A. Marinetti, Synthesis and resolution of 2-(diphenylphosphino)heptahelicene, *J Organomet Chem.* 692 (2007) 1156–1160. <https://doi.org/10.1016/j.jorganchem.2006.11.022>
- [39] S. Vanicek, M. Podewitz, J. Stubbe, D. Schulze, H. Kopacka, K. Wurst, T. Müller, P. Lippmann, S. Haslinger, H. Schottenberger, K.R. Liedl, I. Ott, B. Sarkar, B. Bildstein, Highly Electrophilic, Catalytically Active and Redox-Responsive Cobaltoceniumyl and Ferrocenyl Triazolylidene Coinage Metal Complexes, *Chemistry - A European Journal.* 24 (2018) 3742–3753. <https://doi.org/10.1002/chem.201705051>
- [40] M. Deimling, M. Kirchhof, B. Schwager, Y. Qawasmi, A. Savin, T. Mühlhäuser, W. Frey, B. Claasen, A. Baro, T. Sottmann, S. Laschat, Asymmetric Catalysis in Liquid Confinement: Probing the Performance of Novel Chiral Rhodium–Diene Complexes in Microemulsions and Conventional Solvents, *Chem Eur J* 25 (2019) 9464–9476. <https://doi.org/10.1002/chem.201900947>
- [41] J. Nowakowski, S. Nowakowska, G. Srivastava, M. Baljovic, J. Girovsky, N. Ballav, T.A. Jung, Probing the Reactivity of Functionalized Surfaces by Porphyrin Metalation, *ChemistrySelect.* 1 (2016) 891–895. <https://doi.org/10.1002/slct.201600215>
- [42] T. Nishimura, Y. Maeda, T. Hayashi, Asymmetric cyclopropanation of alkenes with dimethyl diazomalonate catalyzed by chiral diene-rhodium complexes, *Angew Chem Int Ed* 49 (2010) 7324–7327. <https://doi.org/10.1002/anie.201003775>
- [43] P. Das, P. Chutia, D. Kumar Dutta, Efficient Carbonylation of Methanol Catalyzed by Rhodium(I) Cyclooctadiene Complexes with Triphenylphosphinechalcogenide Ligands, *Chem Lett* 7 (2002) 766–767, <https://doi.org/10.1246/cl.2002.766>
- [44] R. Bonnaire, D. Diavoust, N. Platzer, Rh NMR Studies of Organometallic Rhodium(I) Derivatives, *Org Mag Reson* 22, (1984) 80–85, <https://doi.org/10.1002/mrc.1270220205>
- [45] M. Ibrahim, M.M. Wei, E. Deydier, E. Manoury, R. Poli, P. Lecante, K. Philippot, Rhodium nanoparticles stabilized by ferrocenyl-phosphine ligands: Synthesis and catalytic styrene hydrogenation, *Dalton Trans* 48 (2019) 6777–6786. <https://doi.org/10.1039/c9dt01006h>
- [46] A. Serrano-Maldonado, E. Martin, I. Guerrero-Ríos, Pyridine-Stabilized Rhodium Nanoparticles in Ionic Liquids as Selective Hydrogenation and Transfer Hydrogenation Catalysts, *Eur J Inorg Chem.* 2019 (2019) 2863–2870. <https://doi.org/10.1002/ejic.201900223>
- [47] S.A. Stratton, K.L. Luska, A. Moores, Rhodium nanoparticles stabilized with phosphine functionalized imidazolium ionic liquids as recyclable arene

hydrogenation catalysts, *Catal Today*. 183 (2012) 96–100. <https://doi.org/10.1016/j.cattod.2011.09.016>

[48] M.L. Buil, M.A. Esteruelas, S. Niembro, M. Oliván, L. Orzechowski, C. Pelayo, A. Vallribera, Dehalogenation and hydrogenation of aromatic compounds catalyzed by nanoparticles generated from rhodium bis(imino)pyridine complexes, *Organometallics*. 29 (2010) 4375–4383. <https://doi.org/10.1021/om1003072>

[49] C. Vollmer, E. Redel, K. Abu-Shandi, R. Thomann, H. Manyar, C. Hardacre, C. Janiak, Microwave irradiation for the facile synthesis of transition-metal nanoparticles (NPs) in ionic liquids (ILs) from metal-carbonyl precursors and Ru-, Rh-, and Ir-NP/IL dispersions as biphasic liquid-liquid hydrogenation nanocatalysts for cyclohexene, *Chem Eur J* 16 (2010) 3849–3858. <https://doi.org/10.1002/chem.200903214>

[50] E. Baralt, Z.J. Sandra Smith, Z. Jamie Hurwitz, Z.T. István Horváth, R.H. Fish, *Homogeneous Catalytic Hydrogenation. 6. Synthetic and Mechanistic Aspects of the Regioselective Reductions of Model Coal Nitrogen, Sulfur, and Oxygen Heteroaromatic Compounds Using the (η^5 -Pentamethylcyclopentadienyl)rhodium Tris(acetonitrile) Dication Complex as the Catalyst Precursor*. *J Am Chem Soc* 114, (1992) 5187-5196, <https://doi.org/10.1021/ja00039a033>

[51] H. Imai, T. Nishiguchi, K. Fukuzumi, *Transfer Hydrogenation and Transfer Hydrogenolysis. 13. Hydrogen Transfer from Cyclic Amines to Aromatic Nitro Compounds Catalyzed by Noble Metal Salts*, *J Org Chem* 42 (1977) 431-434, <https://doi.org/10.1021/jo00433a024>

[52] E. Baráth, *Hydrogen Transfer Reactions Of Carbonyls, Alkynes, And Alkenes With Noble Metals In The Presence Of Alcohols/Ethers And Amines As Hydrogen Donors*, *Catalysts* 8 (2018) 671, <https://doi.org/10.3390/catal8120671>

[53] M. Studer, C. Wedemeyer-Exl, F. Spindler, H.-U. Blaser, *Enantioselective Homogeneous Hydrogenation of Monosubstituted Pyridines and Furans*, *Monatsh Chem* 131 (2000) 1335–1343, [https://doi.org/10.1016/S1381-1169\(98\)00200-3](https://doi.org/10.1016/S1381-1169(98)00200-3)

[54] C. Betti, J. Badano, C. Lederhos, M. Maccarrone, N. Carrara, F. Coloma-Pascual, M. Quiroga, C. Vera, *Kinetic study of the selective hydrogenation of styrene over a Pd egg-shell composite catalyst*, *Reaction Kinetics, Mechanisms and Catalysis*. 117 (2016) 283–306. <https://doi.org/10.1007/s11144-015-0910-8>

[55] Z.A. Piskulich, O.O. Mesele, W.H. Thompson, *Removing the barrier to the calculation of activation energies: Diffusion coefficients and reorientation times in liquid water*, *J Chem Phys* 147 (2017) 134103 <https://doi.org/10.1063/1.4997723>

[56] H. Rafatijo, D.L. Thompson, *General application of Tolman's concept of activation energy*, *J Chem Phys* 147 (2017) 224111 <https://doi.org/10.1063/1.5009751>